# A STUDY OF POWER ELECTRONIC BUILDING BLOCK (PEBB)-BASED INTEGRATED SHIPBOARD POWER SYSTEMS DURING RECONFIGURATION

A Dissertation

by

ADEOTI T. ADEDIRAN

Submitted to the Office of Graduate Studies of
Texas A&M University
in partial fulfillment of the requirements for the degree of

DOCTOR OF PHILOSOPHY

December 2003

Major Subject: Electrical Engineering

# A STUDY OF POWER ELECTRONIC BUILDING BLOCK (PEBB)-BASED INTEGRATED SHIPBOARD POWER SYSTEMS DURING RECONFIGURATION

A Dissertation

by

ADEOTI T. ADEDIRAN

Submitted to Texas A&M University
in partial fulfillment of the requirements
for the degree of

DOCTOR OF PHILOSOPHY

Approved as to style and content by:

| | |
|---|---|
| Karen L. Butler-Purry<br>(Chair of Committee) | |
| Karan Watson<br>(Member) | Prasad Enjeti<br>(Member) |
| Graham Donald Allen<br>(Member) | Chanan Singh<br>(Head of Department) |

December 2003

Major Subject: Electrical Engineering

# ABSTRACT

A Study of Power Electronic Building Block (PEBB)-Based Integrated Shipboard Power Systems During Reconfiguration. (December 2003)

Adeoti T. Adediran, B.Sc., University of Ibadan;

M.S., University of Tennessee

Chair of Advisory Committee: Dr. Karen Butler-Purry

The U.S. Navy has developed in their ships, and is continually improving, electric propulsion, ship service power, and electric loads. The latest topology under design is the integrated power system (IPS). The IPS entails the all electric ship concept with electric propulsion, direct current (DC) distribution, and modular technology. In the all electric ship concept, ship propulsion and ship service loads are powered by alternating current (AC) generation. For the IPS, power electronics conversion is to be utilized to convert alternating current (AC) generation to direct current (DC) distribution. As state-of-the-art power electronics, the Navy plans to use power electronic building blocks (PEBB) technology in its IPS.

A U.S. naval shipboard power system is required to be a highly reconfigurable system to enhance its survivability and reliability. Reconfiguration is a change in the shipboard power system state for various reasons such as new topology, changing missions and emergencies. It was decided to study the behavior of a PEBB-based integrated shipboard power system during reconfiguration. Since no real time operation data was available, the

problem was studied through the simulation of reconfiguration scenarios on a scaled-down computer model of an IPS in MATLAB.

Reconfiguration scenarios were determined and staged, and an AC/DC power system stability assessment methodology was applied by decoupling the IPS test system around an intrazonal bus. The coupled system of the test IPS, consisted of two dynamic 4160 VAC generators, two rectifiers, two DC-DC converters between the rectifiers' output looped bus and the downstream intrazonal 775V busses, inverters, buck converters, AC loads and DC loads. There was modeling of excitation perturbations which introduced errors in the assessment of the stability requiring an approximation analysis.

The study found that the DC bus of interest was stable for all nine reconfiguration scenarios staged, but it found that other busses were not stable for two of the scenarios. The study further found that lower stability margins occurred at lower frequencies of about 1Hz for stable scenarios. It concluded that there were tangible benefits to advancing the shipboard power system architecture to the IPS topology because of the good stability results.

To my twin sister, Dr. Adeola K. Adediran, who made these dry bones live again.

# ACKNOWLEDGMENTS

I thank God, the Almighty, whose mercy and grace made this dissertation possible. Many people in my life have contributed to the success of this dissertation and I now recognize my major professor, Dr. Karen L. Butler-Purry, whose kindness, even in the most trying of circumstances, has made this dissertation possible. I recognize my mother, Mrs. Mercy Adediran, for her many prayers and support and I thank the rest of my family for their concern and support. My committee has been exemplary in their patience and consideration. I thank Dr. Watson, Dr. Enjeti, Dr. Allen and Dr. Hardy for their professionalism, mingled with tremendous grace. The research work and the publications produced by me in this Ph.D. program could not have been possible without the help of my lab mates at the Power Systems Automation Laboratory, Texas A&M University. My heartfelt thanks, therefore, goes to my friends at the lab. I thank my editor and friend, Dr. Jean Creighton Bailey, for her work in editing this document. Finally, I thank the staff of the National Emergency Response and Rescue Training Center (NERRTC) for their support financially and emotionally through the final stages of this dissertation.

# TABLE OF CONTENTS

Page

CHAPTER Page

# LIST OF FIGURES

FIGURE Page

FIGURE Page

FIGURE Page

FIGURE Page

# LIST OF TABLES

# CHAPTER I

# INTRODUCTION

## 1.1 Overview

As commercial and military ships have evolved to the present day, there have been numerous changes in their drive and service power design. The US Navy ships are forging ahead with their own evolution by using continually improving electric propulsion, ship service power, and electric loads. The latest topology under design for naval shipboard power systems is the integrated power system (IPS). The IPS entails the all electric ship concept with electric propulsion, direct current (DC) distribution, and modular technology. In the all electric ship concept, propulsion motors and service loads are powered by AC generation. In the IPS, DC distribution is used to supply the zones with power and within the zones there are inverters that convert power to AC for AC loads and buck converters supply power to DC loads. Power electronics conversion is utilized to convert alternating current (AC) generation to DC distribution.

US naval shipboard power systems are highly reconfigurable systems. There are often two paths (normal and alternate) to vital loads and bus transfer switches are used to reroute power to the alternate path in the event of a failure in the normal path to a load. This form of system reconfiguration is in addition to the reconfiguration performed by protective devices such as circuit breakers, fuses, and other protective devices.

---

This dissertation follows the style and format of IEEE *Transactions on Power Delivery*.

Reconfiguration in an IPS is an important issue because of its stability implications. It was inferred that with a proliferation of power electronics devices in a power system, that there would be stability concerns to be addressed

Power electronic building blocks (PEBB) are a proposed technology under development as a part of IPS. Also, PEBB are to be used in other systems such as DC zonal power systems. It is a technology that performs conversion, inversion, and all other types of power modulation. PEBB is a paradigm shift from conventional custom design of converters and controllers to modularized development of standardized designs of converters-submodules and controllers. This technology, when used in the IPS, makes the issue of the behavior of the IPS during reconfiguration an even more complex issue. An example of such complexities is the soft switching of the converter using the PEBB power switches. PEBB modular nature requires standardization of filter interface design and this standardization, among others, is factored into the formulation of the problem complexity.

The study of PEBB-based integrated shipboard power systems during reconfiguration scenarios examines the behavior of an integrated power system (IPS) during reconfiguration assuming PEBB proliferation as is expected to be the case in AC/DC power systems in Naval SPS, generally, in the future, and examines the issue of DC bus stability due to the reconfiguration phenomenon. An AC/DC power system methodology which is less conservative than traditional methodology was applied to study the behavior of the IPS during reconfiguration. A catalog of DC bus stability results of the scenarios was generated of the scaled-down IPS system model. This

dissertation presents results of a study of PEBB-based integrated shipboard power systems performed in order to characterize their stability performance during reconfiguration. The tasks involved in this dissertation research were system analysis, system modeling, system simulation and data generation, reconfiguration scenario generation, perturbation modeling, stability assessment, multiplier design, stability margin determination and results presenting. The aim of the dissertation research was to learn how a PEBB-based integrated shipboard power system responded to reconfiguration.

## 1.2 Motivation

One of the motivations of the dissertation research was to make a contribution to the ongoing discussion on the all-electric ship concept which forms one of the main thrusts of the research by the Office of Naval Research (ONR).

It has been observed and elaborated on in this dissertation that there are several issues involved in reconfiguration. A very critical issue is the issue of stability, because of its often catastrophic effect on power system behavior. Stability can become as undefined and complex in the IPS as in traditional AC systems because of the large number of power-electronics components within the system. The theoretical importance of stability within the context of AC/DC shipboard power systems is also a motivation for the study.

## 1.3 Reconfiguration Behavior of PEBB-Based Integrated Shipboard Power Systems

The IPS entails the all electric ship concept with electric propulsion, direct current (DC) distribution, and modular technology. In the all electric ship concept, propulsion motors and service loads are powered by AC generation. The PEBB-based integrated shipboard power system has DC distribution, where PEBB is used for the power conversion modules in converting AC to DC and back to AC. PEBB can also be used for the controller modules. The IPS is an AC/DC power system. The concept of PEBB is new, being introduced in recent years. The expected progression of events is to exclusively utilize PEBB for power modulation in future naval ships [1]. Before the advent of the PEBB idea in shipboard power system (SPS), an SPS was already a highly reconfigurable system. There is use of redundant power paths to vital loads to ensure power continuity to these vital loads during ship operation. However, the use of PEBB in the IPS is causing some issues of stability of the PEBB-based integrated system during reconfiguration to be addressed. Starting with the reconfiguration phenomenon and the PEBB-based integrated shipboard power system characteristics, complete understanding of the issue of stability is required.

An example of a reconfiguration action performed in an SPS is shown in Fig. 1.1. It depicts an automatic bus transfer (ABT) unit changing a vital load from its normal path to its alternate path as a result of a fault on the normal path. Typical components utilized during reconfiguration are bus transfer units, circuit breakers, fuses, switches, and low-voltage relays.

Characterizing the PEBB-based AC/DC power systems has become of high priority since the announcement by the Department of Defense of their intention to use the IPS for their newest land attack destroyer. This announcement has moved what would have been a natural progression of PEBB use in AC/DC power system into high gear and precipitated this study and others like it to ascertain the limitations of the chosen topology and its optimal use.

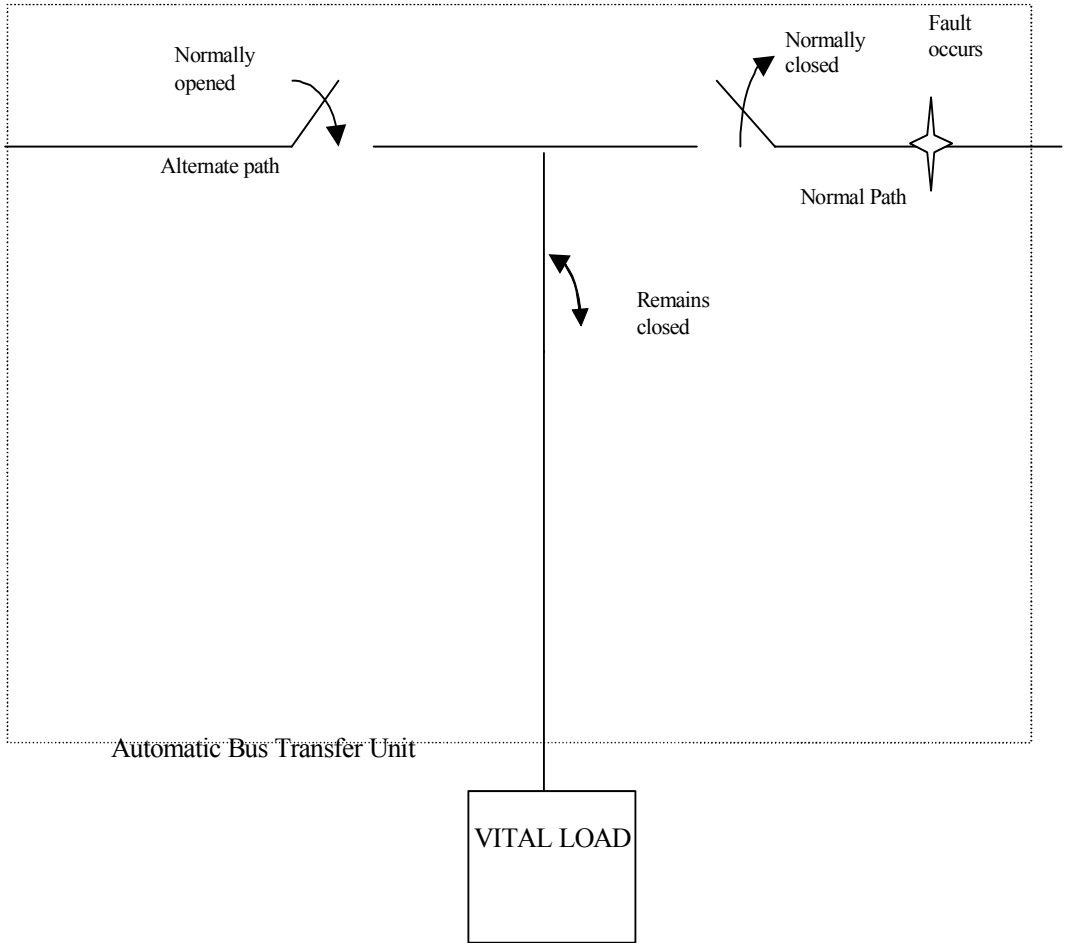


Fig. 1.1 Reconfiguration concept, ABT transferring load from normal to alternate paths

## 1.4 Problem Statement

The problem addressed herein was the development of a methodology for studying reconfiguration behavior of a PEBB-based integrated shipboard power system within the context of DC bus stability. The research to address this problem included the modeling of a small scale PEBB-based integrated shipboard power system and the stability assessment of the PEBB-based integrated shipboard power system by applying an existing stability assessment methodology. It further involved generating results on system performance, developing methodology's error analysis, and methodology's merit indices.

In this study, nine reconfiguration scenarios were staged on a small scale PEBB based IPS. Stability assessments were made on the intrazonal bus on the port side by first running the scenarios on a test system and then decoupling the test system about the intrazonal bus on the port side and perturbing the decoupled subsystems with signals containing the reconfiguration information from the scenarios and obtaining the stability contours. These contours were required to not have violated the forbidden regions of the contour space for stability to have occurred. How far the contours were from the forbidden regions were taken as a merit index. Errors obtained from generating signals with the reconfiguration information were quantified and minimizing these errors was another merit index.

## 1.5 Summary and Outline

This chapter presented an overview of the dissertation research. The dissertation research motivation was presented giving reasons for the research. The purpose of the dissertation research was outlined, a preliminary discussion of dissertation research topic, and a formulation of a concise problem statement were discussed.

The rest of this dissertation is organized in the following way: Chapter II contains a Literature Review that addresses PEBB, reconfiguration, PEBB-based integrated shipboard power system and present status of reconfiguration in PEBB-based integrated shipboard power system. In Chapter III the problem formulation is presented and chapter IV pertains to the analysis of the study. The results discussing the scenarios included in the study are presented in Chapter V. Similarly, chapter VI contains the catalog of reconfiguration scenarios performed on the test system and the summary of stability assessments. Chapter VII contains the conclusions of the study, summary of work, project applicability, and future work.

# CHAPTER II

# LITERATURE REVIEW AND THEORETICAL CONCEPTS

## 2.1 Overview

PEBB-based integrated shipboard power system is a new technology. Concepts that come to play are very rarely covered in the literature. The PEBB idea was developed in the late 1990s. The PEBB and IPS technologies are military technologies. The use of PEBB for IPS is still in conceptual stages. Reconfiguration is a more established concept for the Navy. Due to the need for power continuity for vital loads within a shipboard power system, and the need for change of priority on loads for different missions, reconfiguration was used as a tool to facilitate the realization of the itemized objectives. For vital power security, redundant paths were connected to vital loads in the shipboard power systems. Use of these different paths to loads causes a change of the topology of the system. Reconfiguration is an uncharted territory to understand in newer ship power architectures like the IPS. This novelty gives this dissertation research sufficient work in the area. Stability in shipboard power system is not like the utilities, where generator angle coherency is the main concern and where generation is often far from distribution. Rather, the main concern for the SPS is signal (e.g. voltage) instability (or collapse) and ship power is generated and distributed to load over fairly short cables. Work in the area of stability for novel shipboard power system was gathered in literature under stability of distributed power system DPS [2-10]. In the following sections, more in depth study of the background of concepts mentioned in this section is made.

## 2.2 Integrated Power System

Figure 2.1 [11] shows the latest schematic of the IPS from the ONR. It consists of two AC generator busses to which the propulsion induction motors are connected. The voltage at these busses is 4160VACrms and this is converted to 1000VDC through a power supply (PS) that is a rectifier. Two busses, the port bus and the starboard bus deliver power to all the zones on the ship, running, one on the right and the other on the left of the mid line of the ship. When the power is at the zonal level it is stepped down to 800VDC (or 775VDC) through the ship service converter module (SSCM). From this level it can be transformed to 450VAC rms or 155VDC and used by the loads. Zonal vital loads that need redundant power are fed from both the starboard entry into the zones and the port entry. DC distribution for the IPS affords it frequency decoupling, so that generator design does not have the 60Hz limitation [12].

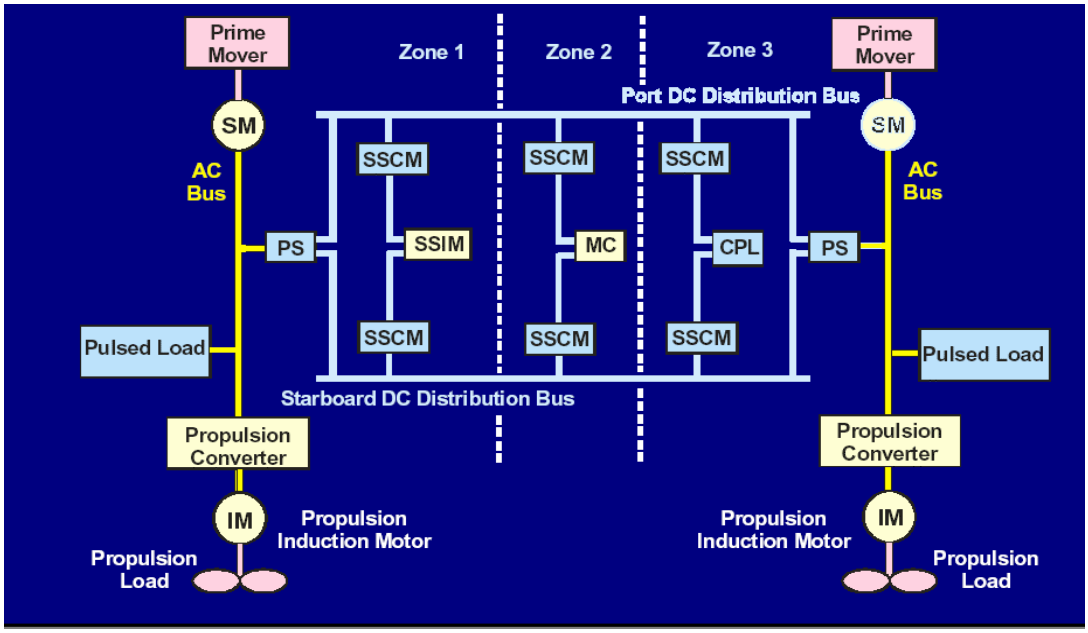


Fig. 2.1 Latest IPS schematic from ONR [11]

## 2.3 Power Electronic Building Blocks (PEBB)

PEBB stands for power electronic building block. This concept stands for a radical shift in current paradigms in the way power electronics is designed, developed and manufactured. It utilizes established concepts in other fields but novel to power electronics like open plug and play architecture, cellular design, hierarchical design, integration and concurrent engineering [13]. The idea of an open plug and play architecture is to build power electronics systems in much the same way as personal computers are built. Power modules are plugged into their applications and operational settings are made automatically [13]. Cellular design means that an entire three-phase inverter can be integrated into a single block or a five-terminal PEBB at small power levels (100kW or less). At slightly higher power levels (less than 1MW), the phase leg becomes the primary unit of integration (this is a three terminal PEBB), and at even higher power levels, (greater than 1MW) the switching cell or two terminal PEBB is the unit of integration [13].

An example of a PEBB phase leg is in Fig. 2.2. It forms the integration unit for medium power PEBB, whereas, a low power PEBB could be the bridge as shown in Fig. 2.3. A switching cell is as shown in Fig. 2.4. A switching cell is one unit of power switches like the MOSFET, while the phase leg is two switching cells in series. Hierarchical design is needed in the PEBB design because integration and snapping elements together require intelligence and hierarchical control.

Starting with the switching cell, embedded intelligence is needed to allow two cells to be snapped together to form a voltage source or current source phase legs [13]. Concurrent engineering is needed because the PEBB form is defined primarily by packaging considerations, thermal qualities, EMI, interconnections, interfaces, communications, sensors, control, manufacturing economics, reliability, passive devices, etc. [14]. These various concerns mature at different times, therefore feedback is needed between design and manufacture. The PEBB idea was to encompass standardization and integration. Since the resulting PEBBs were to have small size, be light in weight, have a high reliability and have easy system level configuration, soft switching topologies were needed among other requirements. A PEBB block layout is as shown in Fig. 2.5 [15]. It comprises the power supply to the module, the power switches, and the integrated control module. The integrated control module must be capable of providing the gate drive voltage to the power switches among other requirements [15].

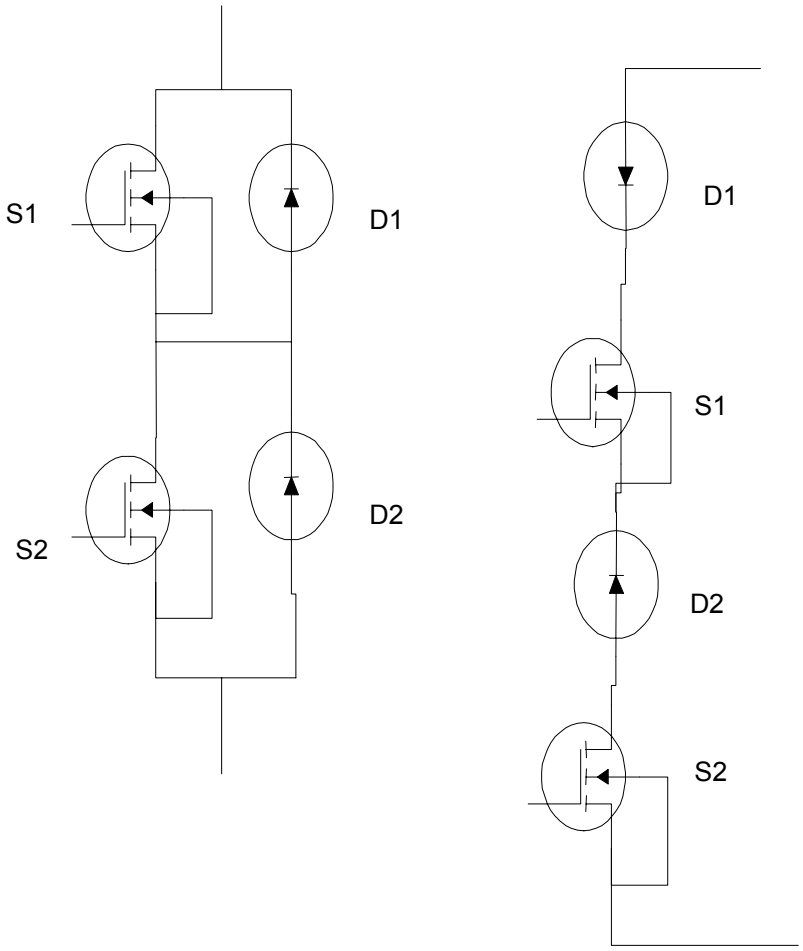


Fig. 2.2 Example of phase leg. Three terminal PEBB

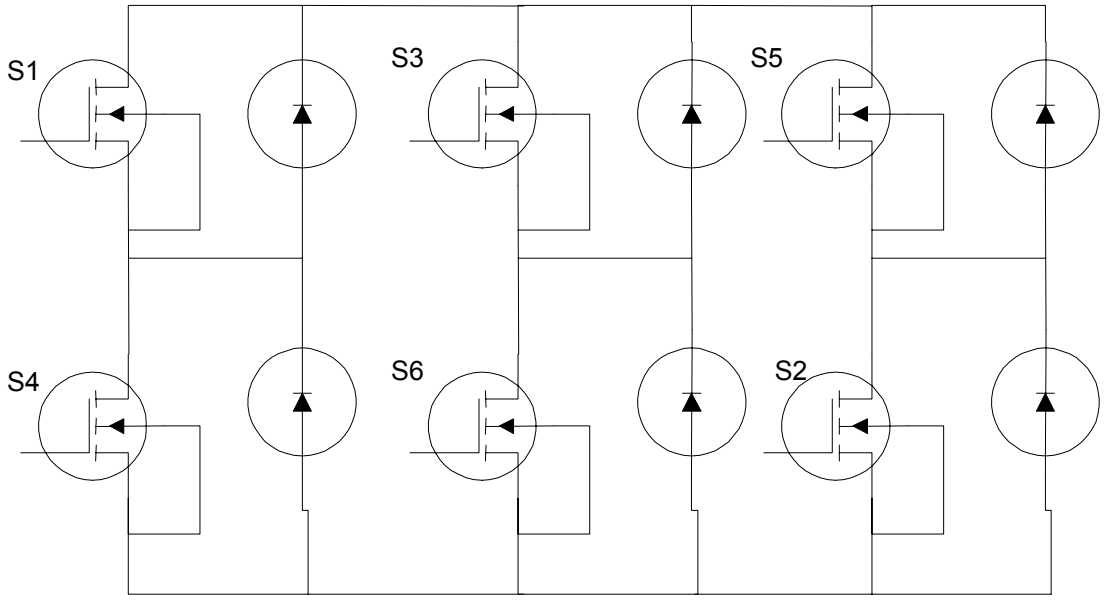


Fig. 2.3 Example of a bridge. Five terminal PEBB

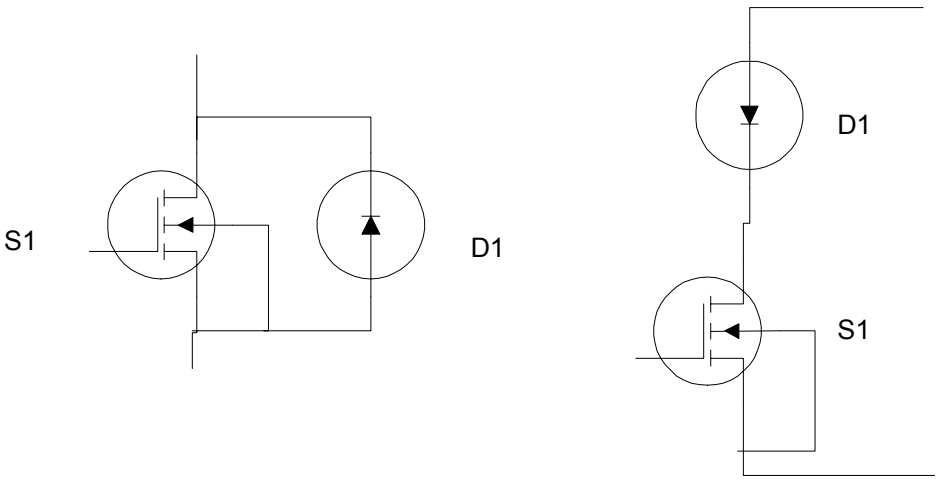


Fig. 2.4 Example of switching cell. Two terminal PEBB

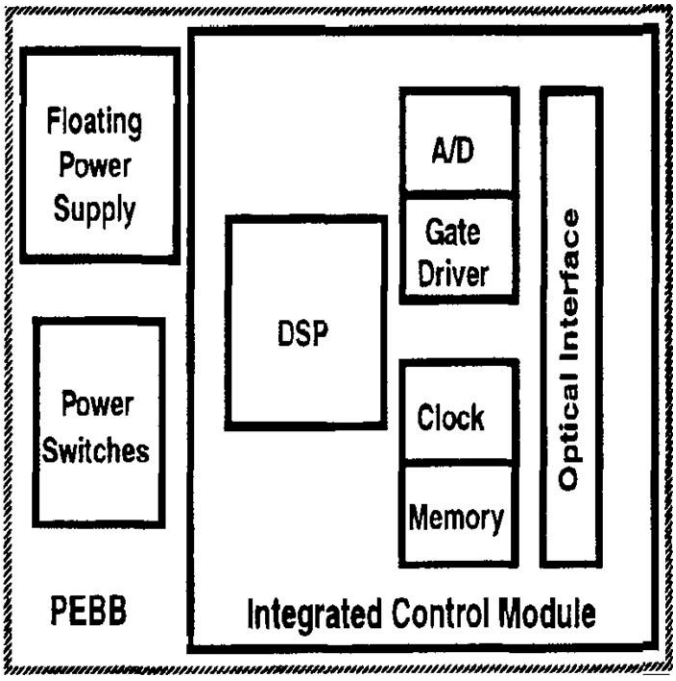


Fig. 2.5 PEBB layout [15]

The PEBB prototyping has several generations. Three generations were carried out within a space of several years, which started in the early 1990s. Each generation underwent the definition, development and demonstration phases [16]. Prevailing concerns during the first generation of PEBBs were PEBB functions, circuit topologies, and the universal controller. For the next generation of PEBBs, the focus was in reducing the size of the PEBB components and achieving standardized interfaces and "foot prints." The last generation of PEBBs' concern was in commercial viability and full implementation [17]. The definition, development and demonstration cycle of each generation was repeated to accommodate novel technologies and improved

methodologies. It was estimated that use of PEBBs in the IPS structure will reduce the ship acquisition cost by $4.4M [16].

There are currently some limitations hindering the PEBB technology. Due to the high switching frequencies proposed for the device, the issue of electromagnetic compatibility is raised. If not properly designed, PEBB devices can produce unacceptably high level of electromagnetic disturbances known as electromagnetic interference (EMI) [15]. With high power density, thermal design becomes critical, and thermal stability of the PEBB device could be a limitation on overall performance. Parasitic parameters introduced by packaging could also be a limitation on overall performance. These could introduce high frequency ringing in the operation [15]. Another concern (in the distributed power system) is the issue of PEBBs interaction with each other. These PEBB interactions, involve issues of stability and degraded system performance [15]. There exist other mechanical and material limitations imposed by device packaging that are issues [15].

Despite all foreseen and encountered challenges, the PEBB concept is expected to revolutionize the field of power modulation, just as the microprocessor did for the field of microelectronics. PEBB's use for the IPS, however, is prompting a look at the reconfiguration phenomenon in IPS, and its stability implications.

## 2.4 PEBB–Based Integrated Shipboard Power System

The IPS entails the all electric ship concept with electric propulsion, direct current (DC) distribution, and modular technology. There are six functional groups within the

IPS family [18]. They are power generation, power distribution, power conversion, power load, energy storage and system control [18].

The power generation functional group (PGM) converts fuel into electrical power [18]. The electrical power is transferred to one or more power distribution functional elements. The power generation functional element communicates with the system control function elements only [18]. A typical PGM is the internal combustion engine (generator-ICE). The power distribution functional group (PDM) comprises elements that transfer electrical power between other functional elements [18]. The PDM only communicates with the system control function elements. The power distribution module (PDM) consists of bus duct, cables, switchgear, and fault protection equipment [18]. The power conversion function group (PCM) converts electrical power from one PDM form to another and exchanges control and information signals with the system control function group. A typical power conversion module (PCM) is the power electronics converter. The power load functional group is the consumer of the electrical power received from one or more PDMs. However, it is possible that the power load module (PLM) can supply power to one or more PDMs [18]. An example of this is the regenerative braking. The propulsion motor [18] is an example of the PLM. The PLM may exchange control and information with the system control function group and other external circuitry [18].

The energy storage functional group stores energy. It connects to the network through one or more PDMs [18]. The energy storage module (ESM) exchanges control and information signals with the system control functional elements only. An ESM may

be a stack of batteries. The system control functional group consists of the software necessary to coordinate multiple other functional elements [18]. It possesses the ability to communicate with all of the other function elements and external systems. A system control module (SCM) resides on an external distributed computer system and does not have a power interface [18]. Within a module, a number of submodules and packages exist, that are made up of components, which are formed from piece parts [18]. Within a function group, there are several modules that make up the function group. For example, there are five PGMs labeled PGM1, PGM2, PGM3, PGM4 and PGM5. A description of the IPS family is given in Table 2.1 [19]. The current IPS idea can be seen in the example test system presented in Fig. 2.6 [19]. The test system depicts the zonal DC distribution of power through the use of PCMs and electric propulsion supplied from the generator bus, at 4160Volts. Zonal power is supplied from two mains – the starboard bus and the port bus. One bus is close to deck level and the other is well below sea level. Within a zone there are intrazonal busses like the AC 450Volts bus seen in the figure and the 155Volts DC bus. Each zone is physically occurring within watertight sections of the ship, with very few connecting ducts, which preserve other zones from the damage suffered in one faulty zone.

This zonal concept is not unique to the IPS. It was first introduced for the AC distribution system in an AC radial SPS, where it was called AC ZEDS. Then it was introduced as a concept for DC distribution systems and was called DCZEDS. The DC ZEDS concept is included in IPS as the method for power distribution.

Table 2.1
IPS family of modules [19]

| Module Type | Module Designation | Description |
|---|---|---|
| Power Generation | PGM 1 | 21MW, 4160Vac, 3phase, 60Hz ICR gas turbine driven generator |
| | PGM 2 | 3.75MW, 4160Vac, 3phase, 60Hz diesel generator |
| | PGM 3 | 3MW,4160Vac, 3phase, 60Hz 501 - k34 gas turbine driven generator |
| | PGM 4 | 8MW, 4160Vac, 3phase, 60Hz diesel driven generator |
| | PGM 5 | 12MW, 4160Vac, 3phase, 60Hz diesel driven generator |
| Propulsion Motor | PMM 1 | 19MW, 150rpm, cage induction motor with power converter |
| | PMM 2 | 38MW, 150rpm, cage induction motor with power converter |
| | PMM 3 | 38MW, 150rpm, tandem cage induction motor with power converter |
| | PMM 4 | 800KW, 360rpm, auxiliary propulsion, retractable and azimuthing |
| | PMM 5 | 52MW, 150rpm, cage induction motor with power converter |
| | PMM 6 | 12MW, 150rpm, cage induction motor with power converter |
| | PMM 7 | 28MW, 150rpm, cage induction motor with power converter |
| | PMM 8 | 1400KW, 360rpm, auxiliary propulsion, retractable and azimuthing |
| Power Distribution | PDM 1 | 4160Vac, 3phase, 60Hz switchgear and cable |
| | PDM 2 | 1000Vdc ship service cable |
| Power Conversion | PCM 1 | Multi - Ship Service Converter Modules, 1000Vdc to 775Vdc |
| | PCM 2 | Multi - Ship Service Inverter Modules 775Vdc to 450Vac, 3phase, 60 or 400Hz |
| | PCM 3 | Multi - Ship Service Converter Modules 775Vdc to 155Vdc or 270Vdc |
| | PCM 4 | Ship Service Converter Module 4160Vac, 3phase, 60Hz to 1000Vdc |
| Power Control | PCON 1 | IPS system level supervisory control software |
| | PCON 2 | Zonal level supervisory control software |
| Energy Storage | ESM 1 | Ship Service, 1000Vdc |
| | ESM 2 | Ship Service, 775Vdc |
| Platform Load | PLM 1 | Uncontrolled 450Vac ship service loads |
| | PLM 2 | Controlled 450Vac ship service loads |
| | PLM 3 | Uncontrolled 155Vdc or 270Vdc ship service loads |
| | PLM 4 | Controlled 155Vdc or 270Vdc ship service loads |

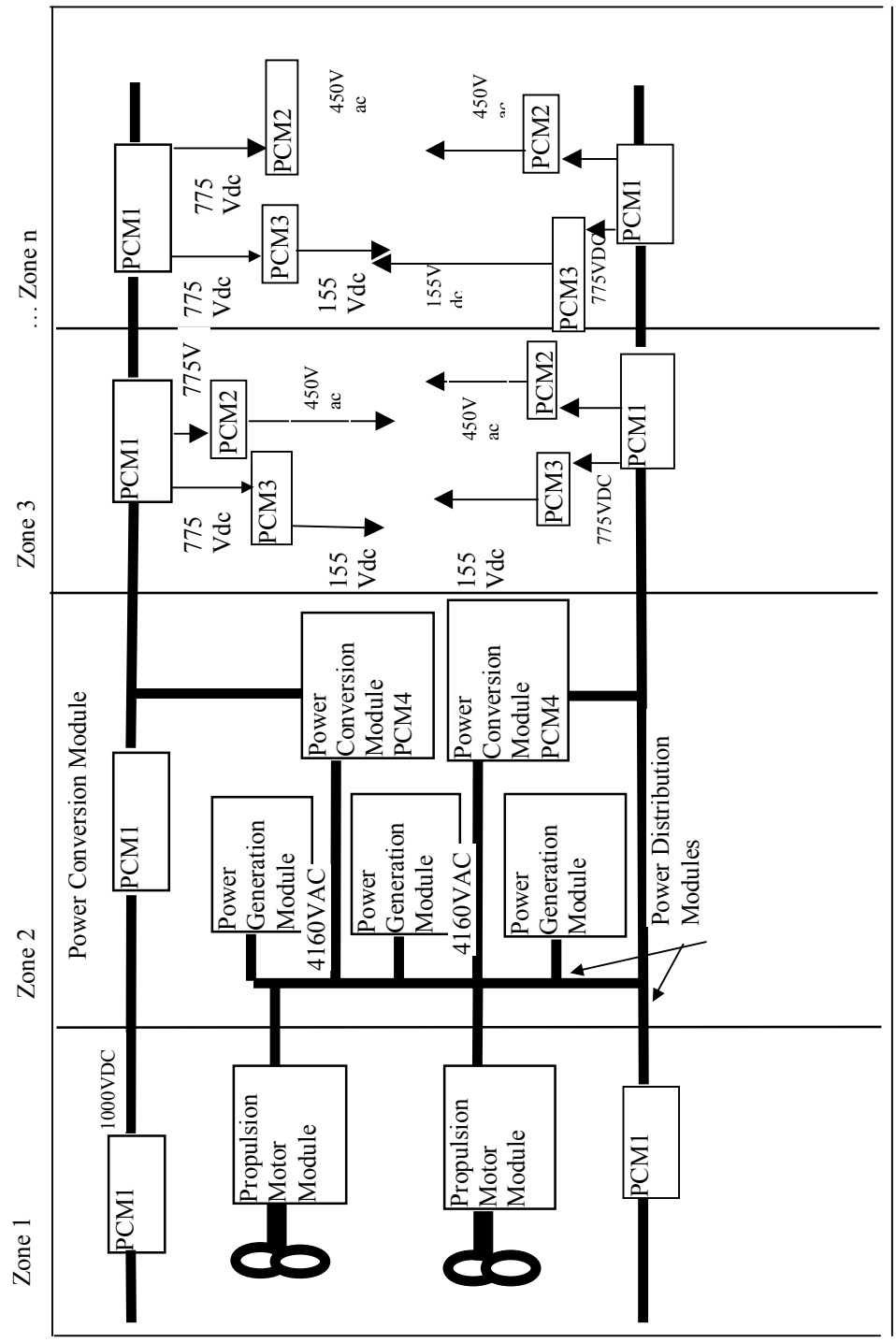


Fig. 2.6 Example of IPS

System studies of multi-converter systems have received attention in the literature. As mentioned in chapter I, a motivation for this work was obtained from the importance with which the Navy regards the IPS system and their intention to use the IPS for their new destroyer. This intention was communicated to scientists by a newsletter email on January 6, of 2000, from a Department of Defense under secretary [20]. This multi-converter system is, therefore, decidedly a new problem. As such, no literature discusses present status of reconfiguration in it – PEBB-based integrated shipboard power system. However, relevant concepts and similar issues have been addressed under system issues from PEBB use [2-10]. The concept of reconfiguration will first be addressed then, system issues from PEBB-based integrated shipboard power system will be addressed.

## 2.5 Reconfiguration

The Navy designers have subdivided reconfiguration phenomenon into three categories; static reconfiguration, mission reconfiguration, and dynamic reconfiguration. Static reconfiguration implies the design of the actual shipboard power architecture, but it also includes platform performance upgrades by means of software and open architecture based equipment upgrades [21]. Mission reconfiguration refers to a change in platform state in response to varying readiness conditions such as, cruise, on-station, anchor, and battle. [21]. Dynamic reconfiguration is a platform response to assure power to vital loads during damage or failure [21]. It is commonly occurring during rapidly

changing conditions such as battle. It is the type of reconfiguration that is addressed primarily in this dissertation research. The dynamic reconfiguration activity comprises changing the status of circuit breakers between open and close, changing the position of bus transfers between normal path and alternate path, and operating the other protective devices such as the low voltage relays between the open and closed positions.

Reconfiguration term used in this dissertation refers to dynamic reconfiguration. The effects of reconfiguration become noticeable in stiffly connected finite inertia systems like the shipboard power system and the international space station (ISS) [3]. In shipboard power system, reconfiguration effects like machine (generator) dynamics, stability and system signal integrity have received little attention in current literature but stability will be dealt with in this dissertation research. The need for reconfiguration on PEBB-based integrated shipboard power systems like the IPS is due to the navy's survivability requirement, changing mission of ships and seasonal load changes.

As a review of the concept of reconfiguration, a reconfiguration scenario arises after a fault or load change has occurred in a system. Typically, there is then some reconfiguration plan activated to bring affected vital loads back on line. A common method is incremental loading for a period of hours. Such load pick up may include black start where the generator starts to pick up load within an area without the presence of external energized circuitry. This scenario is considered desirable reconfiguration. Reconfiguration due to restoration is limited by the presence of protective devices within the system that protect against any anomalies like overloading, standing phase angles, reactive load imbalance, and so on. There is, however, a reconfiguration that takes place

when the system is in an extremis state leading to loads being shed by circuit breakers and paths to vital loads being rerouted this happens in shorter time frame and is more addressed in this dissertation.

## 2.6 System Level Issues Arising in PEBB-Based Integrated Shipboard Power Systems

Many designers of PEBB have addressed the systems issues of multi PEBB use in literature, under multi PEBB systems and multi-converter systems. Pertinent discussions are presented in this section.

Thandi [4] investigated issues arising when two or more PEBB applications are connected through their filter interfaces in a DC distribution system. It was shown that an improper input filter design could affect the stability and performance of a four-leg inverter subsystem. It was found that cascading a boost rectifier and a four-leg inverter to form a two-converter subsystem, with their intermediate filters, the system exhibits a low phase margin. This low phase margin in the system can cause oscillations on the dc bus. Three approaches were then presented to stabilize the system. They were (1) increase the filter damping, (2) increase the dc link capacitance; and (3) decrease the inverter control bandwidth.

Ye [5] presented the small signal characteristics of paralleling PEBB modules. It was explained that to obtain higher power levels and increased reliability, two or more generators with their corresponding three phase power factor correction (PFC) boost rectifiers can be used to supply the DC bus [5]. Potential integration problems were studied. An example of such problems was load-sharing characteristics of parallel

PEBBs. Expressions for the characteristic transfer functions of the two parallel three-phase PFCs with identical parameters were obtained. Compensation techniques were adopted to implement the parallel circuit in the control design. Bus impedance was identified as a significant factor in the paralleling of PFCs. It was also determined that if the parallel PFCs designed were operated independently with this bus impedance included, there was a long transient time and no load sharing occurred at all [5]. The need to utilize load-sharing mechanism was discussed with three such mechanisms presented such as (1) droop method, (2) master / slave control, and (3) master/slave control with democratic current sharing.

Insights have been gained into issues arising from multi-PEBB/multi-converter use in [6]-[9]. An issue discussed in [9] is the DC bus instability issue due to impedance overlap between source and load subsystems. Other issues regarding PEBB, IPS, and reconfiguration were gathered from [10,15,22 - 24]. A salient issue regarding PEBB that have to be addressed in their systems used, is the PEBB design and the problems affecting the PEBB design. Some of these problems affecting the PEBB design are contained in [15] and have been earlier reported.

One issue for multi-converter use found in literature, is the impedance-overlap problem. Ciezki [9] presents some findings of analysis of a multi-converter system. He discusses two criteria for determining instability in these. They are the small gains (Middlebrook's) criterion, and the opposing argument criterion. The small gains criterion is stated as (2.1).

$$\left|\frac{Zs(\omega)}{Zc(\omega)}\right| < 1 \quad for -\infty < \omega < \infty \tag{2.1}$$

Where Zs is complex source impedance (for the rectifier-generator set) and Zc is the complex converter input impedance. The opposing argument criterion is stated as (2.2).

$$\mathrm{Re}\left|\frac{Zs(\omega)}{Zc(\omega)}\right| > -1 \quad for -\infty < \omega < \infty \tag{2.2}$$

These preceding conditions must be met if there is to be a stable operating point. Ciezki [9] further postulated that given a multi-converter system as shown in Fig. 2.7 (made up of constant power loads), for stability, the relationship between the source resistance to the constant power load should be given by (2.3). Fig. 2.7 shows a multi-converter system with constant power loads represented as dependent sources, and their filter interfaces, connected to a common rectifier that is represented as a dc source and source resistance $R_s$. There are three converters connected in parallel in the figure.

$$R_s < \frac{Vs^2}{4*(P_1 + P_2 + P_3)} \tag{2.3}$$

This forms the upper bounds of the stability constraints. The lower bound is given as (2.4)

$$R_s > \sqrt{\frac{23L}{C}} \tag{2.4}$$

Where $L = L_1 = L_2 = L_3$ and $C = C_1 = C_2 = C_3$.

More effects of constant power loads in multi-converter systems were presented by [25]. Belkhayat [25] considered the concept of complete stability, which means the convergence of all trajectories of a system to an equilibrium point. Tightly regulated converters were investigated for constant power characteristics. It was reported that the impedance ratio criterion has been developed for systems with constant power loads to guarantee their stability to small disturbances [25]. However, large signal disturbance is largely unsolved. He proposed a complete stability condition. He stated that conditions under which a test system as shown in Fig. 2.7 had complete stability were if the inequalities in (2.3) and (2.4) were true. It further postulated that the lower bound could be violated to arrive at an Andronov-Hopf bifurcation where the system goes through unstable limit cycles for certain parameters of the system but that if the upper bound were violated, there would be certain loss of complete stability.

The concept of negative impedance stability is added to review of constant power load characteristics in multi-converter systems. Emadi [26] contributed some general rules for negative impedance stability within a multi-converter system – one of which is presented in (2.5).

$$P_{CPL} < P_{CVL} + \frac{R_{eq} C_{eq} V_o^2}{Leq} \tag{2.5}$$

The parameters of (2.5) are as defined in Fig. 2.8 and Fig. 2.9. The Lyapunov direct method [26] was used to produce control laws for the stabilizing controllers in the system using feedback linearization techniques.

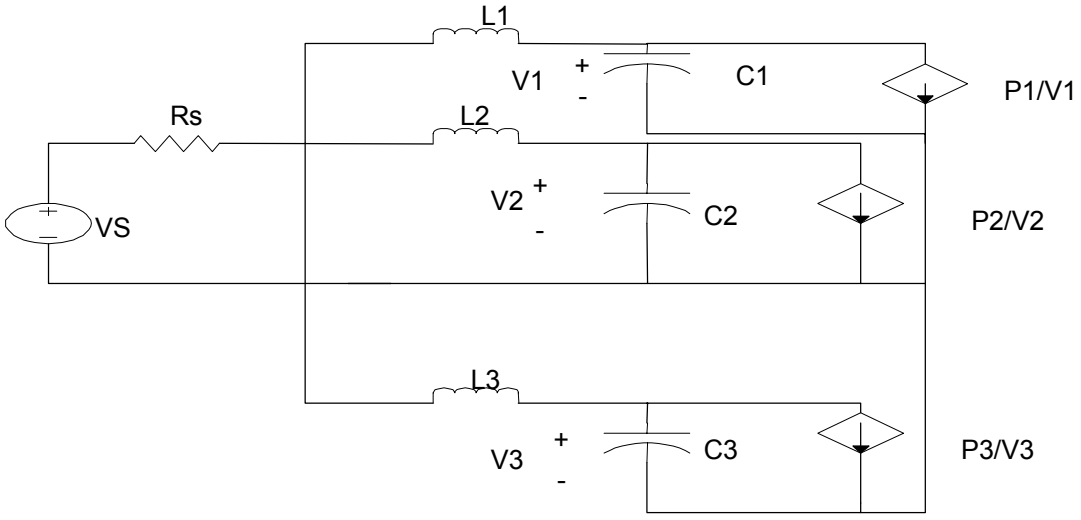


Fig. 2.7 Model of networked high bandwidth converters

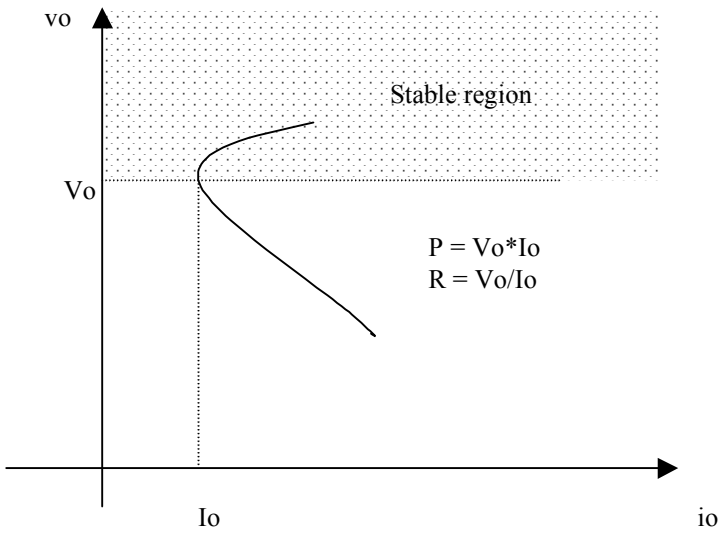


Fig. 2.8 V-I characteristic of a constant power load

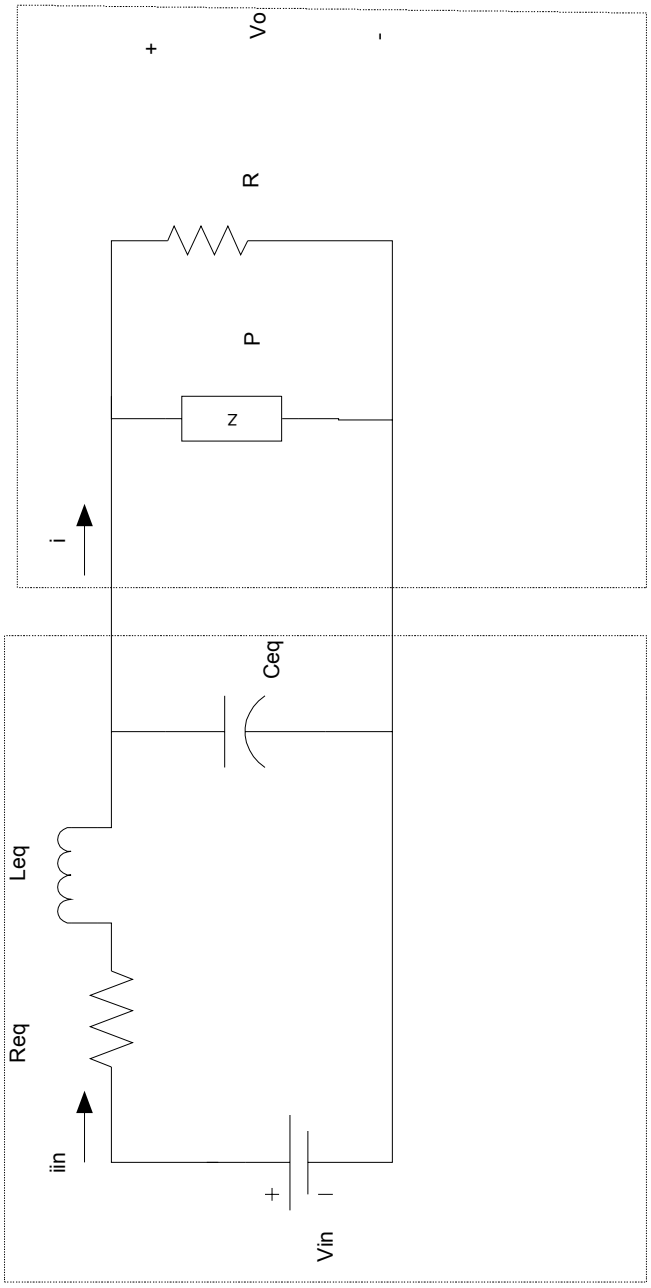


Fig. 2.9 Equivalent circuit of a DC distribution system

Zhang also investigated the PEBB-based integrated DC distributed power system, finding some problems of DC bus instability arising from nonlinear loading effects of the load subsystem. He postulated that depending on the percentage of load unbalance and nonlinearity, the peak-to-peak ripple current drawn from the DC distribution bus could be as large as 100% of the rated current [27]. This was judged unacceptable and solutions were proposed for it. The desired result of the solutions was to keep the ripple currents from entering the DC bus. To do this, an AC load conditioner was proposed to confine the ripple power within the load subsystem. DC bus conditioner was proposed as an alternative solution where the DC bus conditioner acts as an active filter and damper for the DC bus.

This literature raised some questions that were of interest in this research. It was desired to understand if unbalance loads occur frequently during reconfiguration. There was a question of if the 2ω ripple phenomenon posed a real problem for the IPS. It was wondered if there a real chance that reconfiguration could mitigate or exacerbate the 2ω power ripple effect and DC bus instability. And it was questioned, how reconfiguration was constrained by the 2ω ripple power instability.

The nonlinearity of AC/DC systems was addressed in [28]-[30]. Sudhoff [28] made an argument for a new stability criterion that is less conservative than traditional circle theory, in its prediction/determination of stability. It is called the ESAC criterion. Which is similar to the gain margin and phase margin criterion but it occupies a smaller region of the s plane [28]. Sudhoff [28] also addressed the issue of nonlinear systems by

obtaining a load admittance or source impedance space in three dimensions. By trajecting through the system operating points and parameter variation, the nonlinearity of the system was claimed to be accounted for. In dealing with highly reconfigurable (uncertain) systems [29] and [30], Sudhoff advocated generating generalized admittance or source impedance space by obtaining the linear models of all expected reconfigured topologies. He proposed mapping the Nyquist contour of the load/source gains into the generated 3D impedance/admittance space, stating that the system is unstable if the contour traverses the forbidden region of the generated space.

Another method addressing the nonlinearity of AC/DC system was addressed in [31]. Huynh [31] proposed a method that decouples the system at an interface of interest into a source subsystem and a load subsystem. Fig. 2.10 depicts the decomposition. Since Z (the source subsystem impedance) and Y (the load subsystem admittance) are non-linear, the nonlinear analysis involves further decomposition of both Z and Y into linear and nonlinear parts. Any number of methods can be used to obtain the linear parts, e.g., state space representation and system identification. To compute the nonlinear part, the gain of the nonlinear parts was mapped into a conic sector {c,r} where c is the conic center and r is the conic radius. To get the conic sector (and nonlinear gain), (2.6) was used.

$$r(c) \geq \sqrt{\frac{\int_{-\infty}^{\infty} \mathrm{P}_{y-cu}(f)df}{\int_{-\infty}^{\infty} \mathrm{P}_{u}(f)df}} \approx \sqrt{\frac{\sum_i \mathrm{P}^i_{y-cu}(f_i)}{\sum_i \mathrm{P}^i_{u}(f_i)}} \tag{2.6}$$

Where r is the radius of the conic sector and $P_{(.)}$ is the power spectrum density function. $P_{y\text{-}cu}$ is the power spectrum density of the physical system's response to a large signal perturbation, which was modeled in [31] as a binary pseudorandom signal, Ip. The perturbation could be current Ip or voltage Vp. Huynh [31]-[32] developed three stability conditions, which include a composition of the linear gains, the conic radius, and the conic center. Further he introduced a concept of multiplier to reduce the conservativeness of the stability determination.

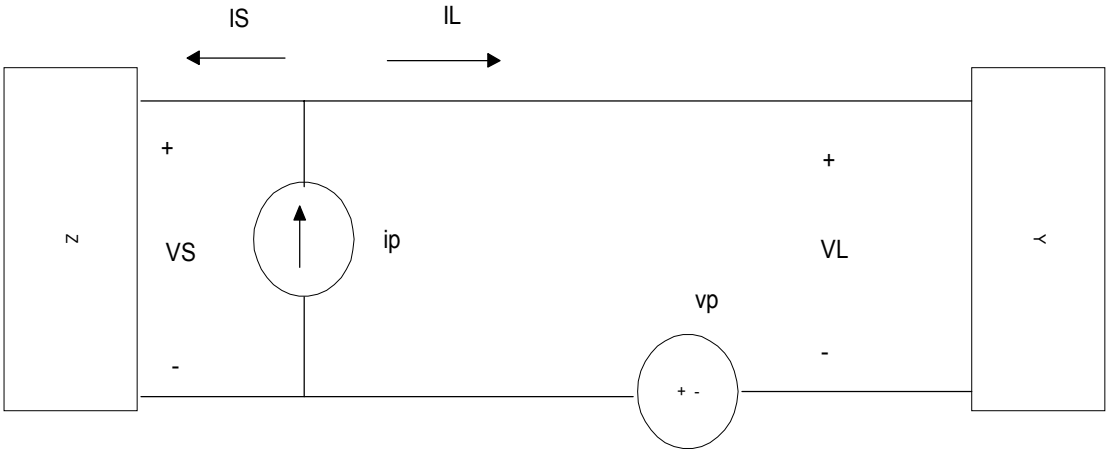


Fig. 2.10 Source and load interconnection

Further review exists for the concept of decomposition and interaction analysis, for an example, the stability analysis in Lui [33] utilizes the voltage and current perturbation at the source/load interface uniquely. He carried out online stability margins monitoring by establishing the relationships between the voltage or current perturbation to stability margin and produced some general rules for the system as shown in (2.7) and (2.8).

$$\left|i_L(j\omega)\right| < \left|i_P(j\omega)\right| \tag{2.7}$$

$$\left|\hat{v}_L(j\omega)\right| \le 2\left|v_P(j\omega)\right| \tag{2.8}$$

where $i_L$ and $v_L$ are load-side response parameters and $i_P$ and $v_P$ are perturbation parameters. He further improved the methodology by advocating permanent components (which were already in the interface) to generate the perturbation signals. The limitation of the stability analysis was that it is a small signal analysis.

While searching for key component topologies, a number of literature reviews were completed. The PCM1 topology was chosen to be the high power active bridge dc to dc converter [34-41]. DeDonker [34] has presented the chosen topology for PCM 1. That topology was the three-phase soft switched high power density DC/DC converter for high power application [34]. Its topology is as shown in Fig. 2.11. The DC/DC converter is capable of boost or buck operation. DeDonker [34] presented the DC/DC converter analysis stating that the circuit operated in soft-switched manner, which reduced EMI and switching losses for high power-density operation. The analysis in [34] produced the output voltage to input voltage, d, of (2.9) and (2.10) depending on the outlined constraints.

$$\begin{aligned} d_l &= 1 - \frac{3\phi}{2\pi} \\ for\ 0 &\le \phi \le \frac{\pi}{3} \end{aligned} \tag{2.9}$$

Where $\phi$ is AC phase shift.

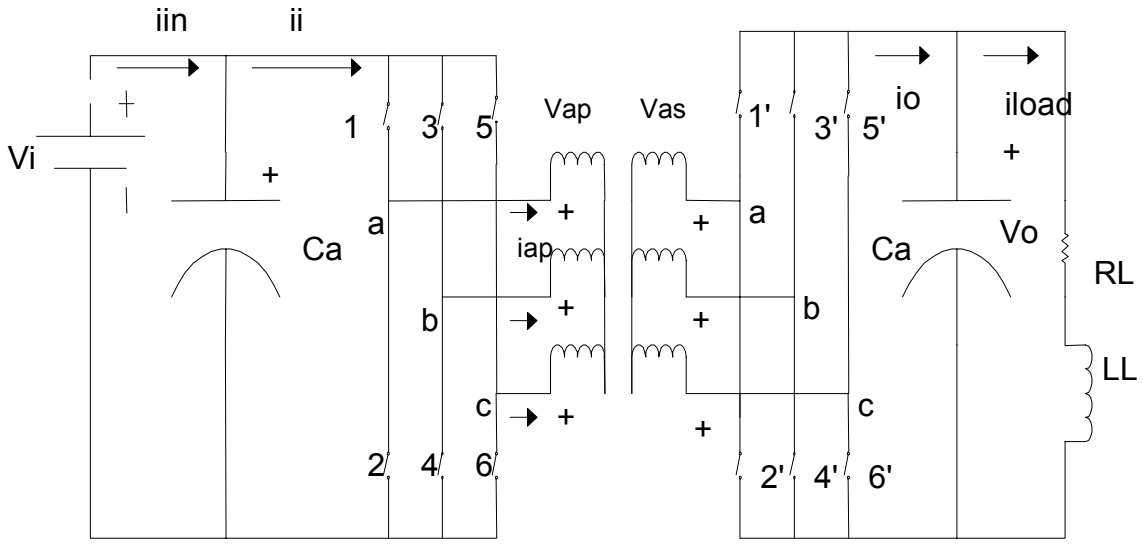


Fig. 2.11 DC/DC converter (dual bridge)

$$d_u = \frac{1}{1-\frac{3\phi}{2\pi}} \qquad for\ \frac{\pi}{3} \le \phi \le \frac{2\pi}{3} \tag{2.10}$$

Similarly, The output power relations were as (2.11) and (2.12).

$$P_o = \frac{Vi^2}{\omega L} d\phi\left[\frac{2}{3} - \frac{\phi}{2\pi}\right] \qquad for\ 0 \le \phi \le \frac{\pi}{3} \tag{2.11}$$

$$P_o = \frac{Vi^2}{\omega L} d\left[\phi - \frac{\phi^2}{\pi} - \frac{\pi}{18}\right] \qquad for\ \frac{\pi}{3} \le \phi \le \frac{2\pi}{3} \tag{2.12}$$

Where Vi = input voltage, $L = \sigma(Lm + Lsl)$, and σ is the ratio of leakage to magnetizing inductance. Lm is the sum of primary or secondary self-inductance and mutual inductance of the AC link transformer and Lsl is the secondary leakage inductance of the AC link transformer. The circuit was also said to be bi-directional.

## 2.7 Summary

This chapter presented the literature review of the research topic and discussed concepts of interest to this research. These concepts were PEBB, reconfiguration and PEBB-based integrated shipboard power system. One important point in the chapter was that there exists only a little discussion in the literature on stability studies of a PEBB – based integrated shipboard power system during reconfiguration.

Chapter III will present the dissertation problem. Details of the problem solutions will be presented

# CHAPTER III

# PROBLEM FORMULATION

## 3.1 Overview

A number of issues have been discovered in this study to be important to the issue of dynamic reconfiguration of a PEBB-based integrated shipboard power system. Six of the issues will be itemized in this chapter and receive in-depth discussion. They are: (1) high DC bus voltage spikes due to inverter - motor back-feed and capacitor switching; (2) inverter/converter control bandwidth limitations; (3) input/output impedance overlap; (4) DC bus stability; (5) cascading failure phenomenon in some paralleling schemes; and (6) DC bus overload. DC bus stability is the issue that is addressed by the work presented in this dissertation. The issue was selected because DC bus stability is a system stability issue and it investigates interaction of stable sub-units after integration. This is a relevant issue with the Navy. In this chapter the six issues will be presented and the problem to be solved will be formulated.

### 3.1.1 High DC bus voltage spikes

When drives or motor loads are taken out of service, necessary braking is done by these drives or motor loads. In this situation, there can be a rise in the DC link voltage. Typically, the DC link is connected with a dynamic braking resistor to dissipate such reverse energy or other loads in the system may use the reverse energy. However, with multiple inverters in an IPS using a common DC link, there exists the potential for a

dangerous rise in DC link voltage due to this braking phenomenon [42], [43]. The reason for the DC link voltage elevation is that when regenerative braking energy enters into the DC link, there are DC link capacitors that are charged momentarily in the form of a spike. During a mission change, there is the possibility that the motor duty factor changes cause this back-feed. This change in the duty factor is a form of reconfiguration. Another instance where DC link voltage spikes occur is when the switching in of a new load causes voltage dips that initiates regenerative braking or backfeed. This load adding is also reconfiguration. There is overvoltage when loads are shed as well. The shedding of load causes a dv/dt change on the filter capacitors causing the voltage spikes. The IPS' architecture, lends itself to this problem. It has common inter and intrazonal DC busses with a number of filter capacitors connected to them.

### 3.1.2 Inverter/converter control bandwidth limitations

Most converters/inverters are designed with large control bandwidths, to ensure their operation under varied conditions. However, the filter interface that comes with these converters is designed to operate similarly at any desired operating point. This makes for a low quality factor, Q. The quality factor Q is the measure of selectivity or sharpness of peak of resonant circuits [44]. Low Q leads to degraded DC link voltage and current, which is undesirable for military circuits. These poor power quality problems can become worse when coupled with transients caused by frequent switching (opening and closing circuit breakers) that is possible during dynamic reconfiguration. Hence, even

though this problem of bandwidth limitation is a static design problem, it can become exacerbated during reconfiguration.

### 3.1.3 Input/output impedance overlap

During static design, the designer seeks to ensure that the system is designed to a stable operating point. This includes matching the source impedance with converter impedance. However, this represents only one operating point. During reconfiguration, this operating point can be deviated from greatly (i.e., during light load and heavy load). Small signal stability, which is the stability of the system in response to small signal disturbance, ensures that the input impedance to the load subsystem is higher than the output impedance of the source subsystem for all frequencies. For a highly reconfigurable system (uncertain system), this impedance inequality cannot always be guaranteed. Impedance matching is a well-known method of ensuring the small signal stability, and impedance overlap is also a well-documented problem. The mismatching affects the filter stage by degrading its performance.

### 3.1.4 DC bus stability

With regards to DC bus stability, the requirement always is to attain a stable operating point for the system statically and dynamically. For years, power electronics engineers have achieved the former, but work is ongoing on the latter. The kind of stability of concern for reconfiguration is mostly large-scale signal stability. Large-scale signal stability is the stability of the system to large signal disturbance. Instability from

this kind of disturbance can be catastrophic in nature. One instance in which the problem of DC bus stability arises is when several converter units are interconnected to each other in a system and reconfiguration is introduced as a disturbance to the system. The controllers in the system must bring the system back to a stable operating point. It would be generally useful to assess for stability of the DC bus of the system during this closed loop phenomenon. Due to the fact that the PEBB modules immediate to the DC bus operate in close loop, any oscillations seen and fedback from this DC bus may result in the malfunction of these modules and would be catastrophic to the system. The condition can further deteriorate, as is the case in IPS, when there are many PEBBs at other busses that may become affected.

### 3.1.5 Cascading failure phenomenon

Typically, two converter/inverter units can be operated in parallel to supply multiple loads or increased power. If there is no mechanism to ensure proper sharing of power to the load, it has been observed that in such paralleling schemes, one converter draws a large part of the load power to the detriment of the other converter(s). Methods have, therefore, been developed to deal with power sharing for parallel converter units. There are four major paralleling strategies [5]-[10]. They are droop, master-slave, central limit control and frequency-based techniques. It has, however, been observed that the operation of these schemes, specifically droop and master-slave, require sensors, feedback signals and a high level of communication between several parallel units, which in the event of failure in one unit may lead to cascading failures in others. Failure

mentioned above refers to the shut down of converter/inverters due to a received control signal to that converter/inverter stipulating for the converter/inverter to shut down. In PEBB-based integrated power systems, the level of communication is expected to be very high between converter units. Therefore, there is a great potential for these cascading failures to become an intolerable problem.

### 3.1.6 DC bus overload

There is a potential for instability of the system to arise due to DC bus overload. These stability problems may include bounded oscillations and limit cycles and it is as a result of the system trying to make the DC bus supply more power than it can deliver. Normally designers match supply with load within some margin to secure stability during contingencies. However, it is not completely improbable that a situation may arise that causes the demands on the DC bus to exceed specification. The likelihood of the DC bus overload scenario occurring is highest during battle casualty when the shipboard system is performing reconfiguration in response to battle damage to the SPS. The system may be required to continue to survive in the presence of finite impedance faults. Considering DC bus overload may change the way reconfiguration is done and it may affect automatic reconfiguration planning and activation.

## 3.2 Research Methodology

The author of this dissertation chose to focus on the DC bus stability issue because: (1) stability is an important issue; (2) large signal Perturbation is catastrophic in nature;

(3) the sub-modules are designed stable and problem can be integration based; (4) approach by which reconfiguration relates to the problem of DC bus stability is clearly defined; and (5) there exists a sufficiently complex problem to solve in DC bus stability. The nature and causes of disturbances on the DC bus will be studied in this research work with the task being to model disturbances, representing reconfiguration actions, assess bus stability during these actions, and determine the constraints on reconfiguration in order to enhance stability.

Five tasks were performed to investigate the DC bus stability issue in PEBB-based integrated SPS: (1) define reconfiguration scenarios; (2) model accurately a scaled-down IPS to serve as a test system; (3) develop an effective methodology to study DC bus stability for PEBB-based integrated shipboard power system during dynamic reconfiguration; (4) perform analyses with the methodology on the reconfiguration scenarios; and (5) infer conclusions on the performance of a PEBB-based integrated shipboard power system for these reconfiguration actions.

### 3.2.1 Reconfiguration scenarios

Defining dynamic reconfiguration scenarios entailed determining how an IPS can be reconfigured, stating the condition of the system during reconfiguration, and incorporating all possible activities occurring during the reconfiguration of the system for that reconfiguration scenario

### 3.2.2 A scaled-down IPS model

A test system was selected that had a zone of an IPS and consisted of two major busses. They are the port bus and the starboard bus. The loads were modeled by load types available on ships with the sizes chosen to be aggregate of such loads in the system. To facilitate modeling of test system, each component in the system was modeled by state space representation with the appropriate parameters of the system chosen as state variables and as algebraic equations. Some parameters were chosen as driving functions while other parameters formed derived variables. Components were connected into a network by use of common variables. For example, the derived variables of component A could become the driving functions of the next component. Each component retained its non-linearity, as such the state space matrices, in their explicit forms, were not possible. The system matrix was not independent of the state variables. The network remains solvable, however, because initial values were provided to all state variables at time, t, equals zero. In the next chapter there will be discussion about the modeling of each component in the system.

### 3.2.3 An effective methodology to study DC bus stability

A method for DC bus stability analysis for large scale AC/DC systems was developed by [31]. The method involves interaction analysis which consists of decoupling the system at the interface of interest into a stable source subsystem (Z) comprising all the upstream modules and a stable load subsystem (Y) comprising all downstream modules and investigating interactions between the two subsystems. The

subsystems (Z and Y) were further decomposed into linear and nonlinear gains [31]. System Identification was used to identify the linear gain using the ARMAX and analytical geometry (conicity) was used to identify the nonlinear effects. In using the ARMAX for the linear gain [31] utilized white noise approximation to excite his subsystem but this dissertation research used an exogenous control variable containing the reconfiguration information instead making the model used as an ARMAX.

The methodology that was developed to study DC bus stability is discussed briefly below. The baseline system was selected by determining the "average system" prior to reconfiguration. The baseline was chosen as two 9MVA generators supplying 80 percent load and 40 percent of the load respectively with no over-power protection on generator models. As such, the system can supply as high as the load and perturbation dictates, so that the protective devices required for reconfiguration were the limitation of the signal levels seen. An example of the limitation was the size of the system circuit breakers.

The system was decoupled into source and load subsystems. This is done at the test system modeling stage. The source system was assumed to serve a well behaved load (i.e. a resistive load) and the load subsystem was assumed to be supplied from ideal source (DC source). The decoupling was performed to investigate the interaction of the subsystems at the interface of interest, which is the intrazonal DC bus on the port side.

The small signal behavior of baseline subsystems was determined by perturbing subsystems with small perturbation and recording interface voltages and currents. This was done to generate data for the ARMAX program. The data generated from the source

subsystem had current as the input data and the output data as the voltage, while the data generated from the load subsystem had voltage as input data and current as output data.

Linear transfer functions were obtained from the ARMAX identification parameter results. The output of the ARMAX identification program was the coefficients of the difference equation describing the source and load subsystems.

Effects of reconfiguration on subsystems were determined and reflected in perturbation models. The perturbed signals within the DC circuit were the voltage and current. Within the AC circuit comprised of the generator, the perturbed signals can be frequency in addition to voltage and current. The perturbed signals were changed from pre-reconfiguration value to post-reconfiguration value. The change was modulated by the differential equations describing the component to which the perturbation was attached. This produced the desired intermediate trajectory. Error analysis was carried out to ascertain how closely the perturbation model signals resembled those of the actual reconfiguration activity. More details on error analysis will be given in Chapter IV.

The subsystems were perturbed with large signal perturbation models and the conic sector parameters were obtained. The perturbation model was applied to selected components and/or interfaces in the subsystems and the DC bus signals were recorded. Based on Huynh [31]-[32], the large signal perturbation effects on the system were represented by conic sector. The conic center and radius fully describes the sector. To obtain the inputs to the computation of the conic sector the input data of the subsystems were fed into the system identification program and the output of the linear part was generated. The output of the linear part formed the input to the conic sector

determination through the multiplier section, which generated the conic sector parameters.

Stability conditions shown in (3.1) were applied to obtained graphical results and checked if forbidden region was traversed. With the linear transfer functions and the conic sector parameters, the stability conditions [32] below were computed and forbidden regions were drawn for conditions 1 and 2 according to the following rules with c and r as shown in (3.2).

$$\delta_z \equiv 1 - \left| \frac{T(s)c_y}{1 + c_z T(s) c_y} \right| r_z > 0$$

$$\delta_y \equiv 1 - \left| \frac{T(s)c_z}{1 + c_z T(s) c_y} \right| r_y > 0$$

$$G \equiv \frac{\delta_z \delta_y}{r_y r_z} - \left| \frac{T(s)}{\left[1 + c_z c_y T(s)\right]^2} \right| > 0 \qquad (3.1)$$

$T(s) = L_z L_y$ product of source and load linear gains

$\{c, r\}$ Center and radius of the conic sector

$$b = c + r$$
$$a = c - r \qquad (3.2)$$

if a>0 The Nyquist must avoid the disc with points -1/a and -1/b on the real axis

if a =0 The Nyquist must stay to the right of the vertical line passing through -1/b

if a<0 The Nyquist plot must stay inside the disc that intersects the real axis at -1/b and -1/a

3.2.4 Analysis of the methodology on the reconfiguration scenarios

A total of nine cases were run utilizing the methodology and designing the reconfiguration scenarios. The reconfiguration scenarios were staged at a definite time in the simulation and the stability assessments were done visually and through the methodology. Data generated from the methodology stability assessments were further analyzed for merits of the performance of the test IPS. Further theory used in the methodology and the staging of scenarios on a scaled-down IPS are contained in Chapters IV and V.

### 3.2.5 Conclusions on the performance of a PEBB-based shipboard power system during reconfiguration

Based on stability assessment, the determination of DC bus stability for the proposed IPS was made basing the judgment on quantitative indices like scenario stability (number of cases unstable), stability margin, error analysis and stability sensitivity. A catalog of the system stability analyses will be presented in Chapter VI.

## 3.3 Summary

This chapter included discussion of issues arising from reconfiguration of an IPS with focus on DC bus stability. The problem to be solved was selected as being DC bus stability of PEBB-based integrated SPS during reconfiguration. The salient point was the discussion of the methodology used to solve the problem. It was a multi-step methodology, which does not make the limiting assumptions of linearization or small signal.

The next chapter discusses the analyses mentioned in Chapter III. These are modeling analysis and reconfiguration methodology details. There will be methodology analysis to present the details involved in conducting the stability assessment.

# CHAPTER IV

# SCALED-DOWN IPS MODELING AND ANALYSIS METHODOLOGY

## 4.1 Overview

Modeling was the first step of the analysis for this work. The strategy of the system modeling was to model each component in the system with state space representation. Each component was described using differential and algebraic equations. Each component used state variables, driving functions and derived variables. The network was formed by passing the derived variables of one component to become the driving function of the next component, or through use of common state variables. The network was made into two function blocks with the starboard bus function block embedded in the function block of the port bus. Source and load subsystems were decoupled on the port intrazonal bus in one system and at the port interzonal bus in another system. The starboard bus was linked to the load subsystem of the port bus through the bus transfer switch located in front of the dynamic load and the starboard was also linked to the source subsystem through the ring of DC distribution at the PCM4 output. More on the connectivity is reported in section 4.2.

Methodology analysis is comprised of the proof that the adaptation to existing methodology was correct (Appendix A), the analysis of the error of the approximation introduced by the adaptation of the methodology, perturbation modeling, multiplier determination and stability margin determination. The stability assessment conditions used for the stability assessment were not a contribution to this work. Section 4.2 is devoted to the modeling methodology, while the DC bus stability methodology is discussed in section 4.3.

## 4.2 Test System

The connectivity of the test system shown in Fig. 4.1 is as follows: The generators (PGM) are connected to the 4160Vac bus feeding two six-pulse rectifiers through three phase transformers. The rectifiers (PCM4) are phase-controlled rectifiers with the firing angles modulated to keep the output DC voltage at no load value. The phase-controlled rectifiers each have an output voltage of 1000Vdc. The primary bus of interest is the intrazonal bus on the port bus. This bus is one component away from the phase-controlled rectifier output bus of 1000Vdc. The 1000Vdc is typically stepped down to 800Vdc value using a DC-DC converter (PCM1) but 775Vdc which was an earlier published [19] value was chosen for step down value in this work.

The 775Vdc bus supplies the load through an inverter (PCM 2) and a DC-DC converter (PCM3). The load is a dynamic load, which is specifically an induction motor, an AC static load and a static load, which is a resistor. Only static loads are put on the starboard bus for the zone of interest. There is static 450Vac load on the output of the PCM2 of the starboard bus and a resistor on the output of the PCM3 on the starboard bus. Furthermore, the starboard bus PCM2 was sized to serve the static load and the induction motor on the port bus with power in the event that the bus transfer switch operated and transferred the induction motor to the alternate path. Similarly, the port bus PCM2 also supplies the induction motor and the AC static load normally. In the test system there is a decoupling done on the port bus at the 775Vdc bus which is not done on the starboard bus. This decoupling is to help determine the interaction between the downstream of the point of decoupling with the upstream of the point of decoupling.

The functionality and the state space model of each component will be elaborated on in the following sections.

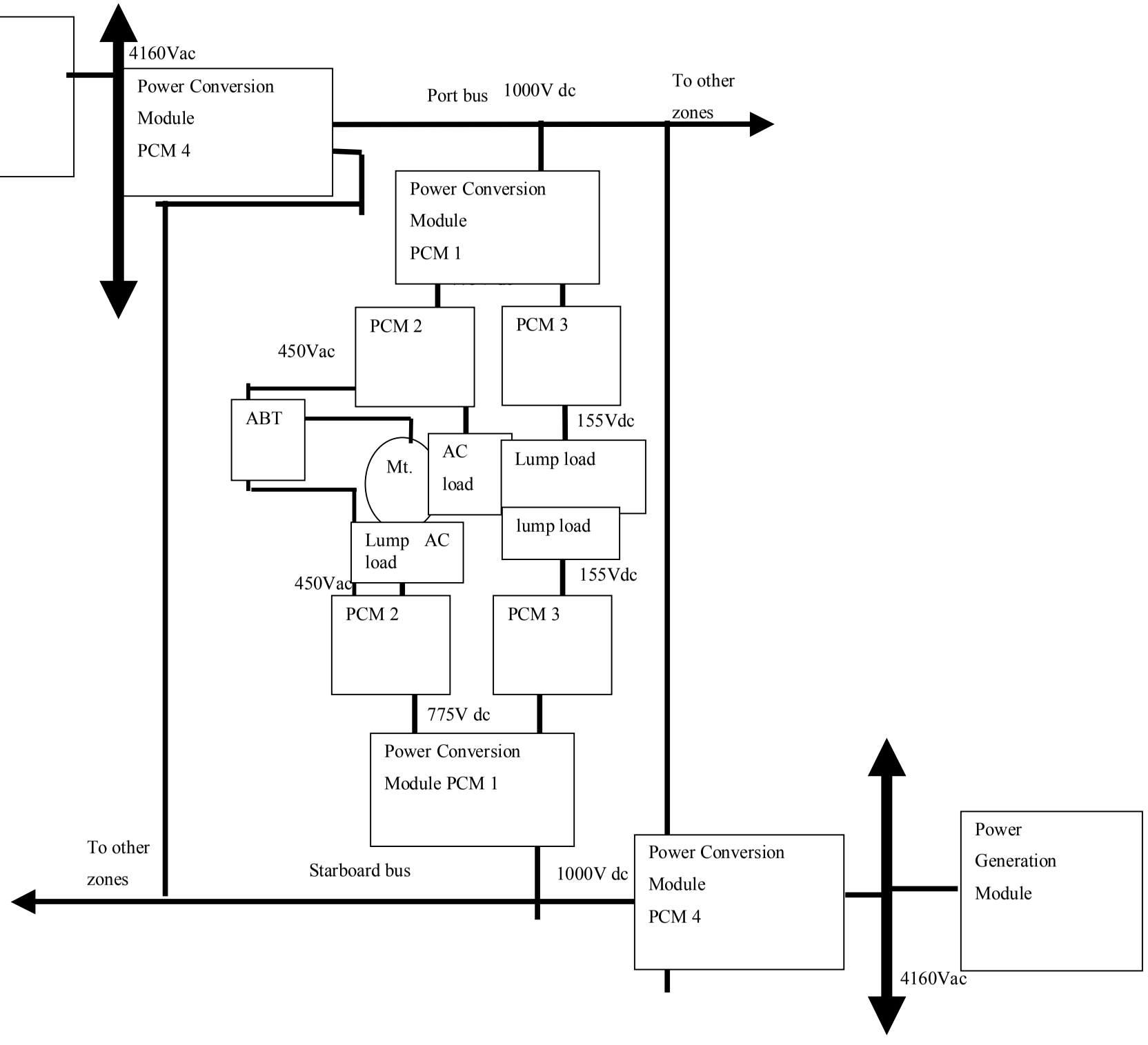


Fig. 4.1 Test system

4.2.1 IPS modules

IPS modules, PGM, PCM1, PCM2, PCM3 and PCM4, were explicitly used in the system. The use of PDM is implied but will not be discussed. The IPS modules consisted of hardware and software necessary for generation, transformation, distribution, and consumption of power. The function of PGM is generation, while transformation is the function for PCM1, PCM2, PCM3 and PCM4. In order to implement these functions and achieve high power density, which is also a characteristic of IPS, the following topologies have been chosen: for the PGM, a 9MVA, 6.9KV (l-n), 0.9PF hydro unit was used [45]. This odd choice for the PGM was made due to the availability of data for the modeling of this particular generator and its comparability in size to the desired generator. PCM1 was modeled as a dual bridge high power density DC/DC converter [34].

The PCM2 was modeled as a three phase Pulse Width Modulated (PWM) Auxiliary Resonant Commutated Pole (ARCP) inverter. PCM3 was modeled as a fixed duty cycle buck converter, which was operated in open loop. PCM4 was modeled as a three-phase phase-controlled rectifier with voltage control implemented with a proportional integral (PI) controller.

There are also some components that are not explicitly IPS modules including the induction motor load, circuit breakers, and bus transfer unit. The induction motor was modeled as a squirrel single cage motor. It has designed output power of 5 MW, a terminal voltage of 450Volts and synchronous speed of 1800 rpm. The circuit breakers are AC and DC, while the bus transfer switch had a pick up voltage of 313 Volts and a dropout voltage of 260 Volts. Filters were T section, L section, and capacitors as desired.

#### 4.2.1.1 Power Generation Module (PGM)

The PGM is a power generation module and it was designed to produce 9MVA power at 6.9kVpeak phase to neutral. The synchronous generator was modeled with currents as state variable [45]. The formulation of the differential equations was based on Anderson [45] and is well treated in literature. The machine equations are as follows in (4.1):

$$
\begin{bmatrix} v_d \\ v_F \\ 0 \\ v_q \\ 0 \\ Tm \\ 1 \\ \frac{K_r V_t}{\tau_R} \\ 0 \\ \frac{K_A(V_{REF}+V_s)}{\tau_A} \\ 0 \end{bmatrix} = -\begin{bmatrix} r & 0 & 0 & \omega L_q & \omega k M_Q & 0 & 0 & 0 & 0 & 0 & 0 \\ 0 & r_F & 0 & 0 & 0 & 0 & 0 & 0 & 0 & 0 & 0 \\ 0 & 0 & r_D & 0 & 0 & 0 & 0 & 0 & 0 & 0 & 0 \\ -\omega L_d & -\omega k M_F & \omega k M_D & r & 0 & 0 & 0 & 0 & 0 & 0 & 0 \\ 0 & 0 & 0 & 0 & r_Q & 0 & 0 & 0 & 0 & 0 & 0 \\ \frac{-L_d i_q}{3} & \frac{-k M_F i_q}{3} & \frac{-k M_D i_q}{3} & \frac{L_q i_d}{3} & \frac{k M_Q i_d}{3} & -D & 0 & 0 & 0 & 0 & 0 \\ 0 & 0 & 0 & 0 & 0 & -1 & 0 & 0 & 0 & 0 & 0 \\ 0 & 0 & 0 & 0 & 0 & 0 & 0 & \frac{-1}{\tau_R} & 0 & 0 & 0 \\ 0 & 0 & 0 & 0 & 0 & 0 & 0 & 0 & \frac{-1}{\tau_F} & \frac{\omega_R k_F}{\tau_F \tau_E} & \frac{-\omega_R k_F (S_E^{'}+k_E)}{\tau_F \tau_E} \\ 0 & 0 & 0 & 0 & 0 & 0 & 0 & \frac{-k_A}{\tau_A} & \frac{-k_A}{\tau_A} & \frac{-1}{\tau_A} & 0 \\ 0 & 0 & 0 & 0 & 0 & 0 & 0 & 0 & 0 & \frac{1}{\tau_E} & \frac{-(S_E^{'}+k_E)}{\tau_E} \end{bmatrix} \begin{bmatrix} i_d \\ i_f \\ i_D \\ i_q \\ i_Q \\ \omega \\ \delta \\ V_1 \\ V_3 \\ V_R \\ E_{FD} \end{bmatrix}
$$

$$
- \begin{bmatrix} L_d & kM_F & kM_D & 0 & 0 & 0 & 0 & 0 & 0 & 0 & 0 \\ kM_F & L_F & M_R & 0 & 0 & 0 & 0 & 0 & 0 & 0 & 0 \\ kM_D & M_R & L_D & 0 & 0 & 0 & 0 & 0 & 0 & 0 & 0 \\ 0 & 0 & 0 & L_q & kM_Q & 0 & 0 & 0 & 0 & 0 & 0 \\ 0 & 0 & 0 & kM_Q & L_Q & 0 & 0 & 0 & 0 & 0 & 0 \\ 0 & 0 & 0 & 0 & 0 & -\tau_j & 0 & 0 & 0 & 0 & 0 \\ 0 & 0 & 0 & 0 & 0 & 0 & 1 & 0 & 0 & 0 & 0 \\ 0 & 0 & 0 & 0 & 0 & 0 & 0 & -1 & 0 & 0 & 0 \\ 0 & 0 & 0 & 0 & 0 & 0 & 0 & 0 & -1 & 0 & 0 \\ 0 & 0 & 0 & 0 & 0 & 0 & 0 & 0 & 0 & -1 & 0 \\ 0 & 0 & 0 & 0 & 0 & & 0 & 0 & 0 & 0 & -1 \end{bmatrix} \begin{bmatrix} \dot{i}_d \\ \dot{i}_f \\ \dot{i}_D \\ \dot{i}_q \\ \dot{i}_Q \\ \dot{\omega} \\ \dot{\delta} \\ \dot{V}_1 \\ \dot{V}_3 \\ \dot{V}_R \\ \dot{E}_{FD} \end{bmatrix} \qquad (4.1)
$$

The exciter equation feeds back a state variable EFD to a driving function vF and (4.2) shows the expression. Similarly the terminal voltage Vt is used in the exciter driving functions.

$$v_F = \frac{\sqrt{3}E_{FD}r_F}{L_{AD}} \tag{4.2}$$

The governor equation supplies the Torque value to the generator depending on the values of the $i_d$, $i_q$, and ω and is as shown in (4.3).

$$Tm = \tau_j \dot{\omega} + \frac{1}{3} i_q (L_d i_d + M_F i_f + M_D i_D) - \frac{1}{3} i_d (L_q i_q + M_Q i_Q) + D\omega \tag{4.3}$$

The k factor in (4.1) is omitted in (4.3) because the base of the per unit expressions have been chosen as manufacturer's not as Anderson's [45]. In (4.1) the k factor was taken as 1. It can be seen in (4.3) that no power limiters have been incorporated in the governor. This is consistent with the presentation in Chapter III where it was stated that the circuit breakers and the bus transfer were the only limitation to the power in the circuit. The definitions of the variables are as follows: Vd, Vq, id, vf, if, iq, iD, iQ, w, δ, V1, Vs, V3, VR, EFD, and Tm are machine variables while Ld, Lq, LF, LD, LQ, rQ, rF, rD, r, MF, MQ, MR, MD, and LAD are machine parameters. Additional parameters for the exciter and the speed governor are KA, KE, KR, τA, τE, τj, τR, τF, and D.

4.2.1.2 Power Conversion Module 4 (PCM4)

The PCM4 was a six-pulse phase controlled rectifier bridge. It converts AC power to DC power. The circuit diagram of the module is as shown in Fig 4.2. The following simplifying assumptions have been made: (1) in order that instantaneous switching and harmonic instability can be ignored the average model equations have been used; (2) and, since there is a controller designed for the rectifier, which operates on voltage control, the effects of AC line inductance (Ls) has been ignored. The very simple main transformation equation therefore becomes as shown in (4.4).

$$Vo = 1.35 V_{LL} \cos(\alpha) \tag{4.4}$$

Vo is the voltage-connecting rectifier to the rest of the DC circuit, whereas VLL is the AC line RMS voltage. $\alpha$ is the firing angle for the bridge.

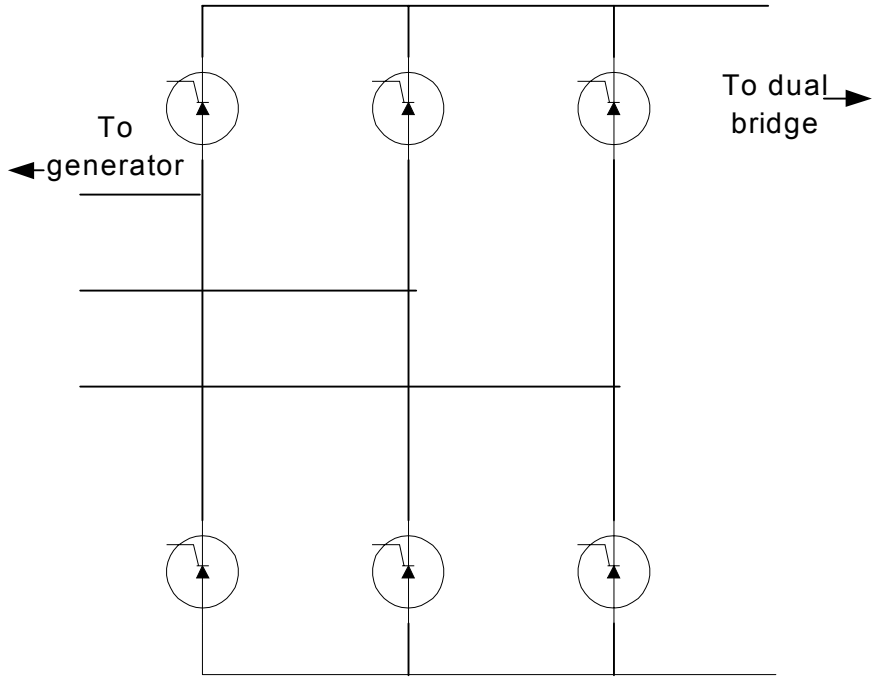


Fig. 4.2 Rectifier bridge (PCM4)

The rectifier voltage controller is shown in Fig. 4.3, and it represents a typical Proportional Integral controller with DC link voltage fed back from the power circuit. The proportional gain, K1, is not a simple constant, but is dependent on the controller output α as shown in (4.5). The derivation of the gain K1 is as follows; in order to obtain a relation ship between alpha and the output voltage, make α subject of formula in (4.4) and obtain that $\dot{\alpha}$ is directly proportional to derivative of output voltage through K1, which integrating gives α.

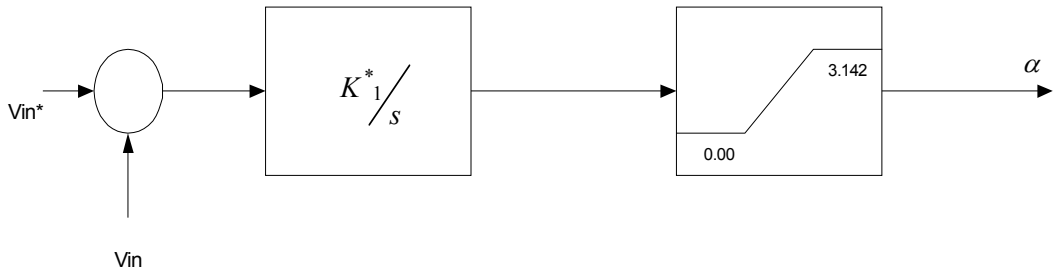


Fig. 4.3 Rectifier voltage controller block diagram

$V_{in}$ is the DC link voltage of the rectifier and α is the firing angle of the phase controlled bridge, with the actual firing angles of the phase legs set at 0, 120, 240 degrees phase shifted from each other, with phase A as reference.

$$K_1^* = \frac{-8.4}{1.35V_{LL}\sqrt{0.5 - 0.5\left|\cos 2(\alpha)\right|}} \tag{4.5}$$

4.2.1.2.1 Power Conversion Module 4 (PCM4) design example

The output specifications for the rectifier are:

$V_{out} = 1000Vdc$
$I_{out} = \text{Full load}$

Input Specifications are

$V_{LL} = 4160VAacRMS$
$I_{in} = ?$

Need to find Iin and α which, is the firing angle for full load and its controller relationship to the power circuit.

$P_{out} = 9MVA$ or 9MW @ unity power factor

$\text{Vout} = 1000\text{V dc}$

$\therefore \text{I}_{\text{out}} = 9000A \text{ dc}$

$\text{Vout} = 1.35\,\text{V}_{\text{LL}}\cos(\alpha)$

$1000 = 4160 * 1.35 * \cos(\alpha)$

$\alpha = 79.75^{\circ}$

$P_{out} = P_{in}$

$\sqrt{3} * V_{LL} I_{in} = P_{in} = 9e6$

$I_{in} = 1249.1AacRMS$

$V_{out} = 1.35 * V_{LL}\cos(\alpha)$

$$\cos(\alpha) = \frac{V_{out}}{1.35V_{LL}}$$

$$\alpha = \cos^{-1}\left(\frac{V_{out}}{1.35V_{LL}}\right)$$

$$d\alpha = -\frac{1}{\sqrt{\left(1-\left(\frac{V_{out}}{1.35V_{LL}}\right)^2\right)}} * \frac{V_{out}^{'}}{1.35V_{LL}}$$

Let $\text{Vout}^{'} = k(Vout^{*} - Vout)$

$$d\alpha = \frac{-k(Vout^{*} - Vout)}{1.35V_{LL}\left(\sqrt{|0.5 - 0.5\cos(2\alpha)|}\right.}$$

*where* $\text{k} = 8.4^2$ Empirically determined

4.2.1.3 Power Conversion Module 1 (PCM1)

The PCM1 was a dual bridge converter with AC link provided by an AC transformer. Divan, et al [34]-[41] invented the topology. The DC/DC converter is suitable for high power operation [34], and it operates in soft-switched manner [34]. This converter consists of two three–phase inverter stages operating in a high frequency six-step mode and uses a three-phase symmetrical transformer as the AC link between the

bridges. The topology is as shown in Fig. 4.4 and it is capable of bi-directional power flow and buck or boost operation. The figure shown in Fig 4.4 is actually the same one shown in Fig. 2.9 for the readers convenience.

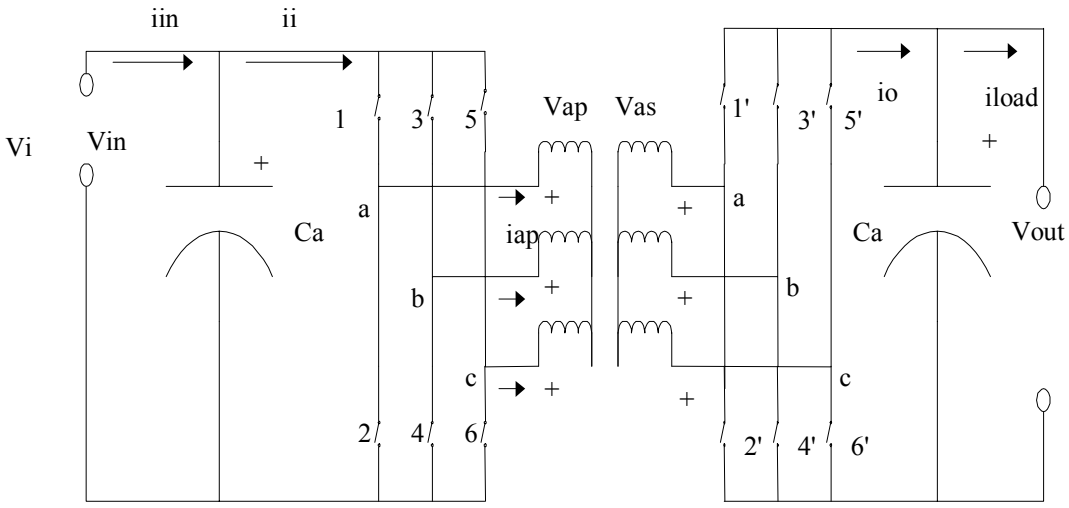


Fig. 4.4 Dual bridge converter (PCM1)

Since there existed only a limited range of operation in which soft switching could be accomplished in the above circuit, the dual bridge was allowed to operate in hard switching regions as well. The dual bridge was, however, constrained to operate in the forward power flow mode only. The equations governing that mode are as follows in (4.6) and (4.7).

$$i_{LOAD} = \frac{(Vin * d * \Psi(0.667 - \Psi/4))}{4FLN} \text{ for } \Psi \text{ between } 0 \text{ and } 0.667 \text{ rads}$$
$$i_{LOAD} = \frac{(Vin * d * (18\Psi - 9\Psi^2 - 2))}{72FLN} \text{ for } \Psi \text{ between } 0.667 \text{ and } 1.333 \text{ rads} \quad (4.6)$$

$$Vout = d * Vin \tag{4.7}$$

The abbreviations in the above equations are the following. $V_{in}$ and $V_{out}$ are as seen in Fig. 4.4; d is the duty ratio from input bridge to output bridge; F is the AC link frequency, L is the transformer leakage inductance, N is the transformer turns ratio, Ψ is ϕ/1.571 radians, and ϕ is the phase shift of the AC link. Ψ is varied by a controller to ensure that the output power is constant at a chosen d. The equations governing the controller are as follows in (4.8) and (4.9).

$$\partial\Psi = \frac{6FL(\partial ia * Vin - \partial Vin * ia)}{Vin^2} \tag{4.8}$$

$$\begin{aligned} &\text{if } \Psi < 0 \\ &\Psi = 0 \text{ and } \partial\Psi \text{ is at floor level} \\ &\text{if } \Psi > 1.333 \\ &\Psi = 1.333 \text{ and } \partial\Psi \text{ is at ceiling level} \\ &\text{else} \\ &\Psi = \text{actual and } \partial\Psi = (4.8) \end{aligned} \tag{4.9}$$

During the range, the change of mode from soft switching to hard switching occurs, and the limiters allow this change to hard switching mode to occur. For more details of the design of the dual bridge see [34 – 41].

4.2.1.4 Power Conversion Module 2 (PCM2)

The PCM2 was a DC to AC converter usually called an inverter. For The PEBB development, the auxiliary resonant comutated pole inverter (ARCP) is being considered and is chosen for modeling for this research. The ARCP is soft switching PWM inverter that uses resonant circuits to ensure zero voltage and zero current switching of all its

switches. For use in this research, the ARCP was modeled using average value models where only the average values of the waveforms are represented [46]. Calculating all of the switching times of the switches off line as a function of the load current at the instant of switching generates the gating signals for all of the semiconductor switches. Then a lookup table to load timers with the proper times to control the gating signals at the proper time is used. Fig. 4.5 shows a diagram of an ARCP phase leg. The other two phases are identical to the shown phase leg.

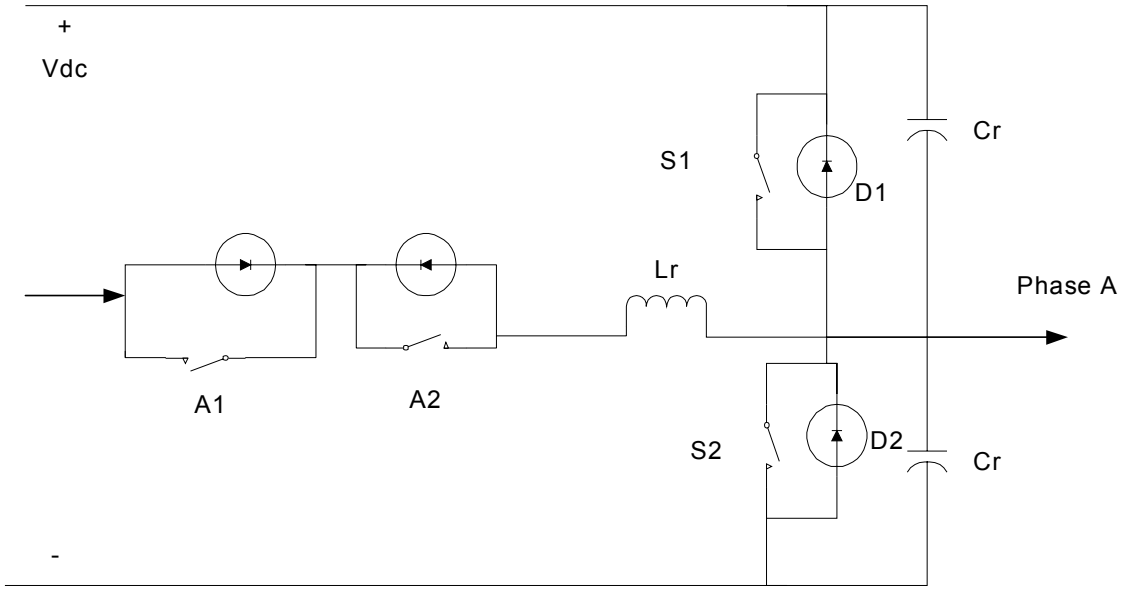


Fig. 4.5 Diagram of an ARCP phase leg (PCM2)

To generate the gating signals, the method explained above requires one sensor to measure the load AC current. This makes the ARCP current controlled to produce constant RMS voltage needed by the ARCP load. The governing operations for the ARCP follow to produce the duty cycle for the ARCP, the duration of the following

periods are determined and stored in a lookup table. They are: (1) linear charging time of the resonant circuit for both transition from high to low and from low to high ($T_{x1hl}$ and $T_{x1lh}$); (2) Resonant time for the resonant circuit for both the high to low and low to high ($T_{x2hl}$ and $T_{x2lh}$); and, (3) discharging time also for both high to low and low to high ($T_{x3hl}$ and $T_{x3lh}$). High to low transition means that phase X voltage changes from DC voltage to zero while low to high transition means the phase X voltage changes from zero volts to DC link voltage. X stands for any phase. The duty cycle modulates the peak fundamental phase to ground voltage seen at the output of the ARCP. (4.10), (4.11), (4.12), (4.13), (4.14), (4.15) [46] are the determination of the periods just presented.

$$T_{x1lh} = \begin{Bmatrix} \dfrac{2L_r(i_{db}+i_x)}{v_{dc}}; & i_x \geq 0 \\ \dfrac{2L_r i_{swb}}{vdc}; & -i_{thresh} < i_x < 0 \\ 0\ ; & i_x \leq -i_{thresh} \end{Bmatrix} \tag{4.10}$$

$$T_{x2lh} = \begin{Bmatrix} \dfrac{2}{\omega_o}\arctan\left(\dfrac{C_r\omega_o v_{dc}}{i_{db}}\right); & i_x \geq 0 \\ \dfrac{2}{\omega_o}\arctan\left(\dfrac{C_r\omega_o v_{dc}}{i_{swb}-i_x}\right); & -i_{thresh} < i_x < 0 \\ \dfrac{2C_r v_{dc}}{-i_x}; & i_x \leq -i_{thresh} \end{Bmatrix} \tag{4.11}$$

$$T_{x3lh}=\left\{\begin{array}{ll}\dfrac{2L_r i_x}{v_{dc}}+\dfrac{1}{\omega_o}\sin(\omega_o T_{x2lh})+\dfrac{2L_r(i_{db}+i_x)}{v_{dc}}\cos(\omega_o T_{x2lh}); & i_x\geq 0\\ \dfrac{2L_r i_x}{v_{dc}}+\dfrac{1}{\omega_o}\sin(\omega_o T_{x2lh})+\dfrac{2L_r i_{swb}}{v_{dc}}\cos(\omega_o T_{x2lh}); & -i_{thresh}<i_x<0\\ 0; & i_x\leq -i_{thresh}\end{array}\right\} \tag{4.12}$$

$$T_{x1hl}=\left\{\begin{array}{ll}\dfrac{2L_r(i_{db}-i_x)}{v_{dc}}; & i_x\leq 0\\ \dfrac{2L_r i_{swb}}{v_{dc}}; & 0<i_x<i_{thresh}\\ 0; & i_x\geq i_{thresh}\end{array}\right\} \tag{4.13}$$

$$T_{x2hl}=\left\{\begin{array}{ll}\dfrac{2}{\omega_o}\arctan\left(\dfrac{C_r\omega_o v_{dc}}{i_{db}}\right); & i_x\leq 0\\ \dfrac{2}{\omega_o}\arctan\left(\dfrac{C_r\omega_o v_{dc}}{i_{swb}+i_x}\right); & 0<i_x<i_{thresh}\\ \dfrac{2C_r v_{dc}}{i_x}; & i_x\geq i_{thresh}\end{array}\right\} \tag{4.14}$$

$$T_{x3hl}=\left\{\begin{array}{ll}\dfrac{-2L_r i_x}{v_{dc}}+\dfrac{1}{\omega_o}\sin(\omega_o T_{x2lh})+\dfrac{2L_r(i_{db}-i_x)}{v_{dc}}\cos(\omega_o T_{x2lh}); & i_x<0\\ \dfrac{-2L_r i_x}{v_{dc}}+\dfrac{1}{\omega_o}\sin(\omega_o T_{x2lh})+\dfrac{2L_r i_{swb}}{v_{dc}}\cos(\omega_o T_{x2lh}); & 0<i_x<i_{thresh}\\ 0; & i_x\geq i_{thresh}\end{array}\right\} \tag{4.15}$$

$I_x$ is the phase current, $I_{db}$ is the anti-parallel diode boost current, $L_r$ and $C_r$ are resonant circuit parameters as shown in Fig. 4.5. $I_{thresh}$ is the current threshold used to decide if the auxiliary circuit is required to aid in the commutation process [46]. $I_{swb}$ is a

current that indicates that there will be enough current to make the capacitor, Cr, rise to DC link voltage. $\omega_o$ is the resonant circuit frequency in radians per second, and $v_{dc}$ is DC link voltage. The average line to ground output voltage of the ARCP is related to the DC link voltage through the determined duty cycle through (4.16).

$$v_{xg} = d_{xeff} v_{dc} \tag{4.16}$$

$d_{xeff}$ is defined as (4.17) – (4.21) [46].

$$d_{xeff} = \frac{T_{sw} d_x^* - T_{x1lh} - 0.5T_{x2lh} + T_{x1hl} + 0.5T_{x2hl}}{T_{sw}} \tag{4.17}$$

$$d_{xeff\ \min} = \frac{0.5T_{x2lh} + T_{x3lh} + T_{x1hl} + 0.5T_{x2hl} + T_{su}}{T_{sw}} \tag{4.18}$$

(4.18) will be valid when (4.19) is true

$$T_{sw} d_x^* < T_{x1lh} + T_{x2lh} + T_{x3lh} + T_{su} \tag{4.19}$$

$$d_{xeff\ \max} = \frac{T_{sw} - (0.5T_{x2hl} + T_{x3hl} + T_{x1lh} + 0.5T_{x2lh} + T_{su})}{T_{sw}} \tag{4.20}$$

(4.20) is valid when (4.21) is true

$$T_{sw}(1 - d_x^*) < T_{x1hl} + T_{x2hl} + T_{x3hl} + T_{su} \tag{4.21}$$

when (4.19) is satisfied $d_{xeff}$ in (4.16) is as given in (4.18). However if the inequality in (4.21) holds then the $d_{xeff}$ in (4.16) is as given in (4.20). Otherwise the equation for $d_{xeff}$ is (4.17). $T_{sw}$ is the switching period, $T_{su}$ is the setup time for the ARCP $d_x^*$ is the duty cycle for the corresponding regular hard switched PWM inverter of the ARCP. The fundamental AC voltages of the ARCP are assumed to be produced by the ARCP for this research purpose.

4.2.1.5 Power Conversion Module 3 (PCM3)

The Buck converter was the topology chosen for the PCM3. It is a 775V DC to 155V DC converter. Assuming the circuit operates in continuous mode, the state space averaged model can be obtained by using the following analysis. A brief discussion of state space averaging is given at the end of this chapter. The Buck converter is as shown in Fig. 4.6. The analysis shown follows the model developed in [47]. The model is based on the fact that there are only two states of the circuit. The first is called the on interval and the other is the off interval. The on interval is described generally with (4.22) and (4.23), and (4.24) and (4.25) describes generally the off interval.

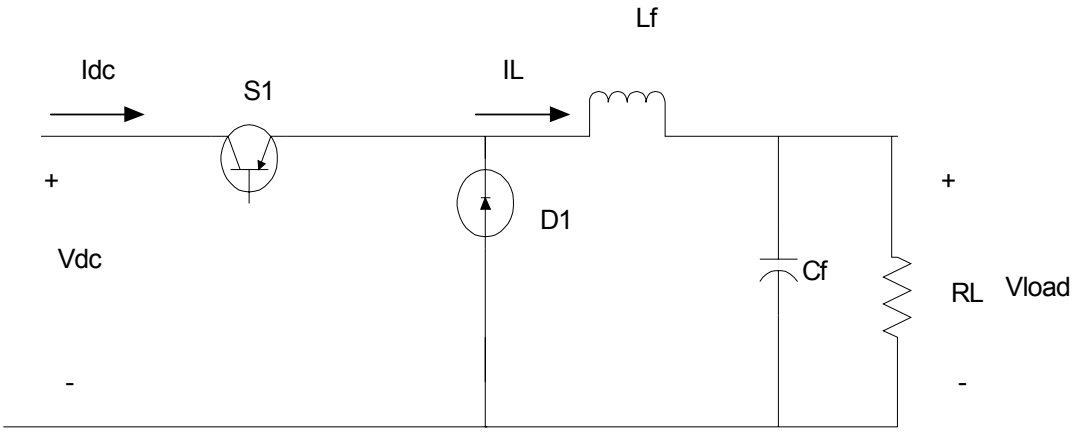


Fig. 4.6 Buck converter (PCM3)

$$\dot{x} = A_1 x + b_1 v_{dc} \tag{4.22}$$

$$y_1 = c_1^{\ T} x \tag{4.23}$$

$$\dot{x} = A_2 x + b_2 v_{dc} \tag{4.24}$$

$$y_2 = c_2{}^T x \tag{4.25}$$

A is the system matrix for the converter in both on and off interval. B is the input matrix, c is the output matrix $v_{dc}$ is the driving function as well as the input voltage as shown in Fig. 4.6. y is the derived variable. In the form that (4.22)(4.23)(4.24)(4.25) exist, the state variables are explicit in the state space equation that signifies that the system is linear time invariant system. This kind of model for the buck converter is prevalent in literature and was used in this research for this module because it is consistent with the constant duty cycle operation assumption chosen for the PCM3 module. Further details of the parameters A,b,c and x are given in (4.26) (4.27) (4.28) (4.29) (4.30) (4.31) (4.32).

$$A_1 = \begin{bmatrix} 0 & \frac{-1}{L_f} \\ \frac{1}{C} & \frac{-1}{R_L C} \end{bmatrix} \tag{4.26}$$

$$A_2 = \begin{bmatrix} 0 & \frac{-1}{L_f} \\ \frac{1}{C} & \frac{-1}{R_L C} \end{bmatrix} \tag{4.27}$$

$$b_1 = \begin{bmatrix} \frac{1}{L_f} \\ 0 \end{bmatrix} \tag{4.28}$$

$$b_2 = \begin{bmatrix} 0 \\ 0 \end{bmatrix} \tag{4.29}$$

$$c_1^T = \begin{bmatrix} 1 & 0 \end{bmatrix}$$
$$c_2^T = \begin{bmatrix} 0 & 0 \end{bmatrix} \tag{4.30}$$

$$x = \begin{bmatrix} V_{load} \\ I_L \end{bmatrix} \tag{4.31}$$

$$y = I_{dc} \tag{4.32}$$

The basic average state space description over one period, T, is obtained by combining the on and off interval as shown in (4.33) and (4.34).

$$\dot{x} = (dA_1 + d' A_2)x + (db_1 + d' b_2)v_{dc} \tag{4.33}$$

$$y = (dc_1{}^T + d' c_2{}^T)x \tag{4.34}$$

where d is the duty cycle and d' is (1-d). The buck converter is traditionally a hard-switched converter. There is, however, some variations of the general topology that can be resonant switched for zero transition capability. But these changes have not been implemented.

4.2.1.6 Motor load (PMM)

The motor selected to represent all dynamic loading in the scaled-down IPS was the single cage squirrel cage induction machine. The dynamics of the motor is represented by a set of differential equations as shown in (4.35), (4.36), and (4.37) [48].

$$\begin{bmatrix} \dot{i}_{ds} \\ \dot{i}_{qs} \\ \dot{i}_{dr} \\ \dot{i}_{qr} \end{bmatrix} = \frac{1}{L^2_{\sigma}} \left( \begin{bmatrix} L_r & 0 & -L_m & 0 \\ 0 & L_r & 0 & -L_m \\ -L_m & 0 & L_s & 0 \\ 0 & -L_m & 0 & L_s \end{bmatrix} \begin{bmatrix} v_{ds} \\ v_{qs} \\ v_{dr} \\ v_{qr} \end{bmatrix} + \begin{bmatrix} -R_s L_r & \omega_o {L_m}^2 & R_r L_m & \omega_o L_r L_m \\ -\omega_o {L_m}^2 & -R_s L_r & -\omega_o L_r L_m & R_r L_m \\ R_s L_m & -\omega_o L_s L_m & -R_r L_s & -\omega_o L_s L_m \\ \omega_o L_s L_m & R_s L_m & \omega_o L_s L_r & -R_r L_s \end{bmatrix} \begin{bmatrix} i_{ds} \\ i_{qs} \\ i_{dr} \\ i_{qr} \end{bmatrix} \right) \tag{4.35}$$

$$L_{\sigma} = \sqrt{L_s L_r - {L_m}^2} \tag{4.36}$$

$$T = \frac{2}{3} L_m (i_{qs} i_{dr} - i_{ds} i_{qr}) \tag{4.37}$$

Equation (4.37) is valid for a two-pole machine. Were the induction motor model to change from being a two-pole device the torque equation should be multiplied by P/2. The differential equations are derived in the stationary reference frame and can easily be transformed to the abc frame by the parks transformation. $\omega_o$ is the rotor speed and is assumed fixed with a slip of 3 percent. The rest of the variables in (4.35) (4.36) (4.37) are as follows L stands for inductance with the suffix s and r to signify stator or rotor quantity. Similarly, R is for resistance with the suffix s and r for stator and rotor. $L_m$ is the mutual inductance. I is for current and T is the mechanical torque.

4.2.1.7 Filters

A filter is a frequency sensitive component and is typically composed of reactive components. There are many configurations of the filter available in literature, but the following ones will be discussed in this section because they were used in this research. They are the T section filter, the L section filter, and the simple capacitor. All three filter - configurations recently mentioned are designed to be low pass filters. Figure 4.7 shows

a simple T section filter composed of two series inductors and a shunt capacitor, while Fig 4.8 shows a series inductor cascaded with a shunt capacitor to make up an L section filter.

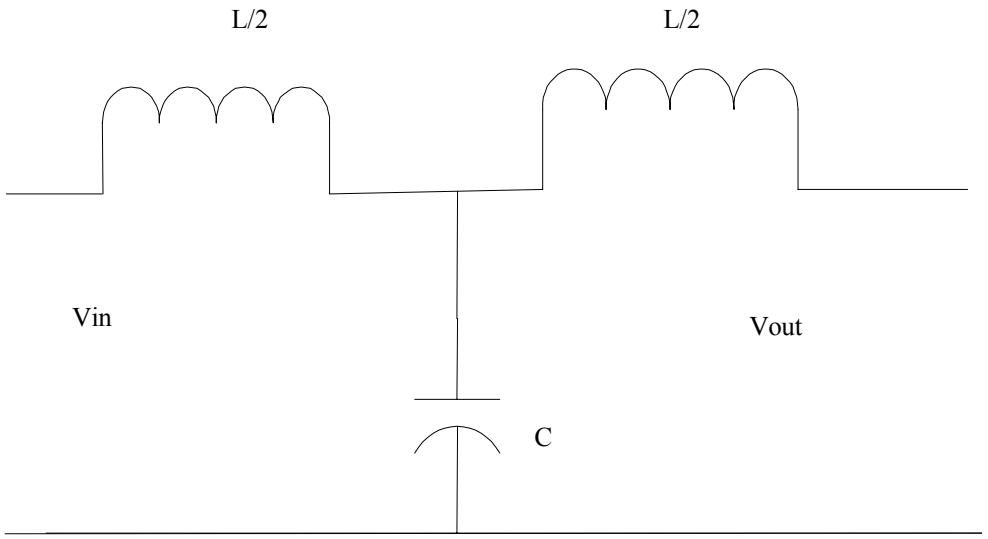


Fig. 4.7 T section filter

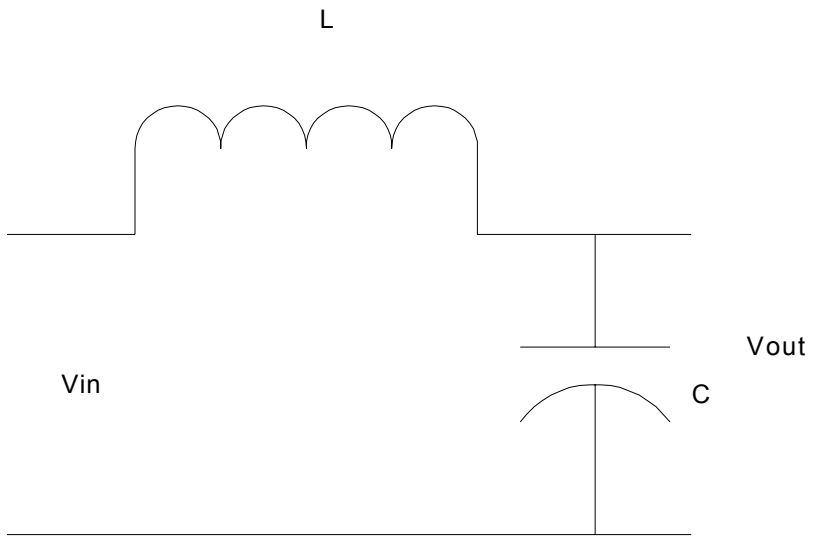


Fig. 4.8 L section filter

Due to the lack of harmonics in the models of the components used in the analysis, the true use of the filters was not made but its effect on the desired signal, which happens to be the fundamental, is investigated. The cut off frequency for the filters within the DC circuit was taken to be 1 hertz and for the AC circuit the cut off frequency was chosen to be 80hertz. The following equations in (4.38)-(4.42) make up the design of the filters [49].

The output impedance of the filter is matched to $R_o$, which is defined as (4.38) and is designed to be the input full load impedance (DC) of the circuit at the stage the filter is inserted.

$$R_o = \sqrt{\frac{L}{C}} \tag{4.38}$$

$$\begin{aligned} X_L &= 2\pi f \frac{L}{2} \quad \text{for T filter} \\ X_L &= 2\pi f L \quad \text{for L filter} \end{aligned} \tag{4.39}$$

$$\begin{aligned} Z_{OC} &= j(X_L - X_C) \\ Z_{SC} &= j(X_L - \frac{X_L X_C}{X_L - X_C}) \quad \text{for T filter} \end{aligned} \tag{4.40}$$

$$\begin{aligned} Z_{OC} &= j(X_L - X_C) \\ Z_{SC} &= j(X_L) \quad \text{for L filter} \end{aligned} \tag{4.41}$$

$$Z_o = \sqrt{Z_{OC} Z_{SC}} \tag{4.42}$$

For proper design of the filter the output impedance as described by (4.42) must be real at the frequency of interest that is chosen to be the cut off frequency. The filters

were designed as first order differential equations using the standard equations for the inductor and capacitor as shown below in (4.43).

$$v_L = L\frac{\partial i_L}{\partial t}$$
$$i_C = C\frac{\partial V_C}{\partial t} \tag{4.43}$$

4.2.1.8 Circuit breakers

The major characteristics for the circuit breaker modeled were that they protected against overcurrent, and they have no reclosure behavior. The block diagram of the operation of the circuit breaker is as shown in Fig. 4.9. The circuit breaker was modeled with its principal function being the inverse time delay. The time versus current characteristic curve of the air circuit breaker (ACB) was used as a representation of all the different types of circuit breakers that was modeled. The circuit breaker was also modeled as a function call within MATLAB. Figure 4.9 shows a block diagram of the logic steps implementing the inverse time delay function. The key feature for the circuit breaker as is implemented in the figure is the integration unit integrating the line currents flowing through the main contacts of the main switches. This charge (output of the integrator) is compared with preselect boundary values to produce a logic that opens/trips the main switches. The feed forward signal to the logic state is for the logic state to have access to the output of the maximum RMS current detector within the RMS function block for some logic design to implement the no reclosure behavior. The

behavior of the DC and the AC are distinct from each other in the inverse time characteristics within the logic state.

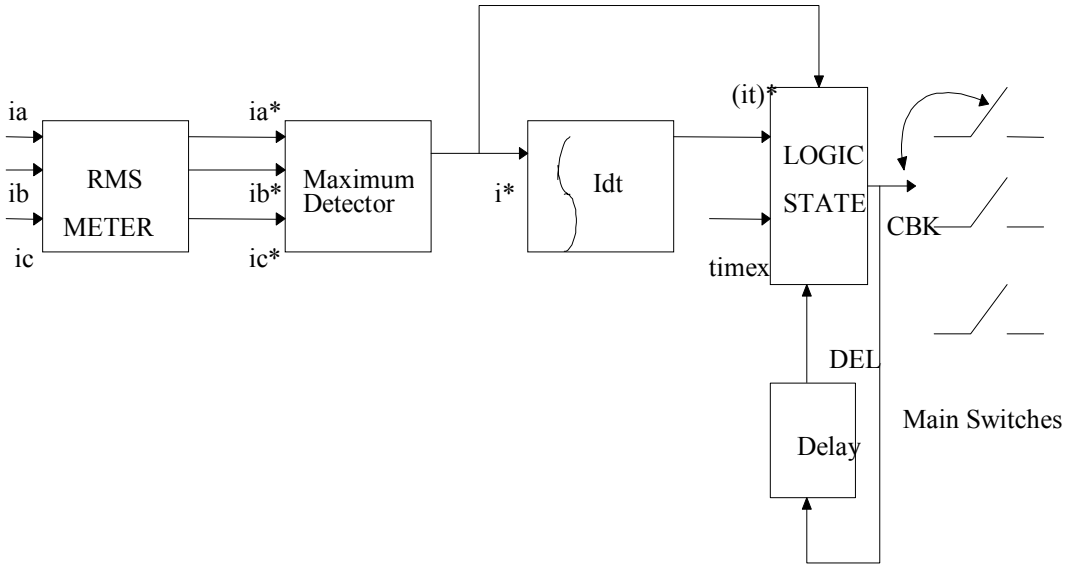


Fig. 4.9 Circuit breaker block diagram

4.2.1.9 Bus transfer unit

The bus transfer unit was modeled as an automatic bus transfer unit (ABT). There are at least nine types of ABTs listed in the military specs DOD-S-17773B. Only one of these types was modeled. The type that was modeled is ABT4A2S400D. In the mentioned model number, ABT denotes the type of component, 4 denotes 450V A.C. A denotes 60Hz, 400 denotes current rating, S denotes special features (like instantaneous tripping), and D denotes cabinet integrity [50].

The ABT is a power continuity protection device. Its operation is automatic with an option for manual operation. This device automatically selects a power source from at least two independent sources. It is designed as a normal power-seeking device, that means when normal power is lost the ABT will automatically shift to the alternate or emergency power source. However, when normal power is restored, the ABT will automatically shift back to the normal power source. The block diagram in Fig. 4.10 shows the implementation of the ABT. The ABT function is implemented as a function call in MATLAB. In the block diagram shown in the figure, the voltages on the normal path are measured and converted to RMS quantities and the minimum value is selected. This minimum value is used in a logic stage for ABT pickup and dropout. The ABT picks up at 313Volts while it drops out at 260V. For every time there is a transfer command initiated by the control logic of the ABT, there is a supplementary logic initiated to insert a transfer time of about 40 milliseconds into the operation of the ABT.

### 4.2.2 Simulation of the test IPS

To connect the described components together in a system the approach used was as follows. Command signals were propagated from generator to load with each component having its controller. The derived variables of the first component in the propagation line become the driving functions of the second component or common state variables are passed from one to the other. Individually the components were represented by a set of differential and algebraic equations.

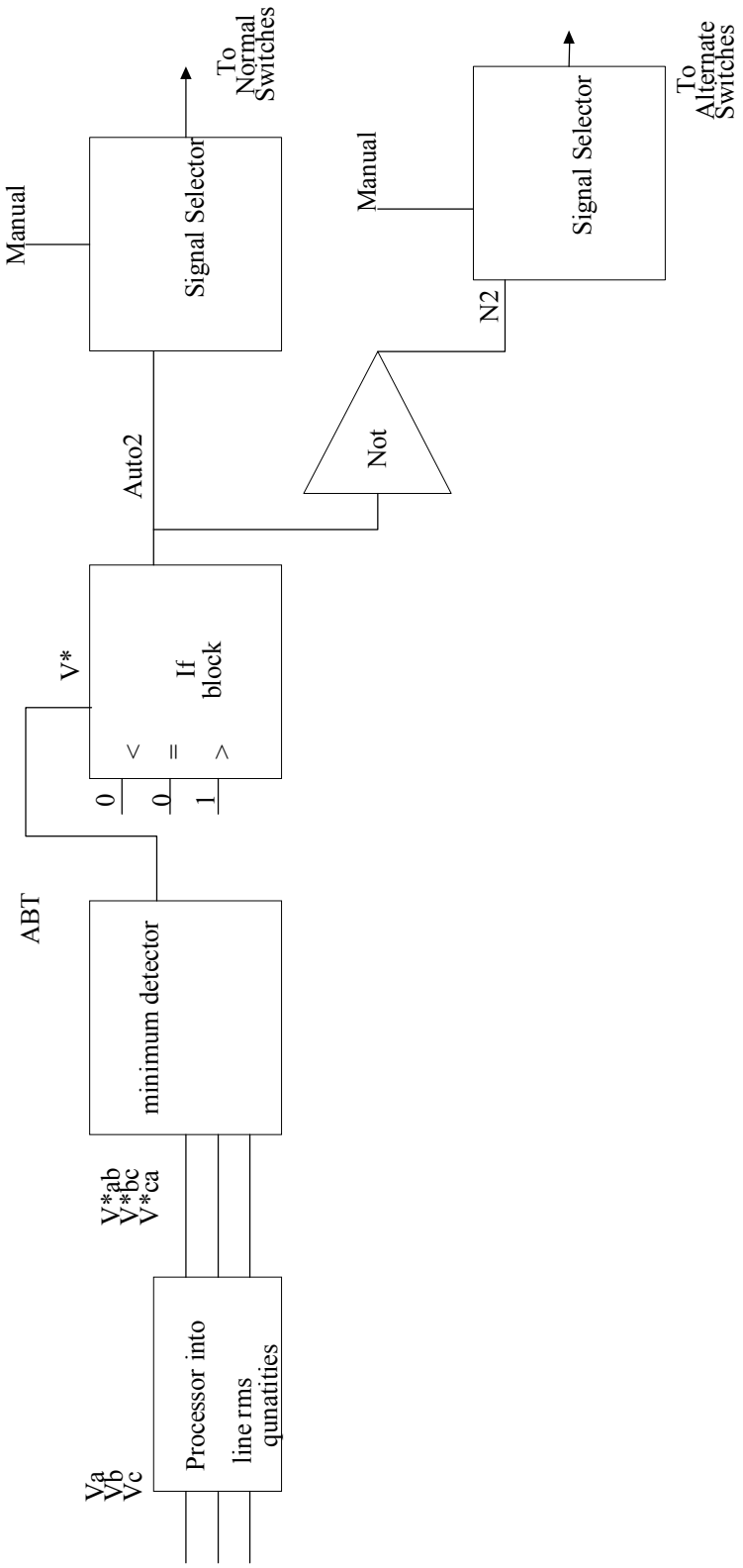


Fig. 4.10 Automatic bus transfer ABT block diagram

The differential equations were passed to the integrator to obtain the instantaneous state variables. The network itself resides within a function block within a simulink program, which is a system of multiplexers and demultiplexers to extract the state solutions of the solver outputs and the derived variables of the system (i.e. network). Common points within the network are designed by fulfilling Kirchoff's law of simple addition of currents. The solution of the state space equations were obtained by setting them as initial value problems so that the problem had only one solution and numerical means were used to obtain that solution. There are many numerical techniques for solving an initial value problem and this dissertation will not discuss them but the solver used in MATLAB for solving the differential equations of the component models was a fixed time step solver. It is called ODE 3 and is authored by Bogacki and Shampine [51], [52]. The ODE 3 is a fixed step solver and is well adapted to solving moderately stiff problems. A stiff problem is one in which the behavior of interest to the simulation is a slowly varying phenomenon even though the behavior might contain a high frequency component.

## 4.3 DC Bus Stability Methodology

The 7 steps for assessing DC bus stability for the intrazonal 775V port side bus in the test system are: (1) Actual scenarios simulations and observation, (2) models and simulation of reconfiguration scenarios (small signals), (3) Error analysis and order of ARMAX determination, (4) Models and simulation of reconfiguration scenarios (large signals), (5) Large signal error, (6) Multiplier design, and (7) Stability margin.

### 4.3.1 Scenarios simulation and observations

Each reconfiguration scenario was staged on the simulated system representing the system shown in Fig. 4.1. Fig. 4.1 represents the baseline system. The scenario simulation involves leaving the port bus coupled at the 775V DC bus and implementing a fault or reconfiguration action at the selected location in the system. Visual observations were made of the relevant node signals in the system. This observation was done to ascertain if the system was stable. Also, the other nodes (less relevant busses) were observed to see if they were stable.

### 4.3.2 Models and simulation of reconfiguration scenarios

The coupled system was set aside and a decoupled system containing the baseline was worked on. Using the tripuls, rectpuls and randn functions of the MATLAB signal processing toolbox, the voltage and current signals of the system constituting perturbed variables were ramped to their post perturbation values from the pre perturbation values. Their correct intermediate response was obtained by attaching the shaping functions to the new states of the state variable so that the system response to the shaping function such as a ramp or step is produced by the differential equation. The perturbation models were at first a small signal model.

The small signal perturbation model was applied to the decoupled system and the bus-of-interest data were generated and stored.

4.3.3 Error analysis and order of ARMAX determination

Solving the error equation of the ARMAX model, (4.44), the parameters of the Linear ARMAX model was estimated.

$$y(k) = a_0 + a_1 y(k-1) + ..... + a_{n-1} y(k-n+1) + b_0 u(k) + b_1 u(k-1) + .... + b_n u(k-n) + v(k) \tag{4.44}$$

The coefficients of the difference equation were determined so that the linear response defined in (4.44) was like the actual response of Z or Y to small signal perturbation with v(k) being the error of the approximation. Taking all the sample data of the system output and input into consideration (4.44) becomes (4.45).

$$\begin{aligned} &Y = U\theta + E \\ &where\ \theta = \begin{bmatrix} a_0 & a_1 & ..... & a_{n-1} & b_0 & b_1 & ..... & b_n \end{bmatrix}^T \end{aligned} \tag{4.45}$$

E is the error vector. Let S be the sum square error and be equal to (4.46)

$$S = E^T E = (Y^T - \theta^T U^T)(Y - \theta U) \tag{4.46}$$

we chose θ such that S is minimized as in (4.47)

$$\begin{aligned} &\frac{\partial S}{\partial \theta} = -2U^T Y + 2U^T U = 0 \\ &Therefore\ \theta = \left[\mathrm{U}^{\mathrm{T}} U\right]^{-1} U^T Y \end{aligned} \tag{4.47}$$

The TF function in MATLAB was used to convert the difference equation obtained from the ARMAX model to s domain transfer function.

A program to determine the error of (4.47) and to match this error to the order of the ARMAX model was made. There are two major sources of error. The first is the perturbation model and the other is the order of the ARMAX model. To overcome these

errors, the order with the minimum deviation of estimated y to real y was chosen and then the bode plots gain margins of the actual simulation and the decoupled simulation were compared at 60Hz, 10kHz and 20kHz. A maximum error of 28 percent was obtained for the small signal scenario at 20kHz. Details of the error analysis for the scenarios will be discussed in Chapter V. The results of trying a series of ramp skews, rectpuls heights, and seed for randn while determining the gain margins were used to fine-tune the design of the perturbation.

### 4.3.4 Reconfiguration scenario simulation (large signal)

The actual reconfiguration action was staged on the test system and the large signal data were generated and collected from the interface (bus) of interest. This step was to assess stability visually in a similar fashion as used in section 4.3.1.

Using the perturbation modeling procedure for the small signal model but increasing its magnitude and complexity, the desired large signal perturbation phenomenon was generated. Large signal perturbation was applied to the decoupled test system. The test system then generated data for the large signal function determination. The large signal function was based on conicity. Huynh [31] developed a theory that allowed a series cascade of the linear transfer function with the non-linear function to represent a non-linear system. The theory for the nonlinear function is given below. The stability conditions in (3.1), (3.2) were computed with their constants and variables now determined.

A non-linear system can be represented by a sector gain {a,b} or by a conic sector {c,r}. A nonlinear system with an input u and an output y which belongs to the sector {a,b} or is interior of the conic {c,r} must satisfy (4.48).

$$\|y - cu\| \le r\|u\|$$
$$\textit{therefore} \qquad (4.48)$$
$$\mathrm{r(c)} \ge \sqrt{\frac{P(y - cu)}{P(u)}}$$

where P(.) denotes the average power of signal (.)

The input u of the non-linear function is the output of the linear transfer function. This input u and the large signal output of the subsystem y are used to determine the radius of the conic sector given the center and these two parameters (center and radius) are applied to stability conditions in (3.1) and (3.2).

### 4.3.5 Large signal error

Each large signal perturbation model was verified that it was within acceptable limits determined by an empirically obtained error of approximation whose formula is shown in (4.49). Appendix A gives details of the derivation of (4.49).

$$\frac{R_{(UY)_3}(j\omega) + P_1 - H_2(j\omega)(R_{(UU)_3}(j\omega) + P_2)}{R_{(UU)_3}(j\omega) + P_2} = \varepsilon \qquad (4.49)$$

### 4.3.6 Multiplier design

In between the linear gain of the subsystem and the non-linear function, a multiplier gain was introduced in the subsystem to reduce the conservativeness of the stability assessment. The multiplier gain determination was based on trial and error to make an

unstable case compute to be unstable by the stability conditions. Scenario 9a was globally unstable, and it was used in computing the multiplier gain. The only requirement of the multiplier was that the poles of the gain be in the left-hand side of the s-plane [31].

### 4.3.7 Stability margin

The stability margin was determined from measuring the shortest distance of the system gain from the closest part of the forbidden region. This s distance is composed of two points, which make the start and end of the straight line. The real value of the s function make up this distance and gives the lowest gain difference possible between the reconfiguration scenario and its forbidden region. This is taken as the stability margin. The frequency at which this s distance occurs is evaluated as the frequency of the system gain at the end point of the straight line of the shortest distance which lies on the gain contour.

## 4.4 State Space Averaging Technique

Earlier stated and used for some modules in the test system is state space averaging technique. The technique consists of averaging two exact state space descriptions of the switched models over a single cycle T [47]. The state space averaging method gives the small signal low frequency models of any dc to dc converter [47]. Any switching dc to dc converter operating in the continuous conduction mode can be described by the state space equations for the two switched models as shown in (4.50) - (4.53). Averaging the

two switched models yields the (4.54) which represents the basic averaged state space description over a cycle T [47].

$$\dot{x} = A_1 x + b_1 v_{dc} \tag{4.50}$$

$$y_1 = c_1{}^T x \tag{4.51}$$

$$\dot{x} = A_2 x + b_2 v_{dc} \tag{4.52}$$

$$y_2 = c_2{}^T x \tag{4.53}$$

$$\begin{aligned} \dot{x} &= (dA_1 + d' A_2)x + (db_1 + d' b_2)v_g \\ y &= (dc_1^T + d' c_2^T)x \end{aligned} \tag{4.54}$$

## 4.5 Summary

This chapter has presented the modeling and methodology analysis. All design considerations were discussed. All governing equations in the test system components and the analysis involved in the methodology were presented. The following Chapter V will focus on presentation of graphs, plots, tables and pictures of the results obtained from carrying out section 4.3 several times.

# CHAPTER V

# RECONFIGURATION SCENARIOS SETUP AND SIMULATION

## 5.1 Overview

Within this dissertation research, there was a number of reconfiguration scenarios investigated. However, nine of these scenarios will be presented in this chapter. The scenarios within this chapter are broadly categorized into three categories. They are bus transfer activity, AC load addition, and AC load shedding. Under the bus transfer activity there were three scenarios, differing from each other by the severity of the fault which caused the bus transfer unit to operate. Details of the scenarios under this category and others will be presented in the subsequent sections. The second category, which is AC load addition consists of three scenarios, which were basically addition of three sizes of AC load to the port bus and observing the port side intrazonal DC bus for possible responses. The last category is titled AC load shedding, and it is analogous to the second category in that load on the port bus is shed at a given time. The shed load is comprised of shedding AC static load on port bus alone, shedding motor load on port bus alone and shedding both AC and motor load on the port bus. These constitute three scenarios, while the observed bus remained the port Intrazonal DC bus.

This chapter contains two major parts. (1) The actual scenario simulation in which the port DC bus is simply visually inspected for signs of signal instability and (2) the perturbation model simulation part in which the test system is decoupled and, as such, the features of the actual scenario are only simulated by correct perturbation to the

affected baseline signals. The baseline system was warranted, because the methodology required decoupling so that in order to regain the system during reconfiguration, a point prior to reconfiguration had to be selected for a baseline. The term baseline resulted from the use of the system as a base, from which the reconfigured system is regenerated. The error introduced by the perturbation modeling was assessed in each case, and tables will be presented to indicate the accuracy of the perturbation modeling. The values of error indicate the degree to which the reconfiguration phenomenon was attained in the decoupled system, and so are regarded as level of confidence in the assessment done by the methodology.

## 5.2 Reconfiguration Scenarios

### 5.2.1 Per unit analysis and bases for the results

In this section, the rationale for the per unit values seen in the results will be discussed. As will be seen in the subsequent subsections and sections the results provided are sometimes per unitized or are in raw data. Reasons why power system results are sometimes per unitized are that (1) there are transformers in the system which transforms voltage and current levels so that a raw data does not contain as much information at a glance as desired. (2) Primary impedances of a circuit containing a transformer and their corresponding values when referred to the secondary are the same per unit values though raw data are different [53] and (3) there is meaningful correlation between AC and DC sub circuits when all signal values are normalized as long as the

bases are chosen carefully and are disclosed. In order to discuss the scaled down IPS in Fig 5.1 within the per unit analyses, the sub circuits were identified. The PGM's form sub circuit 1, transformers form sub circuit 2, interzonal busses form sub circuit 3, intrazonal busses form sub circuit 4, AC load busses form sub circuit 5 and DC load busses form sub circuit 6. Table 5.1 contains a list of bases for the various sub circuits mentioned as identified on Fig. 5.1.

Table 5.1
Bases for the scaled down test IPS

| Sub Circuit number | Sub Circuit Description | Base Power | Base Voltage | Base Current | Remarks about bases |
|---|---|---|---|---|---|
| S1 | Power Generation Module (PGM) | 9MVA | 6.9kV peak l-n | 869A peak l-n phase | Manufacturer's ratings |
| S2 | Transformer | 9MVA | 8450V rms p-4160V rms s | 614.93A rms p-1249A rms s | Ideal Transformation at full load conditions |
| S3 | Interzonal busses | 9MVA | 1000V dc | 9000A dc | Full load conditions |
| S4 | Intrazonal busses | 9MVA | 775V dc | 6450A ac input 4000A dc input 11612.9A at bus | Normal loading and full load conditions |
| S5 | AC load busses | - | 450V rms | 6450A rms | Normal loading |
| S6 | DC load busses | - | 155V dc | 4000A dc | Normal loading |

### 5.2.2 Actual scenarios results

In this section, the staging of the actual scenario will be discussed and the distinctions of one scenario from the other scenarios will be made for each scenario. The reconfiguration scenarios staged on the test system in Fig. 5.1 are given in Table 5.2. The reconfiguration scenario and the system response to this are over within seconds which places the stability in transient stability due to the short duration and magnitude of the disturbance.

Table 5.2
Reconfiguration scenarios

| Category | Scenario number | Brief Synopsis |
|---|---|---|
| BT Activity | Scenario 1 | Finite impedance fault on the cable downstream bus of interest |
| | Scenario 2 | Bolted fault on cable downstream bus of interest |
| | Scenario 3 | More severe finite impedance fault on cable downstream bus of interest |
| Load Addition | Scenario 4 | Load addition to 85% on portside |
| | Scenario 5 | Load addition to 150% on port side |
| | Scenario 6 | Load addition to 100% on port side |
| Load Shedding | Scenario 7 | Static load shed -15% value |
| | Scenario 8a | Induction motor shed – 36% value |

Table 5.2 Continued

| Category | Scenario number | Brief Synopsis |
|---|---|---|
| Visually unstable but could not be properly ascertained by methodology | Scenario 8b | Induction motor shed – 36% value. But decoupled subsystems separated about inter-zonal bus |
| | Scenario 9a | Induction motor and static load shed 51% value |
| Visually unstable and Condition 2 demonstrated instability. | Scenario 9b | Induction motor and static load shed 51% value. But decoupled subsystems separated about interzonal bus |

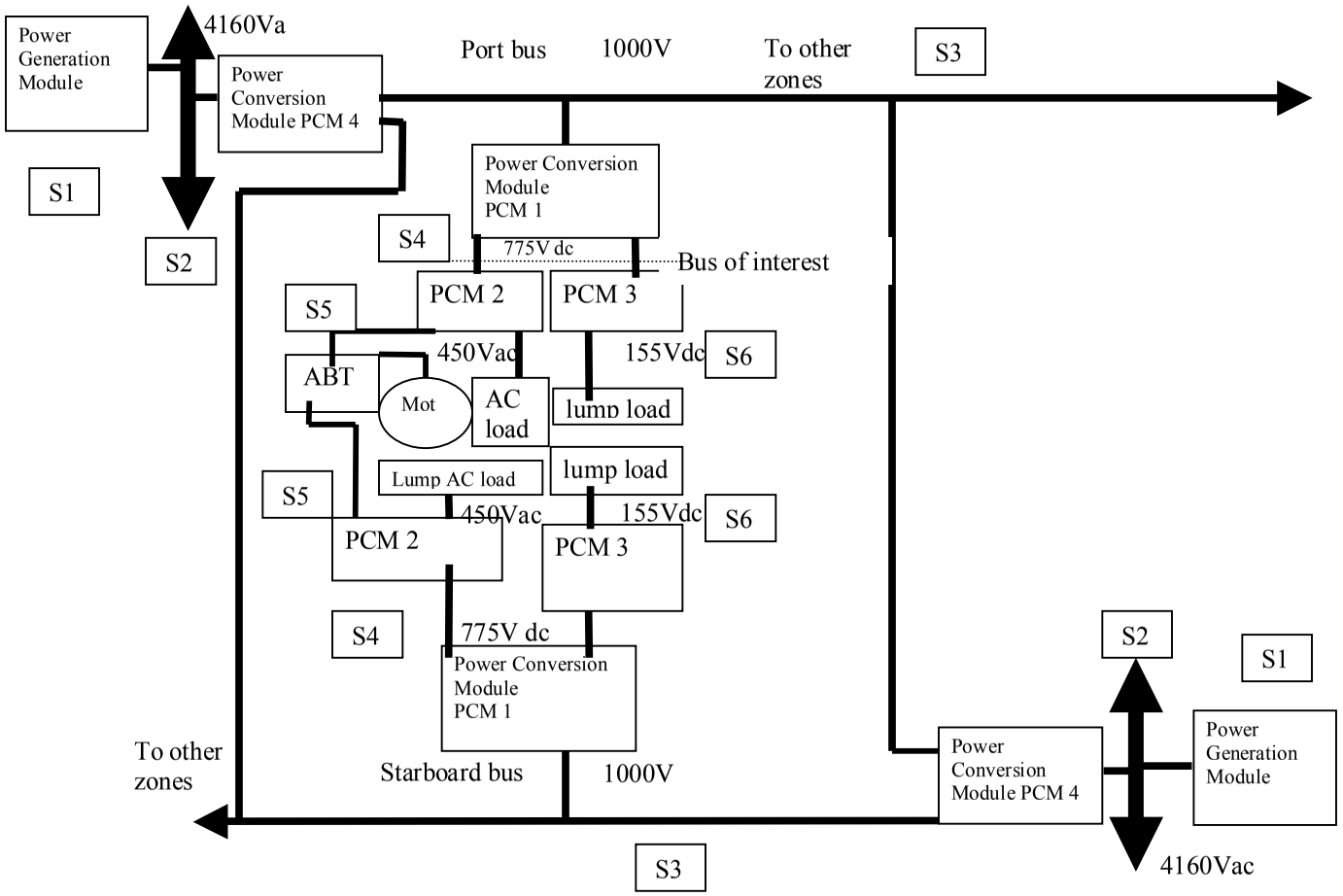


Fig. 5.1 Test system diagram with bus of interest marked

5.2.3 Scenario 1

A finite impedance fault was placed on the cable downstream the port intrazonal DC bus from 0.8 seconds into the simulation till the end of simulation at 1.2 seconds. This finite impedance fault depressed the DC bus voltage, causing the automatic bus transfer (ABT) switch to transfer the induction motor from the port to the starboard bus. The drop out voltage of the ABT was set at 260VACrms, and the pick up voltage was set at 313VAC rms. These values are lower than applicable, but were reduced for the sake of filter attenuation and inverter modulation. The depressed voltage of the load AC bus was 257.85VACrms. The fault impedance for this scenario was 1.042e-2 ohms. The plots shown in Fig. 5.2-Fig. 5.5 are the results of the actual scenario simulation.

The generator inertia causes it to take a while to produce the fault current in Fig. 5.2a and the fault current is produced in the interim from the stored energy in the inductances of the filters in the system. The generator response in the voltage signal is relatively instantaneous, and the generator maintains the 1pu, except during fault time. There exists a voltage regulator with the rectifier that keeps the rectifier output voltage at no load value (which is 1pu), and its effect can be seen in Fig. 5.2c. The circuit breaker operated on the dual bridge to isolate the port source from the fault, but the fault current maximum of 5.3071pu was attained before circuit breaker operation. The circuit breaker on the dual bridge operated in about 40msec as shown in Fig. 5.2d. More system responses follows in Fig. 5.2e-Fig5.2h.

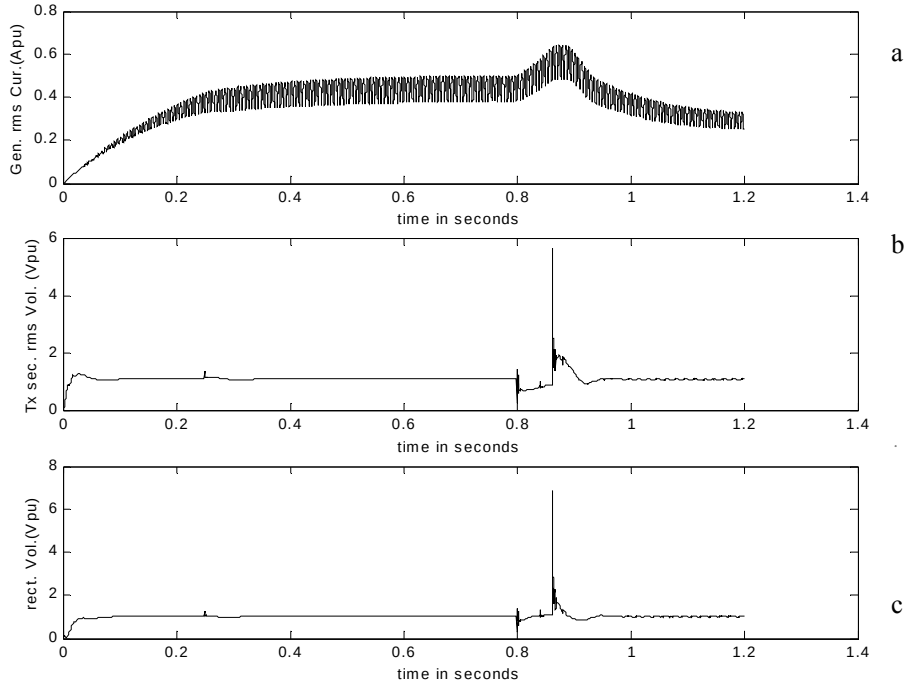


Fig. 5.2 Actual port side simulation results for Scenario 1. a) Port bus generator RMS current in pu

b) Port bus transformer RMS line to line voltage in pu

c) Port bus rectifier output voltage in pu

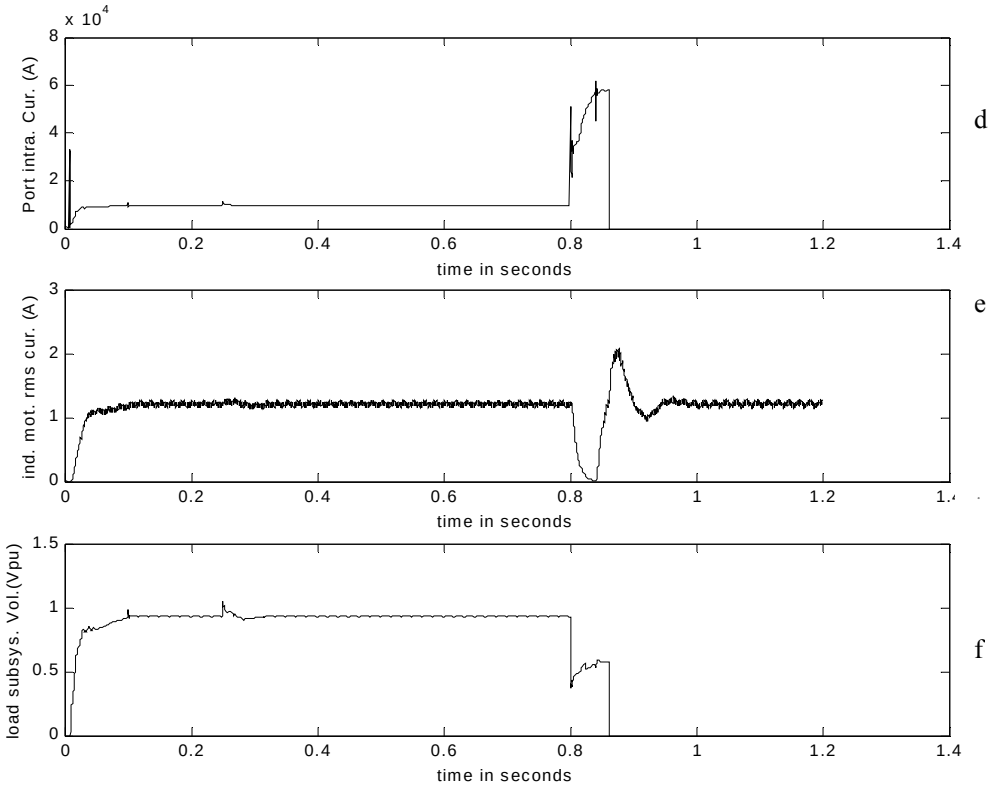


Fig. 5.2 Continued. d) Port bus dual bridge output current in actual

e) Port bus induction motor current from state variables in pu

f) Port bus load subsystem voltage in pu

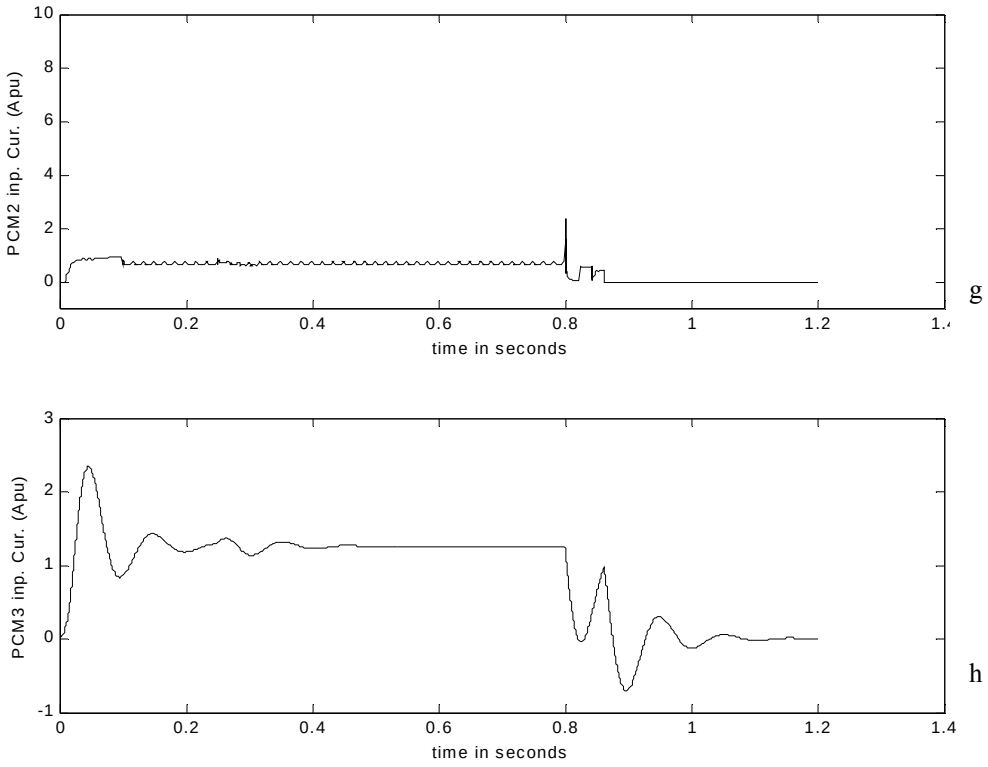


Fig. 5.2 Continued. g) Port bus ARCP input current in pu

h) Port bus buck converter current in pu

The motor current shows bus transfer activity. The first part of the current shown in Fig. 5.1e is port bus current and the latter part is starboard current. The load subsystem voltage shows a dip during fault to 0.3632pu and some slight recovery before circuit breaker operation. There is delay in the start of signals shown in Fig. 5.2e to Fig. 5.2g, and is due to switches in the system that delays the connection of the load to the system's energy. The signals that are of interest are extracted and presented in the per unit basis for view in Fig. 5.3a through Fig. 5.3d. Those of interest are the signals around

the port side intrazonal bus. They are called Voutdualn, ioutdualn, Vdcnewn and Iin. They represent the dual bridge output signals and the load input signals. The responses in the rest of the test system, which is the starboard bus, are also included in Fig. 5.4a through Fig. 5.4h. Fig. 5.3a shows that during the fault, the generators see the motor load on the starboard bus instead of the port bus due to bus transfer activity and reflex this in different loading behavior on both generators. An analogous set of figures of Fig. 5.3a through Fig. 5.3d can be presented for the starboard as was done for the port bus. This is done in Fig. 5.5a through Fig. 5.5d. Though the signals in Fig. 5.5 are not used for stability assessment and as such have not the same amount of interest as Fig. 5.3, nevertheless, they represent the behavior of the starboard bus. Figures presented in Fig. 5.5a through Fig. 5.5d are also presented in per unit basis like those of Fig.5.3.

Visual perception of the signals stored and presented shows no indications of instability, and this assessment is to be made first for all the scenarios. This perception is only qualitative and general and contains few quantitative standards. Quantitative measures taken to assess stability will be presented in Section 5.4.

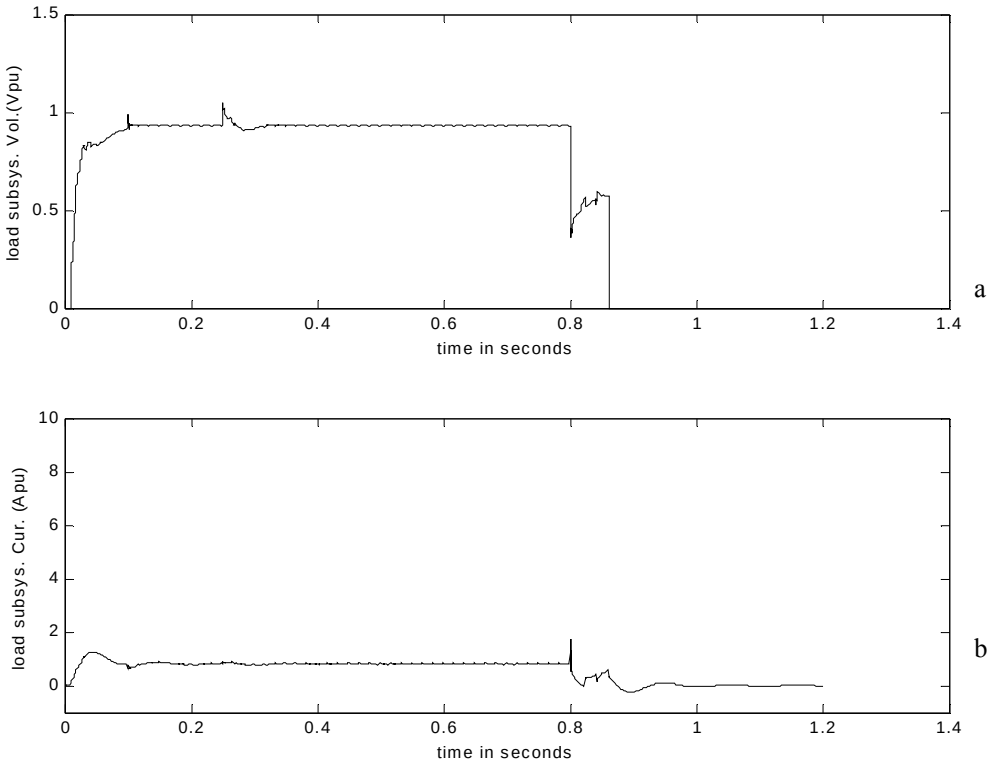


Fig. 5.3 Port side intrazonal bus simulation results for Scenario 1in pu. a) Port bus load subsystem voltage in pu b) Port bus load subsystem input current in pu

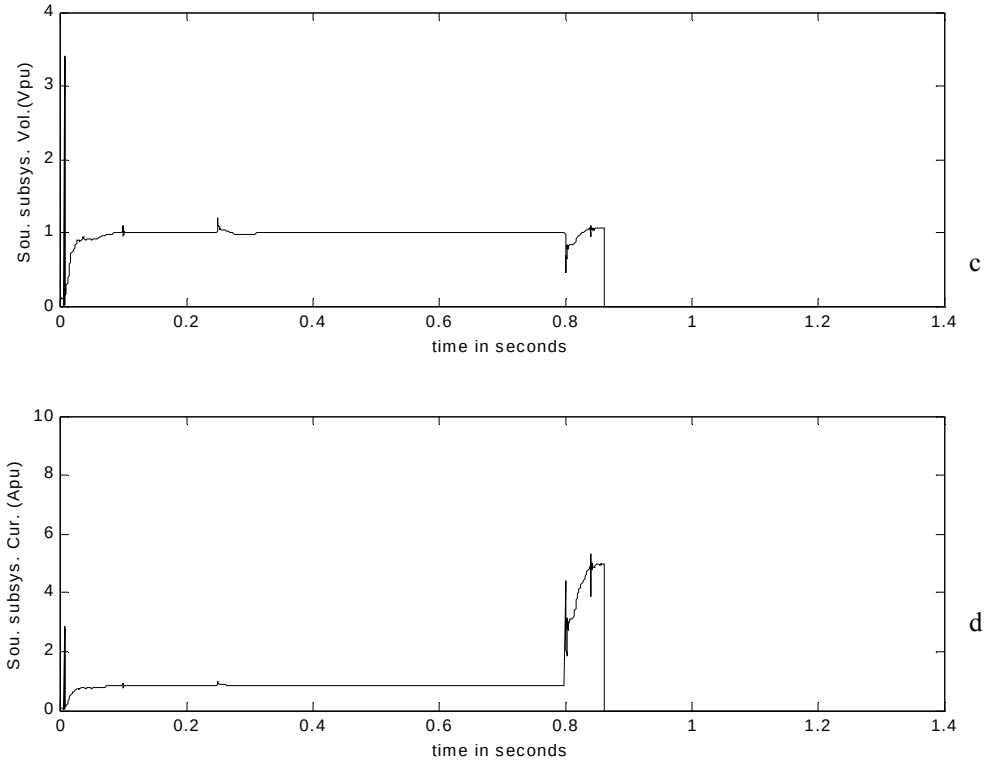


Fig. 5.3 Continued. c) Port bus source subsystem output voltage in pu

d) Port bus source subsystem output current in pu

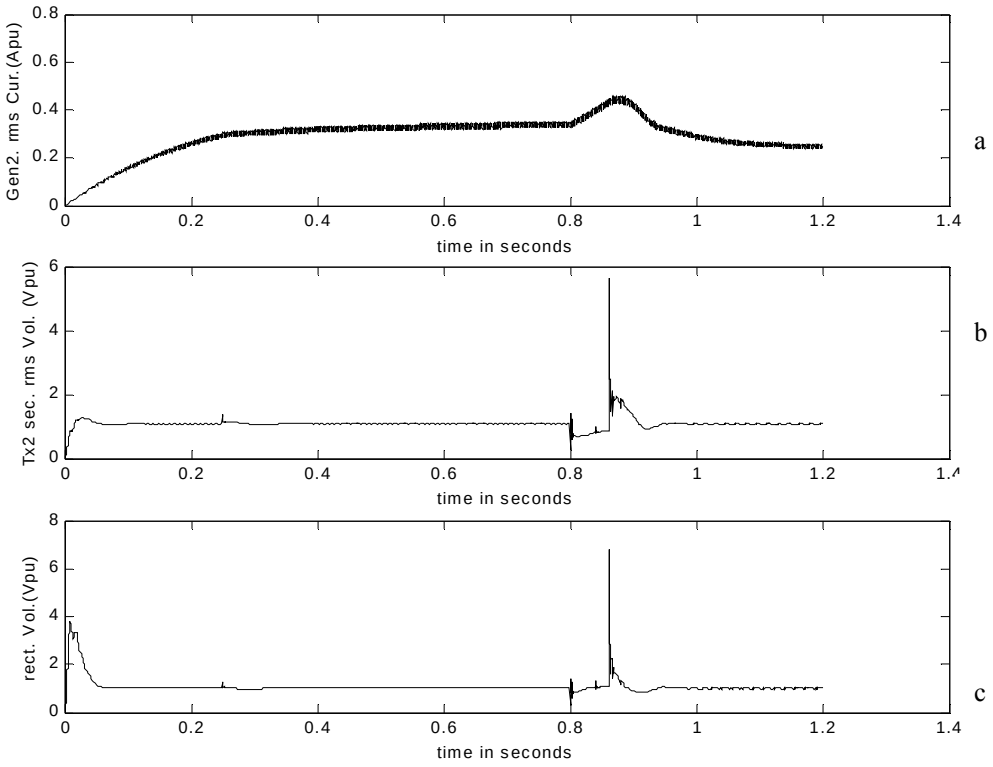


Fig. 5.4 Actual starboard side simulation results for Scenario 1. a) Starboard bus generator RMS current in pu b) Starboard bus transformer line to line voltage RMS in pu

c) Starboard bus rectifier output voltage in pu

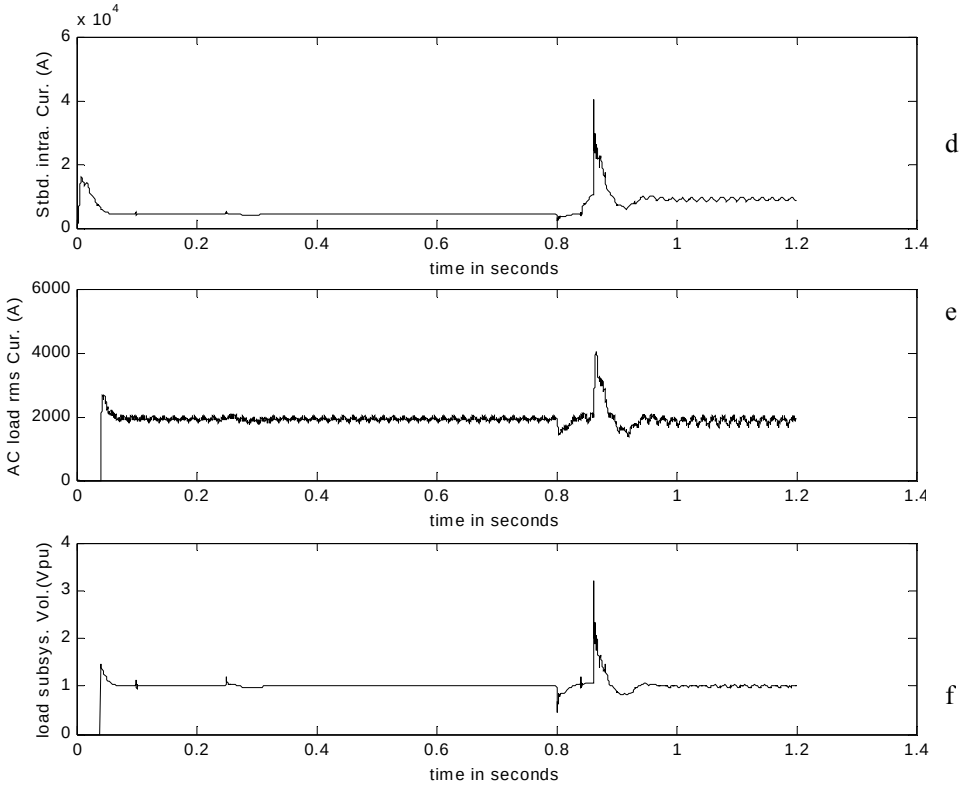


Fig. 5.4 Continued. d) Starboard bus dual bridge output current actual

e) Starboard bus AC RL load current in RMS actual

f) Starboard bus load subsystem voltage in pu

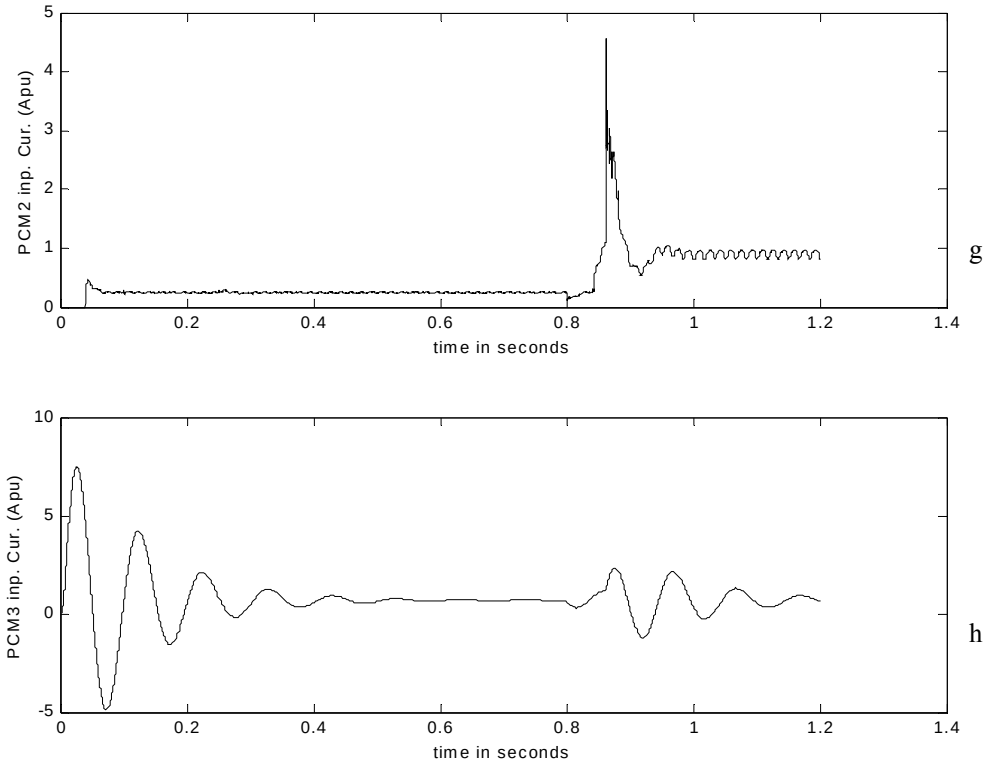


Fig. 5.4 Continued. g) Starboard bus ARCP input current

h) Starboard bus buck converter input current pu

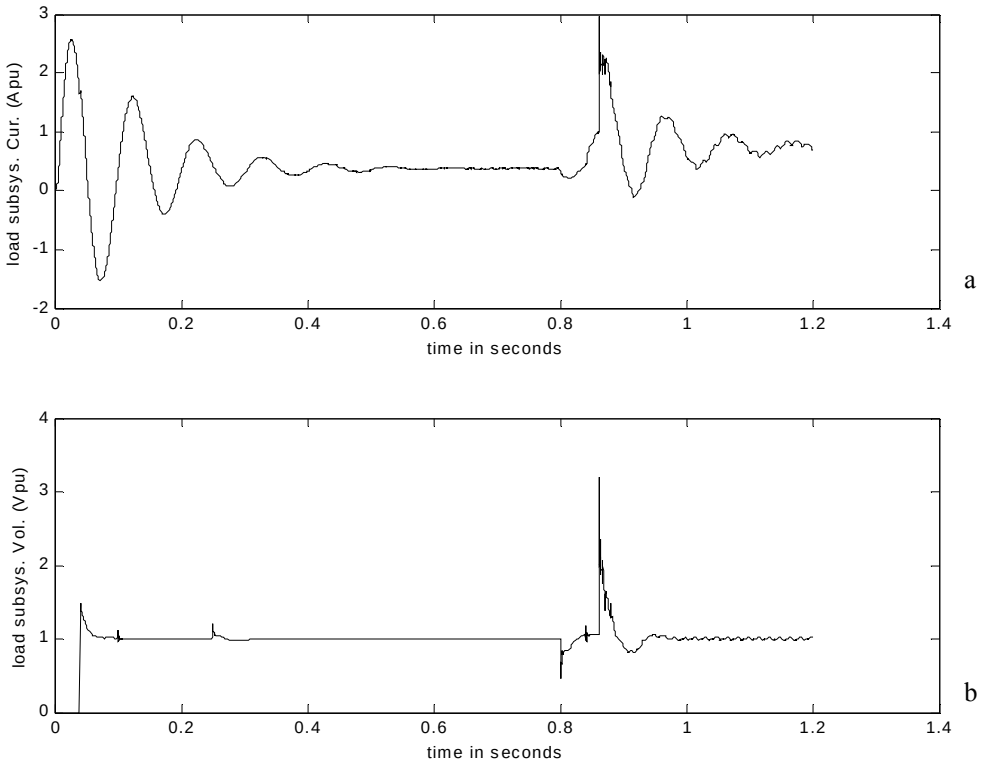


Fig. 5.5 Starboard side intrazonal bus simulation results for Scenario 1 in pu. a) Starboard bus load subsystem current in pu b) Starboard bus load subsystem voltage in pu

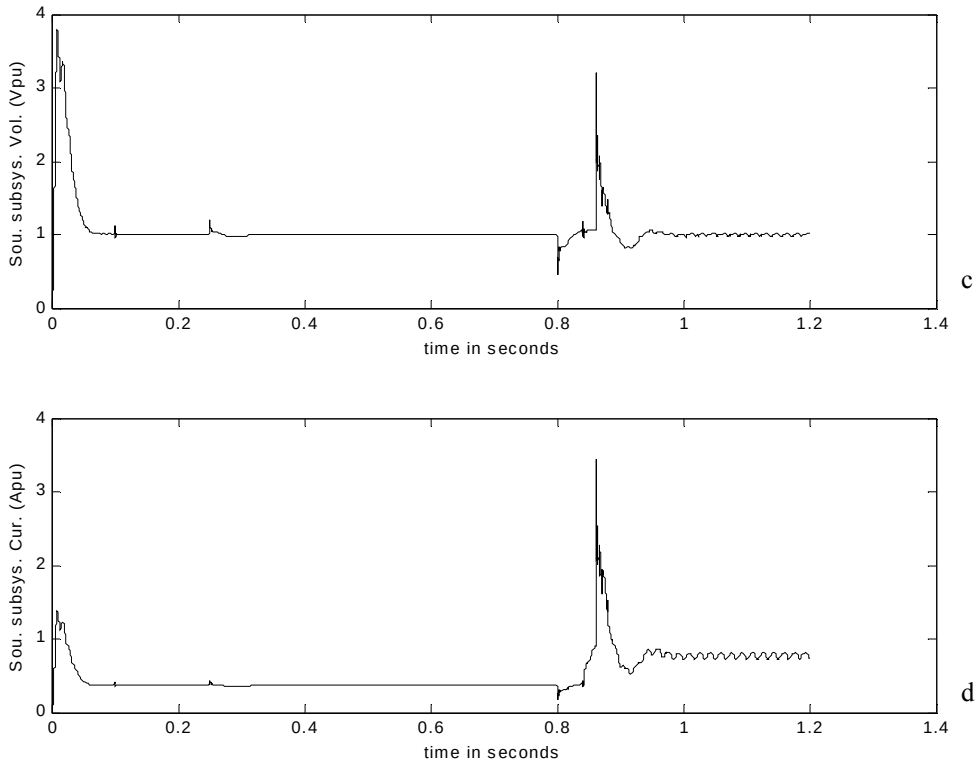


Fig. 5.5 Continued. c) Starboard bus source subsystem output voltage in pu

d) Starboard bus source subsystem output current in pu

### 5.2.4 Scenario 2

A virtually bolted fault was placed on the cable downstream the port intrazonal DC bus from 0.8 seconds and left in the simulation until the end of simulation at 1.2 seconds. This fault depressed the DC bus voltage to 0Volts, causing the ABT to transfer the induction motor from the port bus to the starboard bus. Figures 5.6-5.9 are the results of the actual scenario simulation.

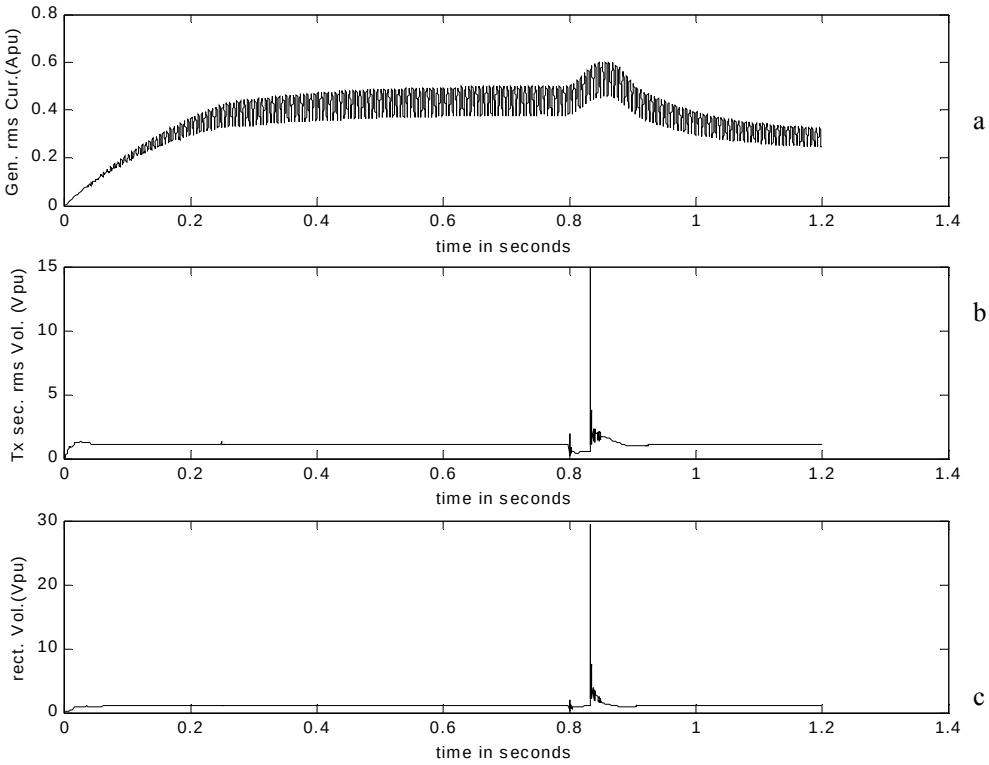


Fig. 5.6 Actual port side intrazonal bus simulation results for Scenario 2. a) Port bus generator RMS current in pu b) Port bus transformer RMS line to line voltage in pu

c) Port bus rectifier output voltage in pu

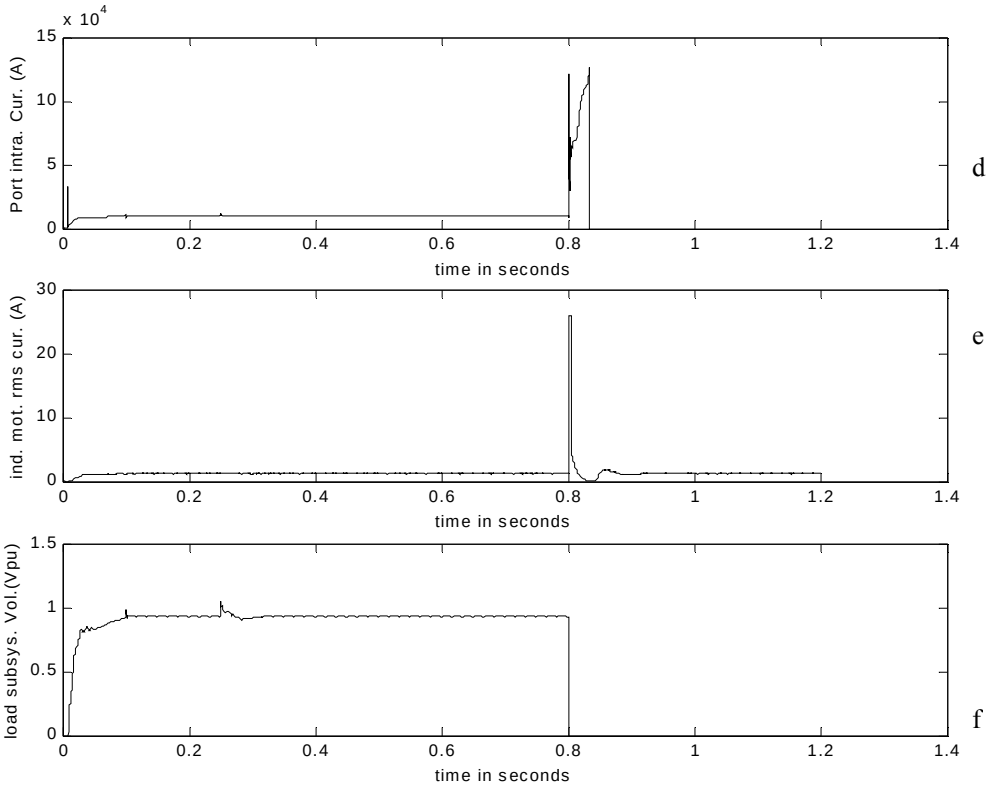


Fig. 5.6 Continued. d) Port bus dual bridge output current in actual

e) Port bus induction motor current from state variables in pu

f) Port bus load subsystem input voltage in pu

The fault current for the bolted fault is higher than the Scenario 1 value. As can be seen in Fig. 5.6d this fault current is 10.85pu peak. Figures 5.6a-c are similar to Scenario 1 profiles, since they represent the same bus transfer activity category, but in this scenario the level of fault severity is higher since this represents a bolted fault situation. More system behavior can be seen in Fig. 5.6e-Fig. 5.6h.

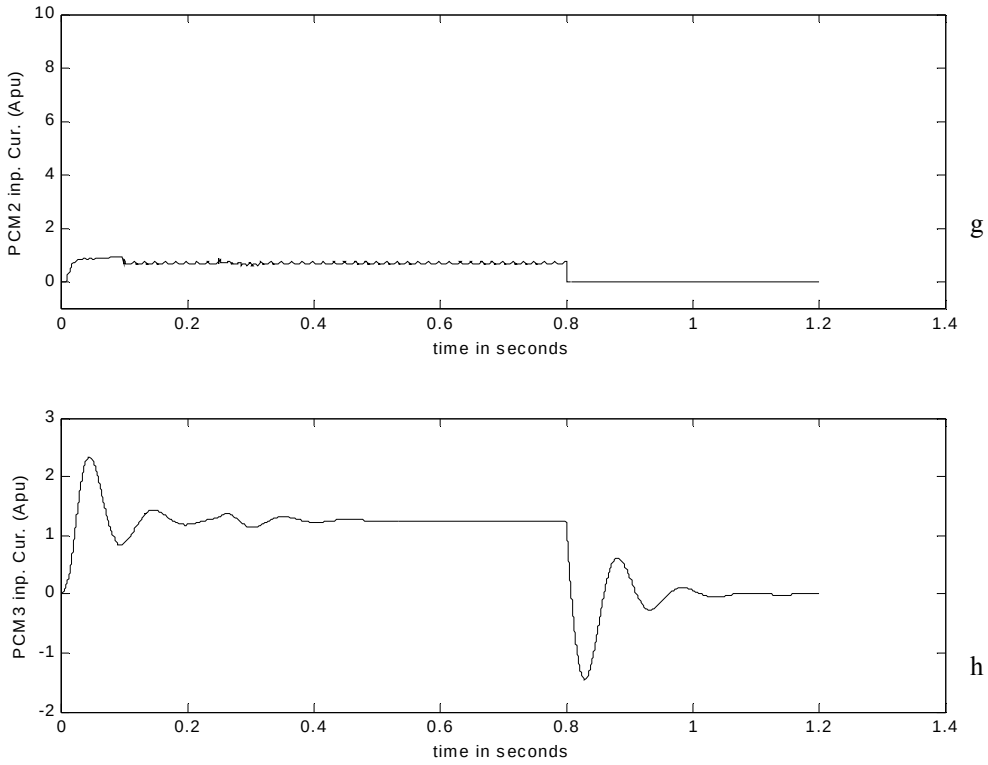


Fig. 5.6 Continued. g) Port bus ARCP input current in pu

h) Port bus buck converter current in pu

With the bolted fault in the system the load voltage downstream the fault shows a zero voltage both during and after the fault. After the fault, because the upstream dual bridge circuit breaker operated, and the downstream circuit lost power, except the motor load regained power when it was transferred to the starboard bus through the ABT, and the activity is captured in Fig. 5.6e which is the motor RMS current. The responses were generally similar to the Scenario 1 response and the signals of interest were similarly extracted and presented in Fig. 5.7a through Fig. 5.7d. They are the same signals of

interest in Scenario 1. The responses in the rest of the test system which is the starboard bus are included in Figs. 5.8a -5.8h. The difference in impedance of the port bus and the starboard bus in this case resulted in the loading difference that the generators of the system saw showing new post fault values different from the pre fault values. This is presented in the Fig. 5.6a and Fig. 5.8a. Similarly signals extracted as signals of interest in the port bus exist in the starboard bus. They are presented in Figs 5.9a through 5.9d.

Visual inspection of signals in the scenario shows no instability similar to the conclusion in Scenario 1. Quantitative analysis will be carried out in Section 5.4.

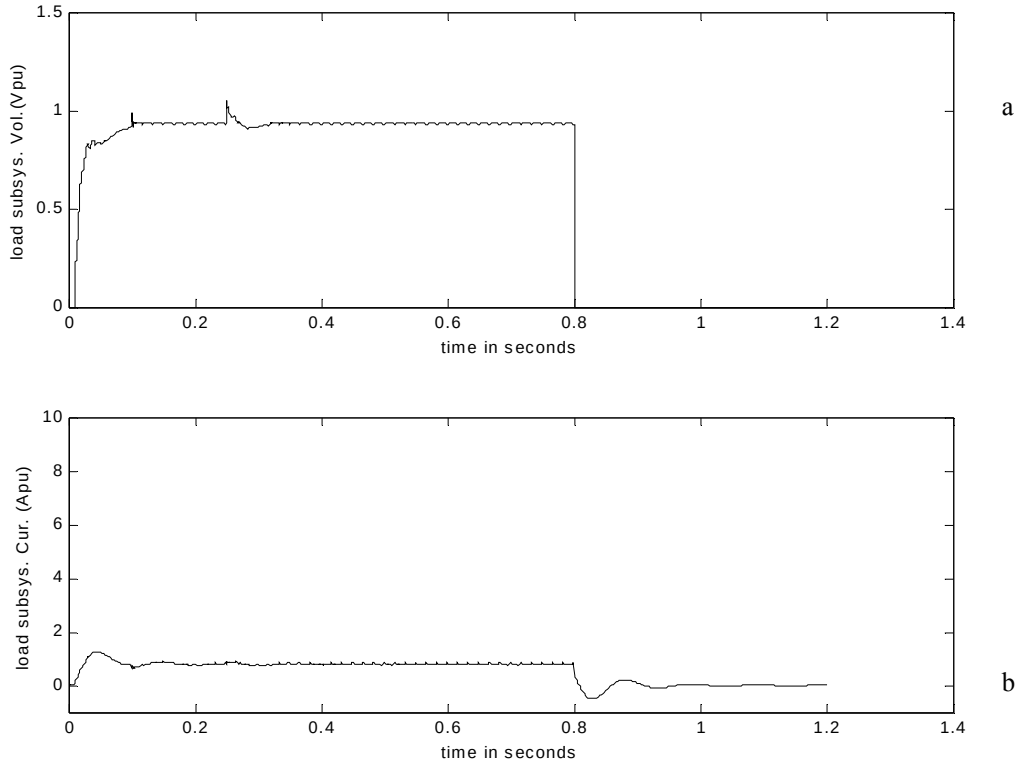


Fig. 5.7 Port side intrazonal bus simulation results for Scenario 2 in pu. a) Port bus load subsystem voltage in pu b) Port bus load subsystem input current in pu

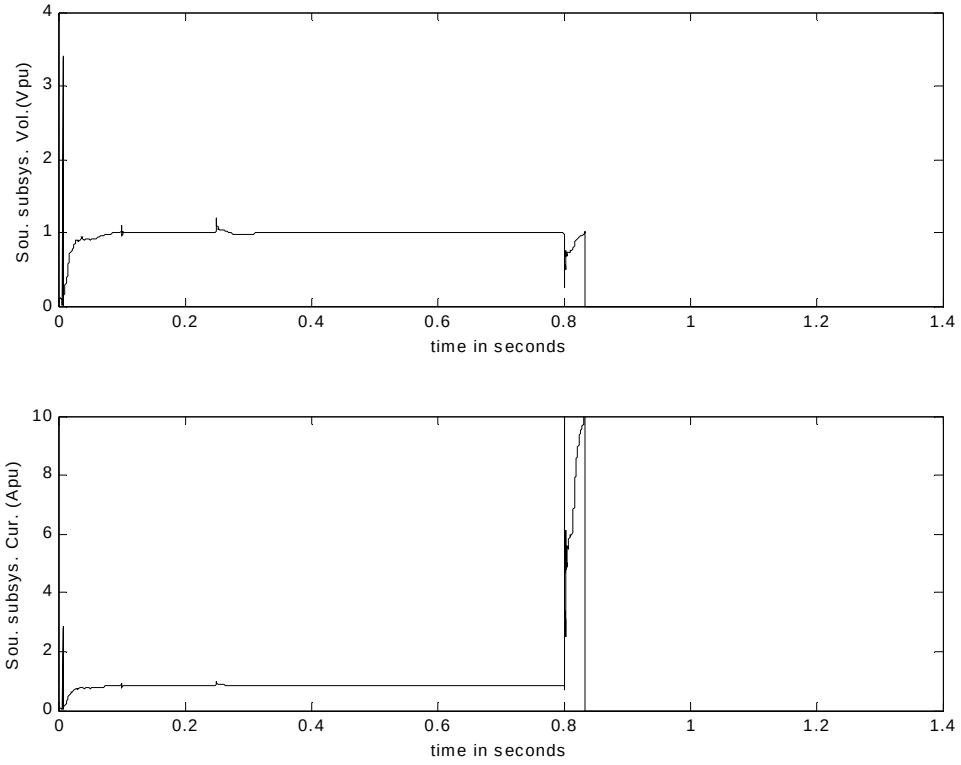


Fig. 5.7 Continued. c) Port bus source subsystem output voltage in pu

d) Port bus source subsystem output current in pu

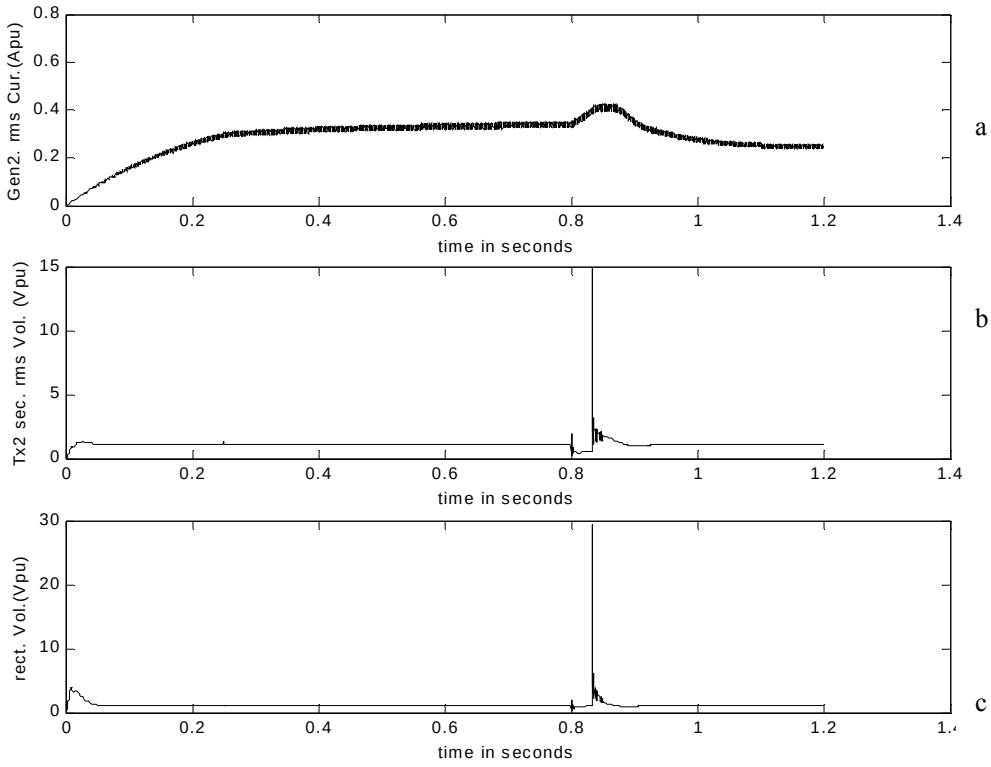


Fig. 5.8 Actual starboard side simulation results for Scenario 2. a) Starboard bus generator RMS current in pu b) Starboard bus transformer line to line voltage RMS in pu

c) Starboard bus rectifier output voltage in pu

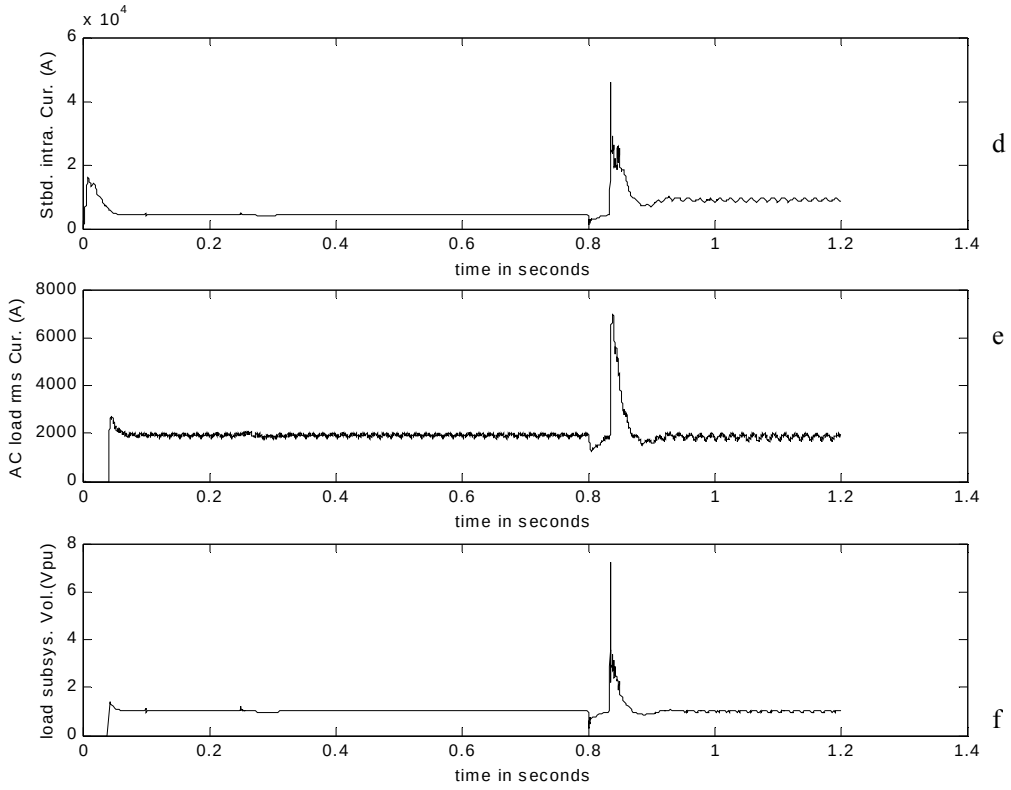


Fig. 5.8 Continued. d) Starboard bus dual bridge output current actual

e) Starboard bus AC RL load current in RMS actual

f) Starboard bus load subsystem input voltage in pu

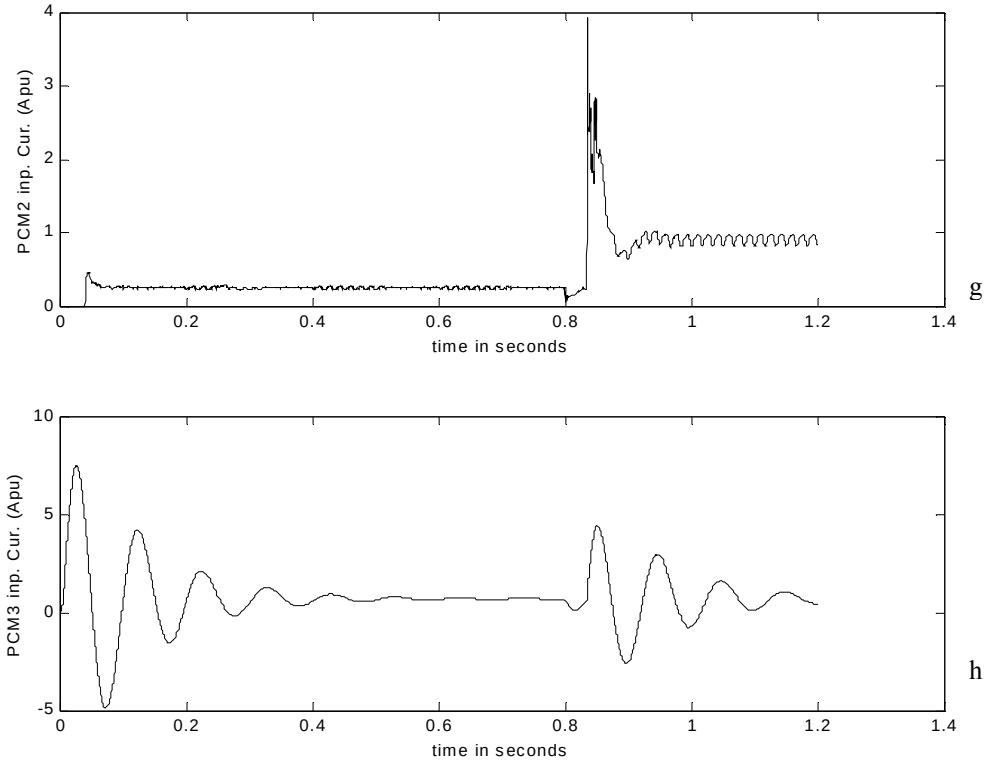


Fig. 5.8 Continued. g) Starboard bus ARCP input current in pu

h) Starboard bus buck converter input current in pu

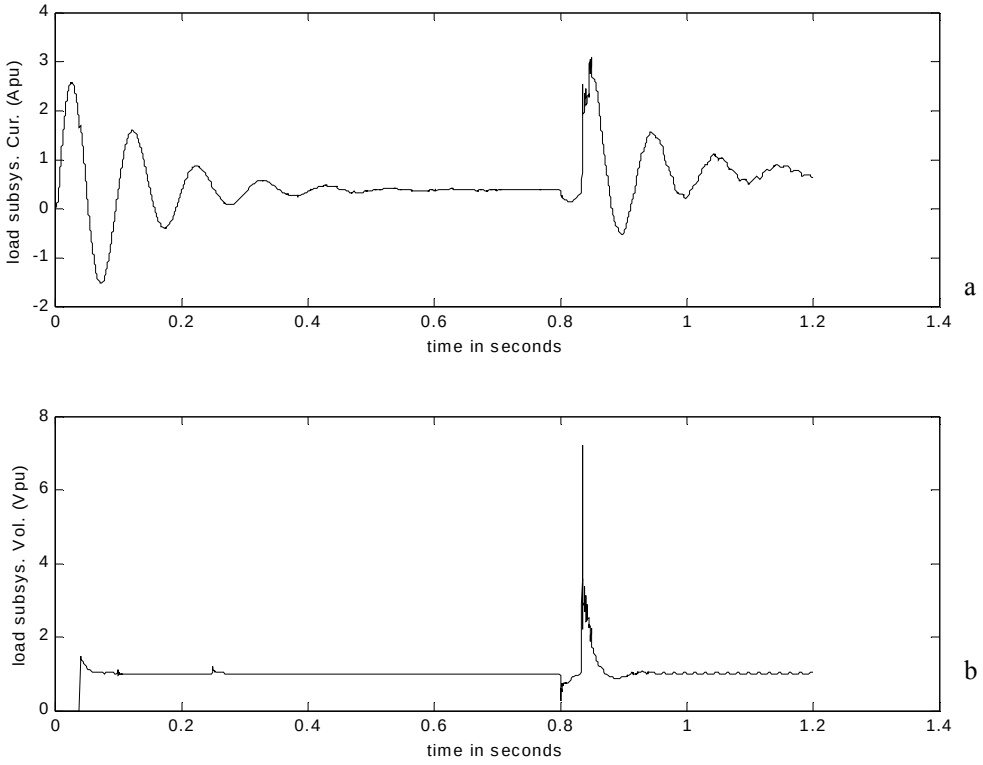


Fig. 5.9 Starboard side intrazonal bus simulation results for Scenario2 in pu. a) Starboard bus load current in pu b) Starboard bus load input voltage in pu

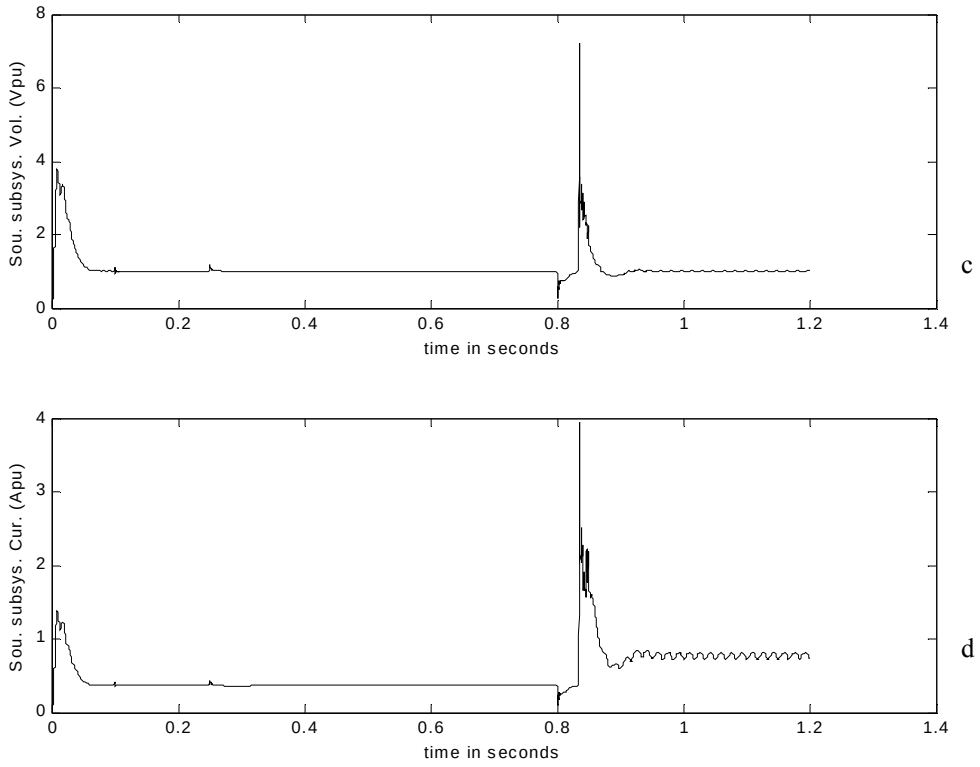


Fig. 5.9 Continued. c) Starboard bus source subsystem output voltage in pu

d) Starboard bus source subsystem output current in pu

### 5.2.5 Scenario 3

A finite impedance fault was placed on the cable downstream port bus from 0.8 seconds into the simulation until the end of the simulation at 1.2 seconds. The fault caused the ABT to see a depressed voltage of 169.52 Volts, causing it to operate and transfer the motor from the port bus to the starboard bus. The fault impedance for the scenario was 4.6311e-3 ohms. The plots shown in Fig. 5.10 through Fig. 5.13 are the results of the actual scenario simulation.

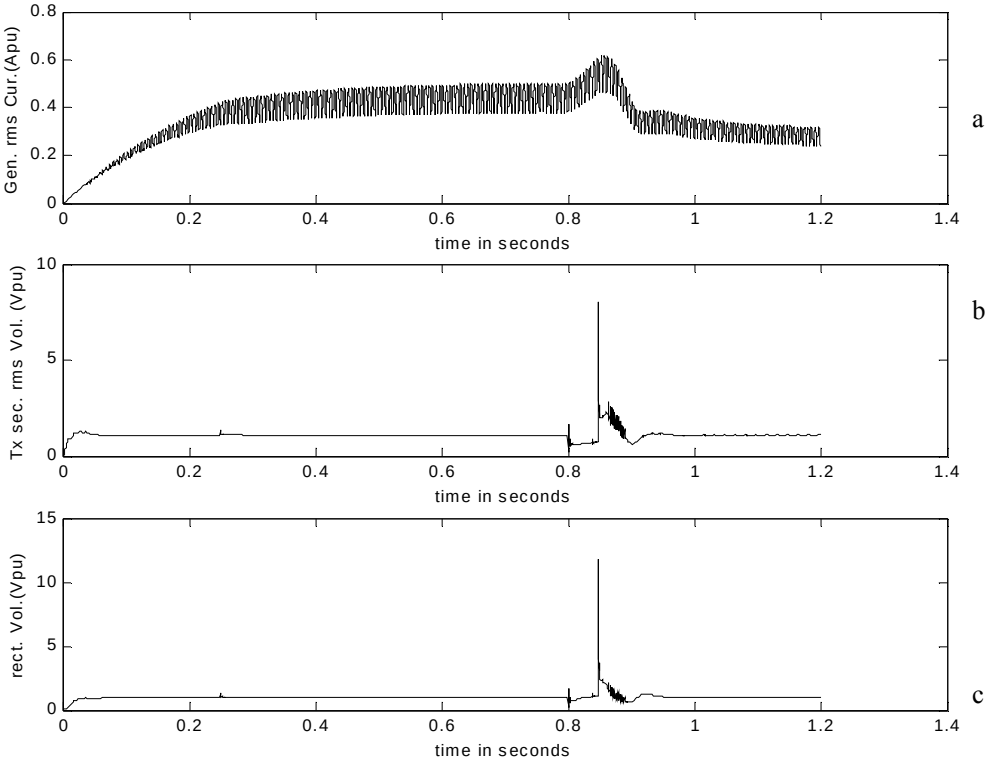


Fig. 5.10 Actual port side simulation results for Scenario 3. a) Port bus generator RMS current in pu

b) Port bus transformer RMS line to line voltage in pu

c) Port bus rectifier output voltage in pu

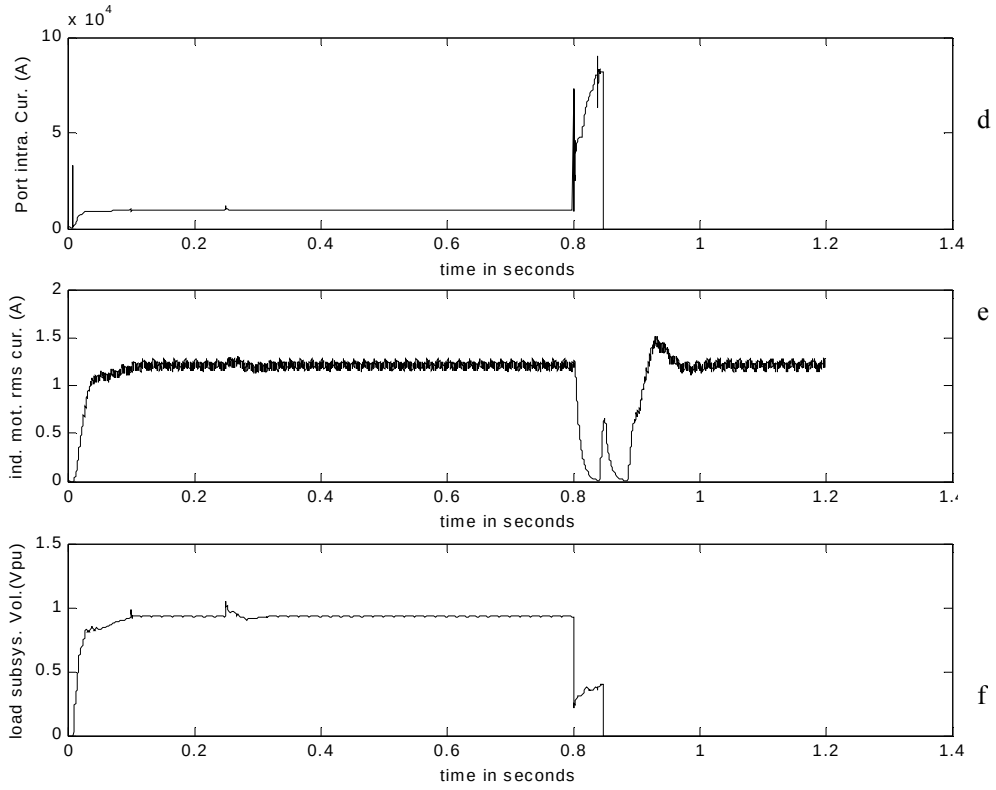


Fig. 5.10 Continued. d) Port bus dual bridge output current in actual

e) Port bus induction motor current from state variables in pu

f) Port bus load subsystem voltage in pu

The response for Scenario 3 is similar to the two previously presented scenarios. But, the severity of the fault is higher than Scenario 1 and less than Scenario 2. This can be seen in the peak fault current seen at the output of the PCM1 on the port bus in Fig. 5.9d. The peak fault current for this scenario is 7.36pu. In Fig. 5.10e it was observed that the low voltage seen by the induction motor was low enough in this scenario to cause the

ABT to operate and after there was complete loss of power there was another response of the ABT. More port bus responses are seen in Fig. 5.9g through Fig. 5.9h

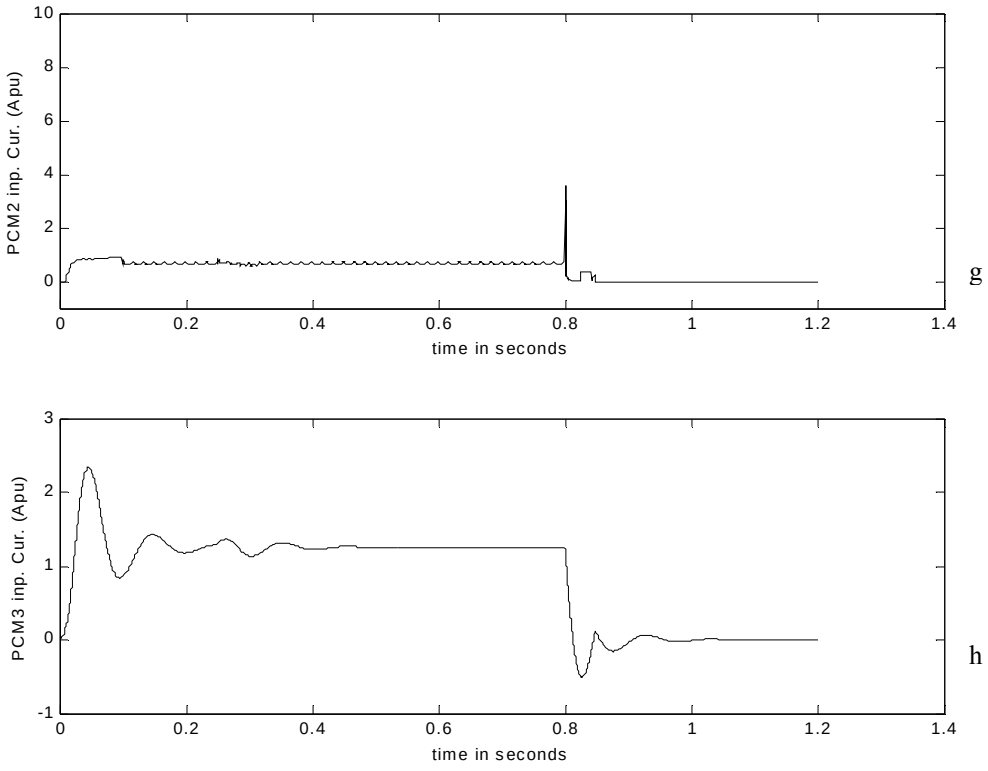


Fig. 5.10 Continued. g) Port bus ARCP input current in pu

h) Port bus buck converter current in pu

As in the two earlier scenarios the motor current shows bus transfer activity. The responses were as expected. The signals of interest for stability assessment were extracted in pu in Figs 5.11a through 5.11d. They are the same signals of all the scenarios, which are the signals around the port intrazonal bus. The rest of the system

responses which belongs to the starboard bus are presented in Fig. 5.12a through Fig. 5.12h. As in the case of Scenarios 1 and 2, Scenario 3 has an analogous set of signals of interest that are not used for stability assessment. They are presented in Fig. 5.13a through Fig. 5.13d in pu.

Visual perception of the signals stored and presented shows no indication of instability for Scenario 3. Quantitative analysis is required to assess the margin of stability.

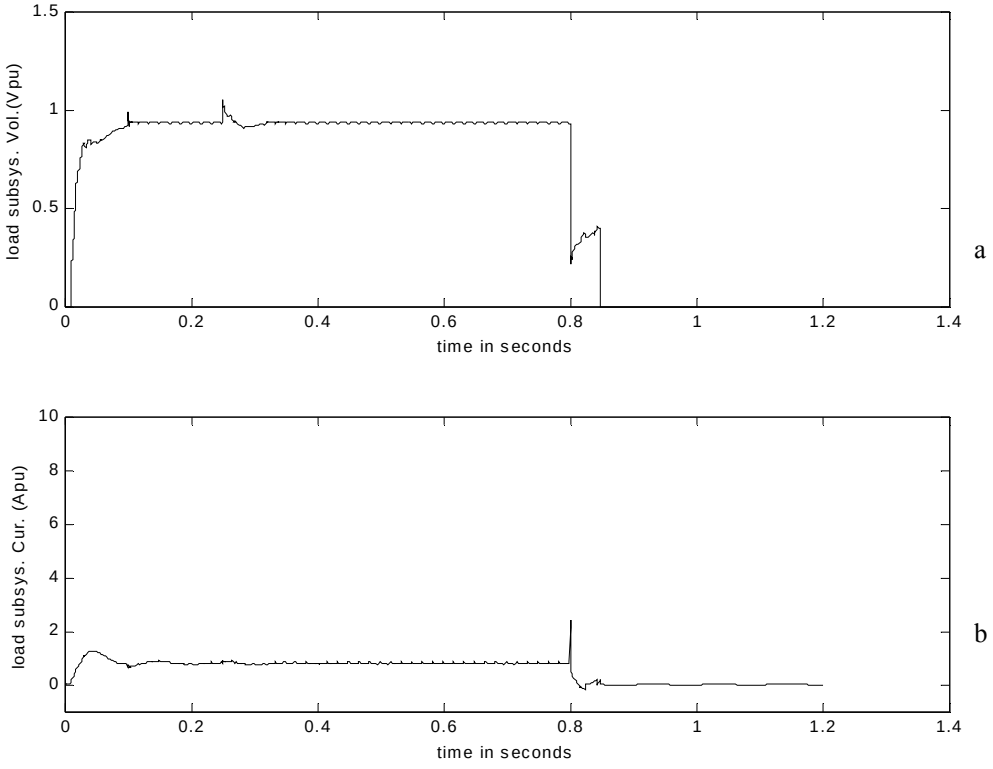


Fig. 5.11 Port side intrazonal bus simulation results for Scenario 3 in pu. a) Port bus load subsystem voltage in pu b) Port bus load subsystem input current in pu

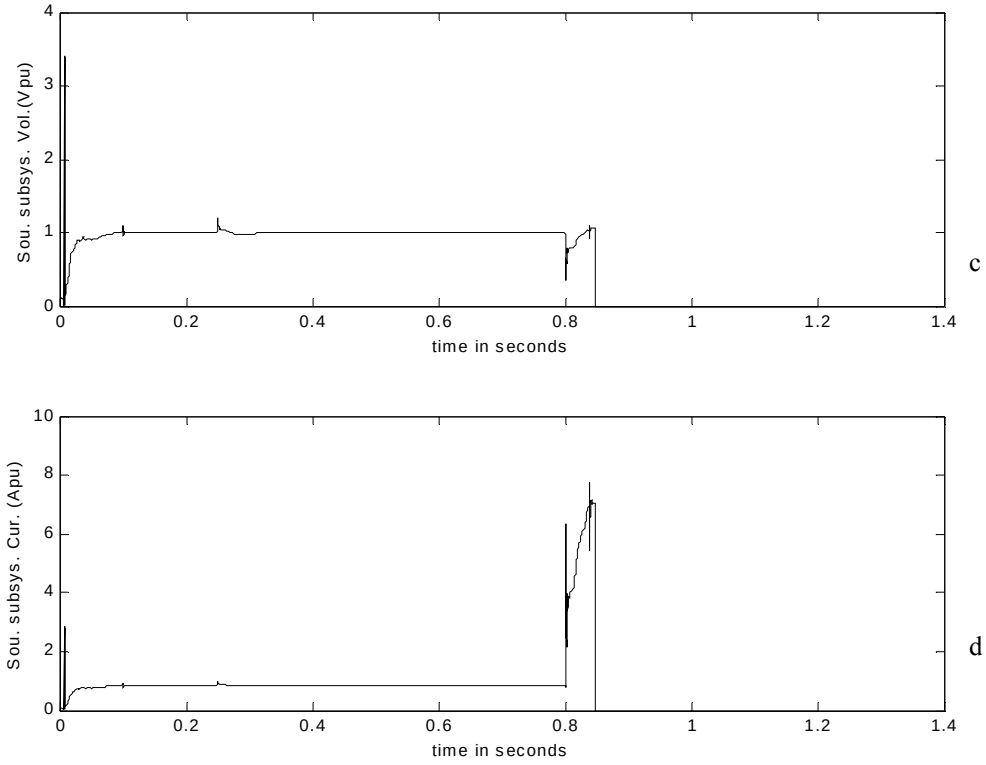


Fig. 5.11 Continued. c) Port bus source subsystem output voltage in pu

d) Port bus source subsystem output current in pu

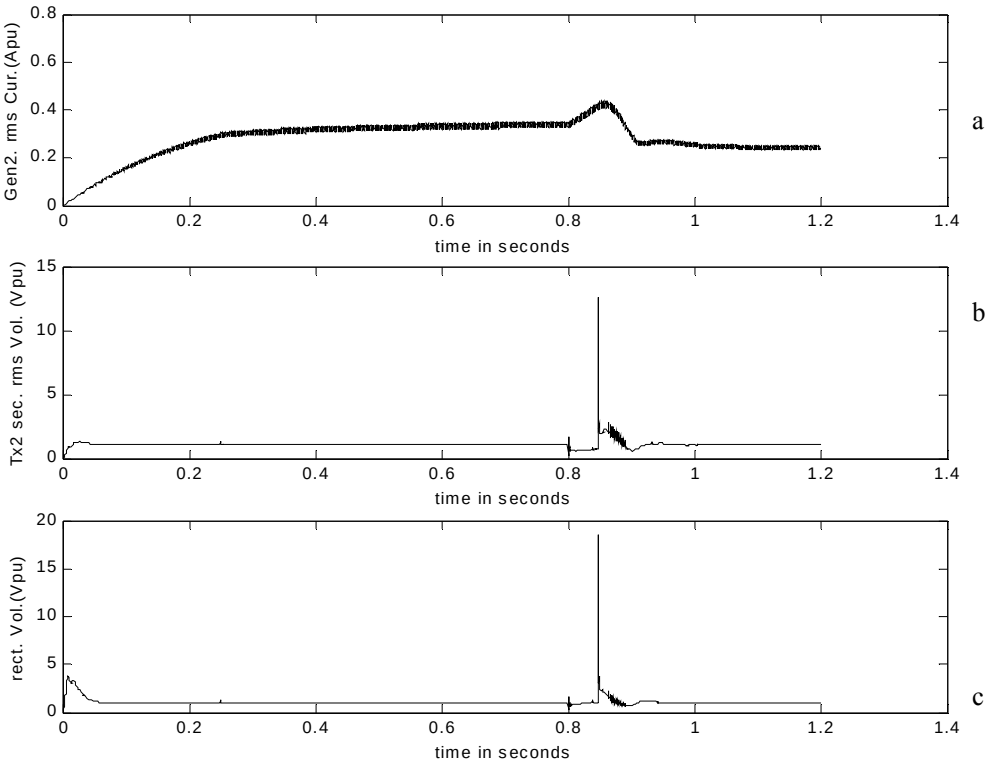


Fig. 5.12 Actual starboard side simulation results for Scenario 3. a) Starboard bus generator RMS current in pu b) Starboard bus transformer line to line voltage RMS in pu

c) Starboard bus rectifier output voltage in pu

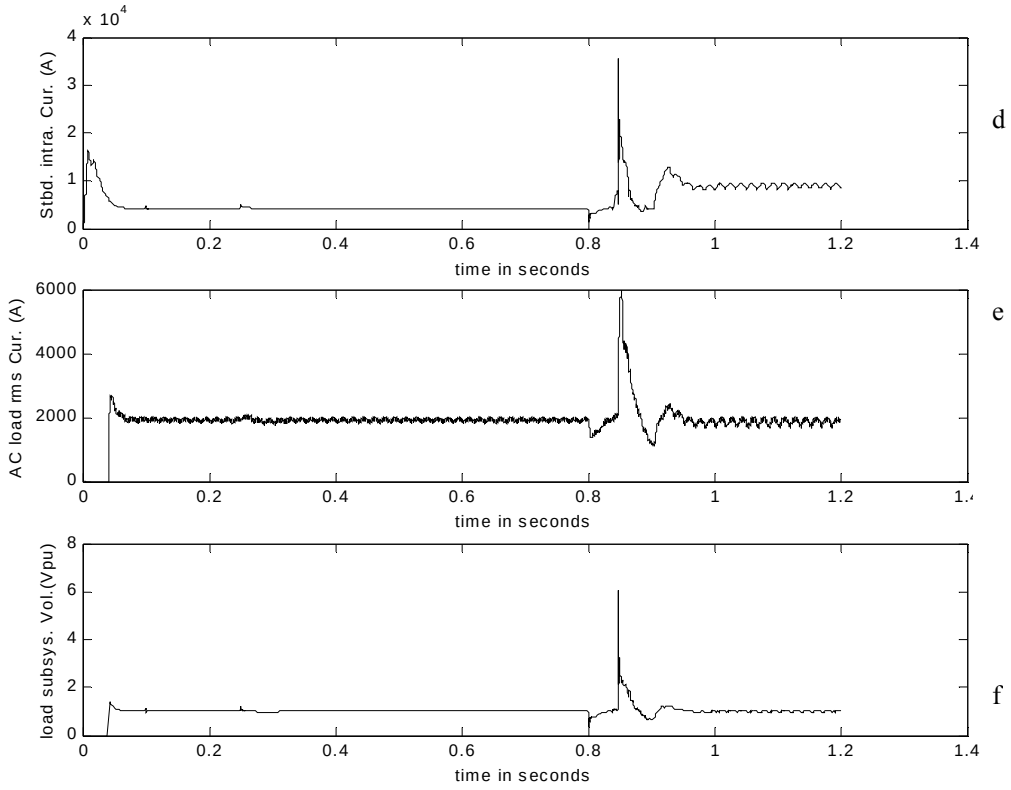


Fig. 5.12 Continued. d) Starboard bus dual bridge output current actual

e) Starboard bus AC RL load current in RMS actual

f) Starboard bus load subsystem voltage in pu

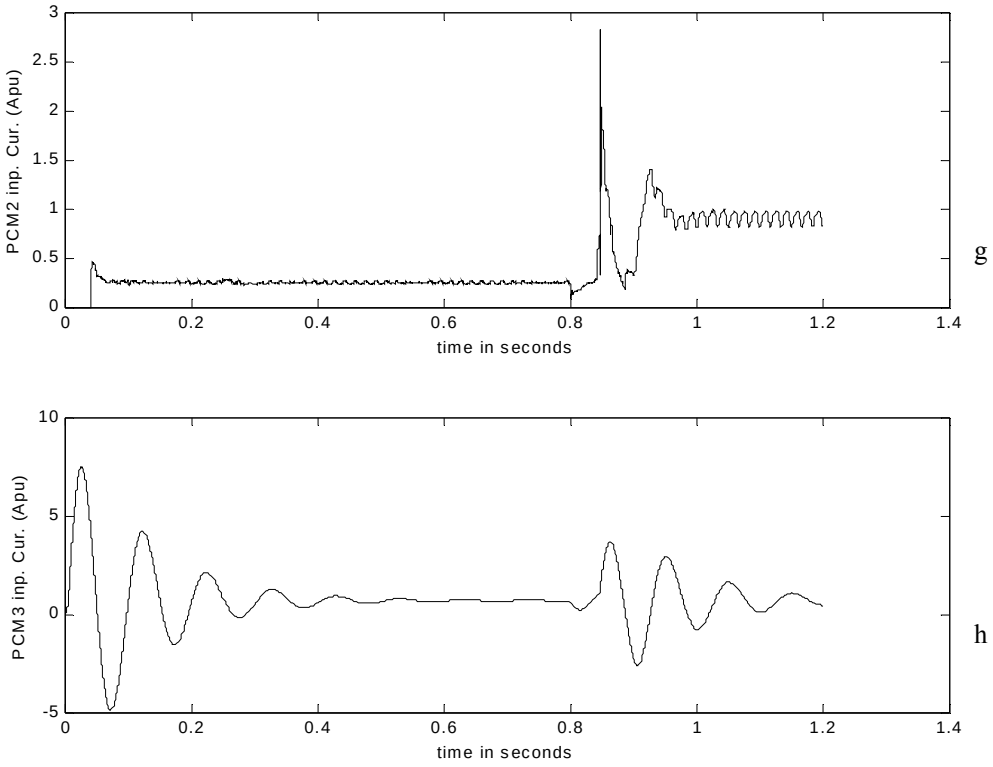


Fig. 5.12 Continued. g) Starboard bus ARCP input current

h) Starboard bus buck converter input current in pu

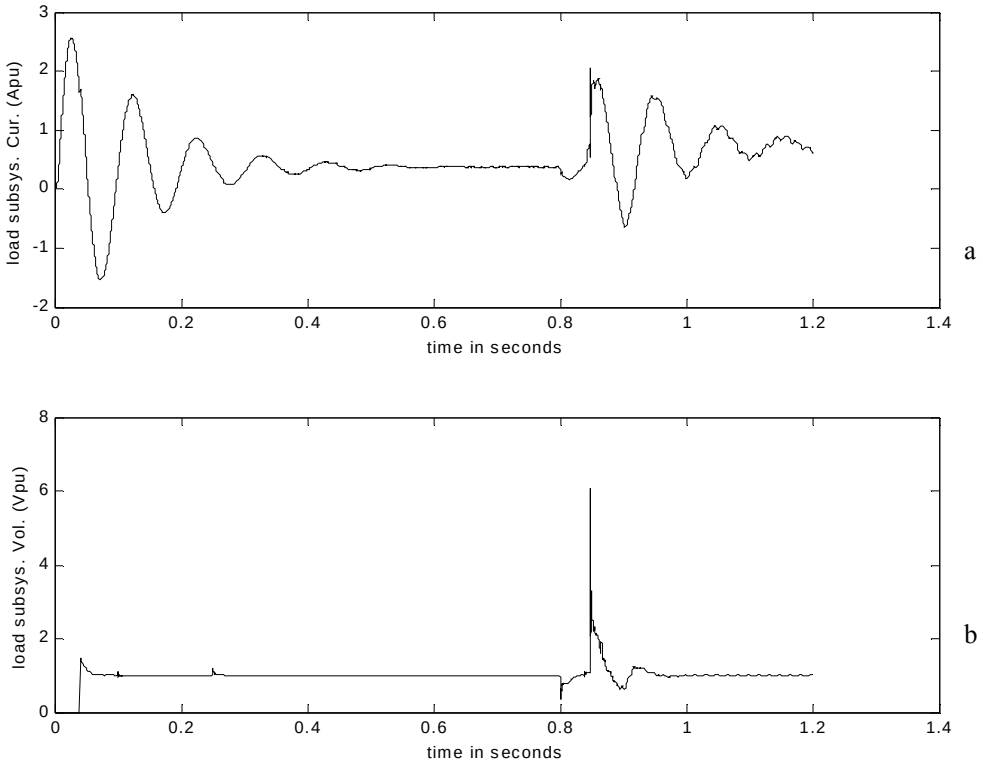


Fig. 5.13 Starboard side intrazonal bus simulation results for Scenario 3 in pu. a) Starboard bus load subsystem current in pu b) Starboard bus load subsystem voltage in pu

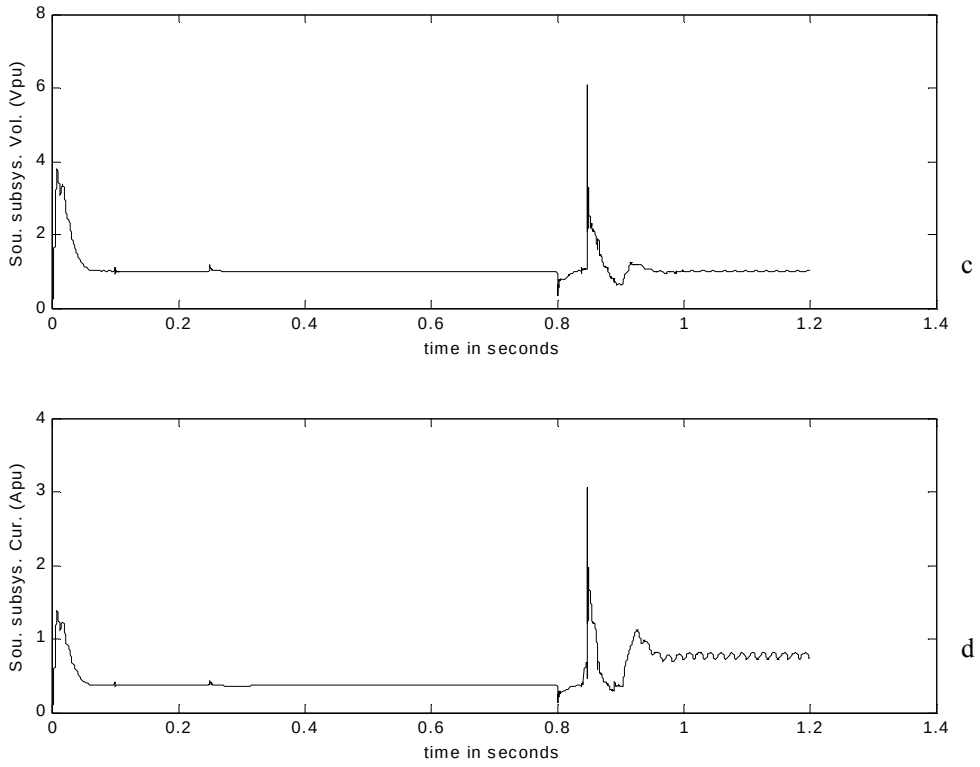


Fig. 5.13 Continued. c) Starboard bus source subsystem voltage in pu

d) Starboard bus source subsystem current in pu

5.2.6 Scenario 4

A finite RL load of impedance value 0.13-j0.079 ohms was added to the output bus of PCM 2 in parallel with the motor load on the same bus. The new load was added at 0.8 seconds into the simulation and remained in the system until end of the simulation of 1.2 seconds. The two generators saw the load instantaneously, but for inertia reasons, responded with definite time constants. During the loading and input power imbalance the system voltage dipped slightly. This dip, even though observable could not be

considered significant. The plots shown in Fig. 5.14 through Fig. 5.17 are the results of the actual scenario simulation.

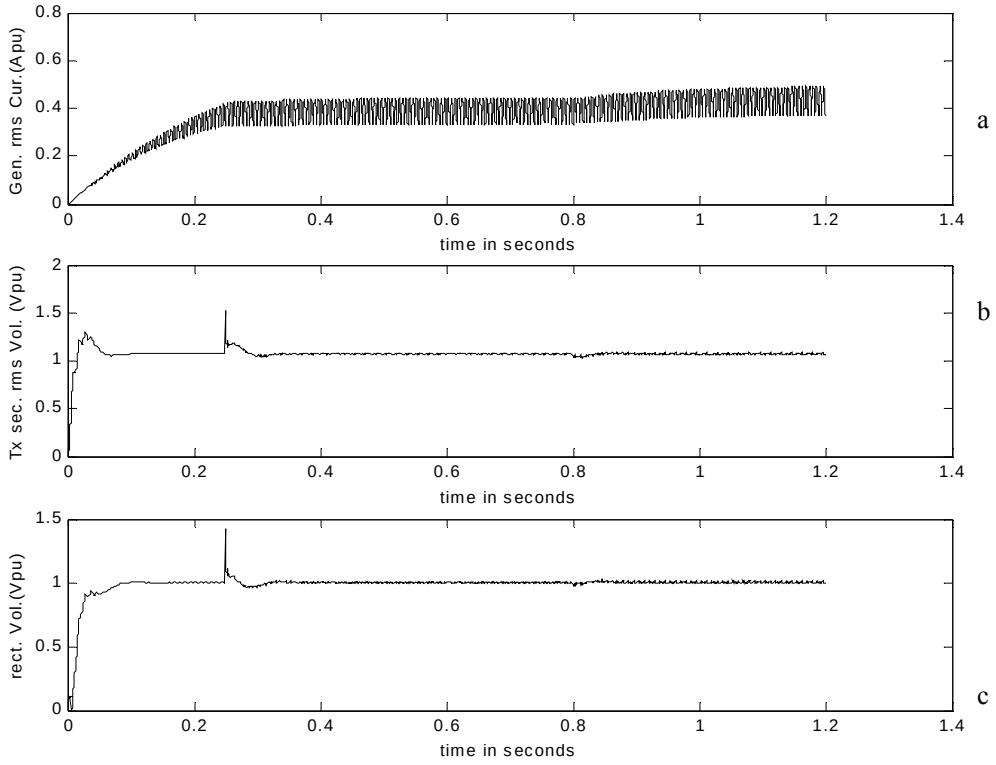


Fig. 5.14 Actual port side simulation results for Scenario 4. a) Port bus generator RMS current in pu

b) Port bus transformer RMS line to line voltage in pu

c) Port bus rectifier output voltage in pu

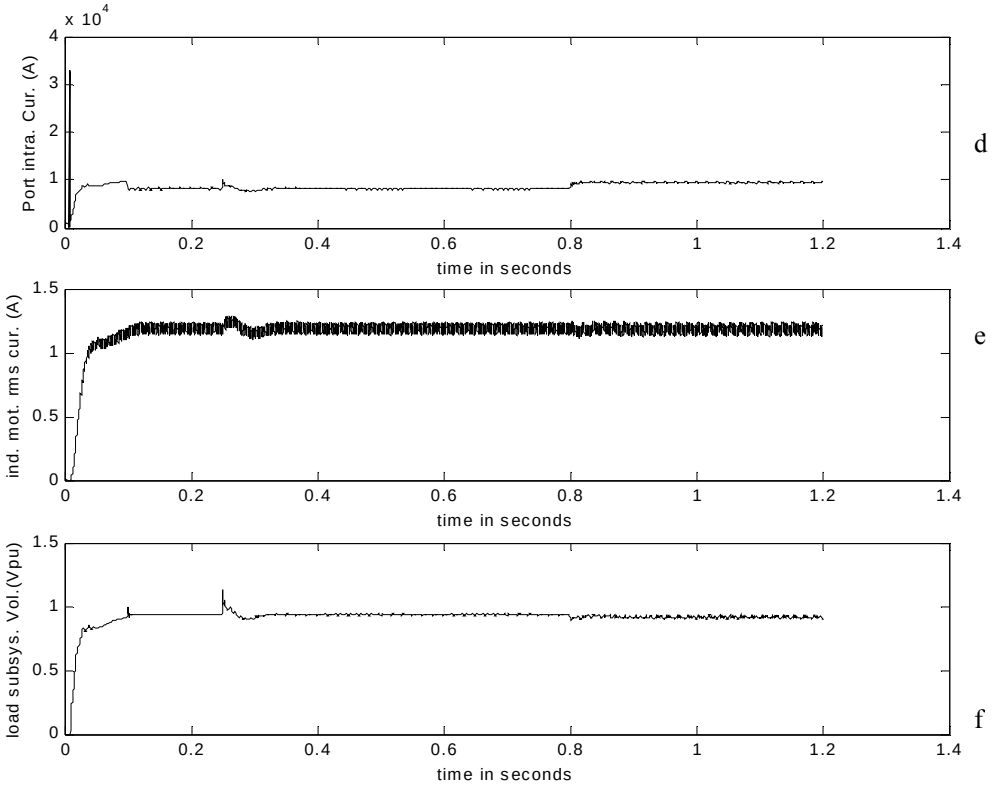


Fig. 5.14 Continued. d) Port bus dual bridge output current in actual

e) Port bus induction motor current from state variables in pu

f) Port bus load subsystem voltage in pu

All signals show signs of stability, which indicates that loading poses no problem in this system. The system responses can be seen for this scenario, which is loading at values corresponding to the onset of large signal disturbance, to be as expected. More system responses shown in Fig. 5.14e through Fig. 5.14h, are as expected.

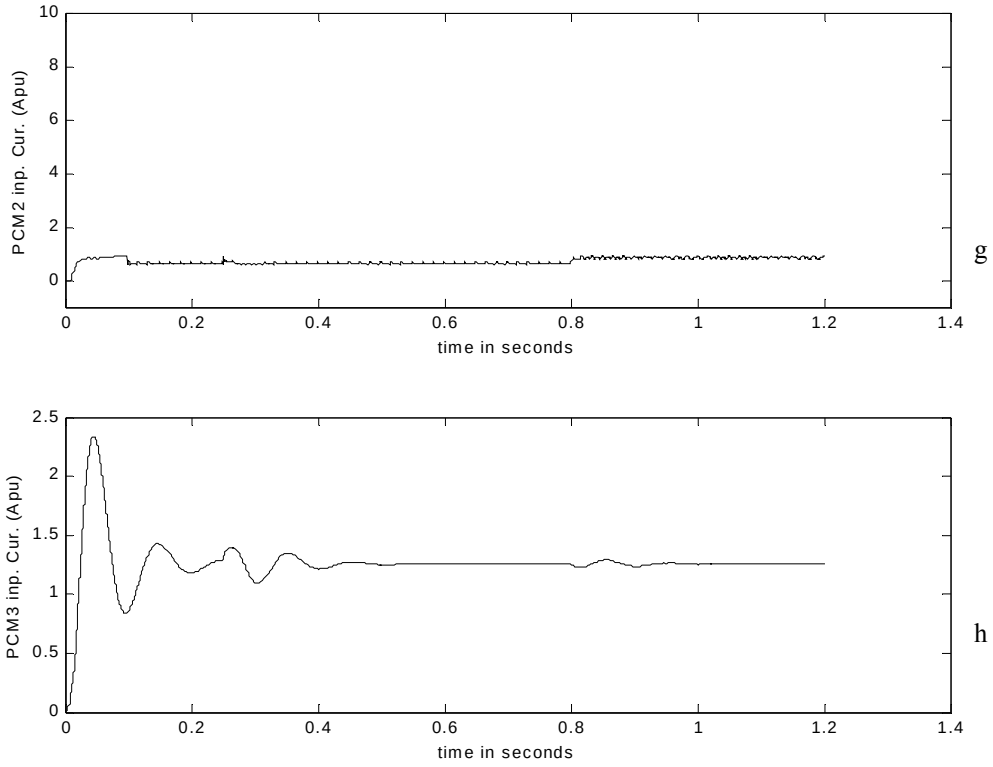


Fig. 5.14 Continued. g) Port bus ARCP input current in pu

h) Port bus buck converter current in pu

The waveforms of interest are presented in pu in Fig. 5.15a through Fig. 5.15d. They show that the 15 percent additional loading on the port bus is not a problem in the system. The starboard bus signals show no change from preloading to post loading as was expected since the loading was within capacity and only on the port bus. The signals are presented in Fig. 5.16a through Fig. 5.16h. The analogous set of signals in Fig. 5.15

(for the starboard bus) are presented in Fig. 5.17a through Fig. 5.17d in pu. They show the unperturbed nature of the starboard bus to this scenario of reconfiguration.

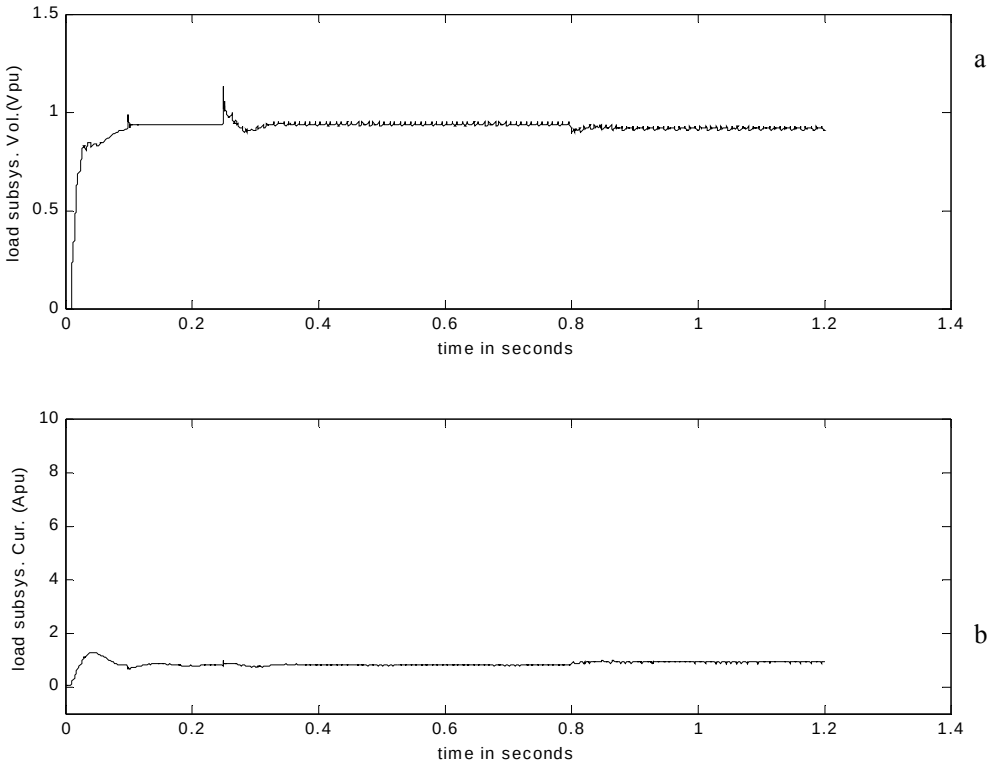


Fig. 5.15 Port side intrazonal bus simulation results for Scenario 4 in pu. a) Port bus load subsystem voltage in pu b) Port bus load subsystem input current in pu

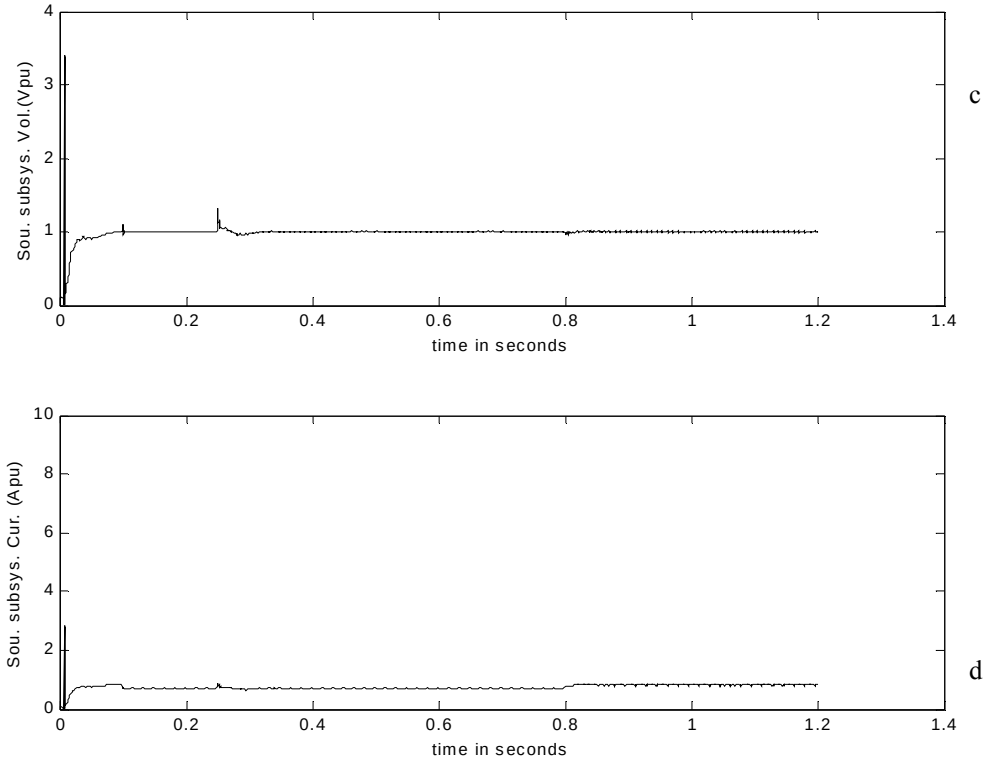


Fig. 5.15 Continued. c) Port bus source subsystem output voltage in pu

d) Port bus source subsystem output current in pu

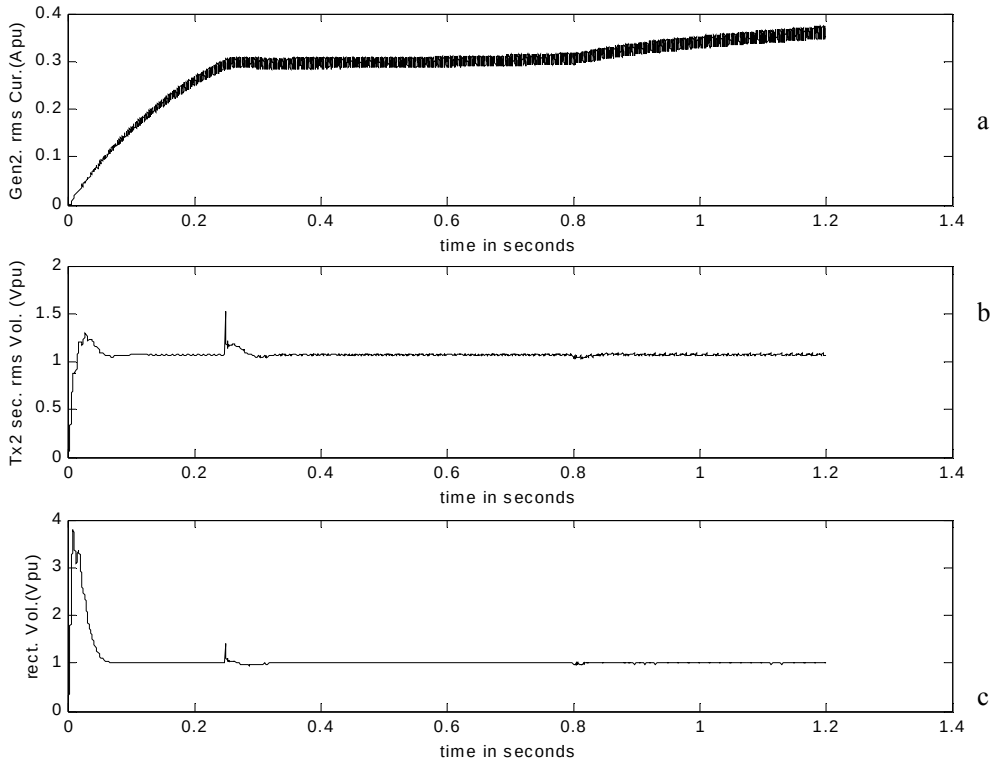


Fig. 5.16 Actual starboard side simulation results for Scenario 4. a) Starboard bus generator RMS current in pu b) Starboard bus transformer line to line voltage RMS in pu

c) Starboard bus rectifier output voltage in pu

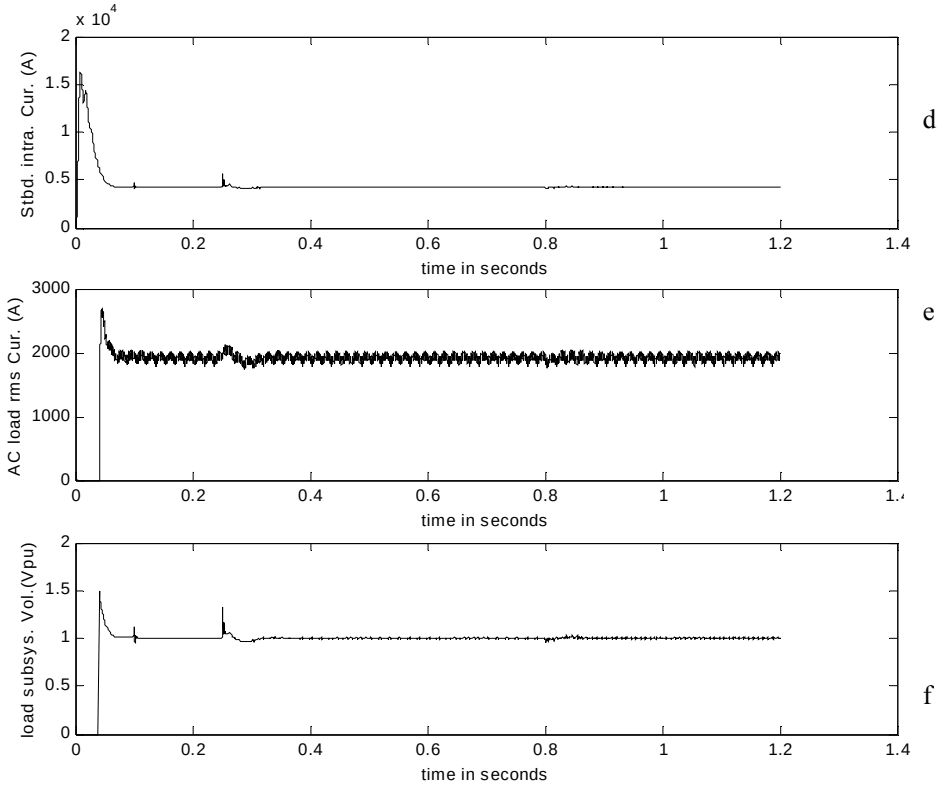


Fig. 5.16 Continued. d) Starboard bus dual bridge output current actual

e) Starboard bus AC RL load current in RMS actual

f) Starboard bus load subsystem voltage in pu

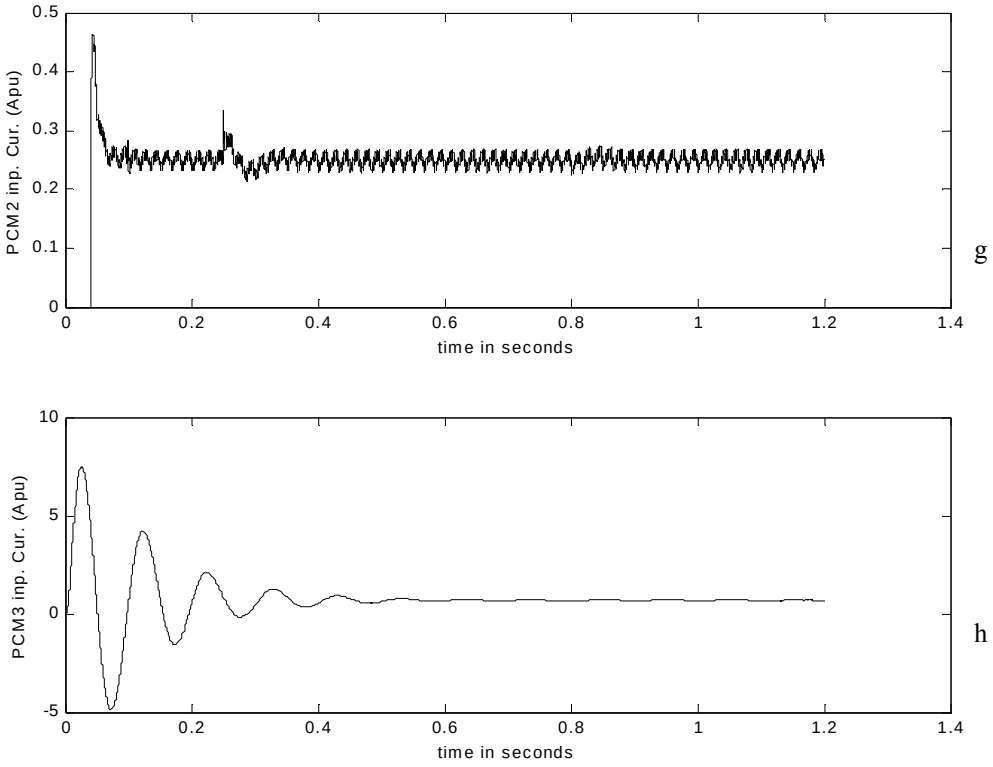


Fig. 5.16 Continued. g) Starboard bus ARCP input current in pu

h) Starboard bus buck converter input current in pu

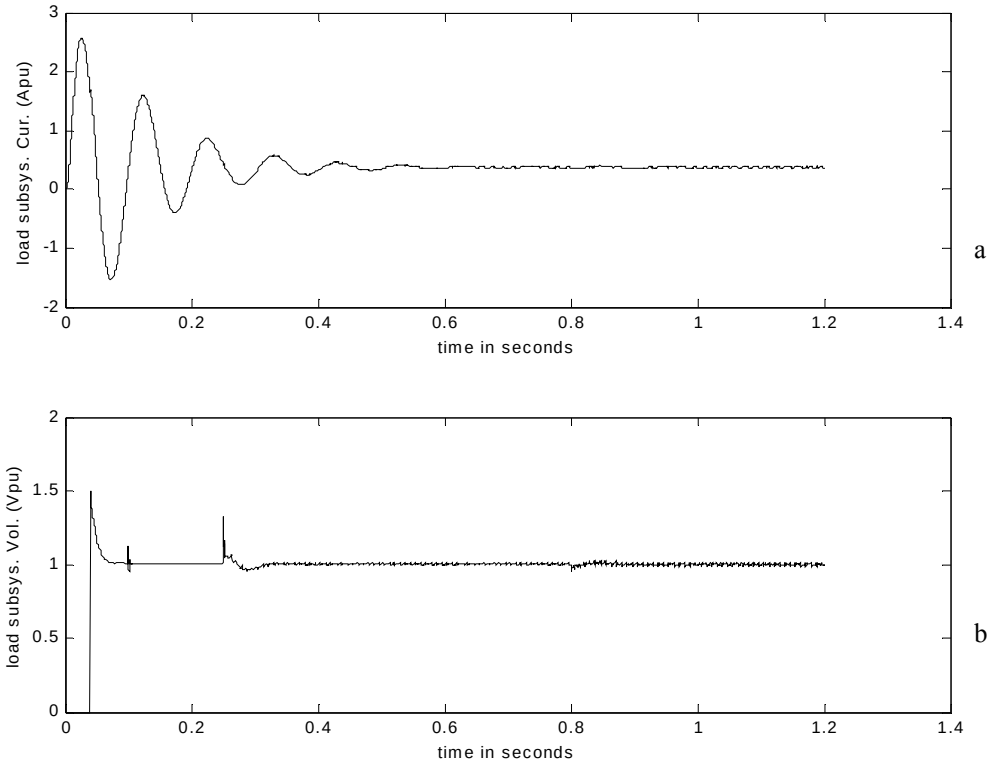


Fig. 5.17 Starboard side intrazonal bus simulation results for Scenario 4 in pu. a) Starboard bus load subsystem current in pu b) Starboard bus load subsystem voltage in pu

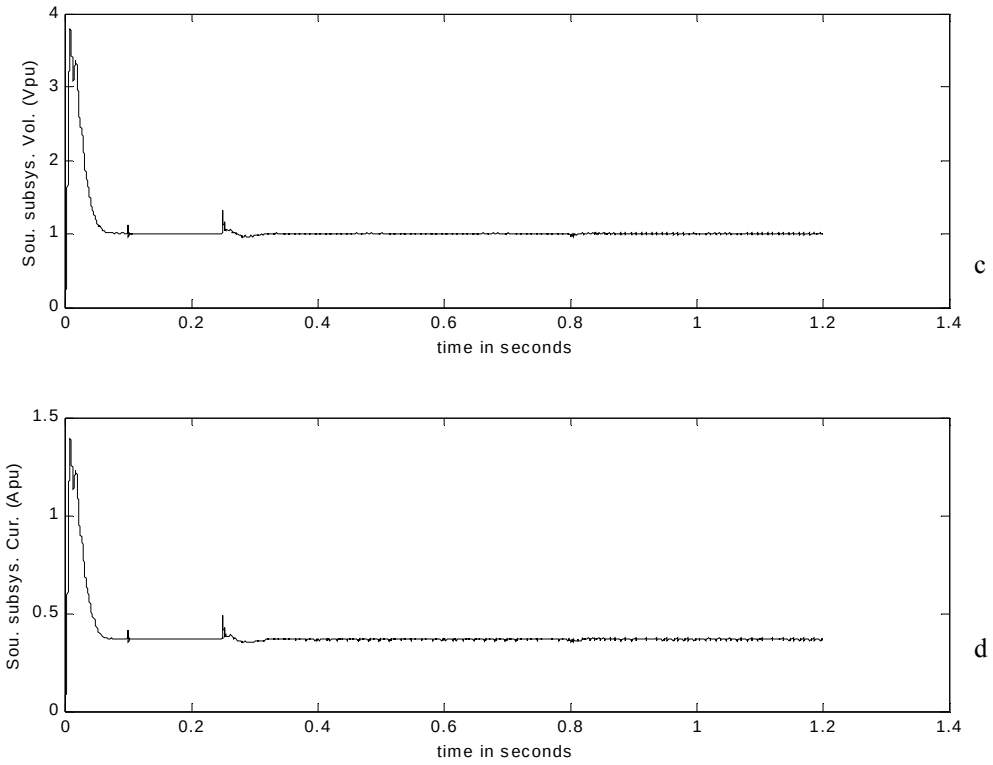


Fig. 5.17 Continued. c) Starboard bus source subsystem output voltage in pu

d) Starboard bus source subsystem output current in pu

### 5.2.7 Scenario 5

For investigation into overload situations during reconfiguration, an AC load was added to the output of the PCM 2 on the port bus in parallel with the induction motor. The AC load made the loading on the Port bus an overload of 150 percent. The static AC Load was added at 0.8seconds into the simulation, and left till protection operated disconnecting the overload. The load addition caused a momentary voltage dip in the system with incomplete recovery of load bus voltage to 372.65Volts RMS (line to line)

at the motor. The bus transfer operation for the induction motor is automatic, but the induction motor did not change to the alternate path, in this case, at the load addition. The plots shown in Fig. 5.18 through Fig.5.21 show the results of the actual scenario simulation.

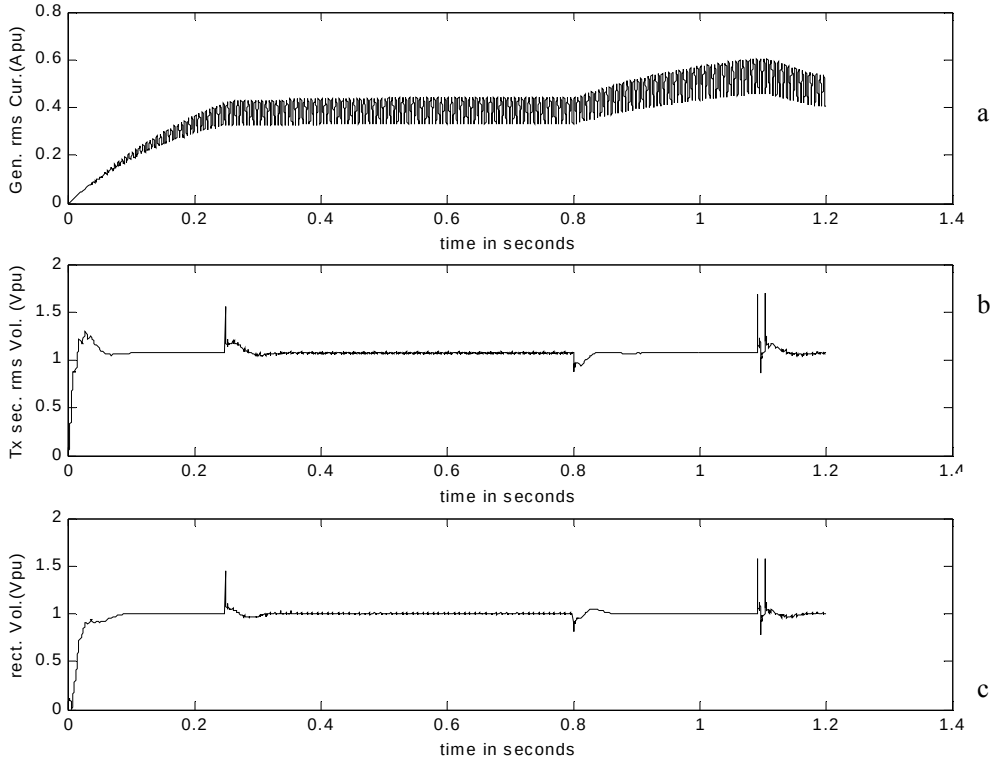


Fig. 5.18 Actual port side simulation results for Scenario 5. a) Port bus generator RMS current in pu

b) Port bus transformer RMS line to line voltage in pu

c) Port bus rectifier output voltage in pu

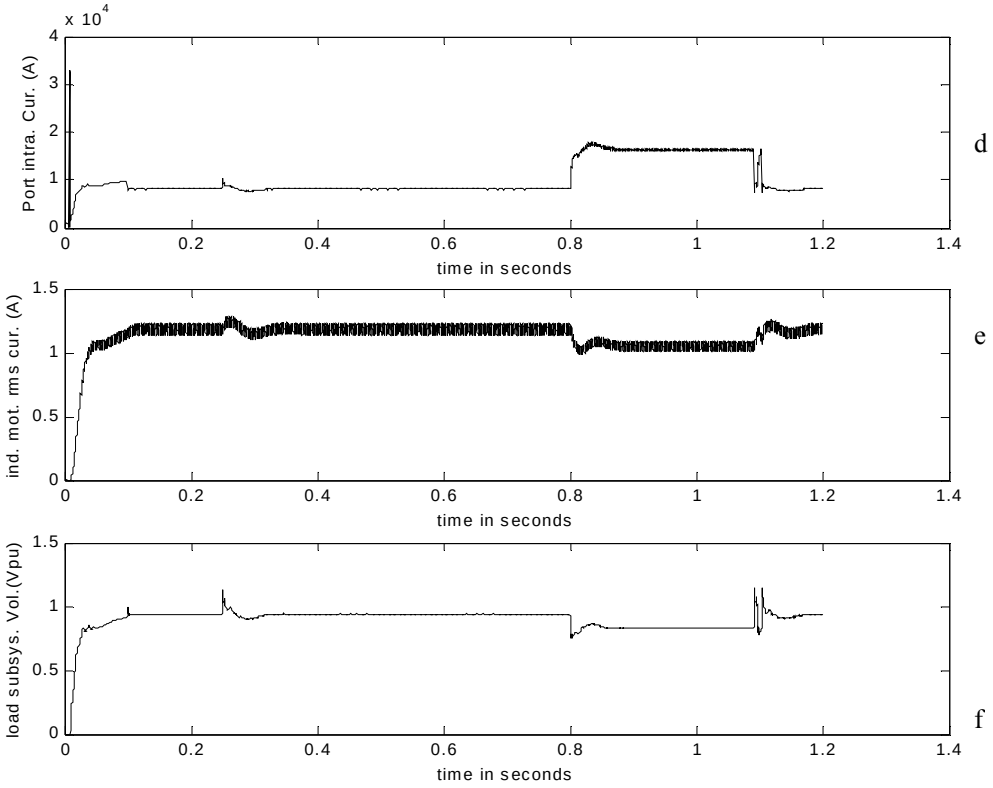


Fig. 5.18 Continued. d) Port bus dual bridge output current in actual

e) Port bus induction motor current from state variables in pu

f) Port bus load subsystem voltage in pu

The behavior in Scenario 5 was as expected with the circuit breaker upstream the load added tripping to isolate the load There was a dip in system voltage due to the loading but the dip was not sufficient to cause ABT operation. The rest of the port side signals are presented in Fig. 5.18e through Fig. 5.18h. Signals of interest to be used for the stability assessment are presented in per unit basis in Fig. 5.19a through Fig. 5.19d.

They comprise the output signals to the PCM1 and the input signals to PCM2 and PCM3.

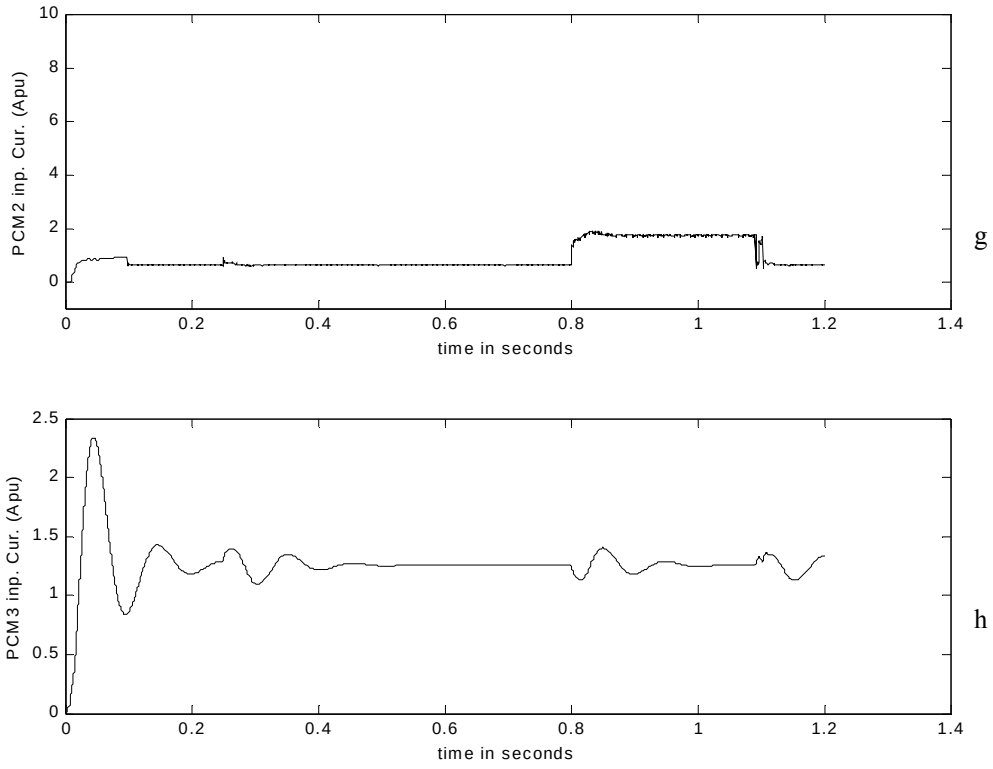


Fig. 5.18 Continued. g) Port bus ARCP input current in pu

h) Port bus buck converter current in pu

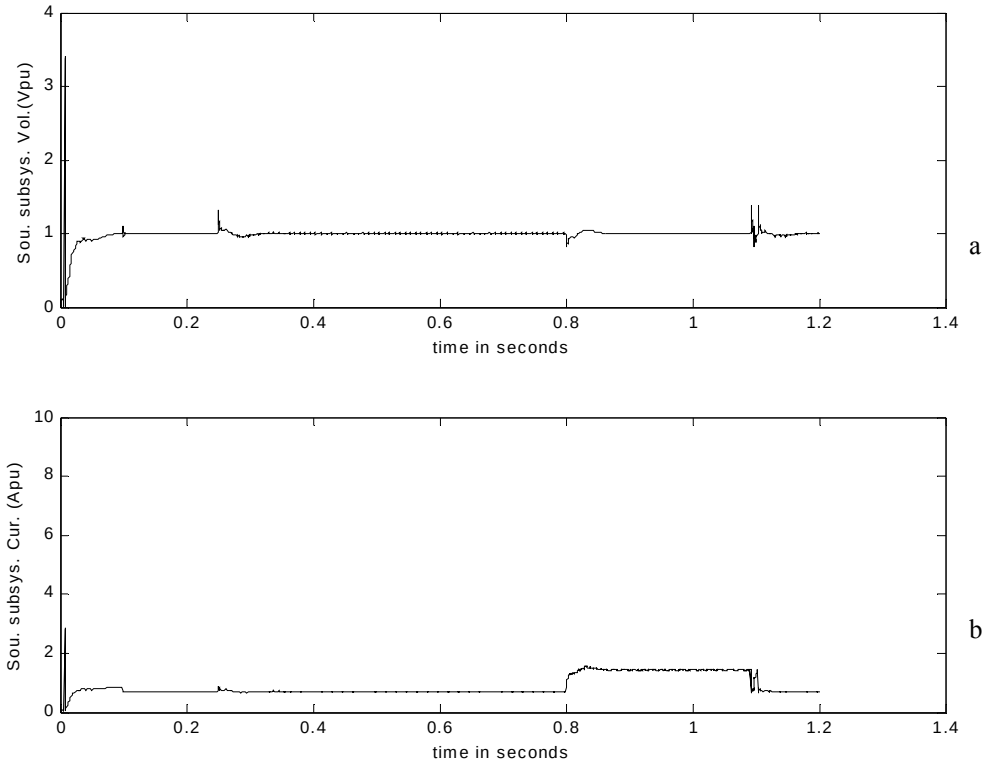


Fig. 5.19 Port side intrazonal bus simulation results for Scenario 5 in pu a) Port bus load subsystem voltage in pu b) Port bus load subsystem input current in pu

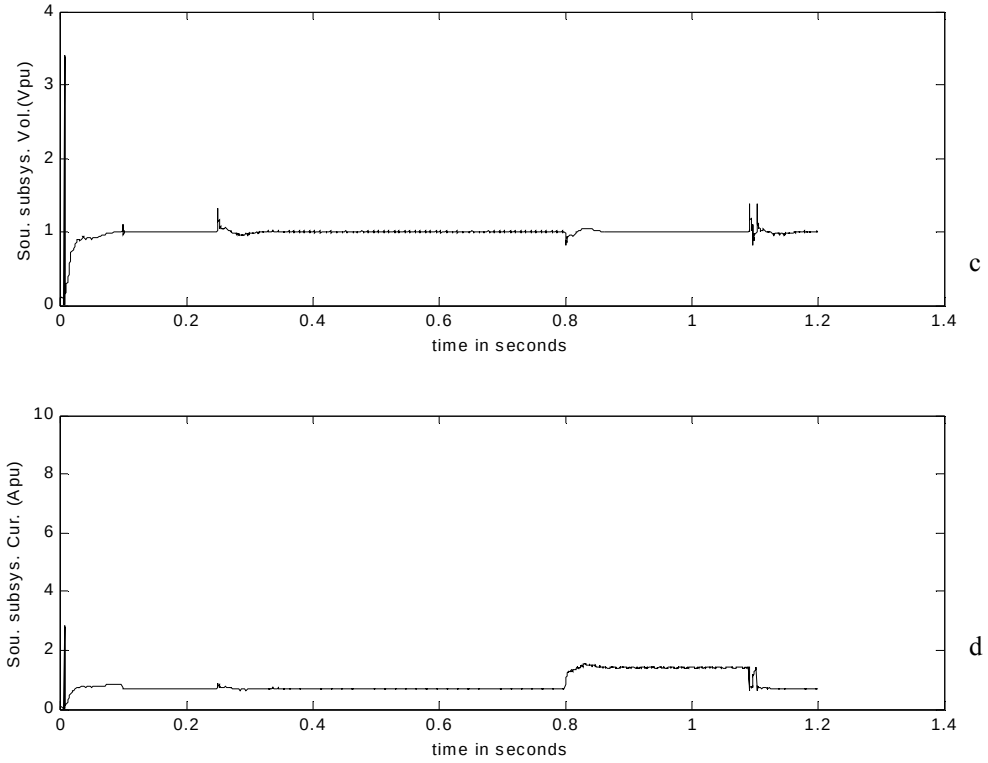


Fig. 5.19 Continued. c) Port bus source subsystem output voltage in pu

d) Port bus source subsystem output current in pu

The starboard side signals are presented in Fig. 5.20a through Fig. 5.20h. Since there was no transfer of the induction motor to the starboard side, the profiles of the starboard side were largely undisturbed. The signals were as expected. The analogous signals to the signals of interest from the starboard side are presented in Fig. 5.21a through Fig. 5.21d. They are not used in stability assessment but are used for observing comparable behavior of port and starboard sides.

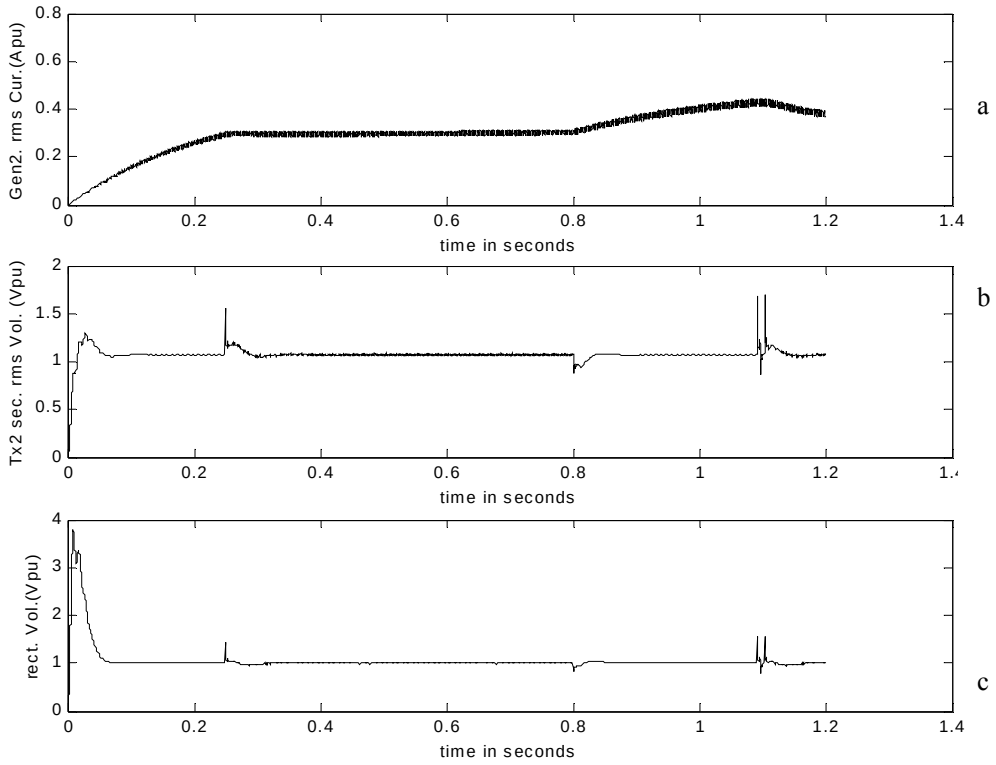


Fig. 5.20 Actual starboard side simulation results for Scenario 5. a) Starboard bus generator RMS current in pu b) Starboard bus transformer line to line voltage RMS in pu

c) Starboard bus rectifier output voltage in pu

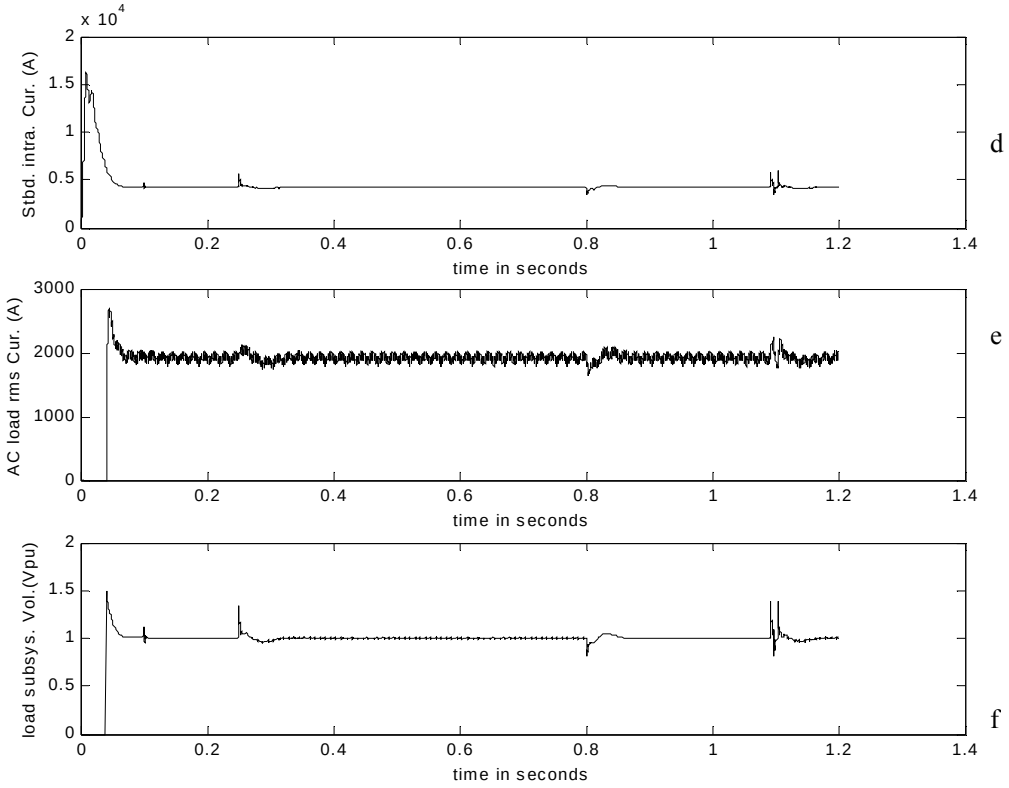


Fig. 5.20 Continued. d) Starboard bus dual bridge output current actual

e) Starboard bus AC RL load current in RMS actual

f) Starboard bus load subsystem voltage in pu

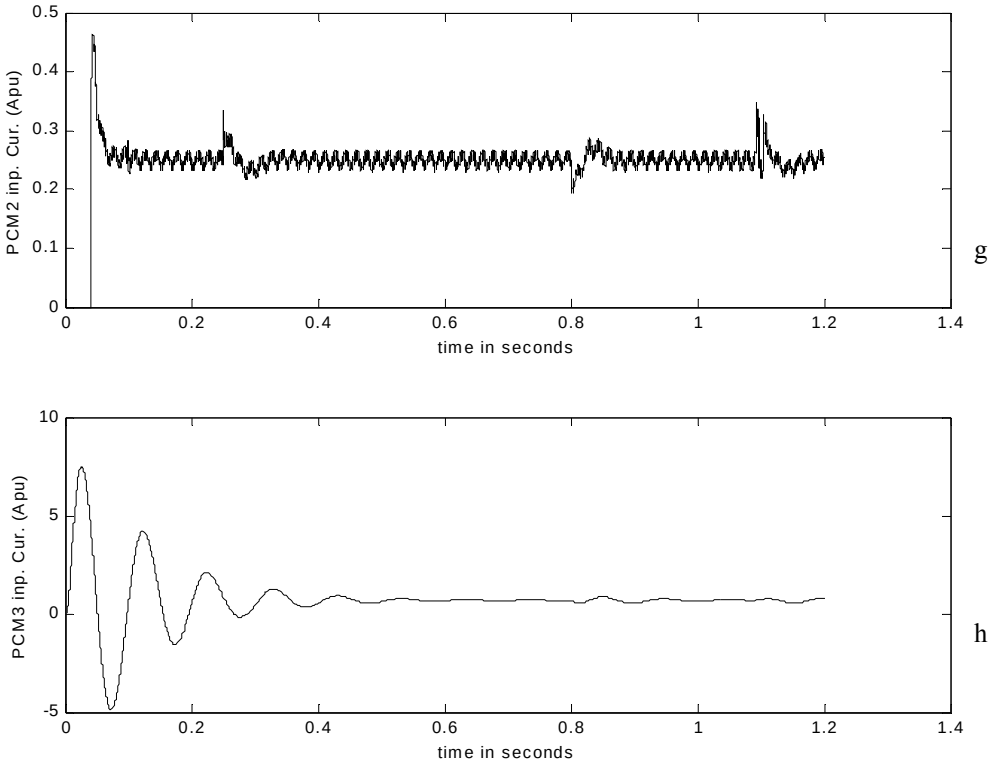


Fig. 5.20 Continued. g) Starboard bus ARCP input current in pu

h) Starboard bus buck converter input current in pu

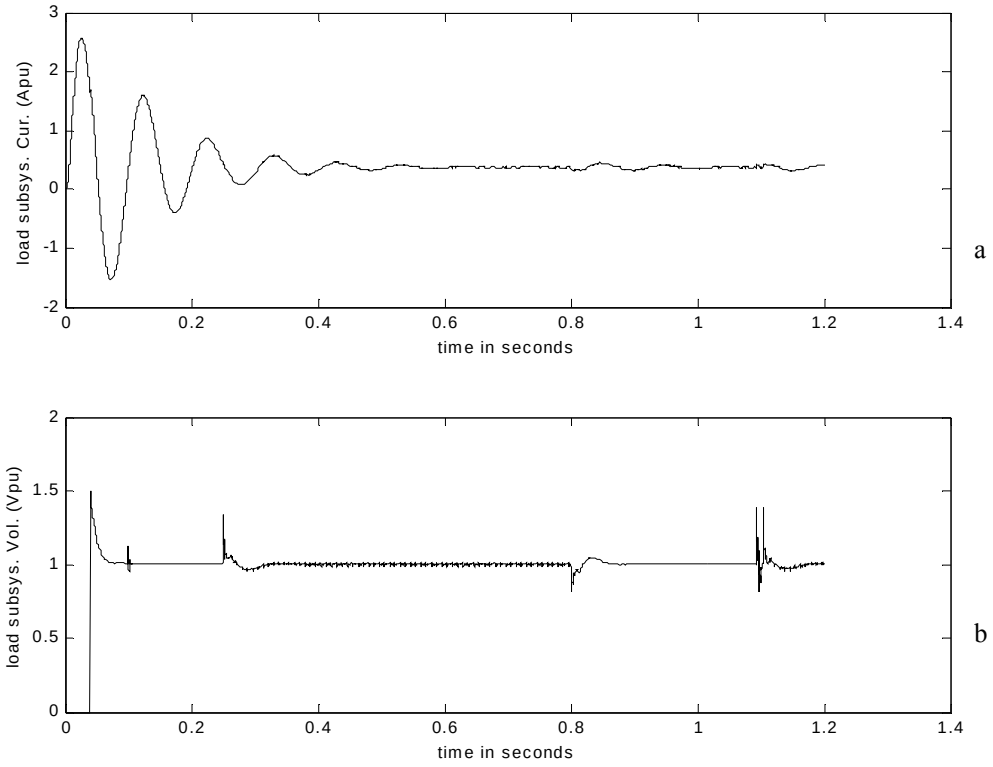


Fig. 5.21Starboard side intrazonal bus simulation results for Scenario 5 in pu. a) Starboard bus load subsystem current in pu b) Starboard bus load subsystem input voltage in pu

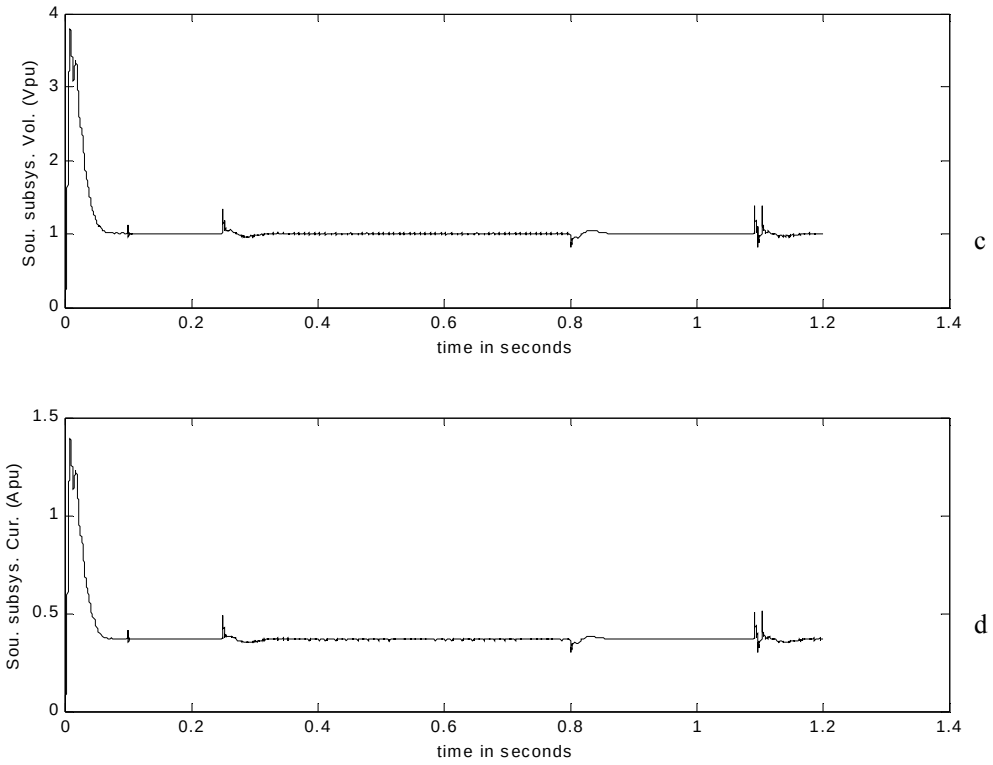


Fig. 5.21 Continued. c) Starboard bus source subsystem output voltage in pu

d) Starboard bus source subsystem output current in pu

### 5.2.8 Scenario 6

The operation of the test system at critical loading was investigated in this scenario. The 775VDC port bus was loaded with AC static load to 100 percent of rated load at 0.8 seconds into the simulation and the new AC static load remained in the system until the end of the simulation at 1.2 seconds. The per phase impedance of the AC static load added was 0.06417-j0.03977 ohms. The plots shown in Fig. 5.22 through Fig. 5.25 represent the results of the actual scenario simulation.

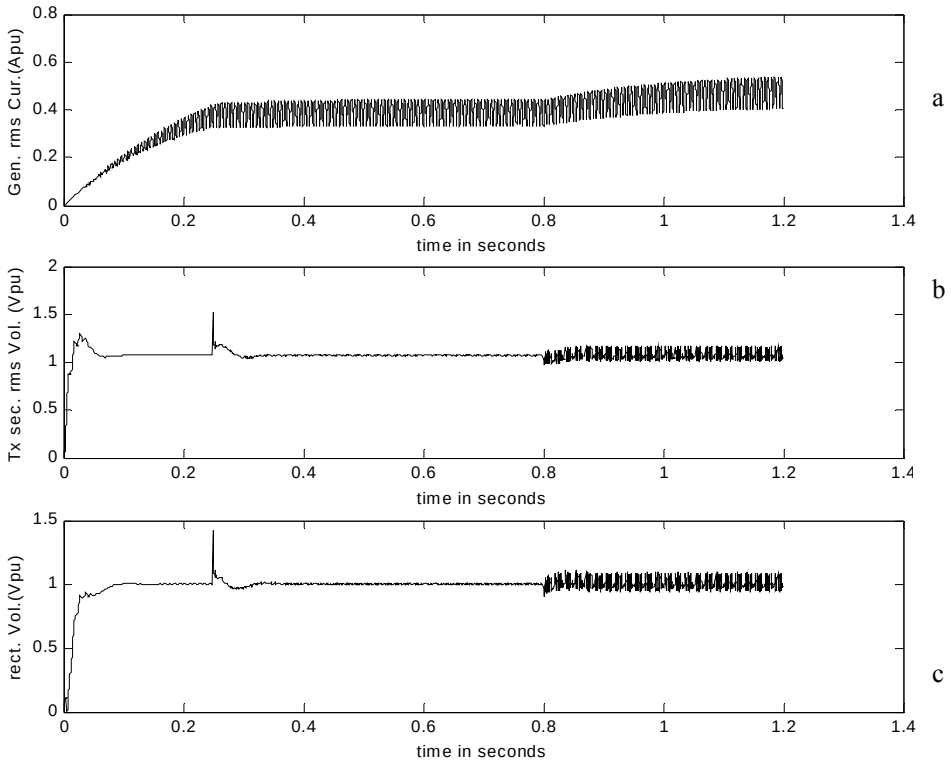


Fig. 5.22 Actual port side simulation results for Scenario 6. a) Port bus generator RMS current in pu

b) Port bus transformer RMS line to line voltage in pu

c) Port bus rectifier output voltage in pu

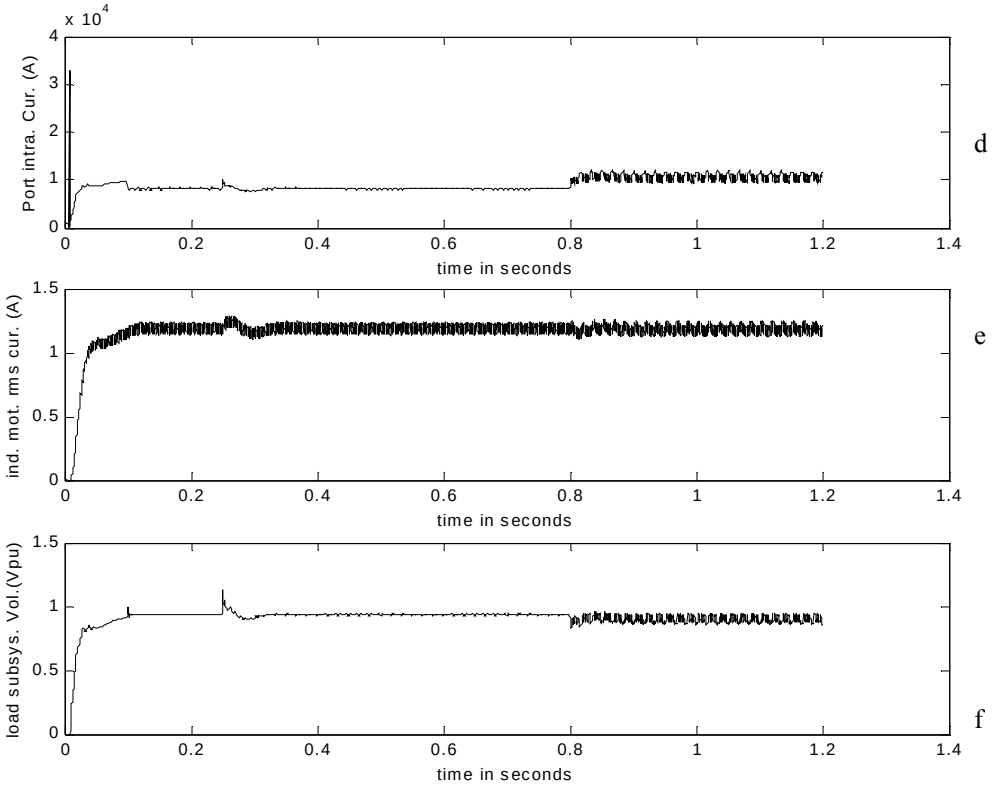


Fig. 5.22 Continued. d) Port bus dual bridge output current in actual

e) Port bus connected induction motor current from state variables in pu

f) Port bus load subsystem voltage in pu

The loading, even though it makes the loading critical, does not pose a problem in the system. It was found, however, that the ARCP introduced noise into the system when its operating point is significantly changed. This can be seen in the noise in the post reconfiguration signals in Fig. 5.22a through Fig. 5.22d. It was observed that when the load was added there was a slight dip in system voltage but this was not sufficient to

cause any protective device to operate. (This is concerning the operation of the ABT more particularly.) More system responses follow in Fig. 5.22e through Fig. 5.22h

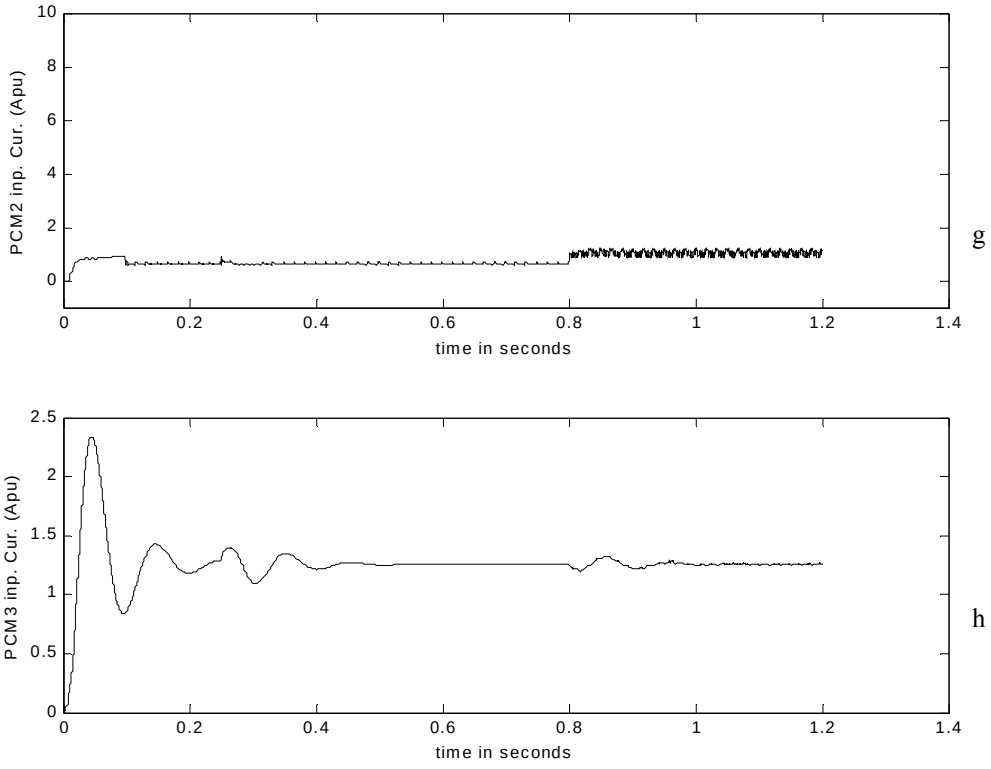


Fig. 5.22 Continued. g) Port bus ARCP input current in pu

h) Port bus buck converter current in pu

From the noise on the PCM2 input current, it is gathered that the integrity of system signals are dependent on the operating points of the various power electronic devices in the system, and reconfiguration can pose a problem to these converters when the loading change is significant. This problem can be alleviated when more adaptive controllers are

used for the converters. Apart from the noise in the ARCP with significant load change, the system can be observed to be stable. Visual perception of the signals stored and presented shows no indication of instability. The signals presented in the figures above are for the port side. An analogous set of figures are available for the star board side and the figures showing the signals of interest for the port side and their starboard side counter part follow in Fig. 5.23 through Fig. 5.25.

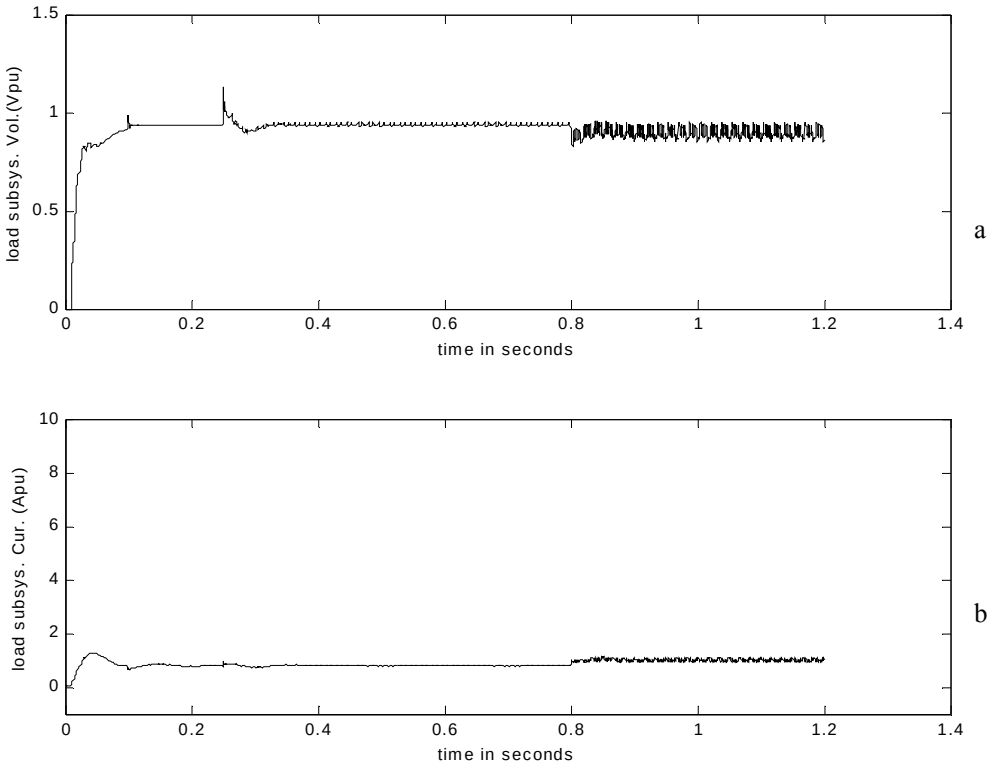


Fig. 5.23 Port side intrazonal bus simulation results for Scenario 6 in pu. a) Port bus load subsystem voltage in pu b) Port bus load subsystem input current in pu

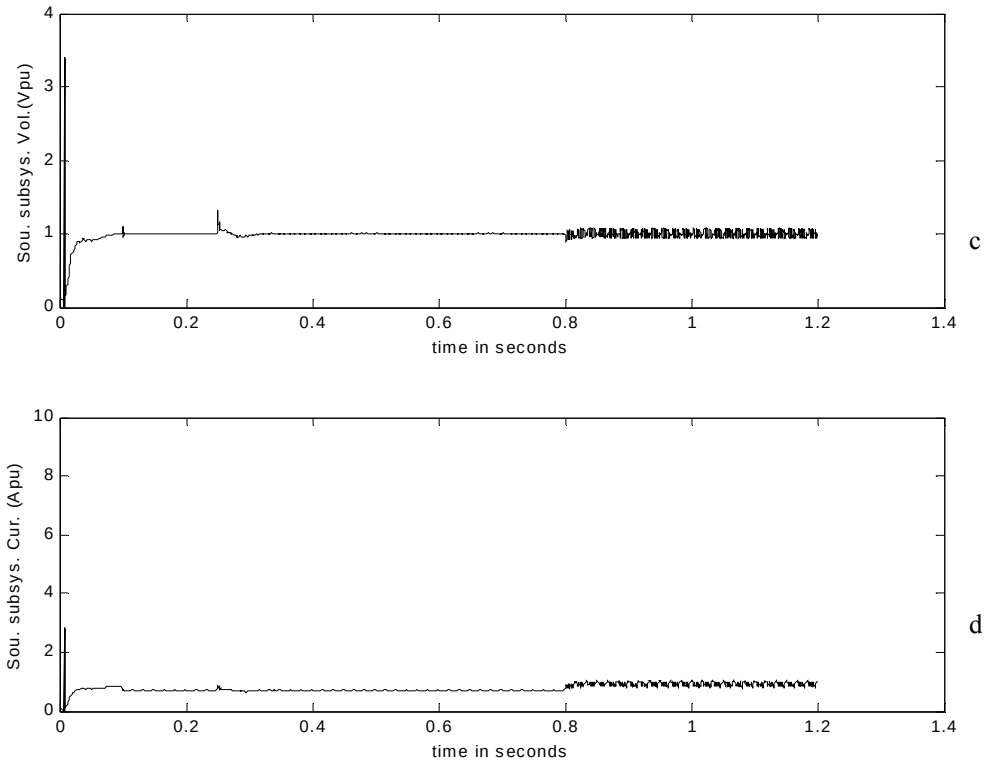


Fig. 5.23 Continued. c) Port bus source subsystem output voltage in pu

d) Port bus source subsystem output current in pu

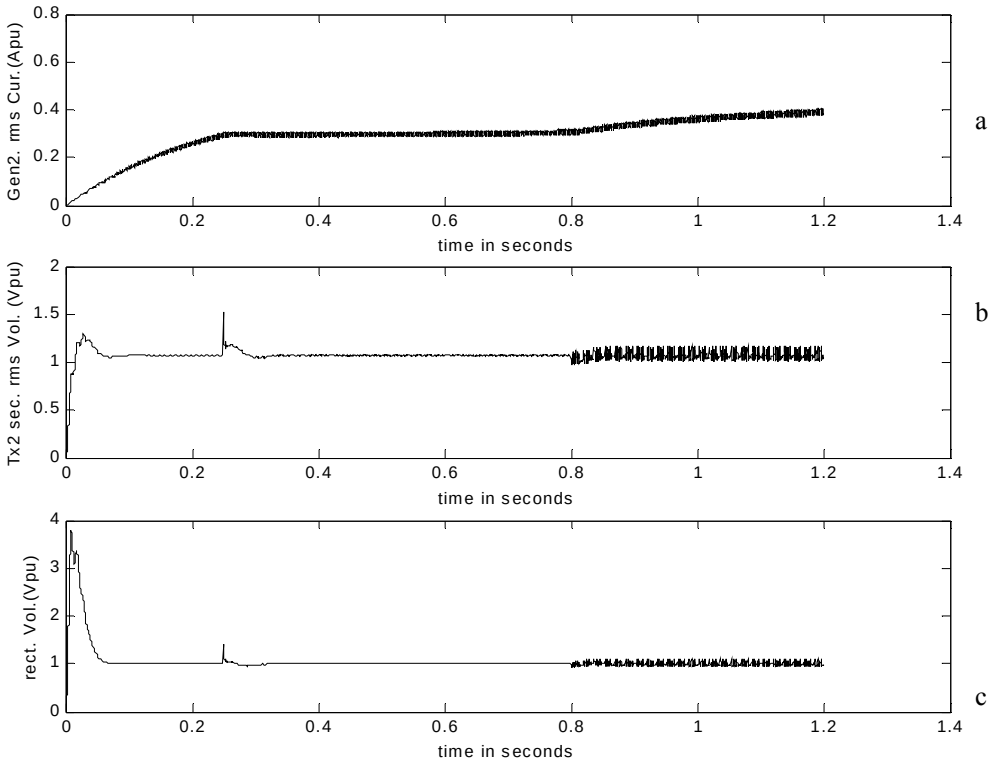


Fig. 5.24 Actual starboard side simulation results for Scenario 6. a) Starboard bus generator RMS current in pu b) Starboard bus transformer line to line voltage RMS in pu

c) Starboard bus rectifier output voltage in pu

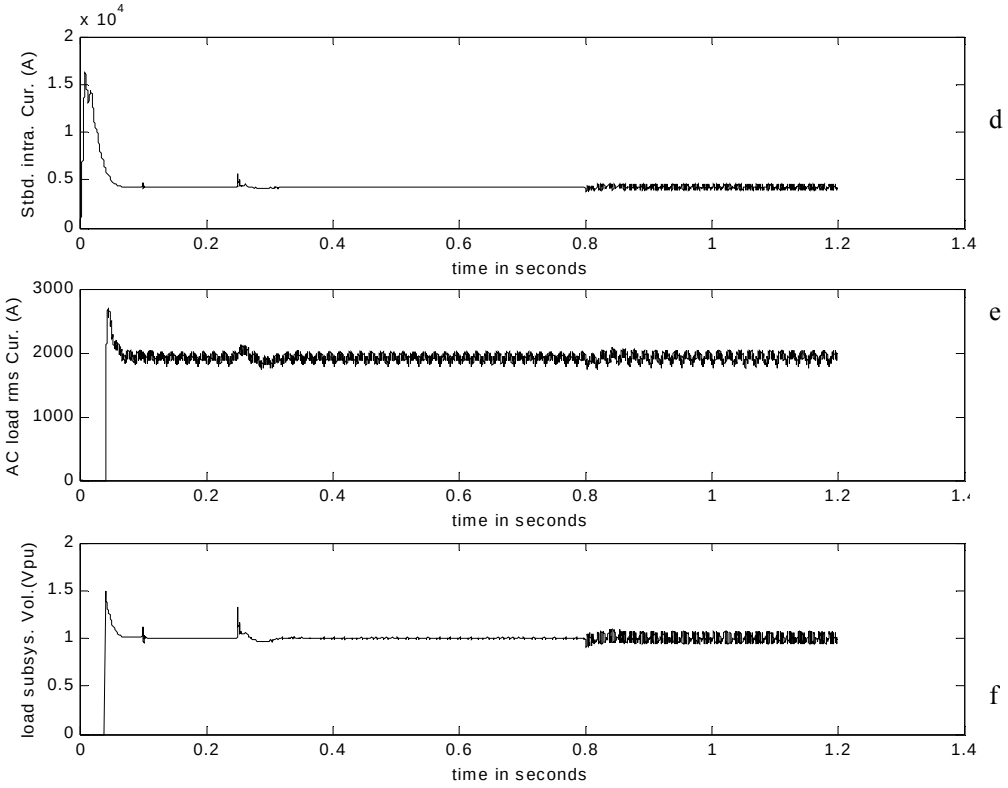


Fig. 5.24 Continued. d) Starboard bus dual bridge output current actual

e) Starboard bus AC RL load current in RMS actual

f) Starboard bus load subsystem voltage in pu

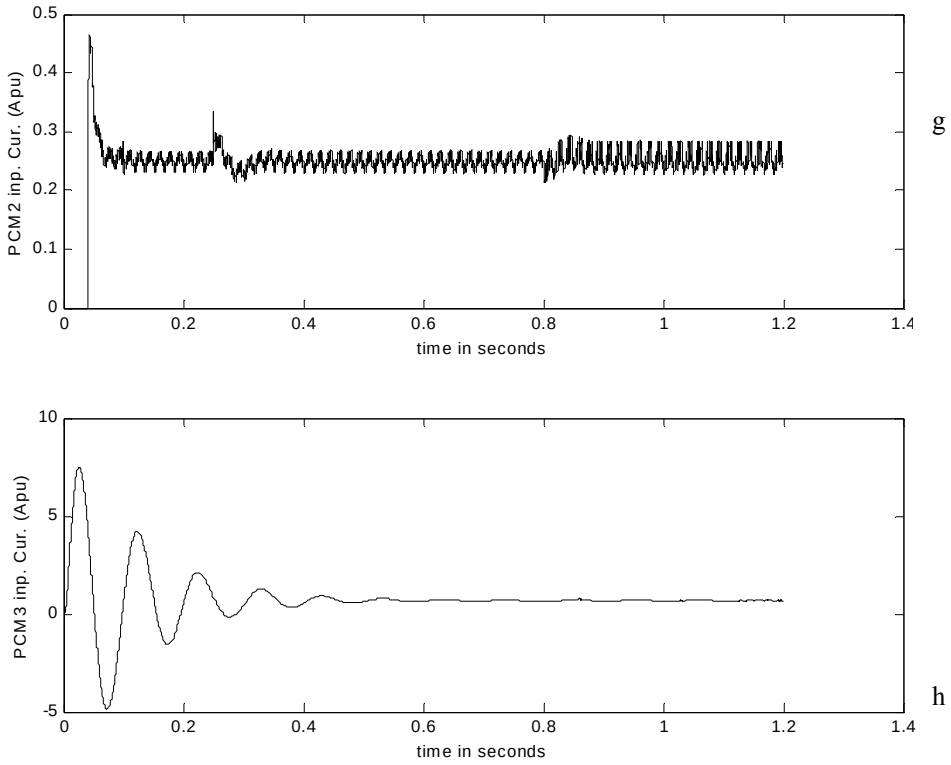


Fig. 5.24 Continued. g) Starboard bus ARCP input current in pu

h) Starboard bus buck converter input current in pu

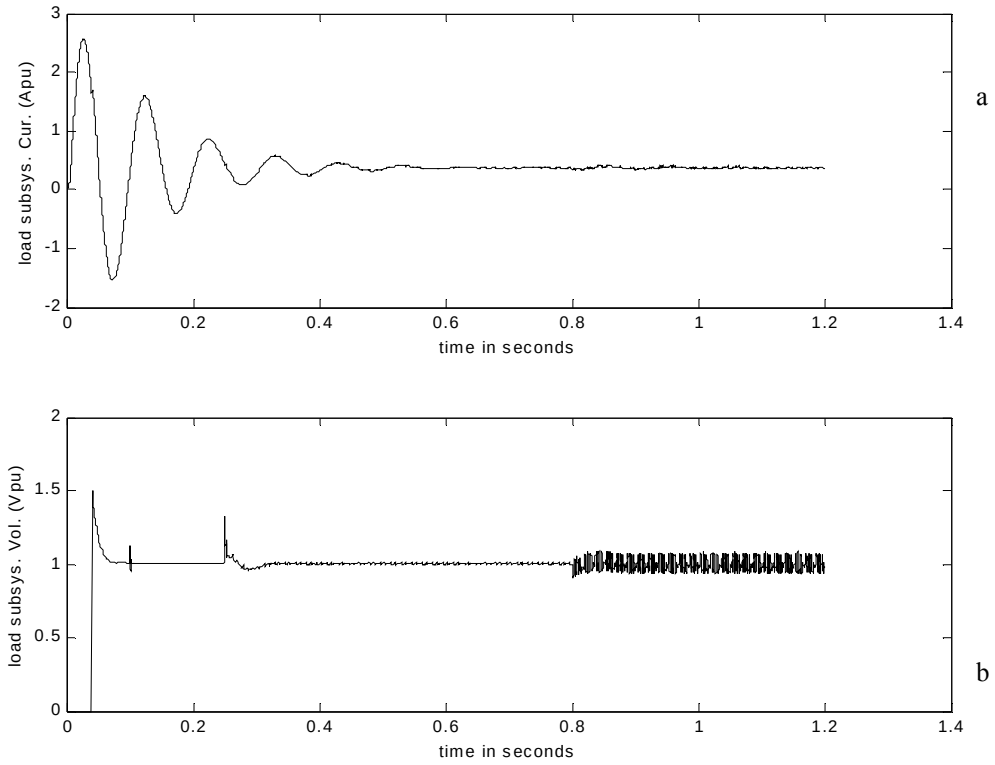


Fig. 5.25 Starboard side intrazonal bus simulation results for Scenario 6 in pu. a) Starboard bus load subsystem current in pu b) Starboard bus load subsystem voltage in pu

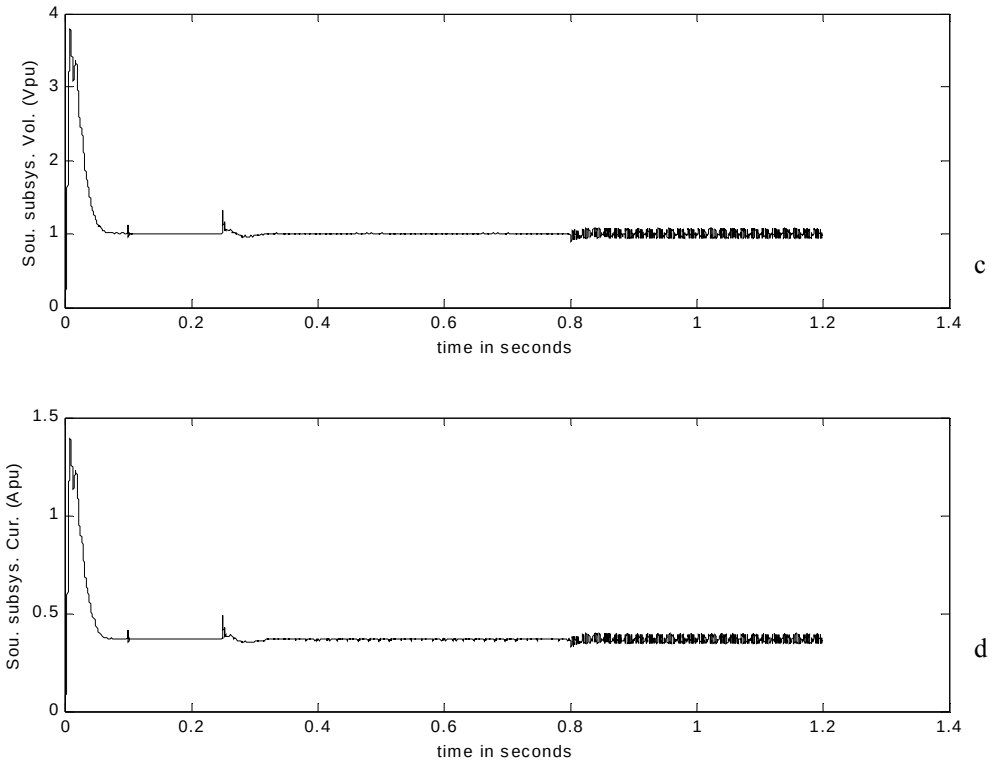


Fig. 5.25 Continued. c) Starboard bus source subsystem output voltage in pu

d) Starboard bus source output current in pu

### 5.2.9 Scenario 7

The last category of reconfiguration investigated was load shedding. The scenario investigated in Scenario 7 was a loss of load on the port side from 80 percent loading to 65 percent loading by the loss of a 15 percent AC static load on the output of the PCM2. This scenario helped to determine if the many filters in the system tolerated low level loading or loading change well. In Fig. 5.1, the intrazonal DC bus on the port side has three loads in the system. They are (1) on the output of PCM3 - a resistive load, (2) on

the output of PCM2 the static AC load and (3) on the output of the PCM2 - the motor. By dropping the AC static load, it was observed that the system responded normally as are seen in the following figures. The impedance value dropped in Scenario 7 was 0.13-j0.079 ohms. The plots of Fig. 5.26 through Fig. 5.29 show the results of the actual scenario simulation for Scenario 7.

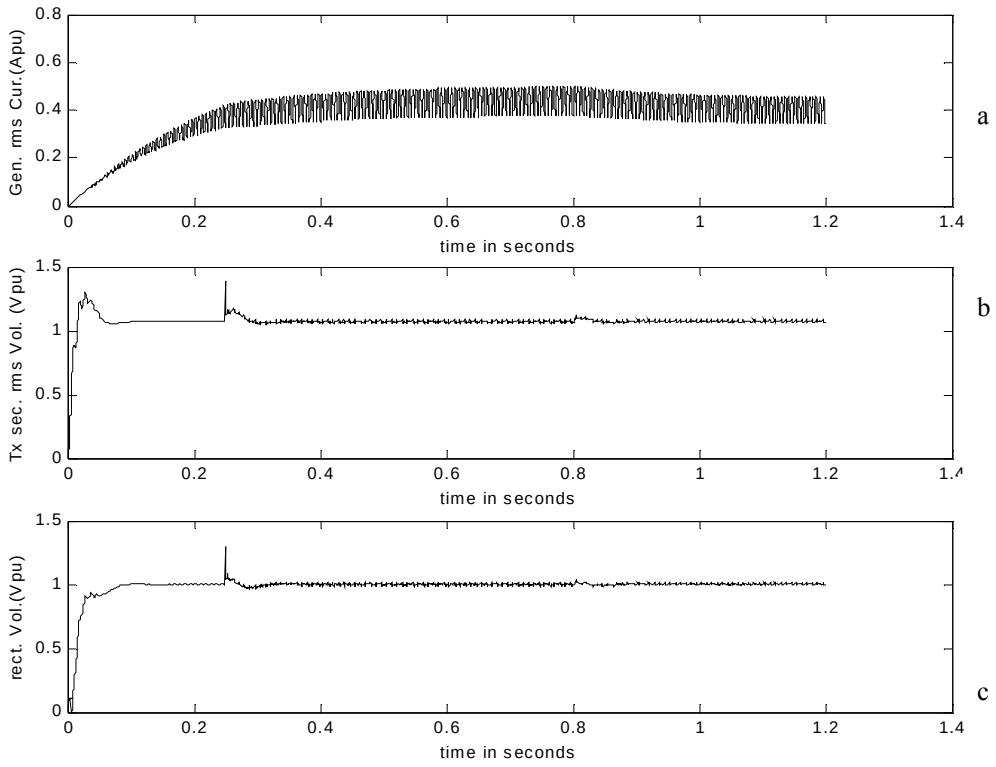


Fig. 5.26 Actual port side simulation results for Scenario 7. a) Port bus generator RMS current in pu

b) Port bus transformer RMS line to line voltage in pu

c) Rectifier output voltage in pu

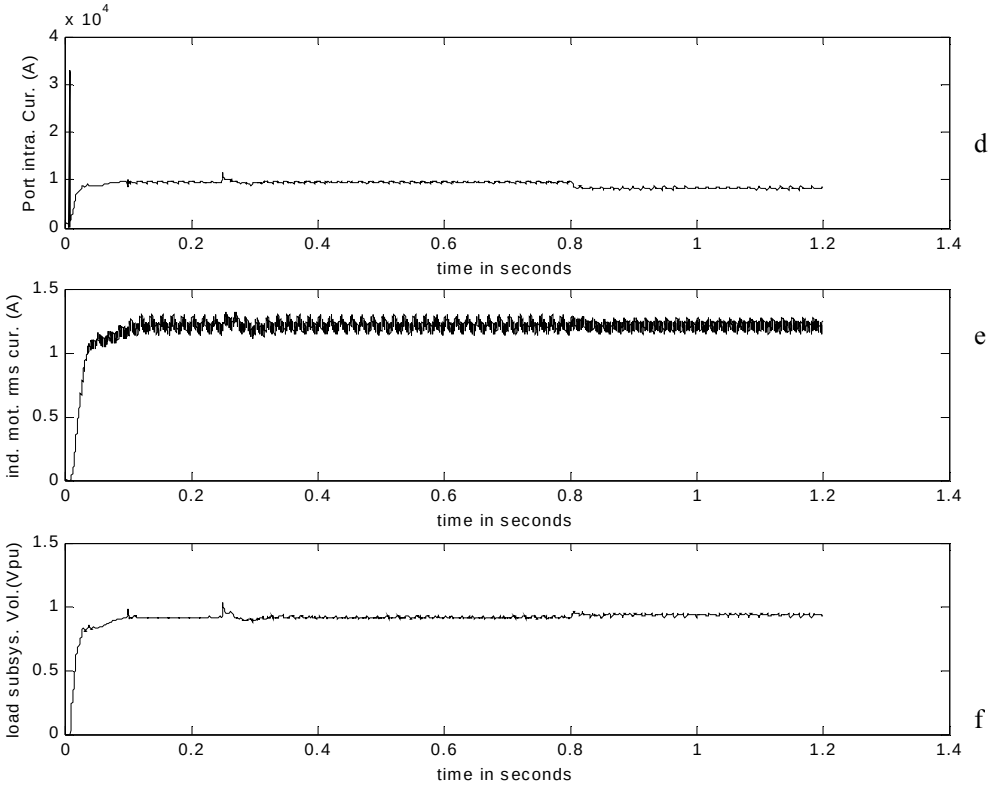


Fig. 5.26 Continued. d) Dual bridge output current in actual

e) Port bus induction motor current from state variables in pu

f) Port bus load subsystem voltage in pu

It was observed that the system responded as expected and was stable to this level of load shedding. The behaviors of the rest of the signals of the port side in this load shedding scenario are presented in Fig. 5.26e through Fig. 5.26h. The signals of interest shows that the system is stable for this scenario with the excursions in the signals to reflect the reconfiguration action as expected. The signals of interest on the port side are presented in per unit form in Fig. 5.27a through Fig5.27d.

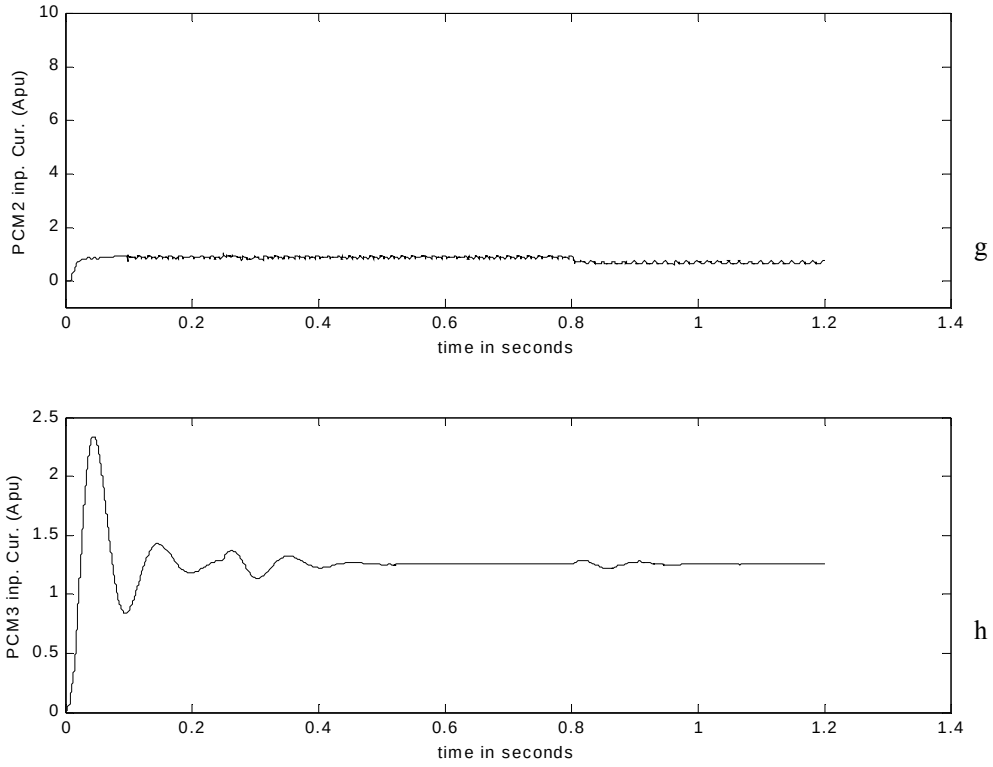


Fig. 5.26 Continued. g) Port bus ARCP input current in pu

h) Port bus buck converter current in pu

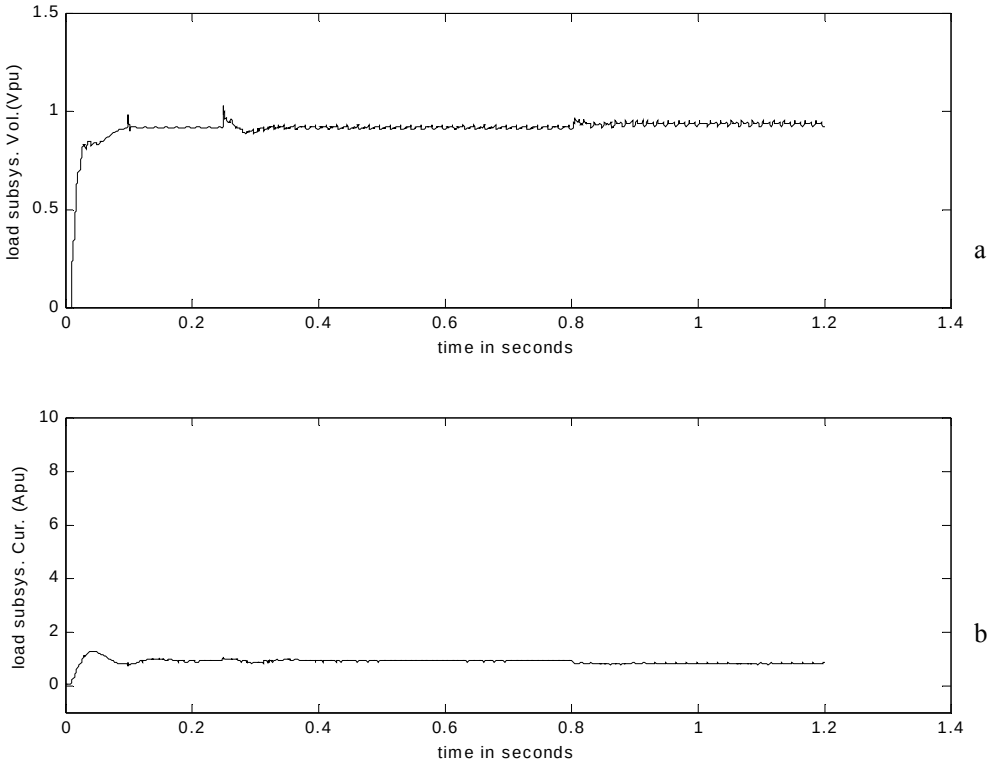


Fig. 5.27 Port side intrazonal bus simulation results for Scenario 7 in pu. a) Port bus load subsystem voltage in pu b) Port bus load subsystem input current in pu

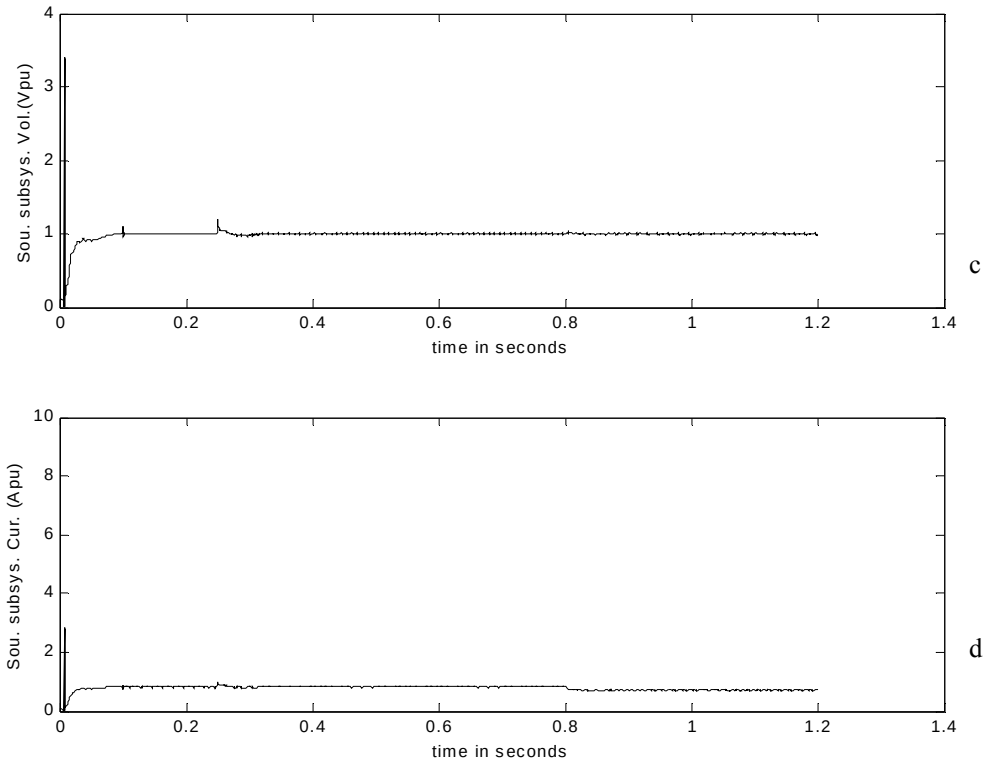


Fig. 5.27 Continued. c) Port bus source subsystem output voltage in pu

d) Port bus source subsystem output current in pu

It was observed that the system was well behaved in the starboard side, as well. The signals in the starboard side were uneventful since the reconfiguration activity did not involve the nodes on that side directly, except for the generator bus and the rectifier bus, which show the loading change as well. The signals for the starboard side are presented in Fig. 5.28a through Fig. 5.28h. The corresponding signals of interest in the starboard side show no reconfiguration activity as expected and are presented in Fig. 5.29a through Fig. 5.29d.

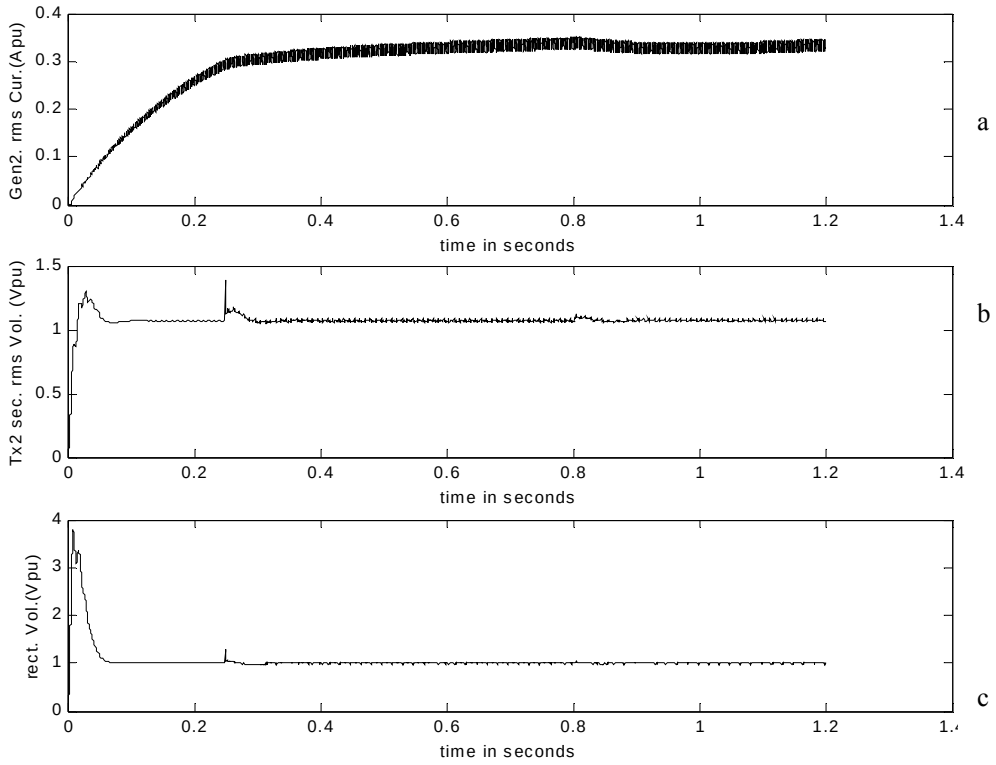


Fig. 5.28 Actual starboard side simulation results for Scenario 7. a) Starboard bus generator RMS current in pu b) Starboard bus transformer line to line voltage RMS in pu

c) Starboard bus rectifier output voltage in pu

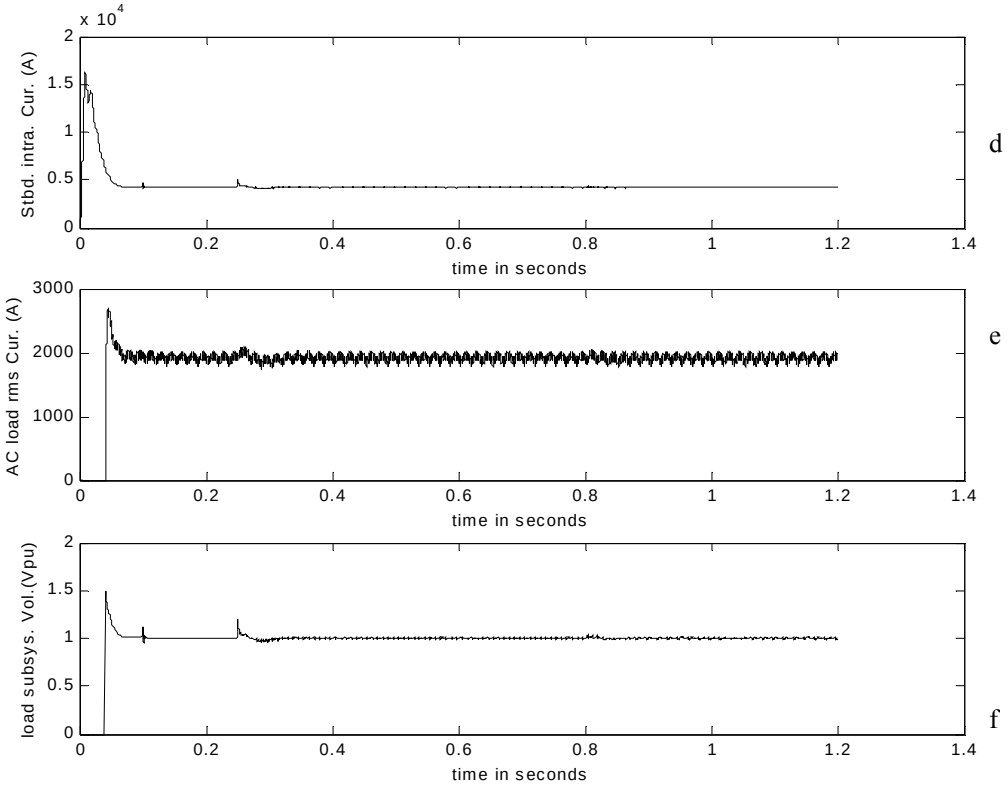


Fig. 5.28 Continued. d) Starboard bus dual bridge output current actual

e) Starboard bus AC RL load current in RMS actual

f) Starboard bus load subsystem voltage in pu

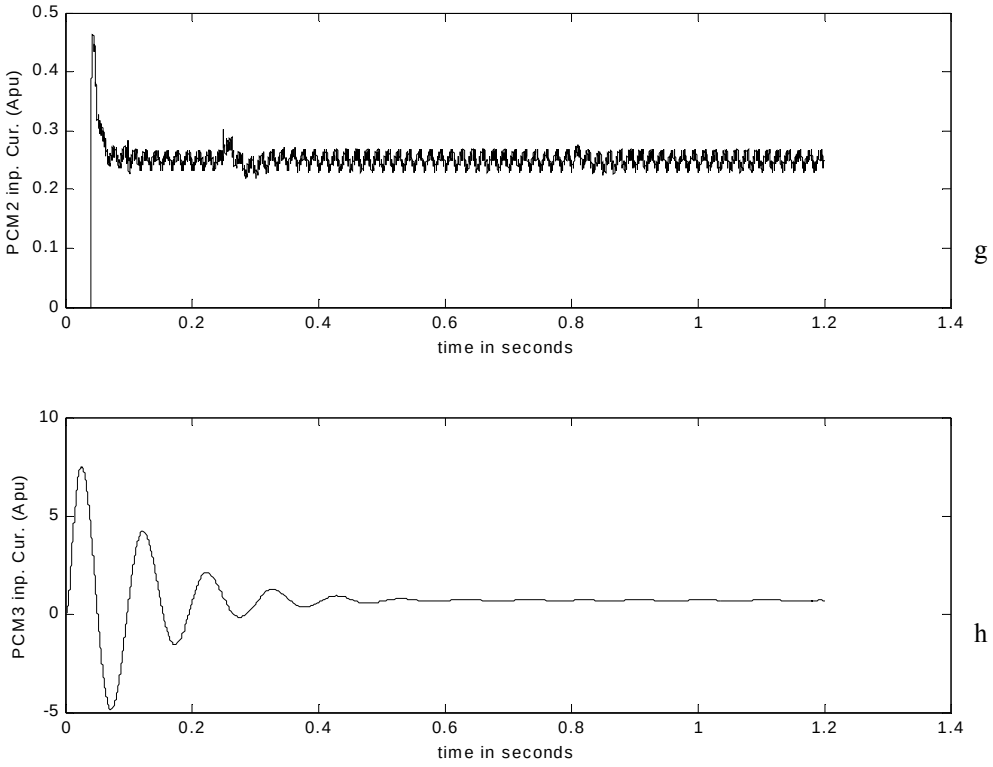


Fig. 5.28 Continued. g) Starboard bus ARCP input current in pu

h) Starboard bus buck converter input current in pu

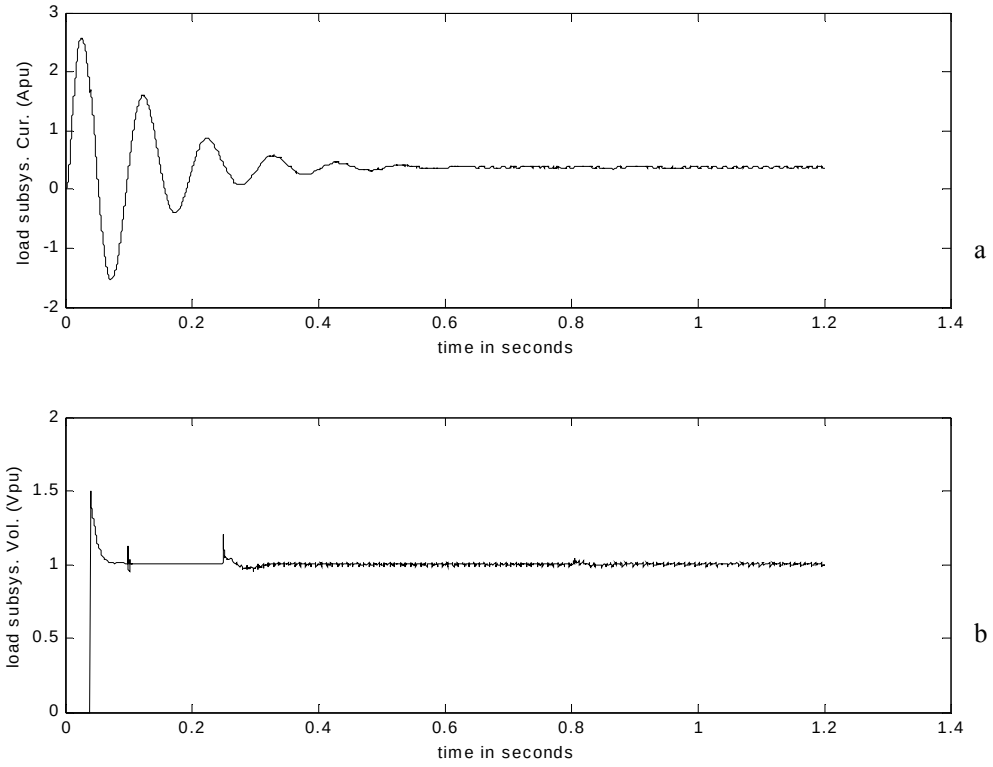


Fig. 5.29 Starboard side intrazonal bus simulation results for Scenario 7 in pu. a) Starboard bus load subsystem current in pu b) Starboard bus load subsystem voltage in pu

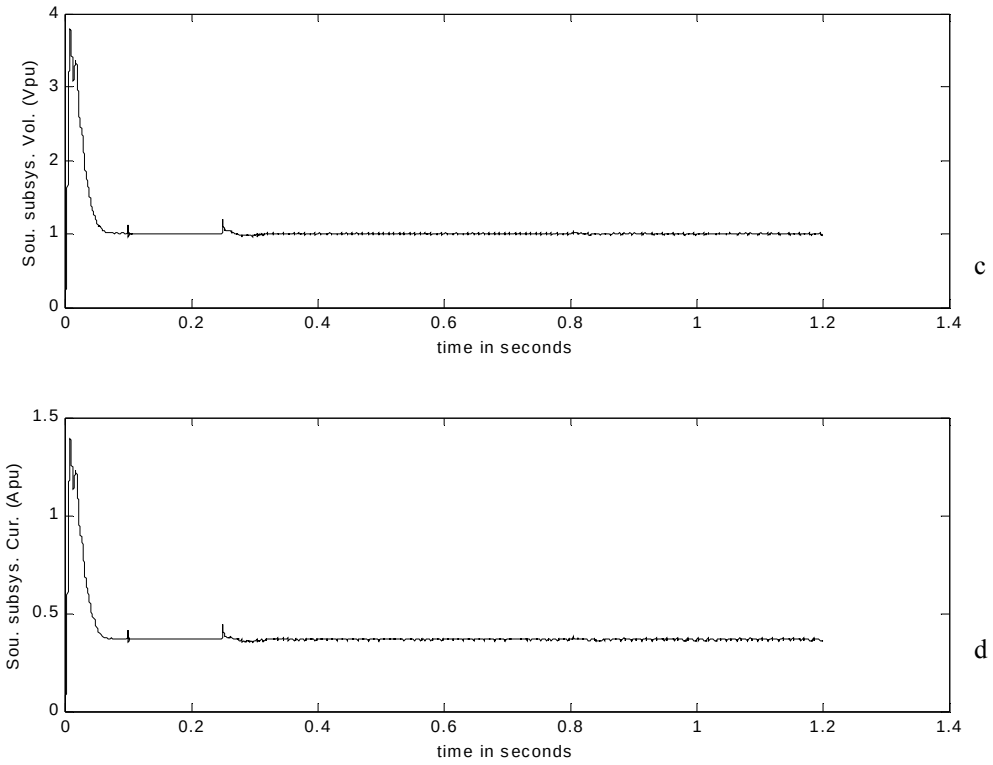


Fig. 5.29 Continued. c) Starboard bus source subsystem voltage in pu

d) Starboard bus source subsystem output current in pu

### 5.2.10 Scenario 8a

With a larger load dropped, it was observed that stability issues arose. In Scenario 8a, the induction motor load on the output of the PCM2 on the port side was switched off at 0.8 seconds into the simulation and was out of the system until the end of the simulation at 1.2 seconds. In this scenario, it was observed that when the PCM2 on the port side input filter saw the drop, it caused an overcurrent to be experienced by its output filter, which was feedback into the upstream nodes as signal degradation. Signal

degradation on the output signals of the upstream filters, especially the rectifier input and output filters occurred in the current and the voltage, and could be seen by the entire system. Overvoltages that characterized the phenomenon were seen by the starboard side loads translating into overcurrent, as can be seen in Fig. 5.32a - Fig 5.32h, tripping the starboard PCM1. But as the PCM1 of the port side was already tripped, the system lost all load resulting in instabilities in some nodes. The size of the motor dropped in this scenario was around 3MW, which is around 33 percent of one generator's capacity. The results of the actual scenario simulation for Scenario 8a are shown in Fig. 5.30 through Fig. 5.33.

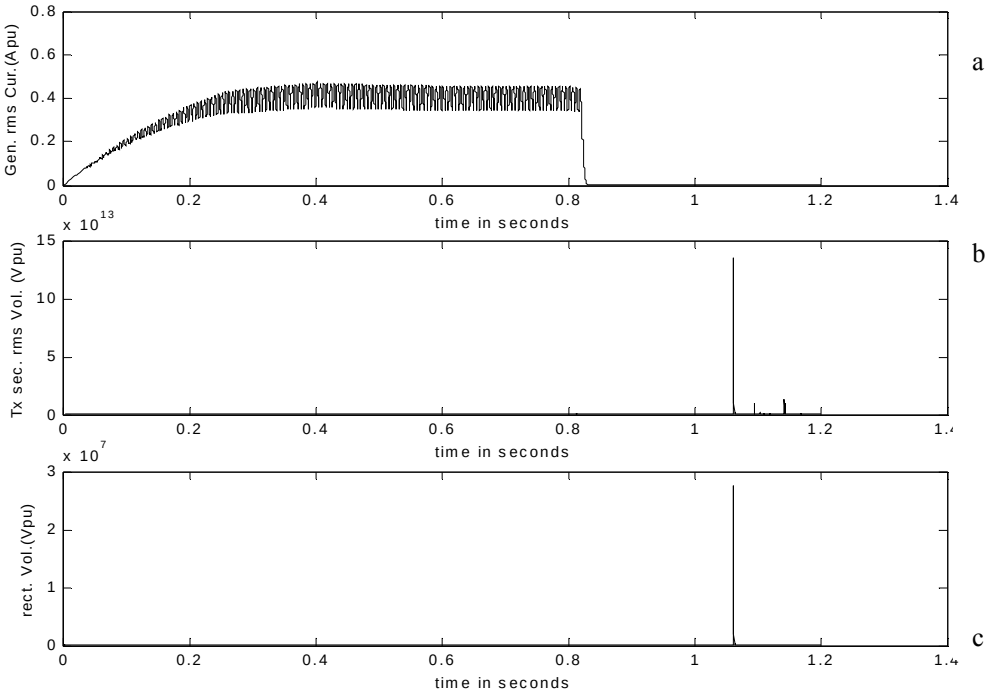


Fig. 5.30 Actual port side simulation results for Scenario 8a. a) Port bus generator RMS current in pu

b) Port bus transformer RMS line to line voltage in pu

c) Port bus rectifier output voltage in pu

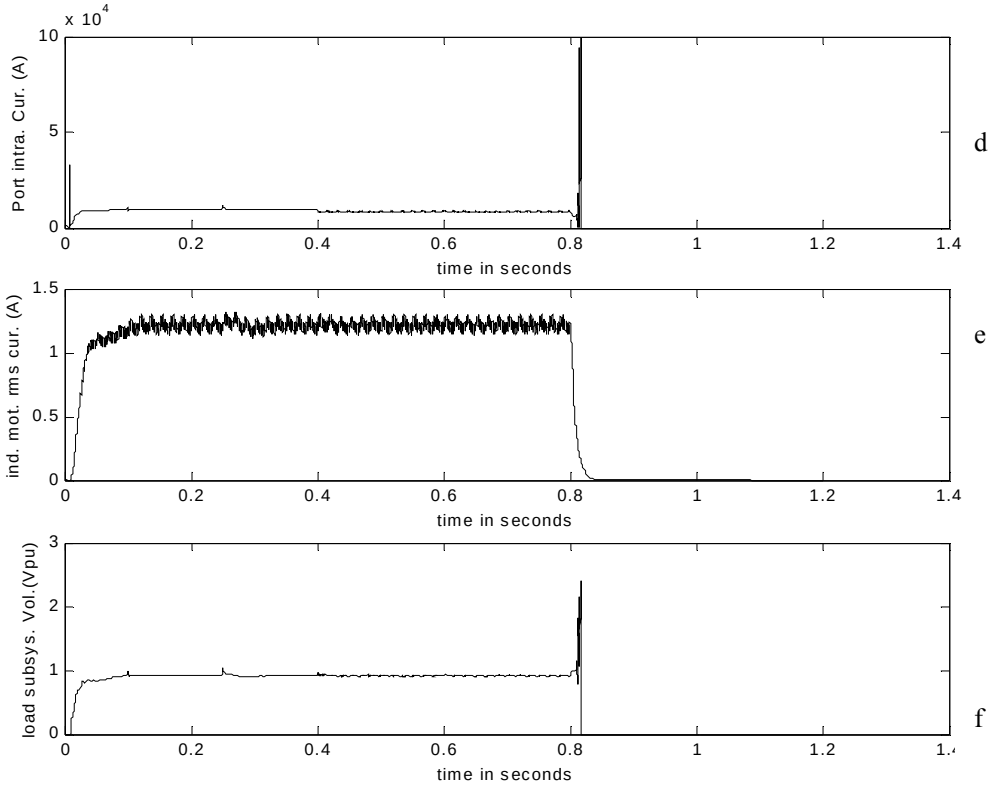


Fig. 5.30 Continued. d) Port bus dual bridge output current in actual

e) Port bus induction motor current from state variables in pu

f) Port bus load subsystem voltage in pu

The instability of Scenario 8a was not seen at the intrazonal bus of the port side but on the generator busses and the ring configuration of the PCM4 bus. It is not detectable at the intrazonal bus, because the protection acted to prevent the loads from experiencing the filter response to the reconfiguration activity. Therefore, it was observed that the system from the zone's entry to the load lost power, but did not exhibit instability, however, the upstream nodes to the zones remained energized but were unstable. More

signals on the port side can be seen in Fig. 5.30e through Fig. 5.30h. The signals used in stability assessment, however, are the port bus intrazonal signals and they are presented in the per unit basis in Fig. 5.30a through Fig5.30d.

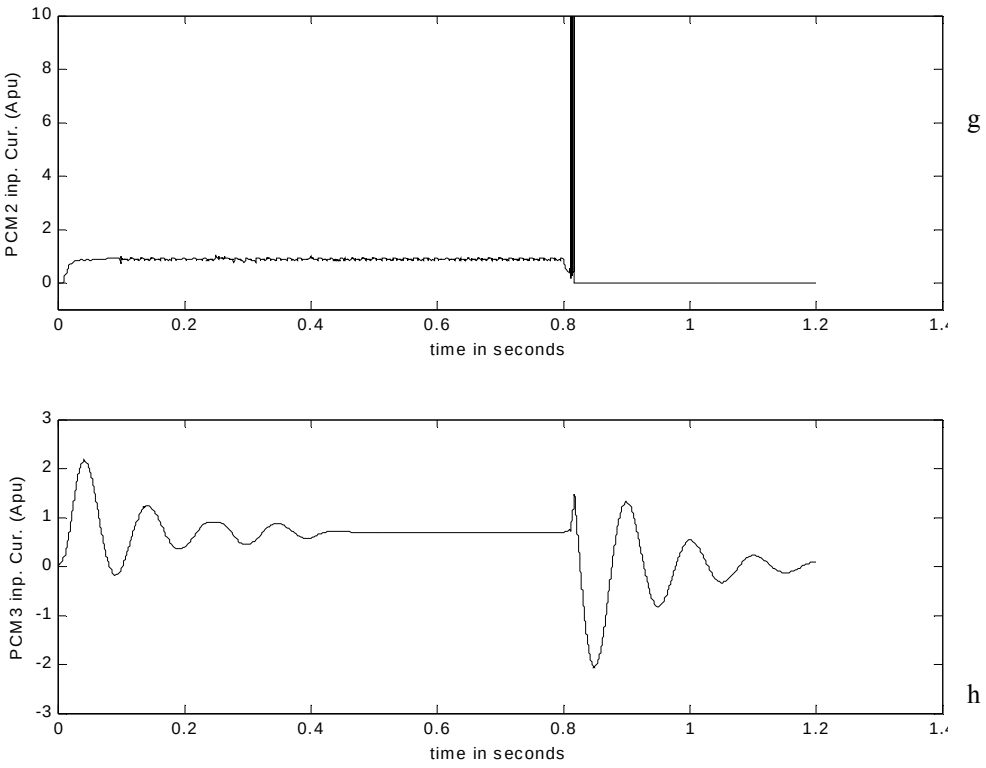


Fig. 5.30 Continued. g) Port bus ARCP input current in pu

h) Port bus buck converter current in pu

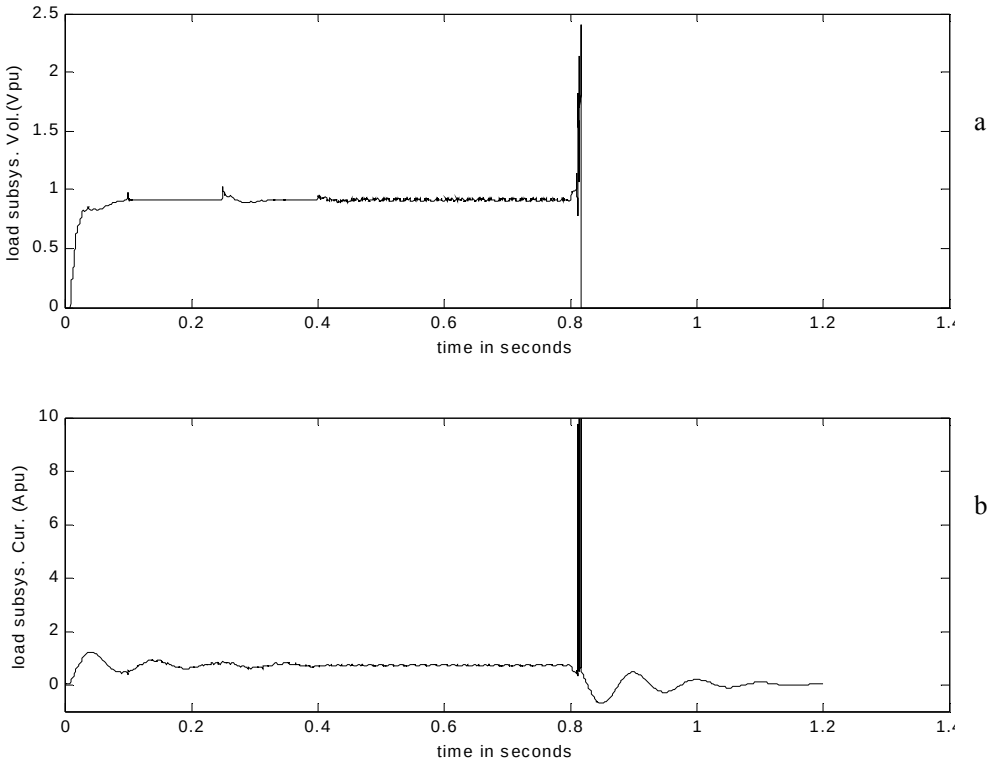


Fig. 5.31 Port side intrazonal bus simulation results for Scenario 8a in pu. a) Port bus load subsystem voltage in pu b) Port bus load subsystem input current in pu

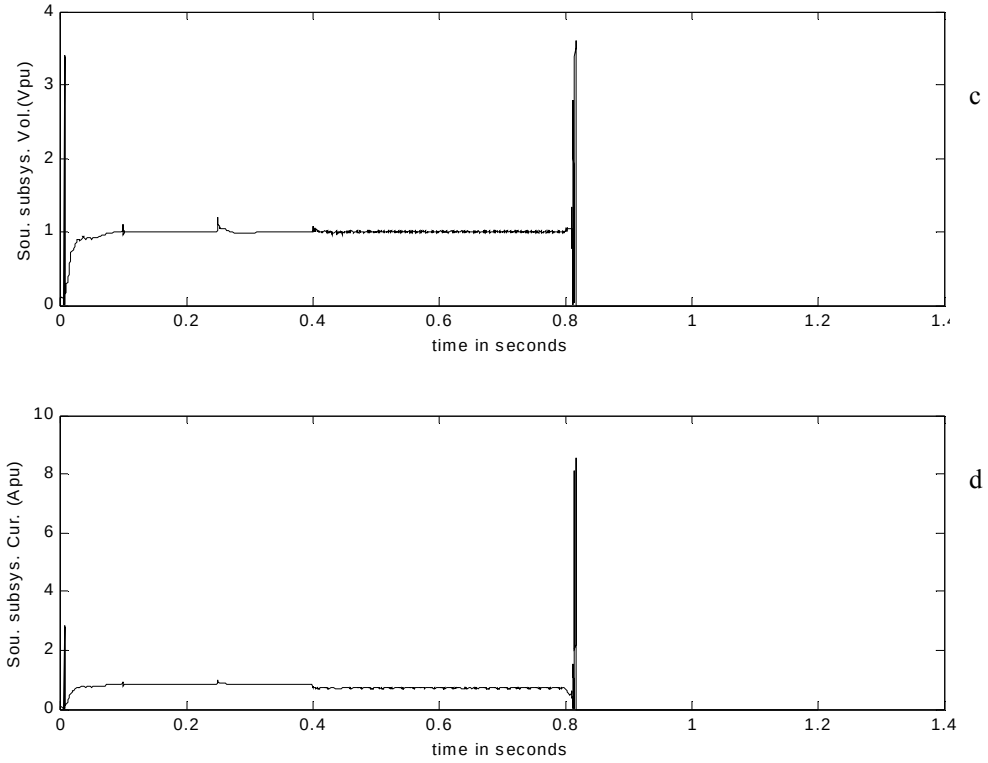


Fig. 5.31 Continued. c) Port bus source subsystem output voltage in pu

d) Port bus source subsystem output current in pu

The starboard side experienced instability because of the degradation of the rectifier (PCM4) signals that contained overvoltages which when applied on the resistive loads in the starboard side, caused overcurrent tripping the intrazonal circuit breakers. The waveforms depicting this are shown in Fig. 5.32a through Fig. 5.32h. The analogous signals to the signals of interest of the port side in the starboard side are presented in per unit basis in Fig. 5.33a through Fig. 5.33d. By visual observation, the system is not stable in Scenario 8a.

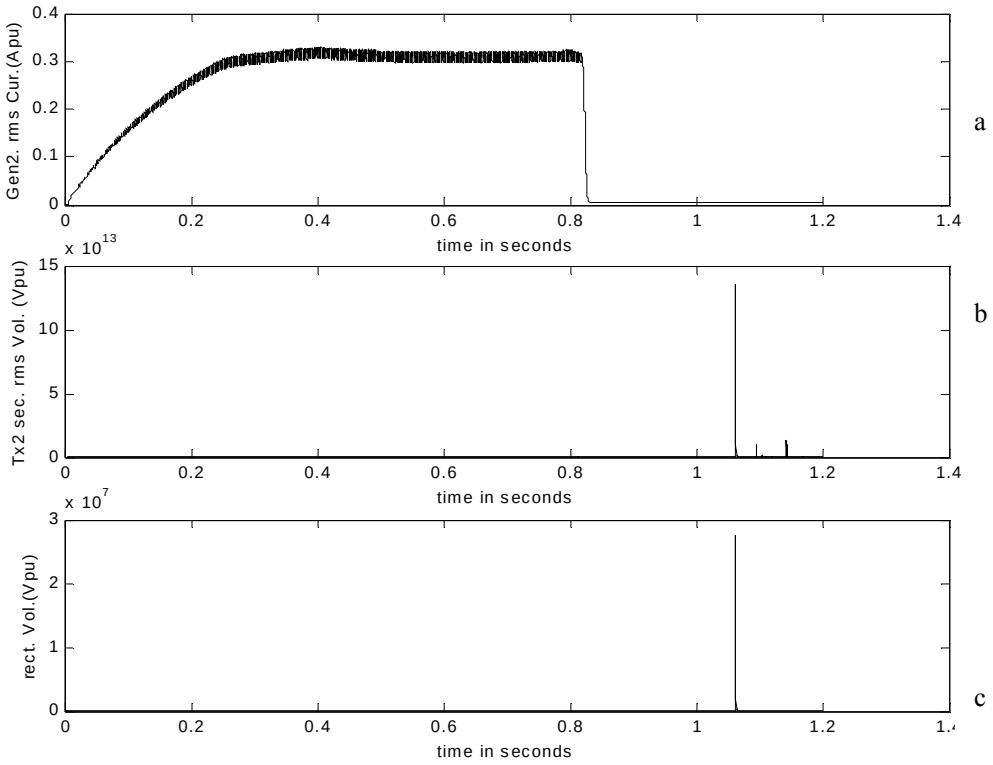


Fig. 5.32 Actual starboard side simulation results for Scenario 8a. a) Starboard bus generator RMS current in pu b) Starboard transformer line to line voltage RMS in pu

c) Starboard bus rectifier output voltage in pu

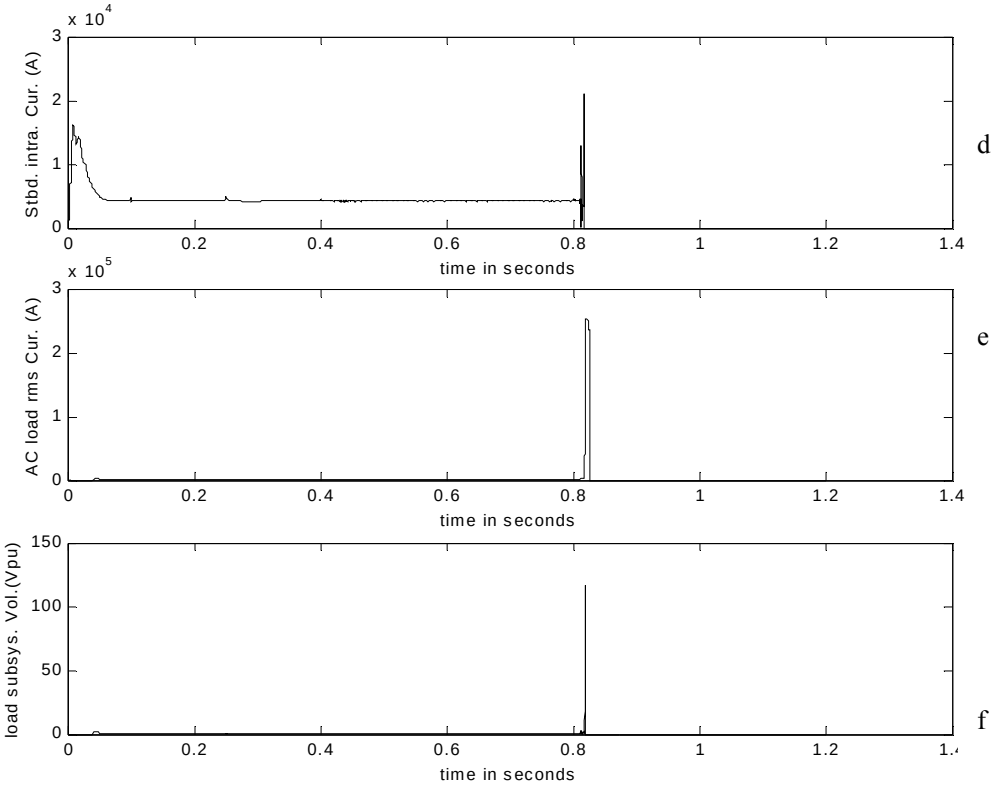


Fig. 5.32 Continued. d) Starboard bus dual bridge output current actual

e) Starboard bus AC RL load current in RMS actual

f) Starboard bus load subsystem voltage in pu

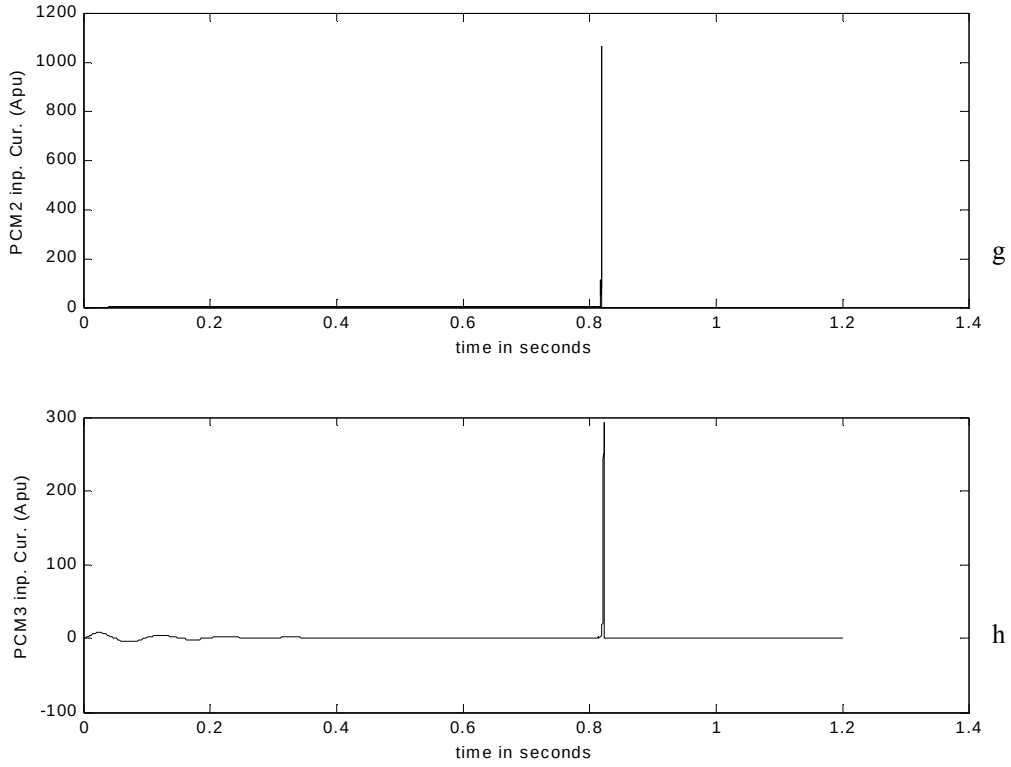


Fig. 5.32 Continued. g) Starboard bus ARCP input current in pu

h) Starboard bus buck converter input current in pu

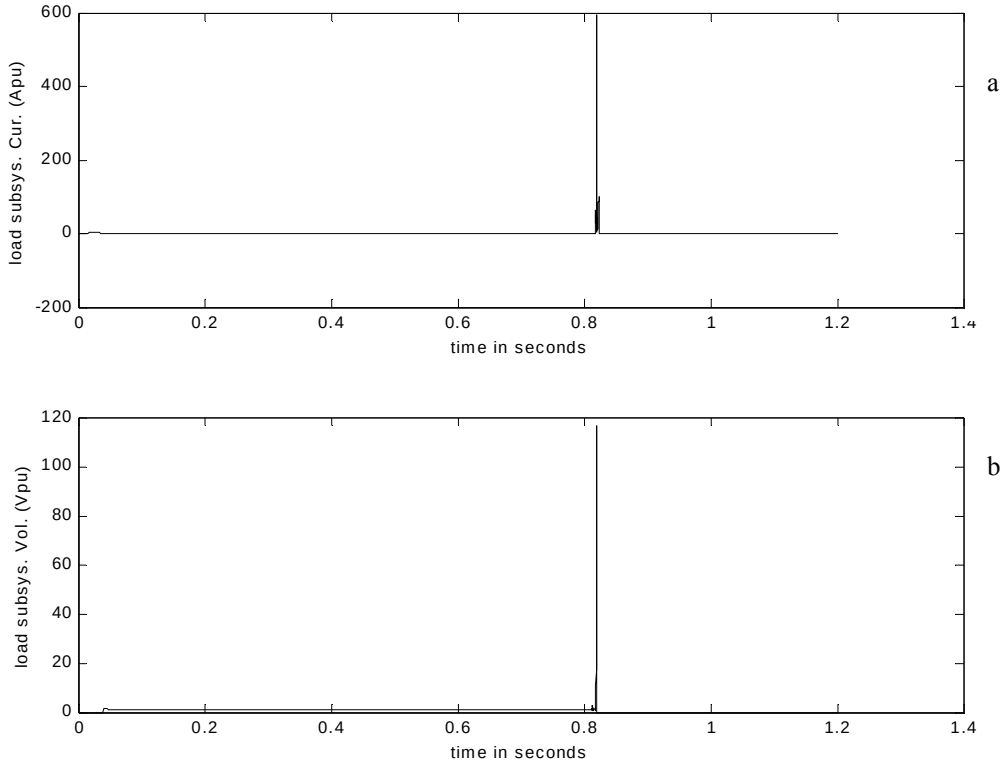


Fig. 5.33 Starboard side intrazonal bus simulation results for Scenario 8a in pu. a) Starboard bus load subsystem current in pu b) Starboard bus load subsystem voltage in pu

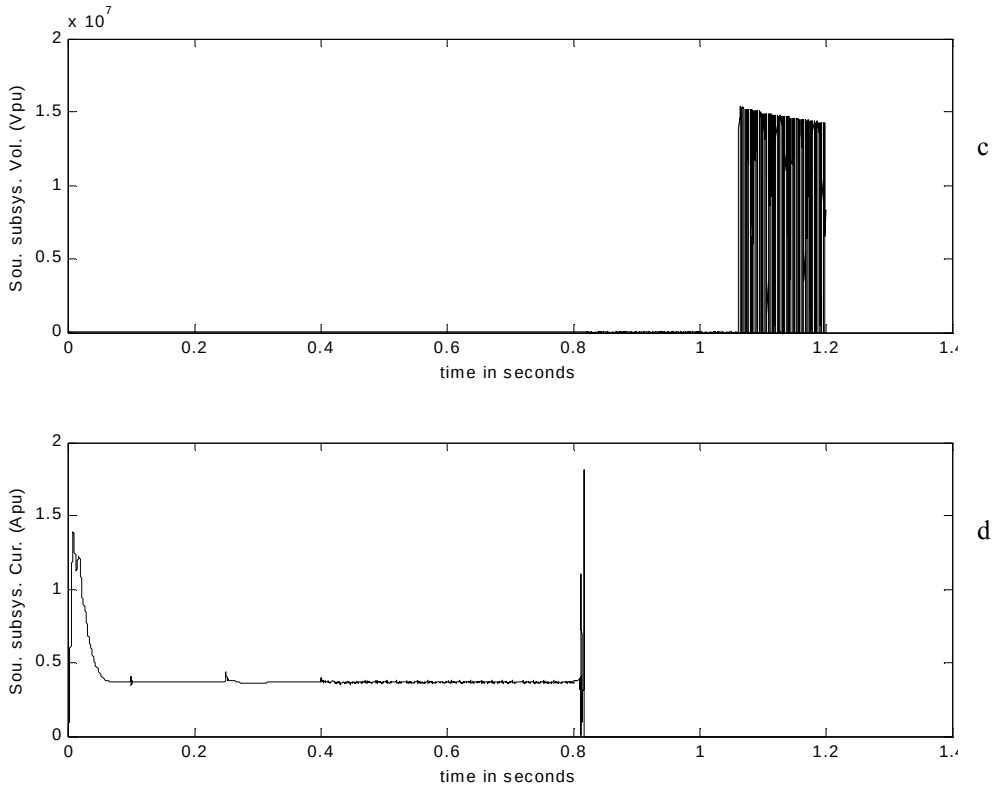


Fig. 5.33 Continued. c) Starboard bus source subsystem output voltage in pu

d) Starboard bus source subsystem output current in pu

### 5.2.11 Scenario 9a

The last scenario within the category for load shedding is the complete loss of load on the PCM2 on the port side. As was the case in Scenario 8a, Scenario 9a was globally unstable due to the same reason for Scenario 8a's poor filter response to the severe load change. The total load lost in this scenario was 4.05MW, and the location of load loss was at the output of the PCM2 on the port side. In Scenario 9a, the induction motor load on the port side and the AC static load were dropped from the system at 0.8 seconds into

the simulation, and remained disconnected from the system until the end of simulation at 1.2 seconds. It was observed that when the loss occurred, the signals upstream of the PCM2 suffered signal degradation and, due to the feedback of signals available in most modules, the degradation was exacerbated until the point of system collapse. The plots shown in Fig. 5.34 through Fig. 5.37 are results of the actual scenario simulation.

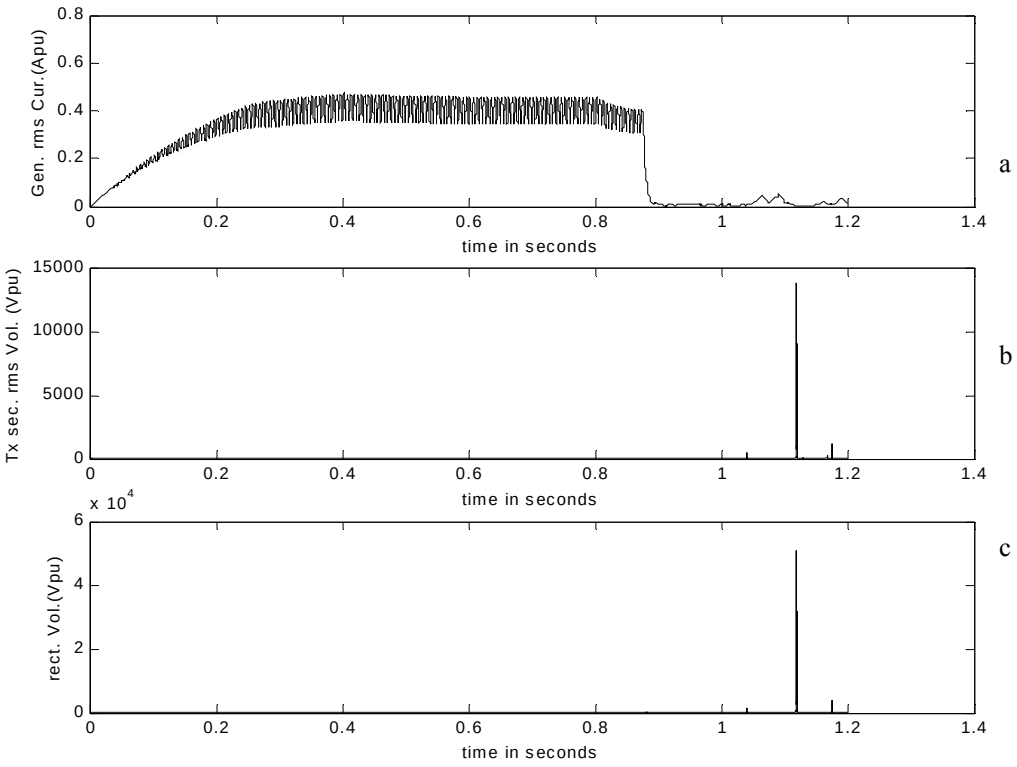


Fig. 5.34 Actual port side simulation results for Scenario 9a. a) Port bus generator RMS current in pu

b) Port bus transformer RMS line to line voltage in pu

c) Port bus rectifier output voltage in pu

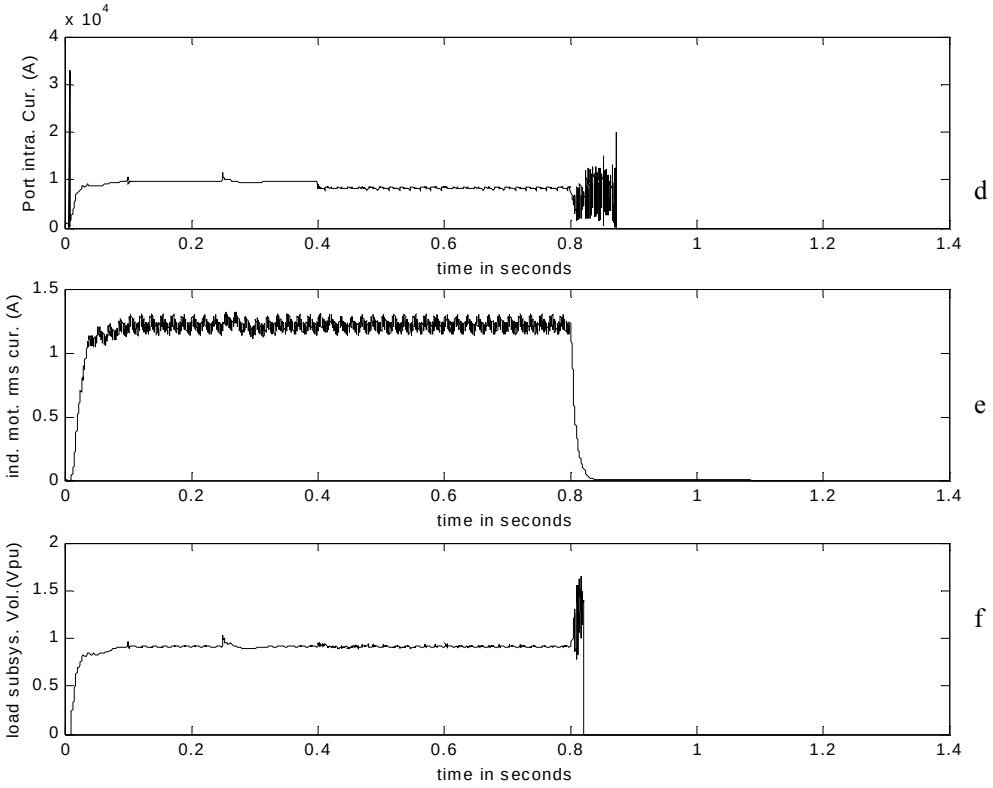


Fig. 5.34 Continued. d) Port bus dual bridge output current in actual

e) Port bus induction motor current from state variables in pu

f) Port bus load subsystem voltage in pu

The generator current (RMS) in Fig. 5.34a shows the system collapse at around 0.9 seconds into the simulation and the second generator shows the same response that is contained in subsequent plots. The rest of the port side signals are available in Fig. 5.34e through Fig. 5.34h. After the system loss of load, the voltage signal of the rectifier (PCM4) was unstable till end of the simulation, and this information is contained in the signals from the starboard side and the port side, as is shown in Fig. 5.36a through Fig.

5.36h for the starboard side signals and Fig. 5.35a-Fig. 5.35d for the port side signals of interest.

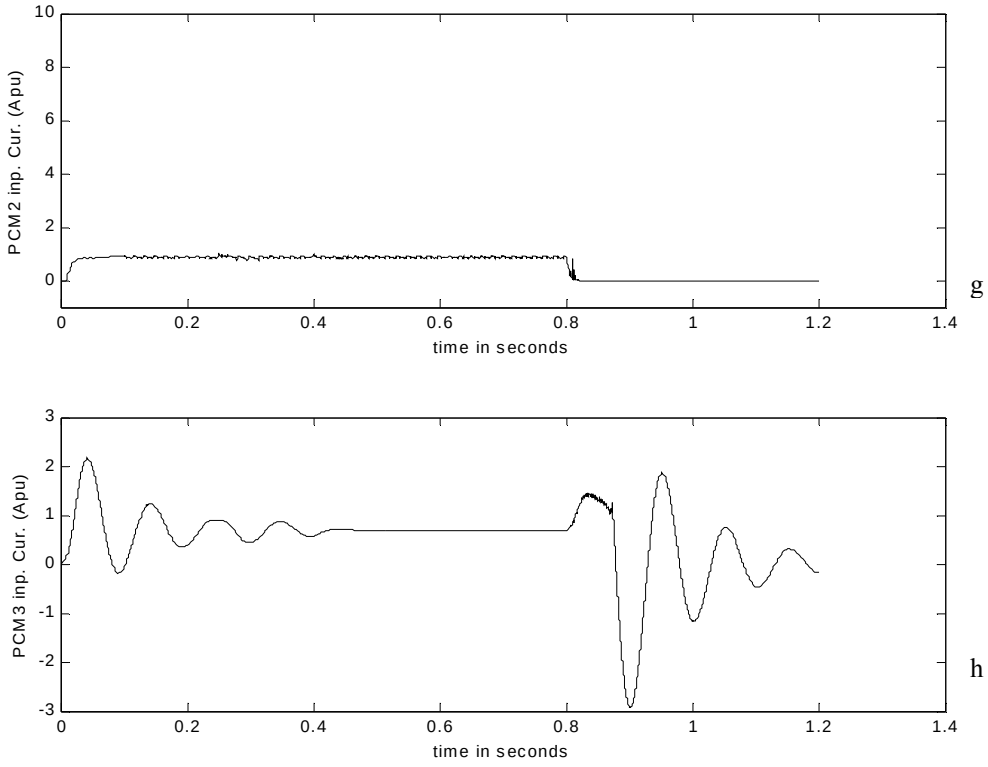


Fig. 5.34 Continued. g) Port bus ARCP input current in pu

h) Port bus buck converter current in pu

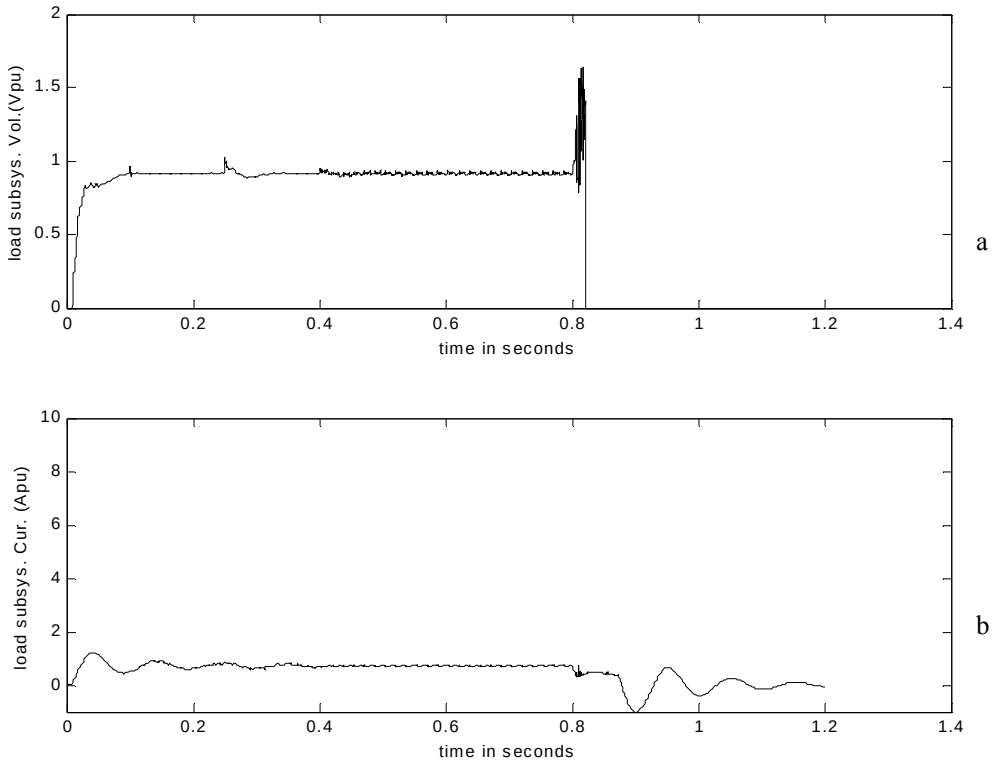


Fig. 5.35 Port side intrazonal bus simulation results for Scenario 9a in pu. a) Port bus load subsystem voltage in pu b) Port bus load subsystem input current in pu

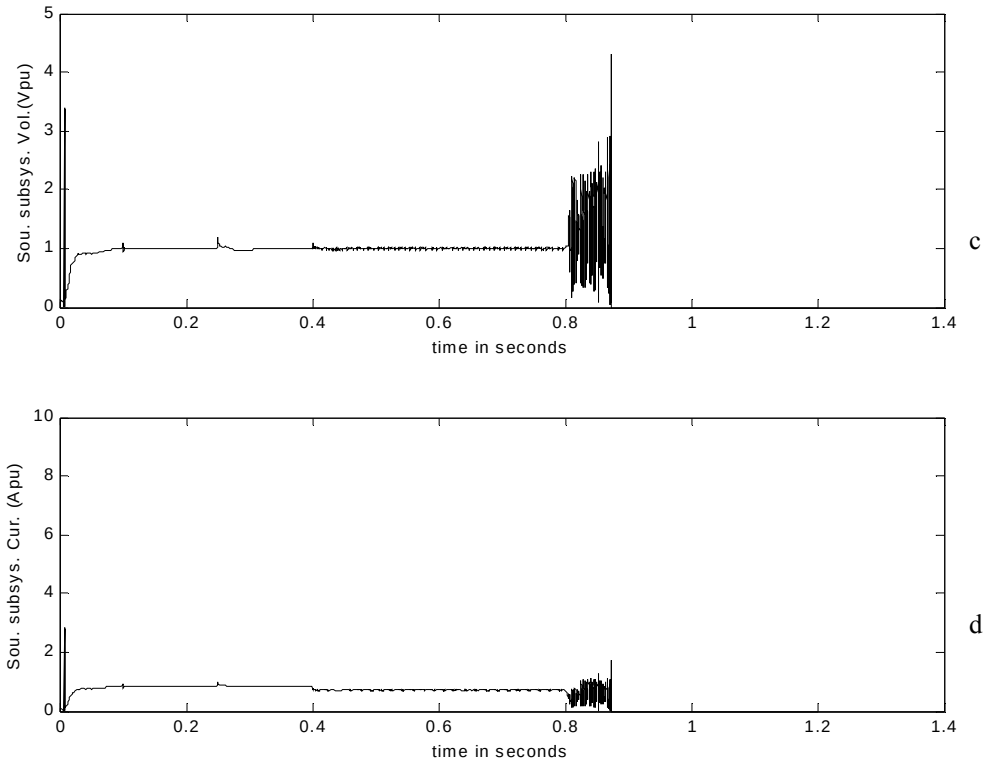


Fig. 5.35 Continued. c) Port bus source subsystem output voltage in pu

d) Port bus source subsystem output current in pu

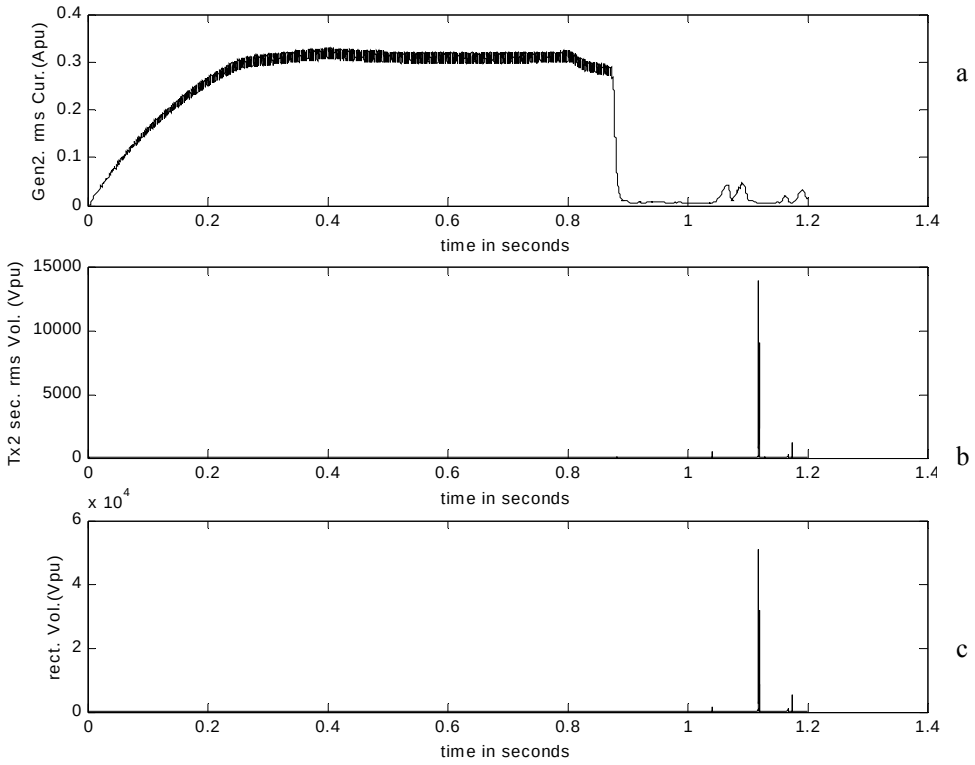


Fig. 5.36 Actual starboard side simulation results for Scenario 9a. a) Starboard bus generator RMS current in pu b) Starboard bus transformer line to line voltage RMS in pu

c) Starboard rectifier output voltage in pu

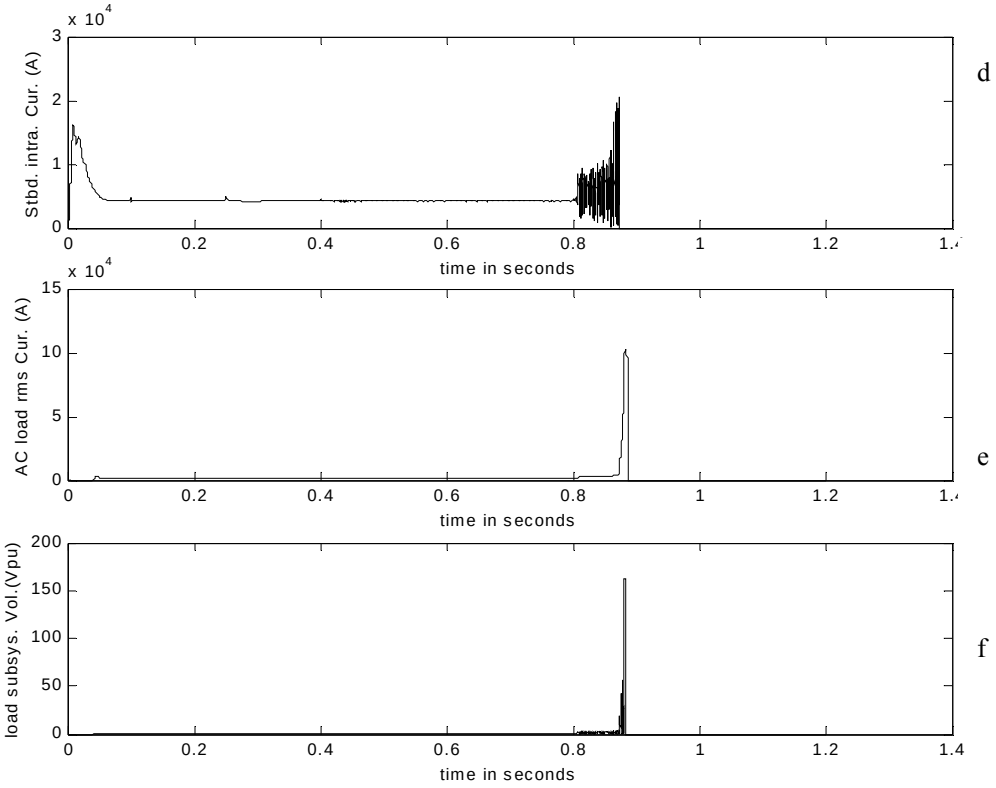


Fig. 5.36 Continued. d) Starboard bus dual bridge output current actual

e) Starboard bus AC RL load current in RMS actual

f) Starboard bus load subsystem voltage in pu

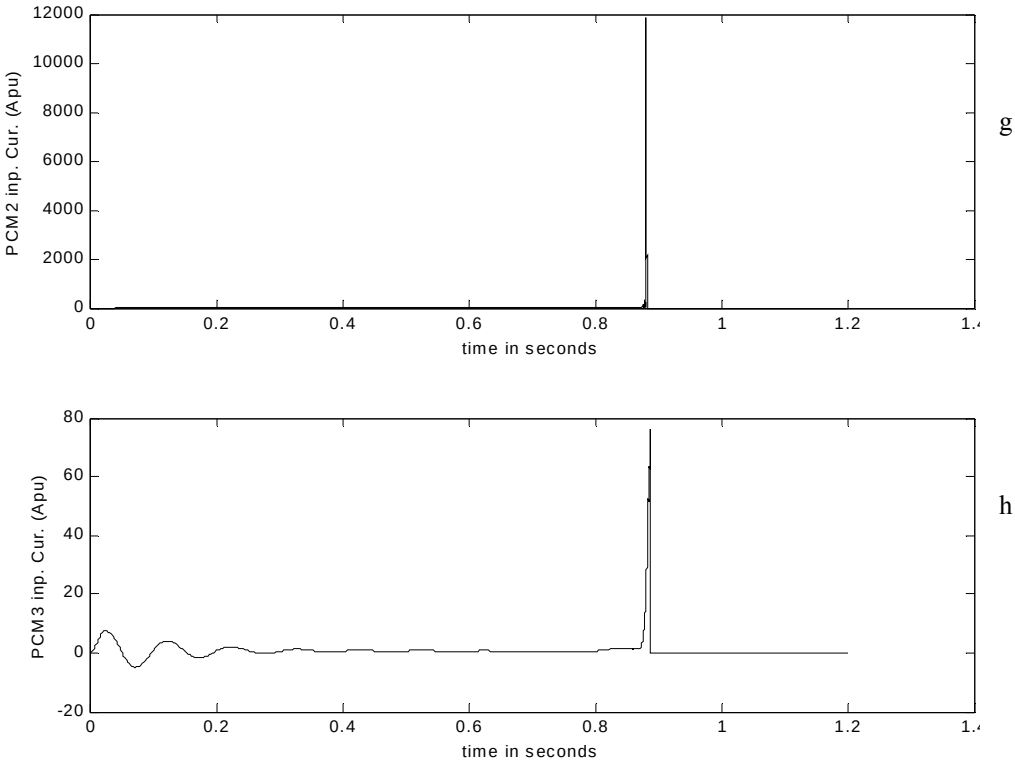


g

h

Fig. 5.36 Continued. g) Starboard bus ARCP input current in pu

h) Starboard bus buck converter input current in pu

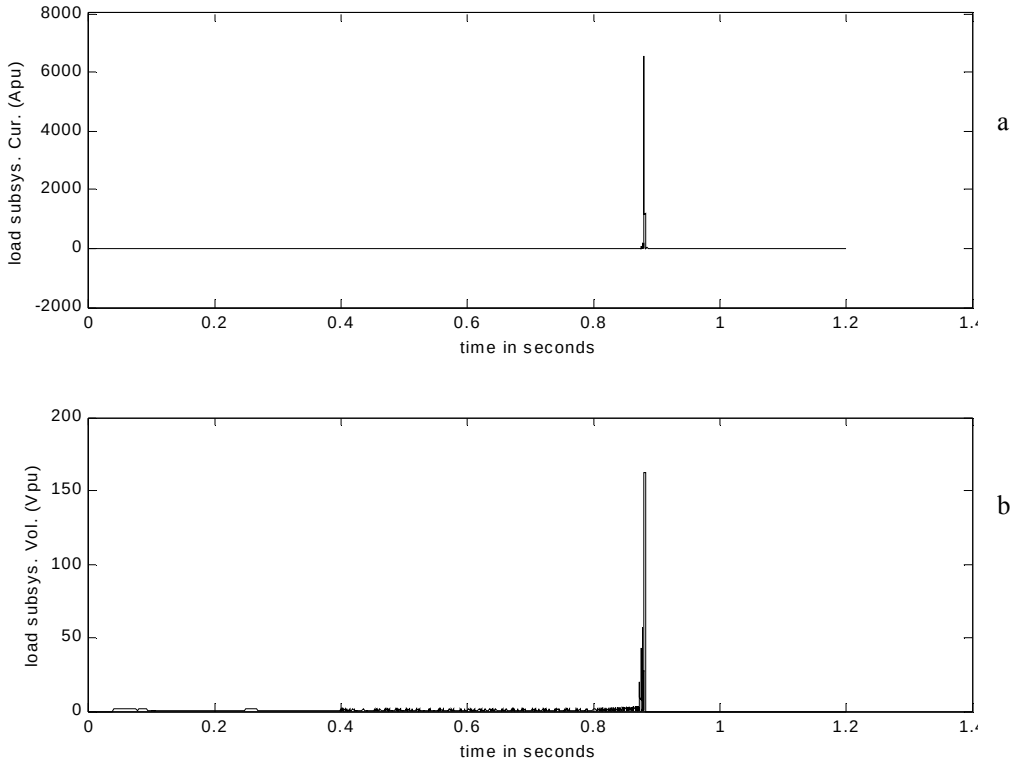


Fig. 5.37 Starboard side intrazonal bus simulation results for Scenario 9a in pu. a) Starboard bus load subsystem current in pu b) Starboard bus load subsystem voltage in pu

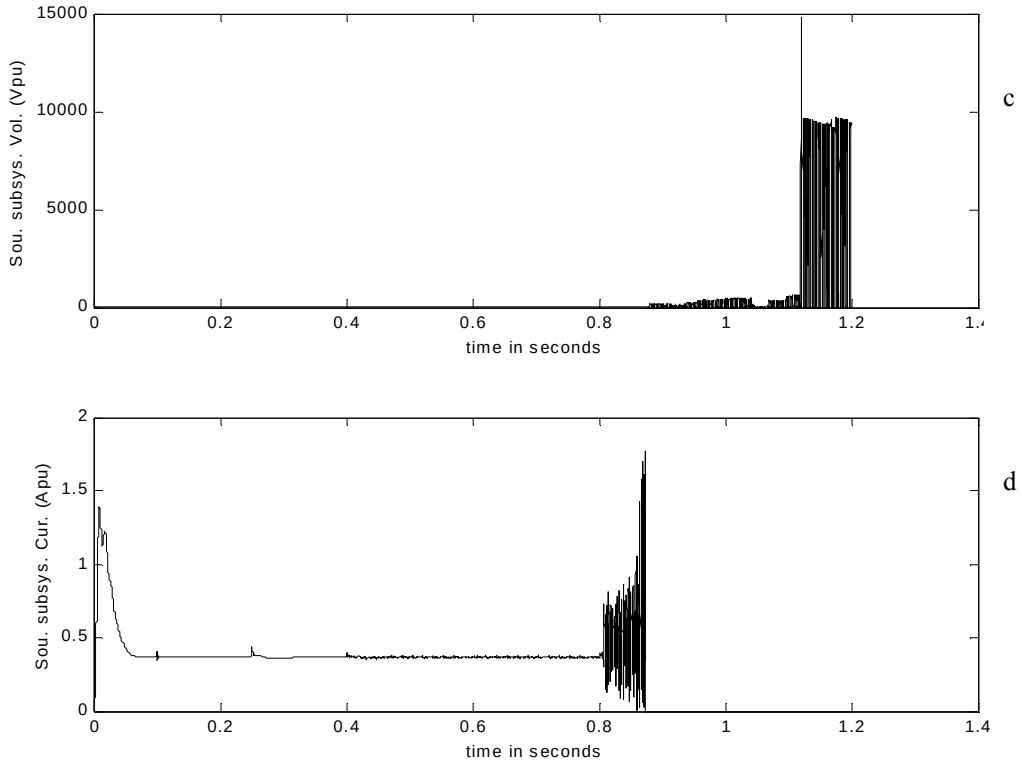


Fig. 5.37 Continued. c) Starboard bus source subsystem output voltage in pu

d) Starboard bus source subsystem output current in pu

By all visual observation, Scenario 9a is unstable at many nodes in the system but it is not observed unstable in the bus of interest as the methodology will show in Section 5.4. In order to use the methodology mentioned, however, the system simulated in this section had to be decoupled about the bus of interest and this decoupling necessitated the use of perturbations to restore the plant gains as obtained in the actual simulation to the same behavior when decoupled. The results and reasons of this exercise are contained in the following section.

## 5.3 Perturbation Models

The methodology, as expressed in the review in Chapter II and recorded in greater detail in Chapter IV, requires that the system be decoupled at the bus of interest with the upstream nodes constituting the source subsystem and the downstream nodes constituting the load subsystem and the source subsystem was to be loaded with perfectly behaved loading, which is the resistor load and the load subsystem was to be excited by well behaved source with perturbation signals introduced into both subsystems at the point of interface. This methodology for assessing stability is well suited for large scale AC/DC systems as is the case in the IPS. The bus of interest for the study is the 775VDC bus, called the intrazonal bus, on the port side. It is within the zone that reconfiguration actions were staged, and it was the response to those actions that the intrazonal bus was investigated for.

Since the main input signals to the subsystems were well behaved, they were of no consequence in the stability assessment, and were modeled as the baseline to the decoupled system. The baseline signals are the signals of this test system at steady state at any particular operating point. The perturbation signals which in the case of this research, contained the reconfiguration activity information were modeled to restore as much as possible, actual scenario behavior to the decoupled system.

In order to change baseline signal the rectpuls was used, when baseline signal was changed ramp wise the tripuls was used when instability or noise was present in the baseline signal to be perturbed then the randn was used. The unique modeling of the system made available all the signals of the system for perturbation purposes, and the

above mentioned signal processing functions are MATLAB functions available within the software used for the simulation analysis. When a perturbation was to be modeled, the actual signal was observed and the information of the reconfiguration action was used. Then the following steps were followed:

The perturbed state variable or derived variable was identified.

The pre-reconfiguration and post-reconfiguration levels were identified

Using the signal processing functions, the baseline was reconstructed to resemble the actual signal behavior.

The perturbation information was attached to the state variable or derived variable.

The controllers and loading feedback were allowed to reconstitute the decoupled system to a new state containing the reconfiguration action information

When the perturbation model is attained there are usually approximation differences between it and the real signal in the actual simulation. This occurred in the small signal simulation and also in the large signal simulation. The proof of the approximation error is contained in Appendix A and the expressions for ε was presented in (4.49). In this section, the numerical values of ε (large signal error) will be presented with a tolerance level chosen to be 15 percent as shown in Tables 5.3 and 5.4. In the analysis, when this error was computed and was below tolerance level, the perturbation model was decided to be acceptable; otherwise it was unacceptable in principle. In sections 5.3.2-5.3.12 each scenario's decoupled profiles about the bus of interest are presented with the treatment of the errors done as follows.

Table 5.3
Large signal error for perturbation models

| Scenario 1 | Error at 60Hz (in Percent) | Error at 20kHz (in Percent) |
|---|---|---|
| Load subsystem | 0 | .8333 |
| Source subsystem | 0 | 9.7e-14 |
| Scenario 2 | Error at 60Hz (in Percent) | Error at 20kHz (in Percent) |
| Load subsystem | 0 | 1.99 |
| Source subsystem | 0 | 0 |
| Scenario 3 | Error at 60Hz (in Percent) | Error at 20kHz (in Percent) |
| Load subsystem | 0 | 0 |
| Source subsystem | 0 | 0 |
| Scenario 4 | Error at 60Hz (in Percent) | Error at 20kHz (in Percent) |
| Load subsystem | 0 | 1.4394 |
| Source subsystem | 0 | 0 |
| Scenario 5 | Error at 60Hz (in Percent) | Error at 20kHz (in Percent) |
| Load subsystem | 8.333 | 0 |
| Source subsystem | 0 | 0 |
| Scenario 6 | Error at 60Hz (in Percent) | Error at 20kHz (in Percent) |
| Load subsystem | 0 | 9.1 |
| Source subsystem | 0 | 0 |
| Scenario 7 | Error at 60Hz (in Percent) | Error at 20kHz (in Percent) |
| Load subsystem | 0 | 0.952 |
| Source subsystem | 0 | 0 |
| Scenario 8a | Error at 60Hz (in Percent) | Error at 20kHz (in Percent) |
| Load subsystem | 8 | 97.3 |
| Source subsystem | 0 | 0 |
| Scenario 9a | Error at 60Hz (in Percent) | Error at 20kHz (in Percent) |
| Load subsystem | 0 | 0.7708 |
| Source subsystem | 0 | 0 |
| Scenario 8b | Error at 60Hz (in Percent) | Error at 20kHz (in Percent) |
| Load subsystem | 26.7 | 22.5 |
| Source subsystem | 25 | 29.1 |

Table 5.3 Continued

| Scenario 9b | Error at 60Hz (in Percent) | Error at 20kHz (in Percent) |
|---|---|---|
| Load subsystem | 30 | 96.053 |
| Source subsystem | 24 | 94.4 |
| | | |

Table 5.4
Small signal error for linear gain computation

| Systems | Frequency (Hz) | Actual subsystem gain (G1) in db | Pert. subsystem gain (G2) in db | Error (in percent) |
|---|---|---|---|---|
| Source | 60 | -67.1 | -77 | 14.75 |
| | 20k | -62.3 | -79.5 | 27.6 |
| | 50k | -68.9 | -82.6 | 19.88 |
| Load | 60 | -33.5 | -33.5 | 0 |
| | 20k | -62.3 | -77.7 | 24.7 |
| | 50k | -69 | -82 | 18.84 |

### 5.3.1 Errors

Large signal errors were mostly within tolerance except for when the system was decoupled about the interzonal bus. In these cases the signals were unstable and hard to replicate in the decoupled system. For these cases which comprise Scenario 8b and Scenario 9b, the best obtained results were reported without consideration for allowable values because it was hard to reduce approximation error to any satisfactory level. This

problem, of unsatisfactory error, was also found in Scenario 8a which showed a 20kHz error in the load subsystem of 97 percent. All other errors in the large signal perturbation were found to be less than 10 percent and mostly zero. This indicated that when signal was well behaved it was possible to replicate the system perfectly with correct perturbation. Source of large signal errors was perturbation modeling. Signal processing tools were used to simulate the actual response of power system to the reconfiguration activity. This served as the perturbation models in the decoupled system giving rise to approximation errors.

Small signal error was obtained by a different means because (4.49) assumed nonlinearity suitable for large signals perturbation modeling. For small signal perturbation modeling, bode plots were used to compare the gain and phase margins of the plant of the actual simulation system and the plant of the decoupled system. The method gave large errors to minor approximations in perturbation models as such low errors were not easily attainable. The small signal errors showed maximum error of 27.6 percent which was deemed acceptable due to the mentioned limitations of the measurement methodology. Sources of small signal errors were the order of the ARMAX and the perturbation modeling.

### 5.3.2 Scenario 1

The perturbation was developed in Scenario 1 to approximate the actual scenario that contained the reconfiguration activity information. Scenario 1 was bus transfer activity with finite impedance fault. The results of the perturbation development are shown in

Fig. 5.38a through Fig. 5.38d. These are the profiles of the key signals used in the stability assessment. Dissimilarities with the actual in Fig. 5.2 are small and are accounted for in ε for Scenario 1.

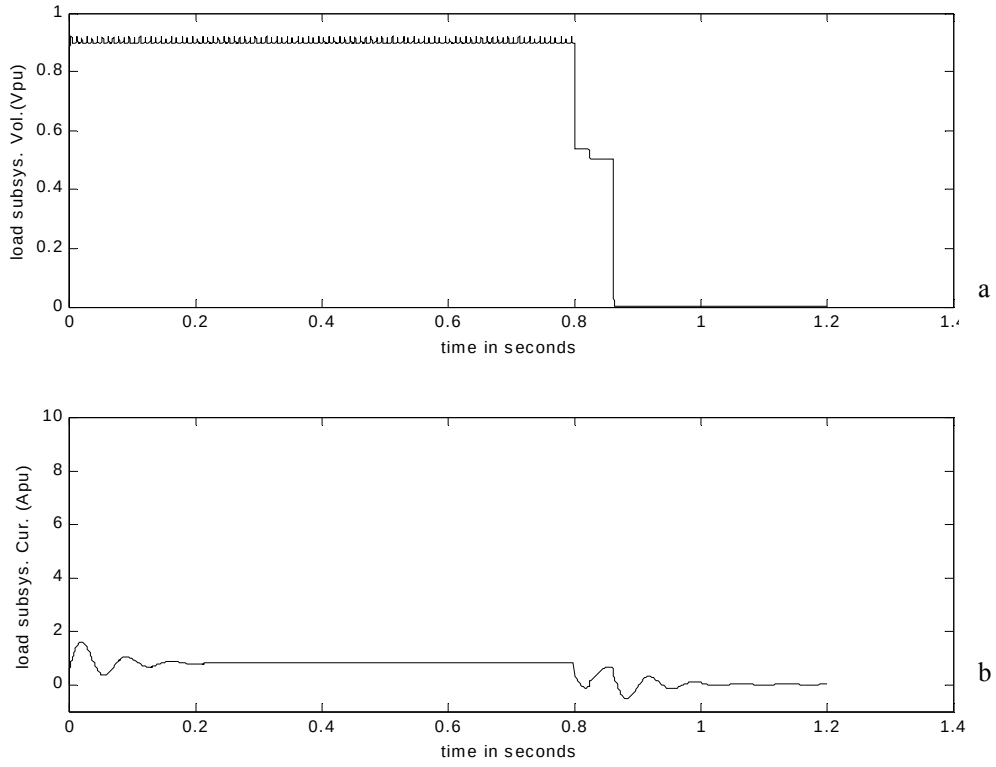


Fig. 5.38 Perturbation model port side simulation results for Scenario 1 in pu. a) Port bus voltage in pu from perturbation model b) Port bus load subsystem input current in pu from perturbation model

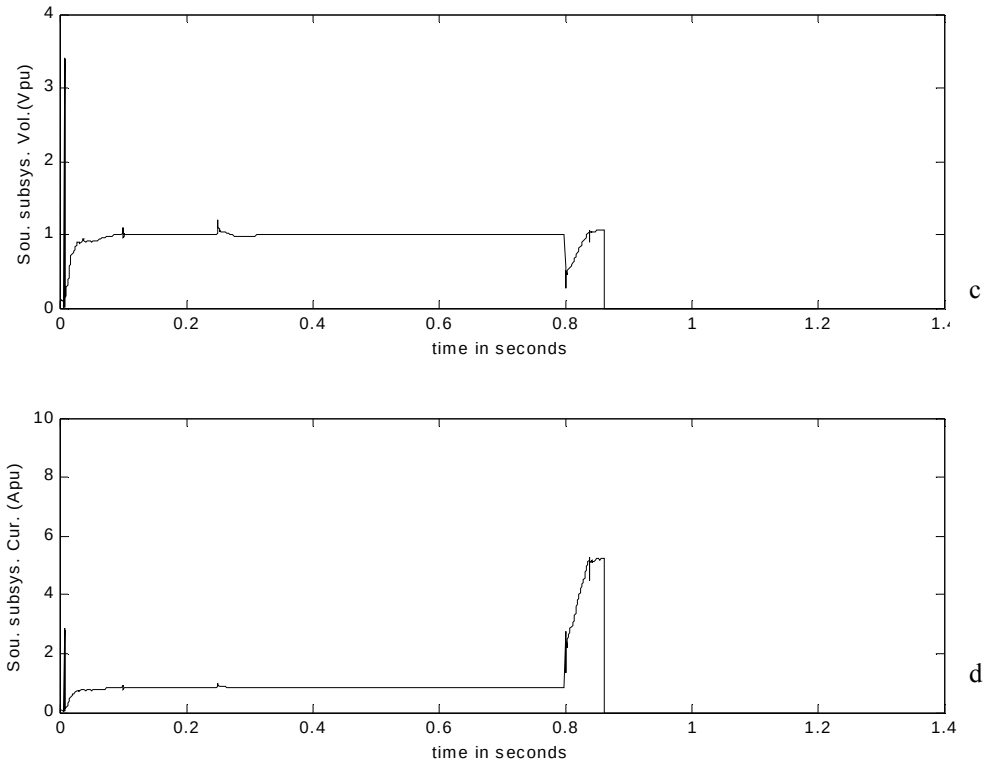


Fig. 5.38 Continued. c) Port bus source subsystem output voltage in pu from perturbation model

d) Port bus source subsystem output current in pu from perturbation model

### 5.3.3 Scenario 2

The perturbation modeling for Scenario 2 was similar to Scenario 1. Scenario 2 was also bus transfer activity (but with bolted fault) and the key signals used in stability assessment of Section 5.4 are presented in Fig. 5.39a through Fig. 5.39d. The signals were developed using the signals processing toolbox as earlier mentioned.

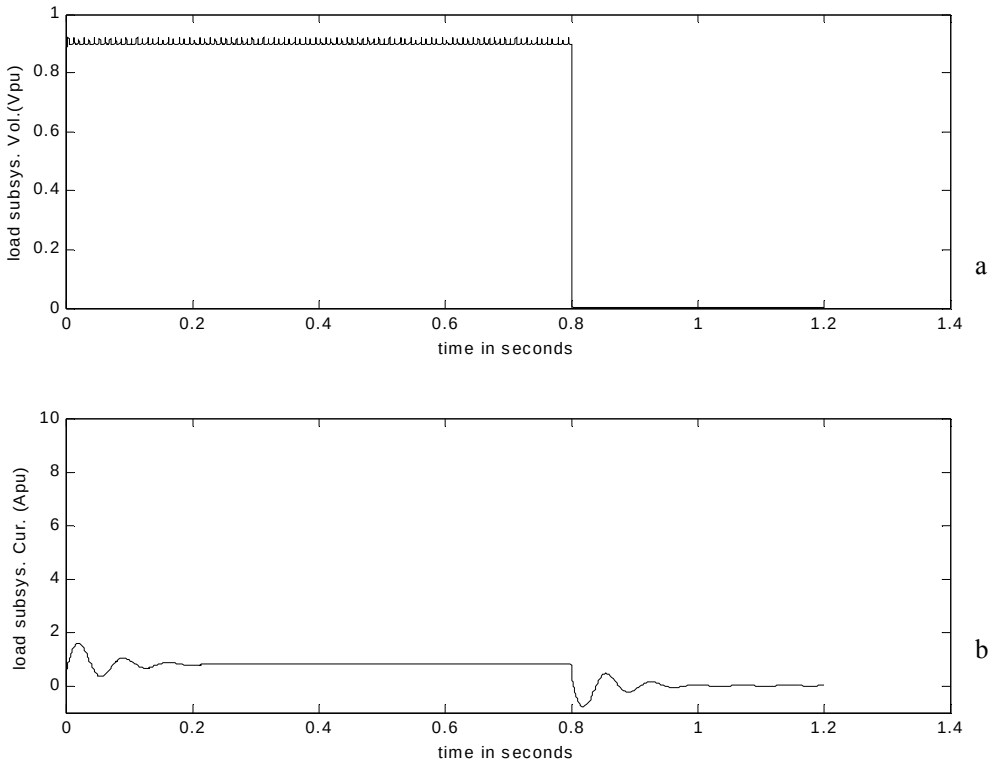


Fig. 5.39 Perturbation model port side simulation results for Scenario 2 in pu. a) Port bus voltage in pu from perturbation model b) Port bus load subsystem input current in pu from perturbation model

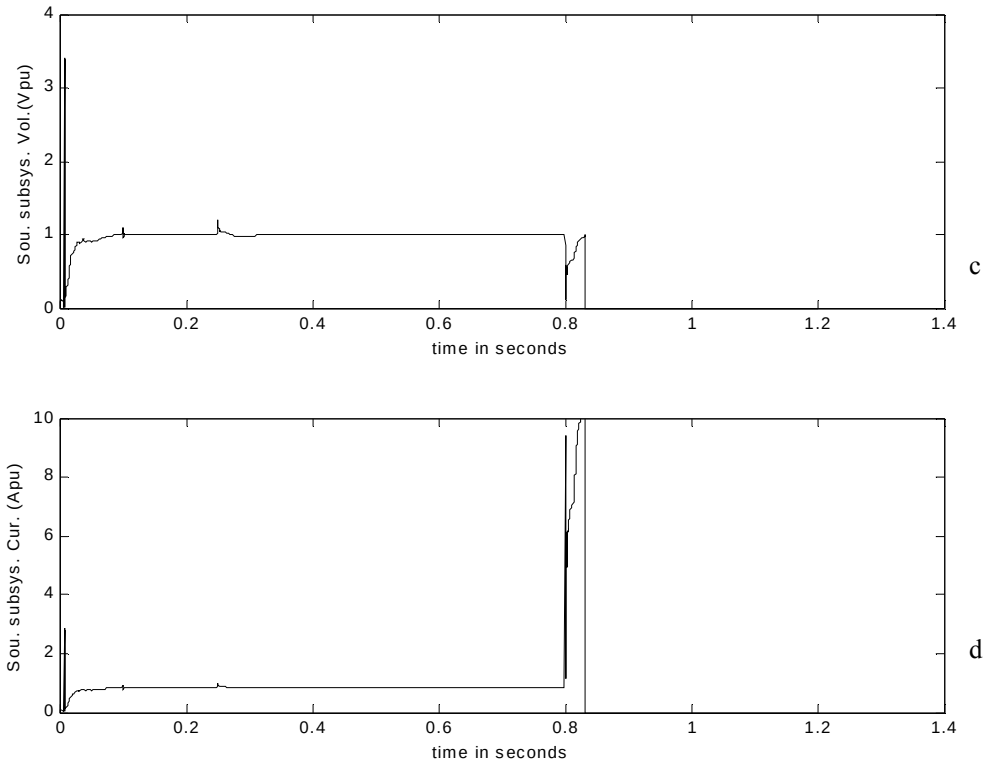


Fig. 5.39 Continued. c) Port bus source subsystem output voltage in pu from perturbation model

d) Port bus source subsystem output current in pu from perturbation model

### 5.3.4 Scenario 3

Scenario 3 is the last in the category of bus transfer activity and it represented the bus transfer due to finite impedance fault with fault impedance lower than the fault impedance of Scenario 1. This scenario was approximated in the decoupled system fairly closely as the error values indicate in Table 5.3. The results of the perturbation modeling for the key signals for stability assessment are shown in Fig. 5.40a through Fig. 5.40d.

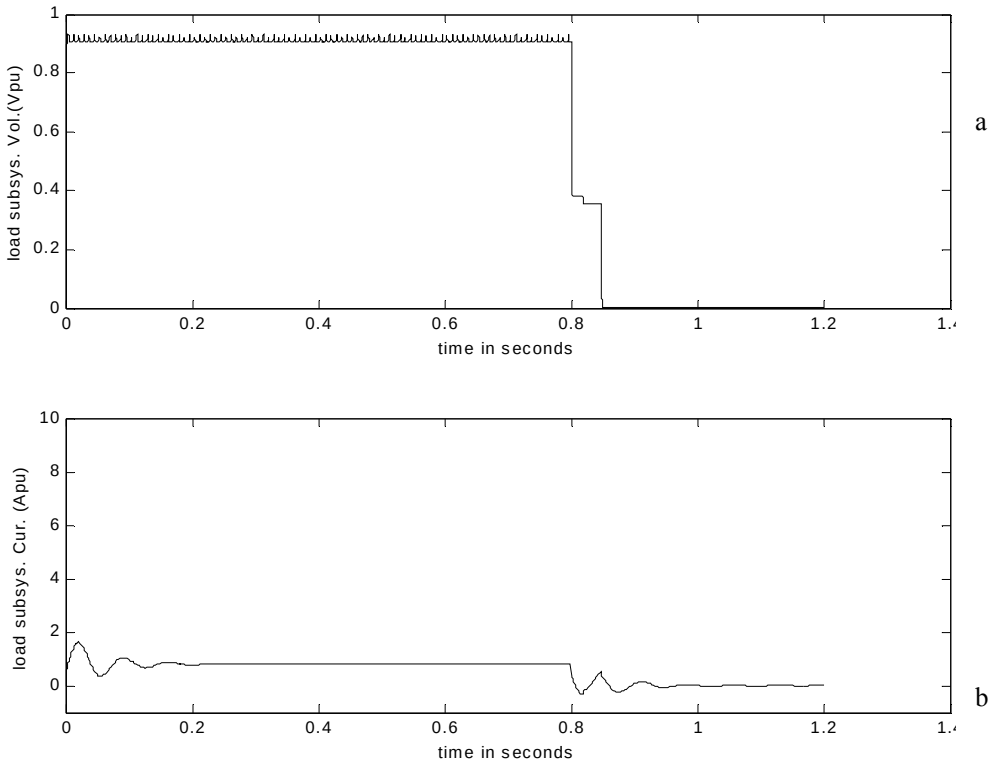


Fig. 5.40 Perturbation model port side simulation results for Scenario 3 in pu. a) Port bus voltage in pu from perturbation model b) Port bus load subsystem input current in pu from perturbation model

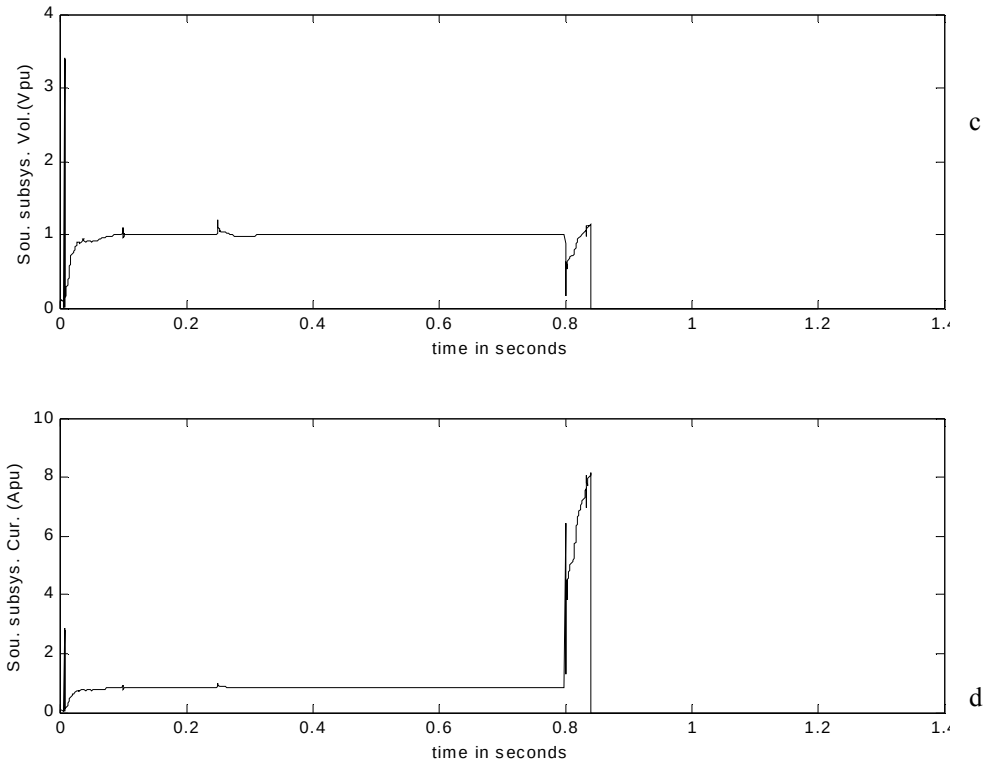


Fig. 5.40 Continued. c) Port bus source subsystem output voltage in pu from perturbation model

d) Port bus source subsystem output current in pu from perturbation model

### 5.3.5 Scenario 4

In Scenario 4, the reconfiguration activity was load addition, and the information to be replicated in the decoupled system was successfully developed in the perturbation model. This scenario represented normal loading and was visually judged stable. The error of approximation was zero for this scenario. The results of the perturbation modeling are presented in Fig. 5.41a through Fig. 5.41d.

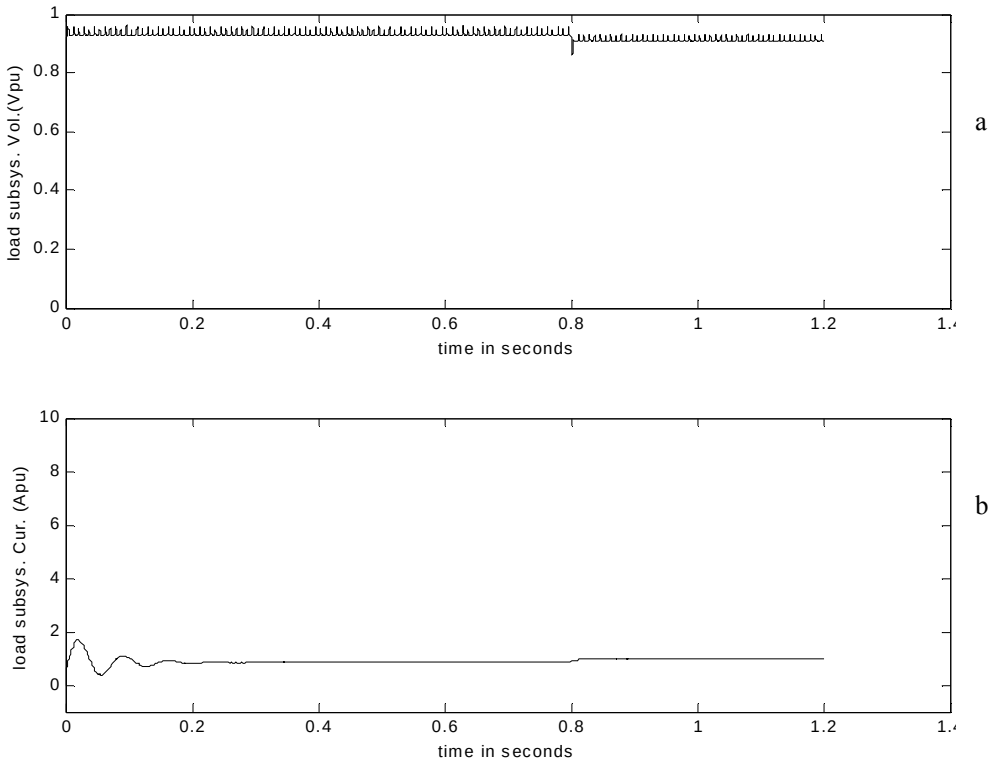


Fig. 5.41 Perturbation model port side simulation results for Scenario 4 in pu. a) Port bus voltage in pu from perturbation model b) Port bus load subsystem input current in pu from perturbation model

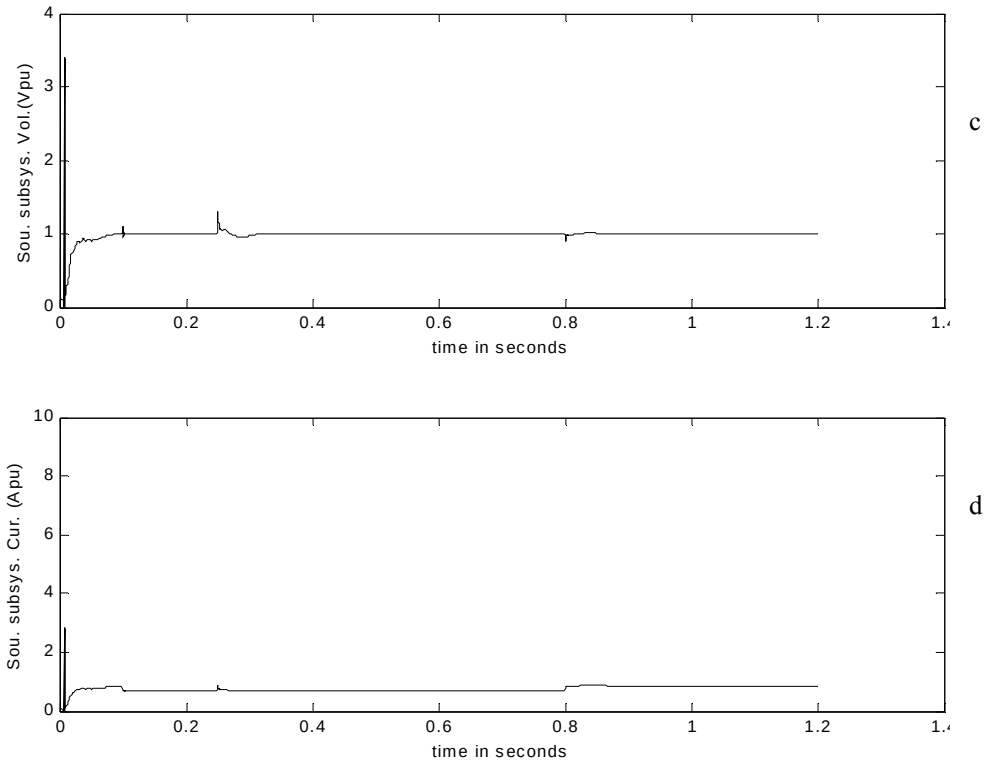


Fig. 5.41 Continued. c) Port bus source subsystem output voltage in pu from perturbation model

d) Port bus source subsystem output current in pu from perturbation model

### 5.3.6 Scenario 5

The case where overload occurs at a bus in the system was investigated in Scenario 5 and it was found to be stable. The overload case was successfully replicated in the decoupled system with mostly small errors as indicated in the error table. The error of Scenario 5 at 60Hz was for the source subsystem was less than 1 percent The results of the perturbation modeling are presented in Fig. 5.42a through Fig. 5.42d.

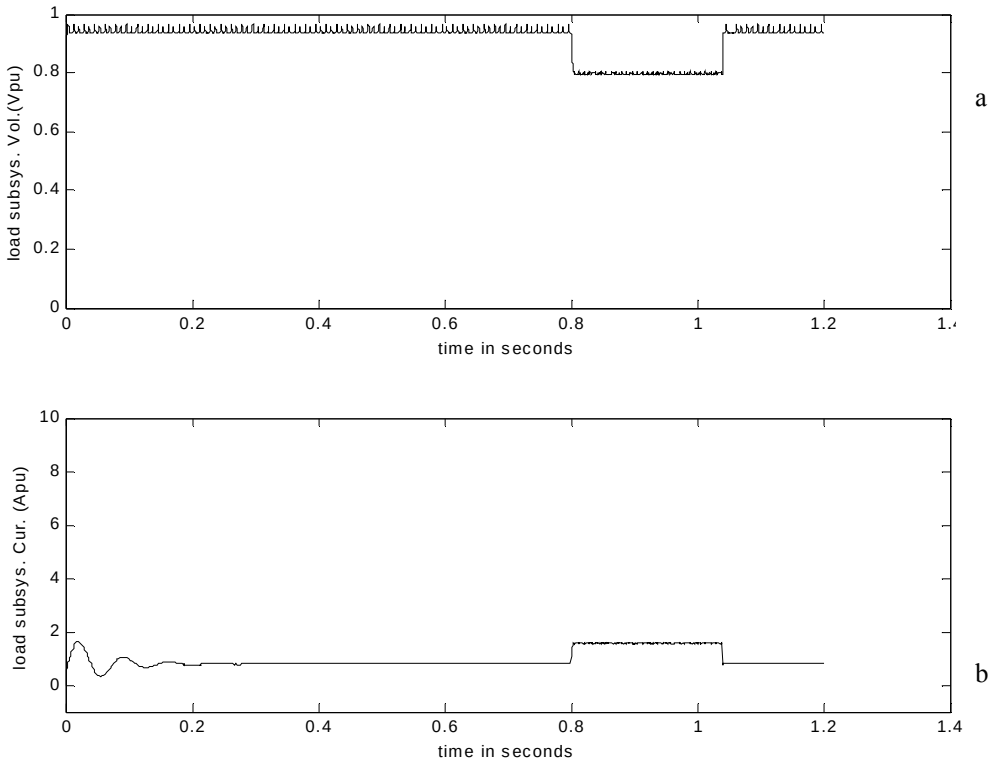


Fig. 5.42 Perturbation model port side simulation results for Scenario 5 in pu. a) Port bus voltage in pu from perturbation model b) Port bus load subsystem input current in pu from perturbation model

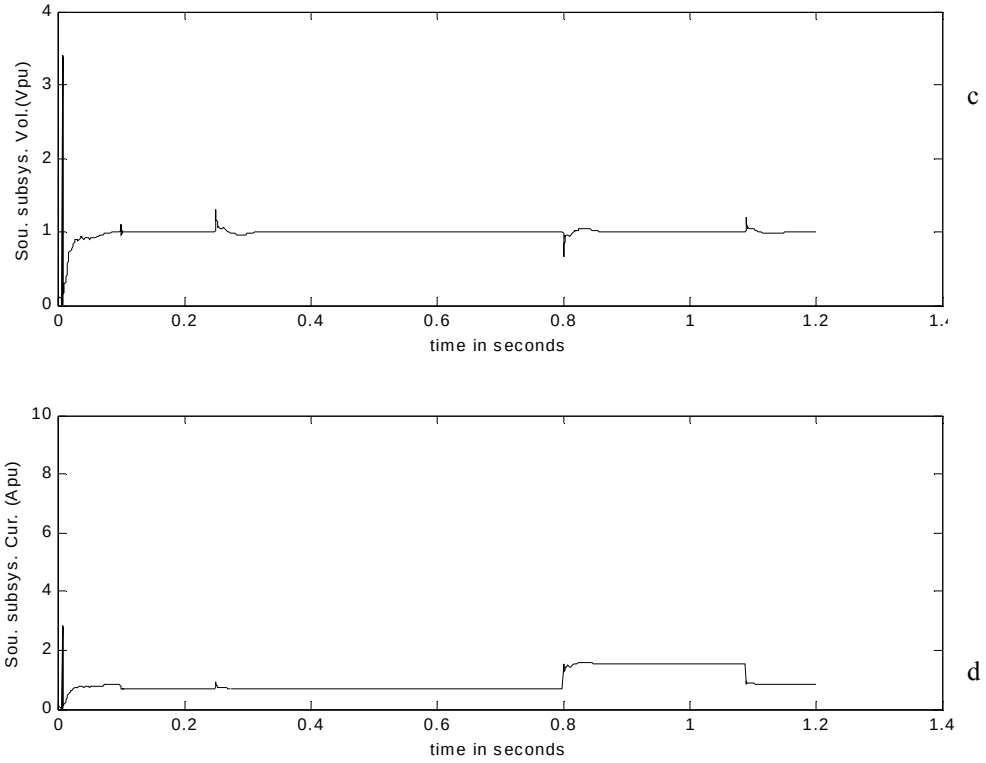


Fig. 5.42 Continued. c) Port bus source subsystem output voltage in pu from perturbation model

d) Port bus source subsystem output current in pu from perturbation model

### 5.3.7 Scenario 6

Scenario 6 is the last of the load addition scenarios category. It represented critically loading the system at a particular bus in the system, and it was easily replicated in the decoupled system. Noise was observed on the post loading profiles in this scenario, due to computer operation conditions. Error of approximation for this scenario was low. Results of the perturbation models are presented in Fig. 5.43a through Fig. 5.43d.

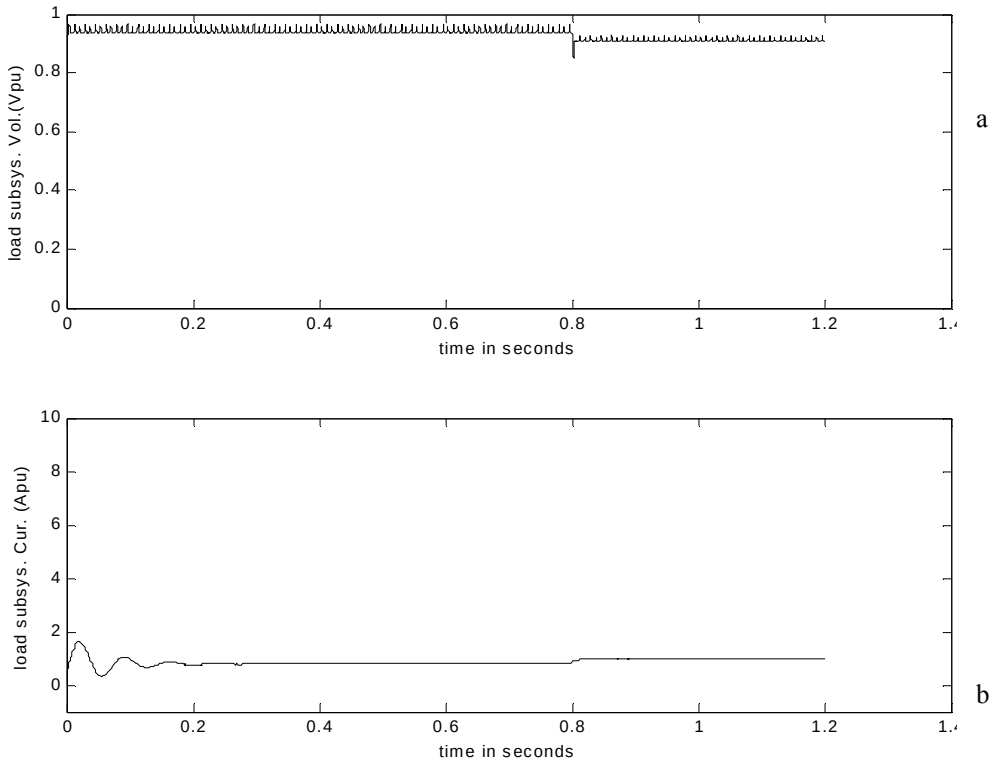


Fig. 5.43 Perturbation model port side simulation results for Scenario 6 in pu. a) Port bus voltage in pu from perturbation model b) Port bus load subsystem input current in pu from perturbation model

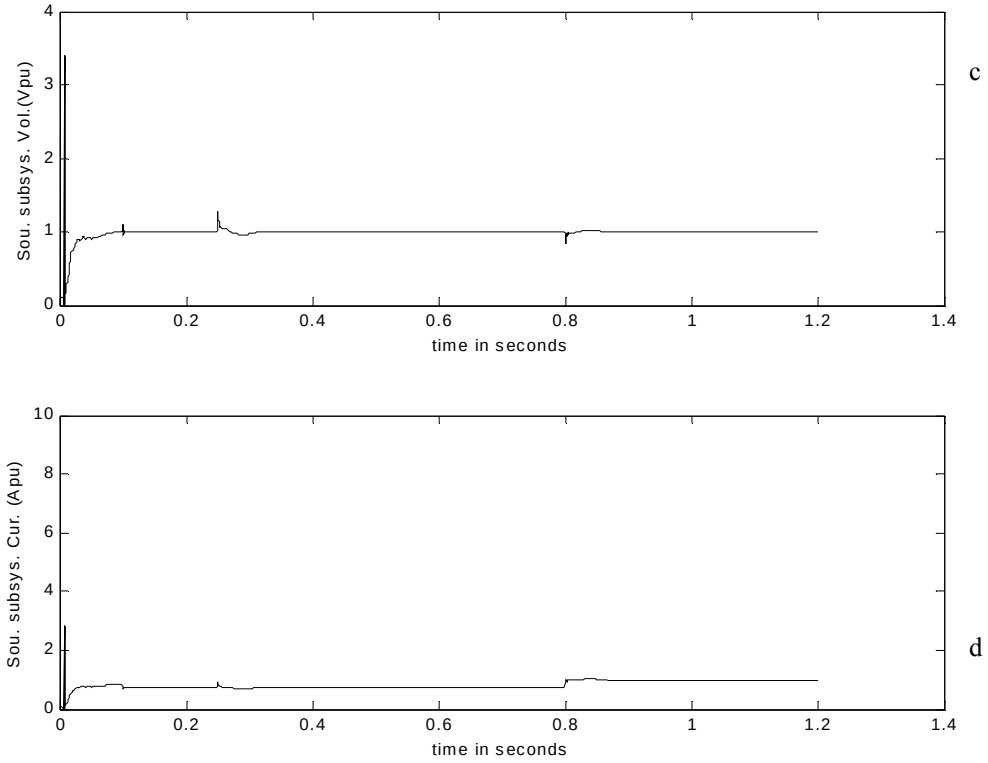


Fig. 5.43 Continued. c) Port bus source subsystem output voltage in pu from perturbation model

d) Port bus source subsystem output current in pu from perturbation model

### 5.3.8 Scenario 7

The last category was load shedding and Scenario 7 represented normal load shedding levels. Scenario 7 was stable and the development of the perturbation models was accurate, with low errors of less than one percent. Results of the perturbation model simulation for Scenario 7 are presented in Fig. 5.44a through Fig. 5.44d.

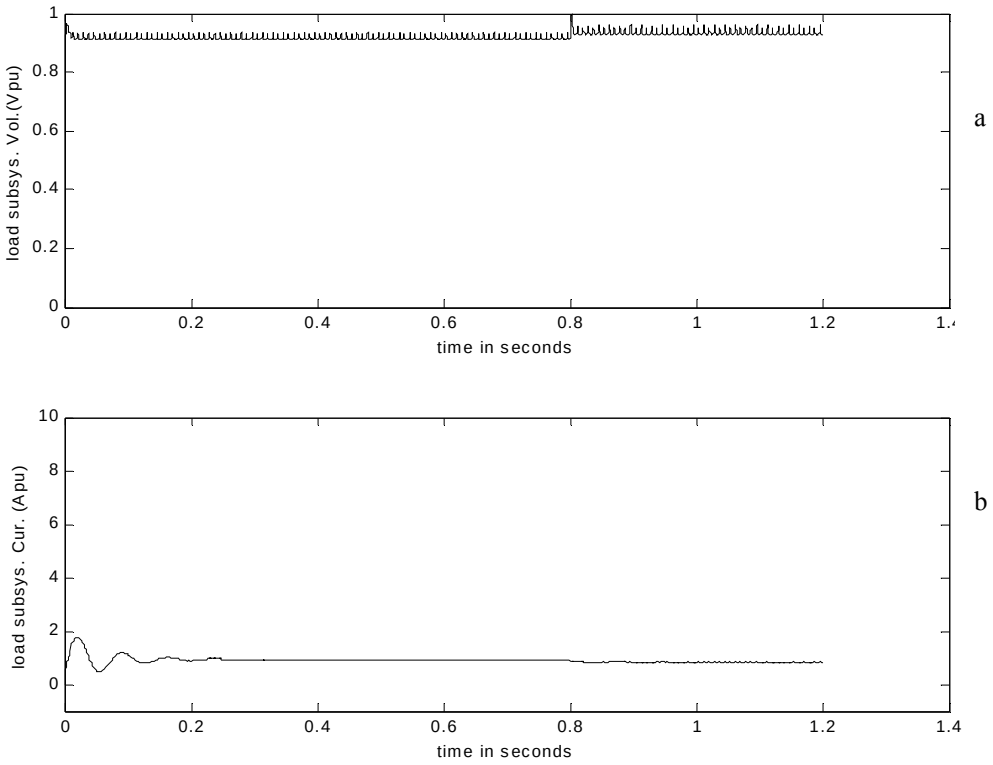


Fig. 5.44 Perturbation model port side simulation results for Scenario 7 in pu. a) Port bus voltage in pu from perturbation model b) Port bus load subsystem input current in pu from perturbation model

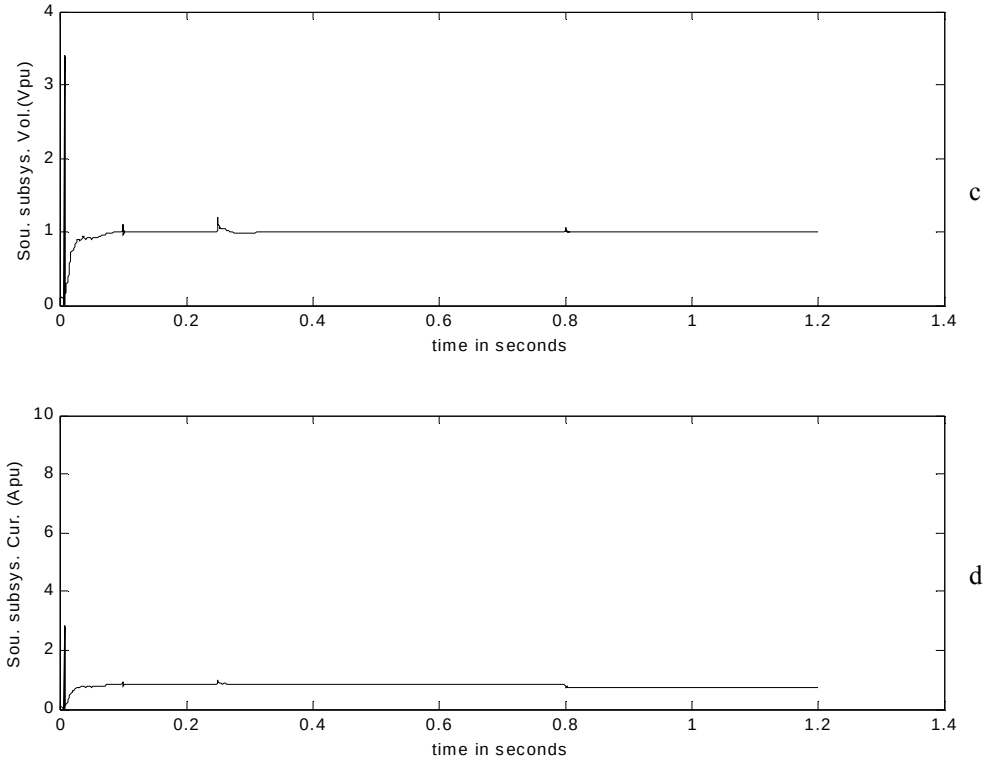


Fig. 5.44 Continued. c) Port bus source subsystem output voltage in pu from perturbation model

d) Port bus source subsystem output current in pu from perturbation model

### 5.3.9 Scenario 8a

When the induction motor was dropped from the system in Scenario 8a, it represented a 3MW load drop sufficient to cause instability within the system. This load, which represented 30 percent the capacity of one of the generators in the system, was able to create the phenomenon of low level loading for most of the filters in the system causing the signal to degrade. It was more complex to model this scenario in the decoupled system for purpose of stability assessment, and this was reflected in the error

presented. An unacceptable 97 percent error was obtained for the 20 kHz gain of the load subsystem, and it was attributed to the difference in system spikes after the motor load was dropped. This difference is a factor of 10 and could not be reduced despite creative attempts. The perturbation modeling was, however, very accurate at all other nodes except for the spikes mentioned. Plots of the results of the perturbation modeling are presented in Fig. 5.45a through Fig. 5.45d.

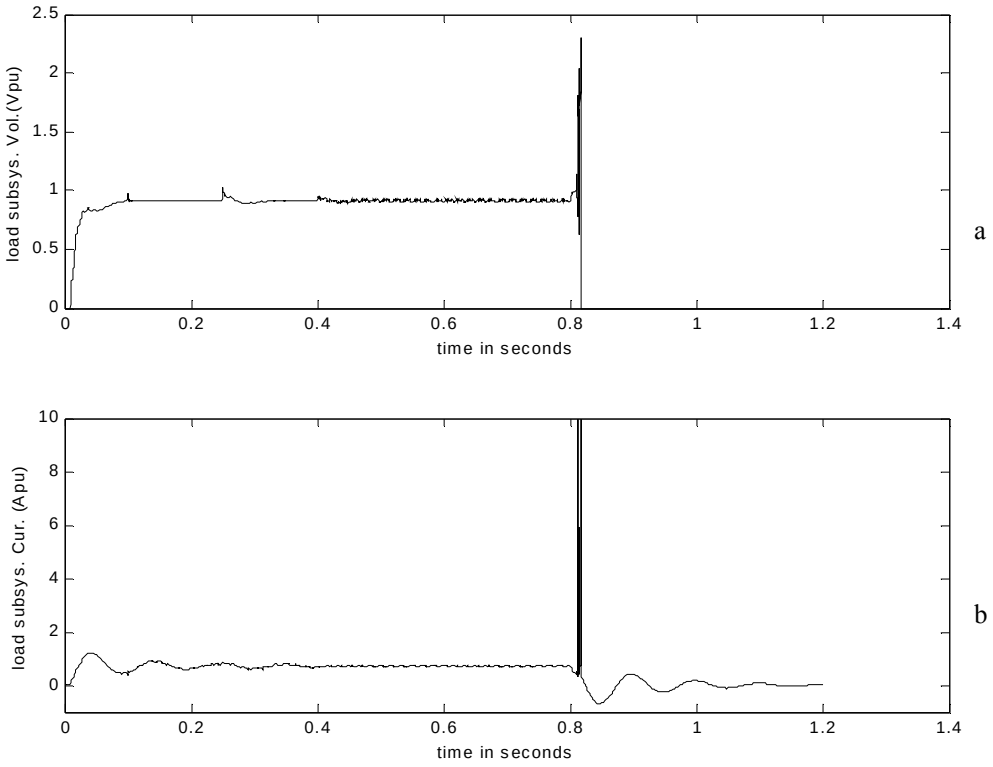


Fig. 5.45 Perturbation model port side simulation results for Scenario 8a in pu. a) Port bus voltage in pu from perturbation model b) Port bus load subsystem input current in pu from perturbation model

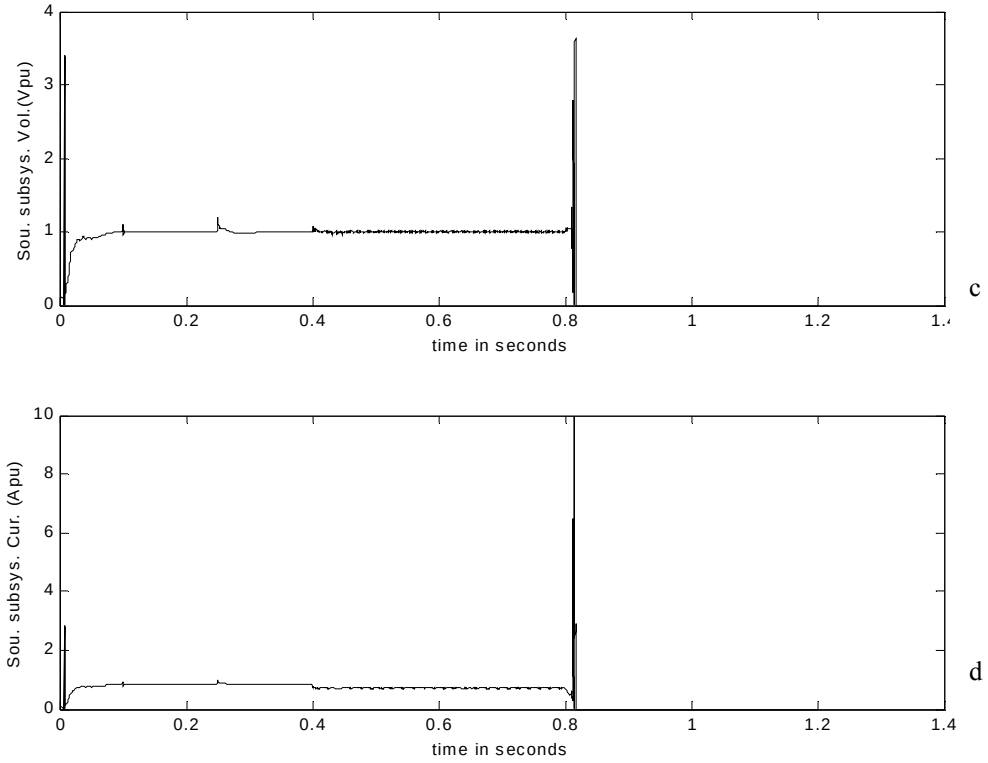


Fig. 5.45 Continued. c) Port bus source subsystem output voltage in pu from perturbation model

d) Port bus source subsystem output current in pu from perturbation model

### 5.3.10 Scenario 9a

The last scenario in the category of load shedding was complete loss of load at a particular bus in the test system. The bus that lost load was the output of the PCM2 on which were connected the induction motor load and the AC static load. It was replicated in the decoupled system with good success and a large signal error of less than 1 percent. The results of the perturbation modeling are presented in Fig. 5.46a through Fig. 5.46d.

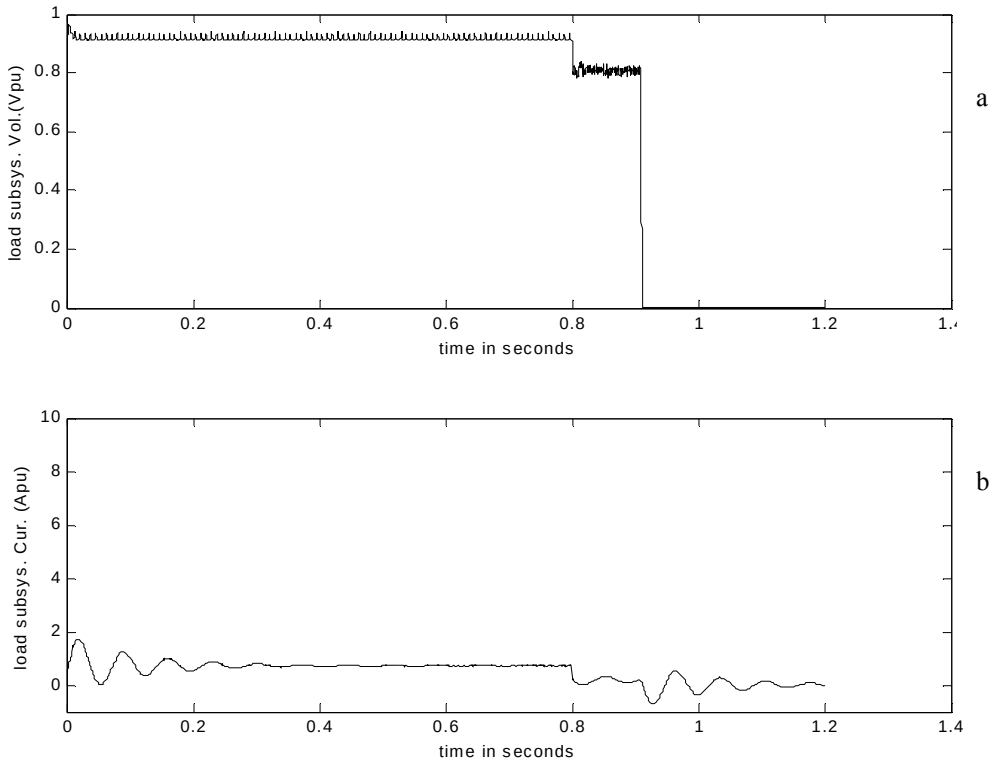


Fig. 5.46 Perturbation model port side simulation results for Scenario 9a in pu. a) Port bus voltage in pu from perturbation model b) Port bus load subsystem input current in pu from perturbation model

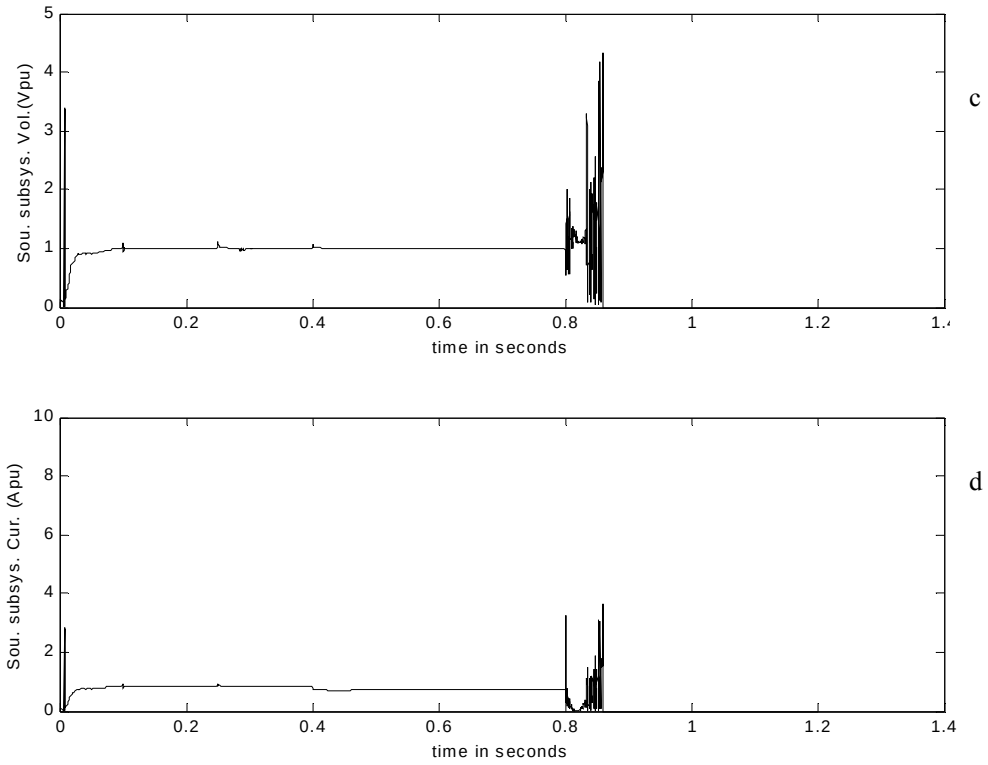


Fig. 5.46 Continued. c) Port bus source subsystem output voltage in pu from perturbation model

d) Port bus source subsystem output current in pu from perturbation model

### 5.3.11 Scenario 8b

Investigating further the instability noticed in Scenario 8a resulted in the system being decoupled about the bus where instability occurred. The reconfiguration activity was the same as in the actual simulation of Scenario 8a but the decoupled system was decoupled about the interzonal bus. Decoupling the system about the interzonal bus resulted in new interface signals which were used for the stability assessment. It was found that replicating the interface signals in the decoupled system was more

challenging at this bus than the other nine scenarios already mentioned owing to the unstable nature of the signals at this bus. However, in order to verify the methodology the best approximation of the instability observed was made and is presented in Fig. 5.47a through Fig. 5.47d.

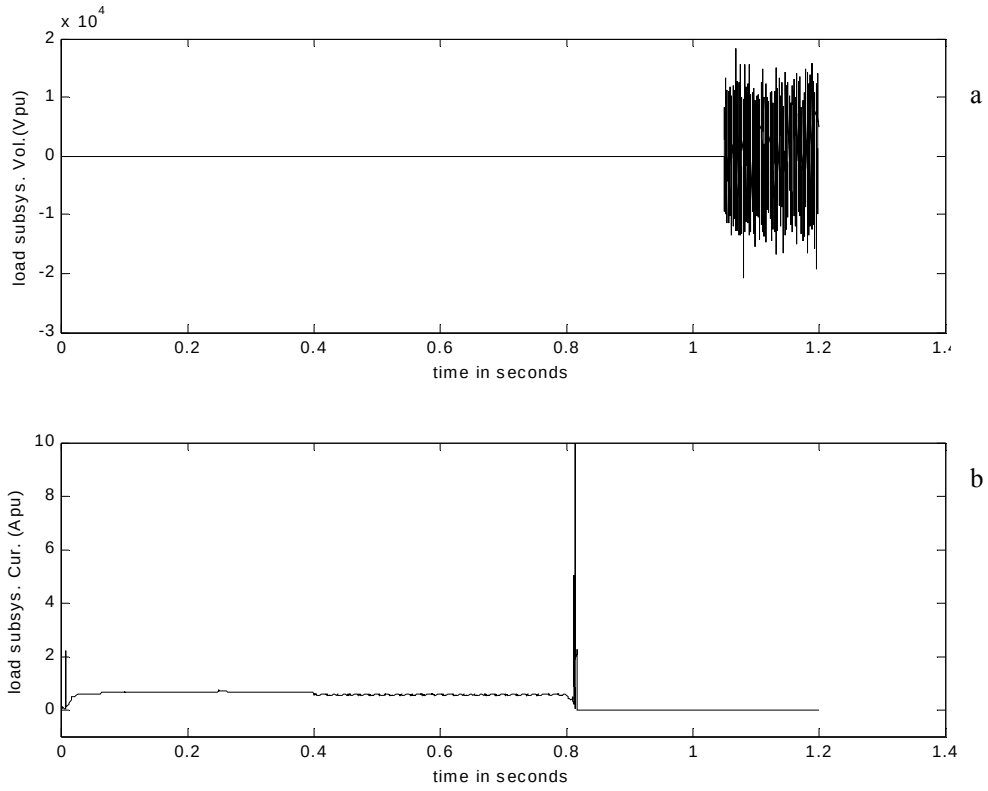


Fig. 5.47 Perturbation model port side simulation results for Scenario 8b in pu. a) Port bus voltage in pu from perturbation model b) Port bus load subsystem input current in pu from perturbation model

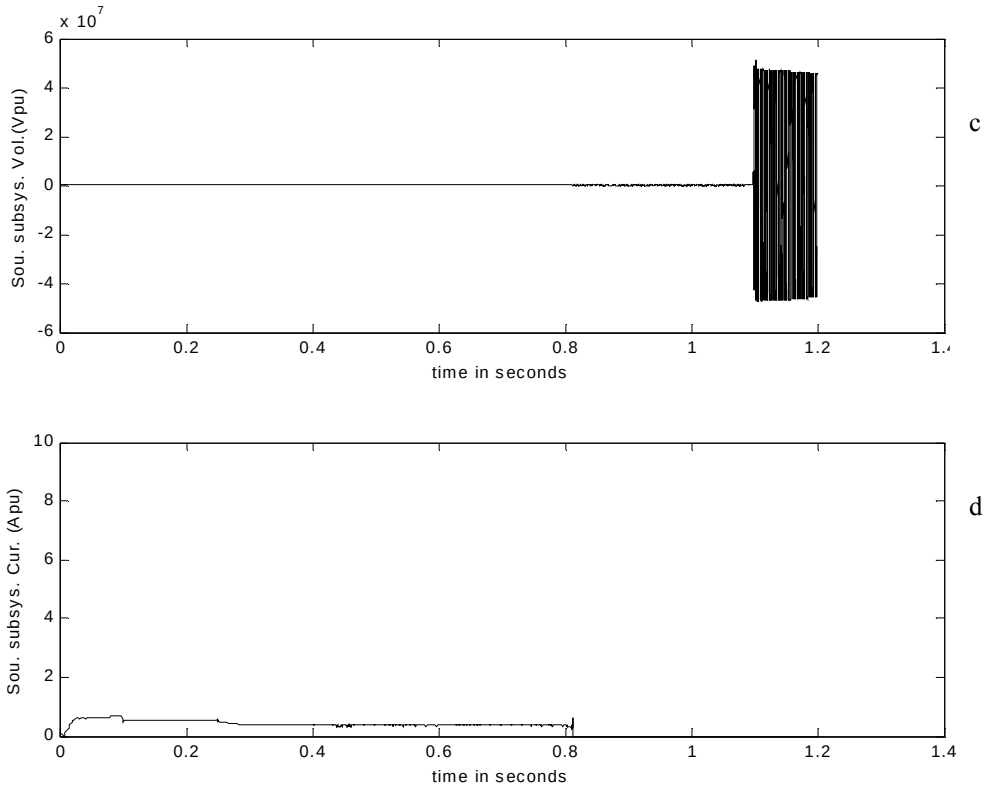


Fig. 5.47 Continued. c) Port bus source subsystem output voltage in pu from perturbation model

d) Port bus source subsystem output current in pu from perturbation model

### 5.3.12 Scenario 9b

Investigating further the instability noticed in Scenario 9a resulted in the system being decoupled also about the bus where instability occurred. The reconfiguration activity was the same as in the actual simulation of Scenario 9a but the decoupled system was decoupled about the interzonal bus. Decoupling the system about the interzonal bus resulted in new interface signals which were used for the stability assessment. It was found that replicating the interface signals in the decoupled system was even more

challenging at this bus than the Scenario 9a already mentioned owing to the unstable nature of the signals at this bus. However, in order to verify the methodology the best approximation of the instability observed was made and is presented in Fig. 5.48a through Fig. 5.48d.

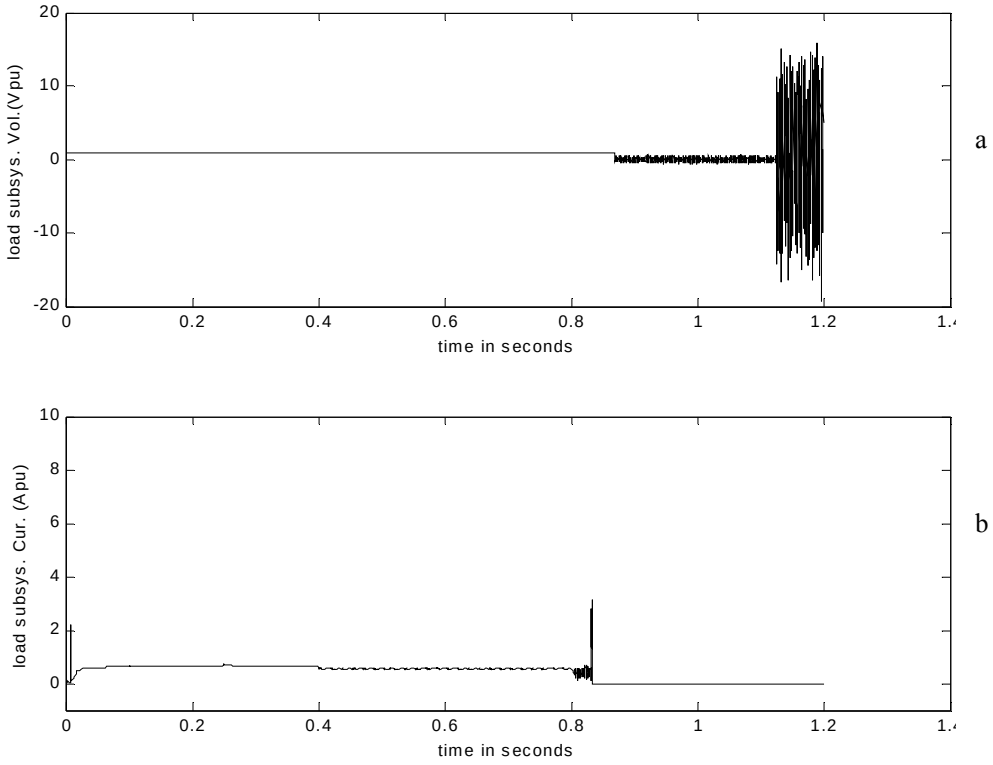


Fig. 5.48 Perturbation model port side simulation results for Scenario 9b in pu. a) Port bus voltage in pu from perturbation model b) Port bus load subsystem input current in pu from perturbation model

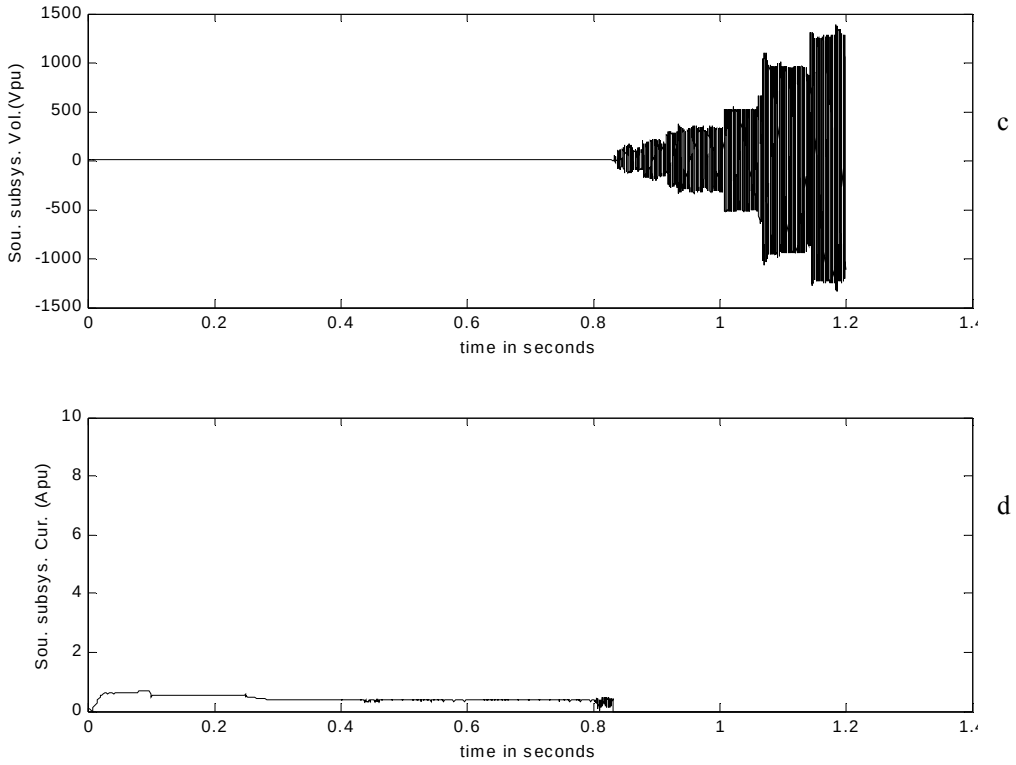


Fig. 5.48 Continued. c) Port bus source subsystem output voltage in pu from perturbation model

d) Port bus source subsystem output current in pu from perturbation model

## 5.4 Stability

Using system identification method and specifically the auto regression moving average with exogenous input model (ARMAX) [54], the linear gain was obtained. The linear gain is as shown in (5.1) and (5.2). The error of the system before the order of the ARMAX was chosen is presented in Table 5.5. In order to obtain the non linear gain, the interface input data, u, for the subsystems are passed into the linear gain for the

subsystems and the intermediate output signals y is passed into a multiplier to generate the output y'. y' and the interface output data yold are used to compute the sector gain from (5.3)[31].

For the transfer function (Linear gain)

$$\text{Gain for source subsystem} = \frac{6.545e-5s^2+10.81s-765.5}{s^2+2359s+2.943e+7} \tag{5.1}$$

$$\text{Gain for Load subsystem} = \frac{6.618\text{e}-5\text{s}^2+14.06s-5.273e+4}{s^2+6677s+2.158e+5} \tag{5.2}$$

$$r(c) \geq \sqrt{\frac{\int_{-\infty}^{\infty} \text{P}_{y-cu}(f)df}{\int_{-\infty}^{\infty} \text{P}_u(f)df}} \approx \sqrt{\frac{\sum_i \text{P}_{y-cu}^i(f_i)}{\sum_i \text{P}_u^i(f_i)}} \tag{5.3}$$

Table 5.5
Small signal error per order of ARMAX model

| Order number | Source subsystem error in db | Load subsystem error in db |
|---|---|---|
| 1.0 | -.8137 | -0.2224 |
| 2.0 | -1.0428 | -1.0562 |
| 3.0 | -1.2983 | -1.2265 |
| 4.0 | -1.6664 | -1.2770 |
| 5.0 | -1.6773 | -1.2994 |
| 6.0 | -1.7685 | -1.3118 |
| 7.0 | -1.7571 | -1.3192 |
| 8.0 | -1.7955 | -1.3243 |
| 9.0 | -1.7882 | -1.3282 |
| 10.0 | -1.8094 | -1.3314 |

The orders used in the stability assessment were Order 2 for the source subsystem and Order 2 for the load subsystem. These were chosen because they gave the best error for the frequency range they contained for the stability assessment. After selecting the conic center to be 200 the corresponding radii for all the nine scenarios were as given in Table 5.6.

Table 5.6
Radii of conic sectors for reconfiguration scenarios

| Center = 200 | rs | rl |
|---|---|---|
| Scenario 1 radius | 199.24 | 199.278 |
| Scenario 2 radius | 199.2769 | 199.3987 |
| Scenario 3 radius | 199.2557 | 199.3361 |
| Scenario 4 radius | 198.9997 | 198.8396 |
| Scenario 5 radius | 198.9969 | 198.5538 |
| Scenario 6 radius | 198.9992 | 198.8533 |
| Scenario 7 radius | 199.0007 | 198.8705 |
| Scenario 8a radius | 199.0012 | 198.9233 |
| Scenario 9a radius | 199.1937 | 199.3091 |

Since the radii were all less than 200, the forbidden regions for the scenarios were within the disk centered at around 0.5, spanning nearly zero and -1 on the left hand plane of the s plane. The stability assessment, therefore, shows no intersections of these forbidden regions with the pseudo nyquist contours for Conditions 1 and 2 for scenarios 1 through 9 but for Scenarios 8b and 9b which were unstable the methodology indicated

that they were unstable. Condition 3 for all the scenarios shows no transversing of the unstable regions that lie above the upper curve in each plot to be presented in the discussion of the scenario stability. The following stability conditions and the rules [31] apply as also shown in Chapter III in (5.4) and (5.5).

$$\delta_z \equiv 1 - \left| \frac{T(s)c_y}{1 + c_z T(s) c_y} \right| r_z > 0$$

$$\delta_y \equiv 1 - \left| \frac{T(s)c_z}{1 + c_z T(s) c_y} \right| r_y > 0$$

$$G \equiv \frac{\delta_z \delta_y}{r_y r_z} - \left| \frac{T(s)}{\left[1 + c_z c_y T(s)\right]^2} \right| > 0 \qquad (5.4)$$

$T(s) = L_z L_y$ product of source and load linear gains

$\{c, r\}$ Center and radius of the conic sector

$$b = c + r$$

$$a = c - r \qquad (5.5)$$

if a>0 the Nyquist (Tscy or Tscz) must avoid the disc with points -1/a and -1/b on the real axis

if a =0 the Nyquist (Tscy or Tscz) must stay to the right of the vertical line passing through -1/b

if a<0 the Nyquist (Tscy or Tscz) plot must stay inside the disc that intersects the real axis at -1/b and -1/a

5.4.1 Scenario 1

Evaluating the conditions in (5.4) for Scenario 1 yielded the results that the scenario was stable as was observed. There are no intersections between the areas within the disk of the forbidden region (of which only a portion is shown left of the full trajectory of the Nyquist contour) and the Nyquist contour of Conditions 1 and 2. Also, the region above the upper curve was not traversed by the lower curve in Condition 3. These results are presented in Fig. 5.49a-Fig. 5.49c.

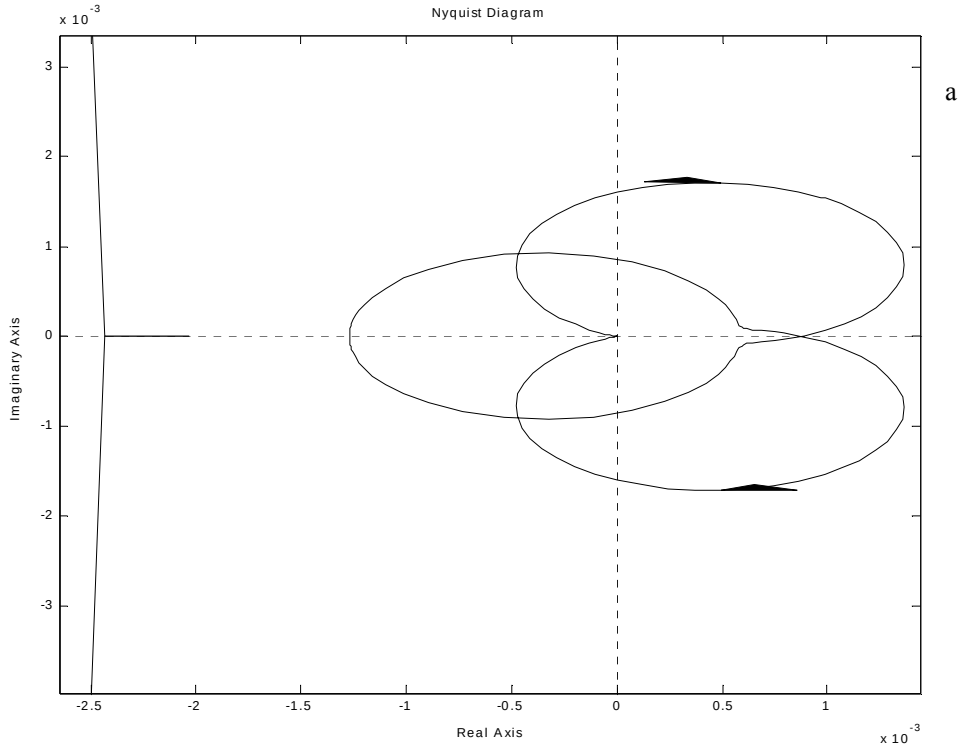


a

Fig. 5.49 Plot of Conditions for Scenario 1. a) Plot of Condition 1 for Scenario 1

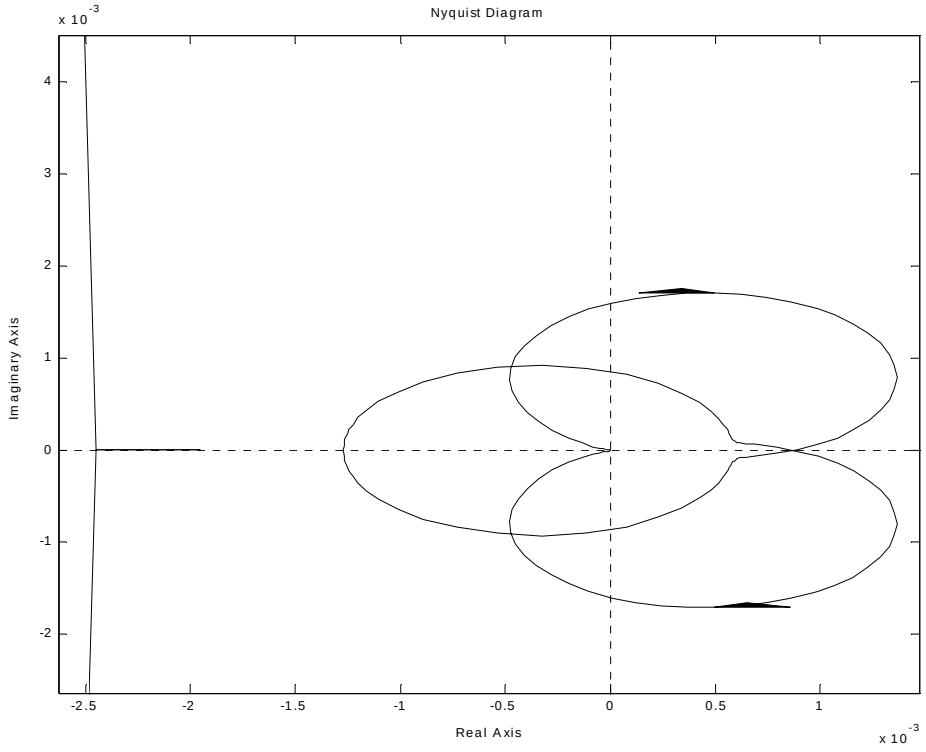


b

Fig. 5.49 Continued. b) Plot of Condition 2 for Scenario 1

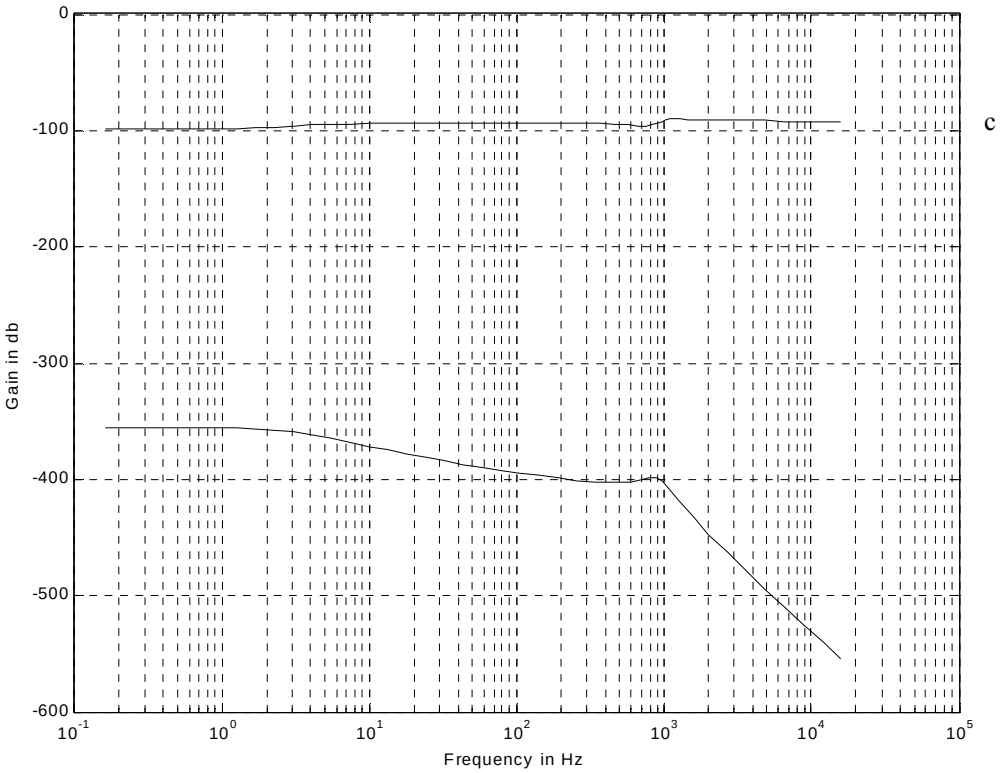


Fig. 5.49 Continued. c) Plot of Condition 3 for Scenario 1

### 5.4.2 Scenario 2

Evaluating the conditions in (5.4) for Scenario 2 yielded the results that the scenario was stable as was observed. There are no intersections between the areas within the disk of the forbidden region (of which only a portion is shown left of the full trajectory of the Nyquist contour) and the Nyquist contour of Conditions 1 and 2. Also, the region above the upper curve was not traversed by the lower curve in Condition 3. These results are presented in Fig. 5.50a-Fig. 5.50c.

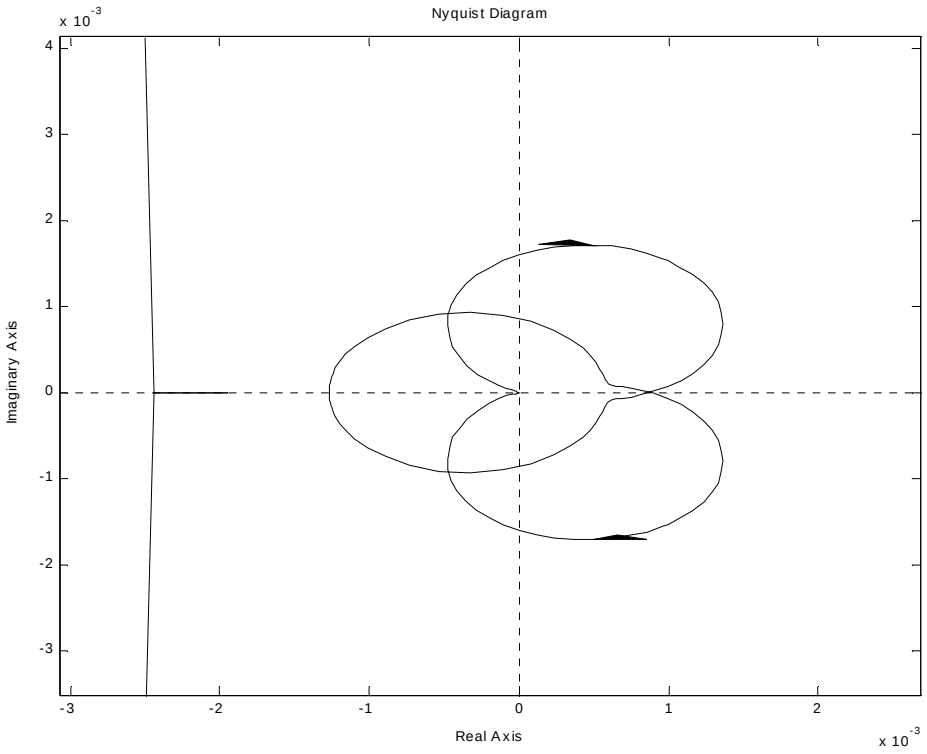


a

Fig. 5.50 Plot of Conditions for Scenario 2. a) Plot of Condition 1 for Scenario 2

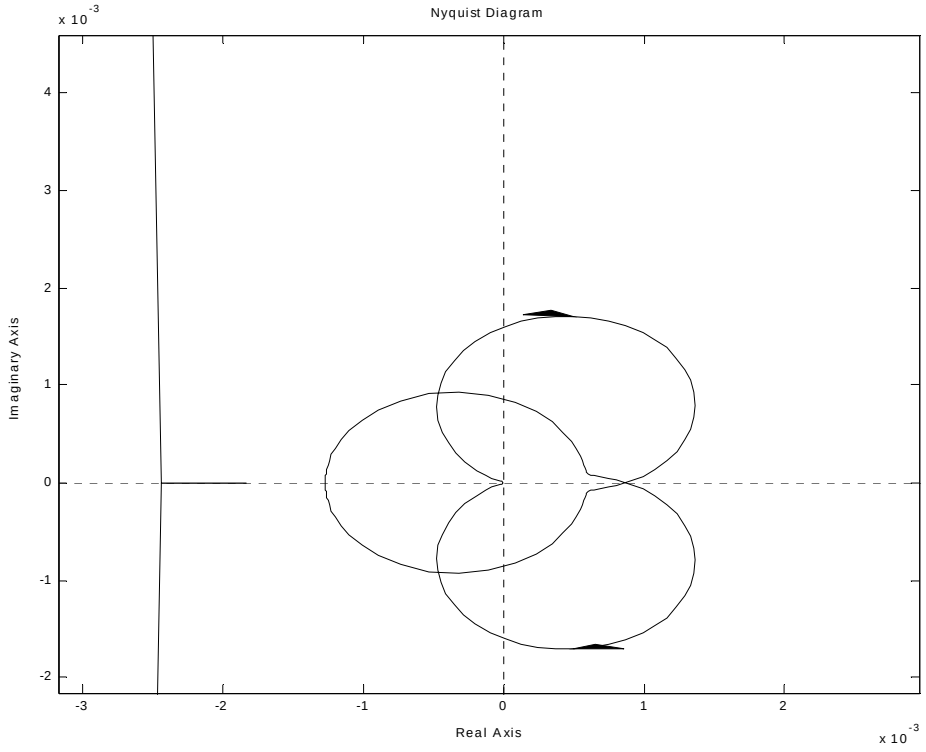


b

Fig. 5.50 Continued. b) Plot of Condition 2 for Scenario 2

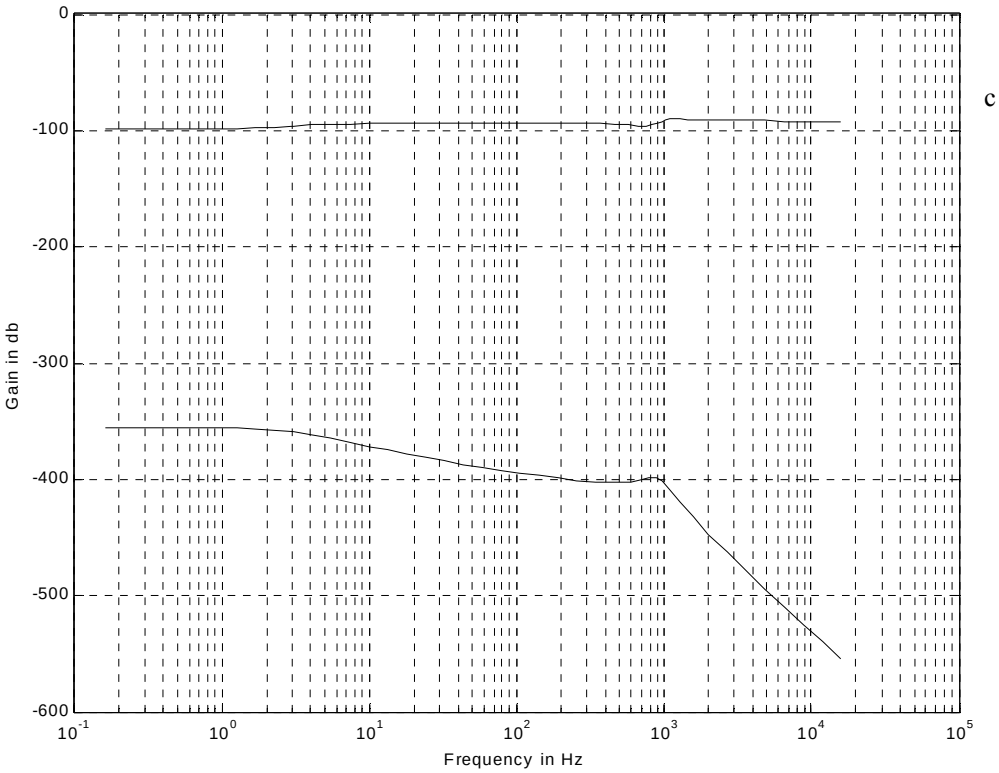


Fig. 5.50 Continued. c) Plot of Condition 3 for Scenario 2

### 5.4.3 Scenario 3

Evaluating the conditions in (5.4) for Scenario 3 also yielded the results that the scenario was stable as was observed. There are no intersections between the areas within the disk of the forbidden region (of which only a portion is shown left of the full trajectory of the Nyquist contour) and the Nyquist contour of Conditions 1 and 2. Also, the region above the upper curve was not traversed by the lower curve in Condition 3. These results are presented in Fig. 5.51a-Fig. 5.51c.

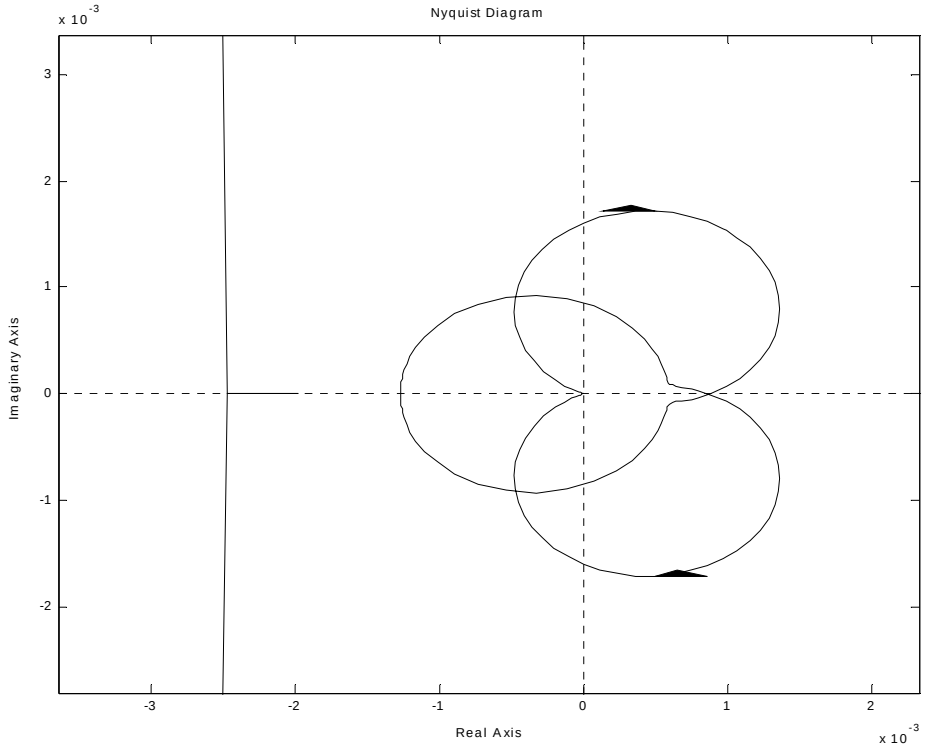


a

Fig. 5.51 Plot of Conditions for Scenario 3. a) Plot of Condition 1 for Scenario 3

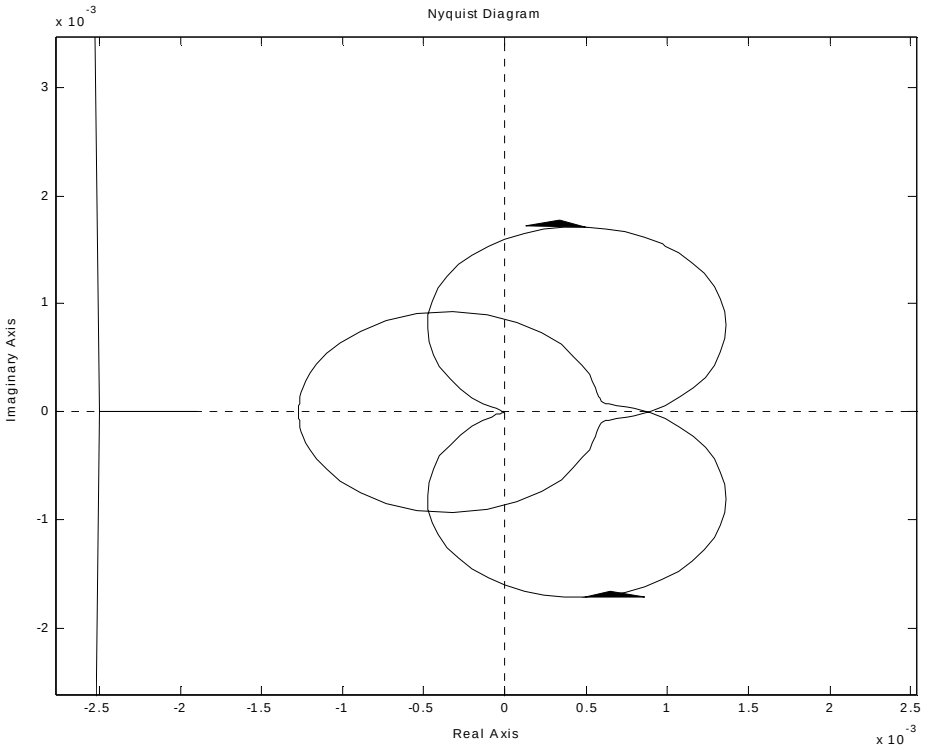


b

Fig. 5.51 Continued. b) Plot of Condition 2 for Scenario 3

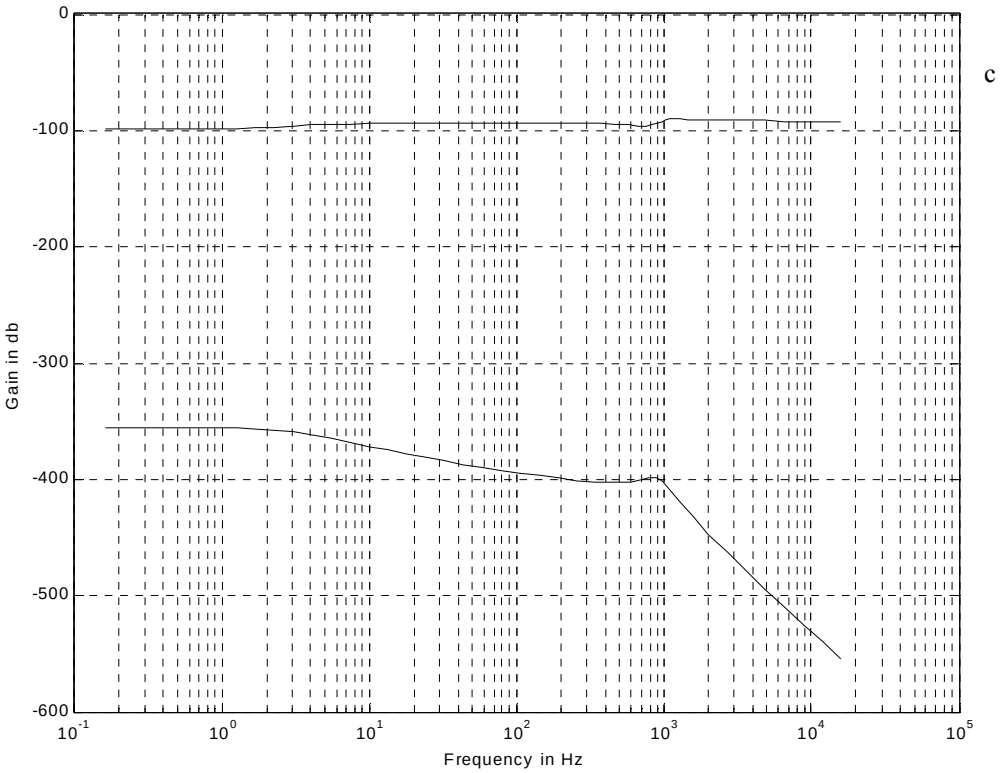


Fig. 5.51 Continued. c) Plot of Condition 3 for Scenario 3

5.4.4 Scenario 4

Evaluating the conditions in (5.4) for Scenario 4 also yielded the results that the scenario was stable as was previously visually observed. There are no intersections between the areas within the disk of the forbidden region (of which only a portion is shown left of the full trajectory of the Nyquist contour) and the Nyquist contour of Conditions 1 and 2. Also, the region above the upper curve was not traversed by the lower curve in Condition 3. These results are presented in Fig. 5.52a-Fig. 5.52c.

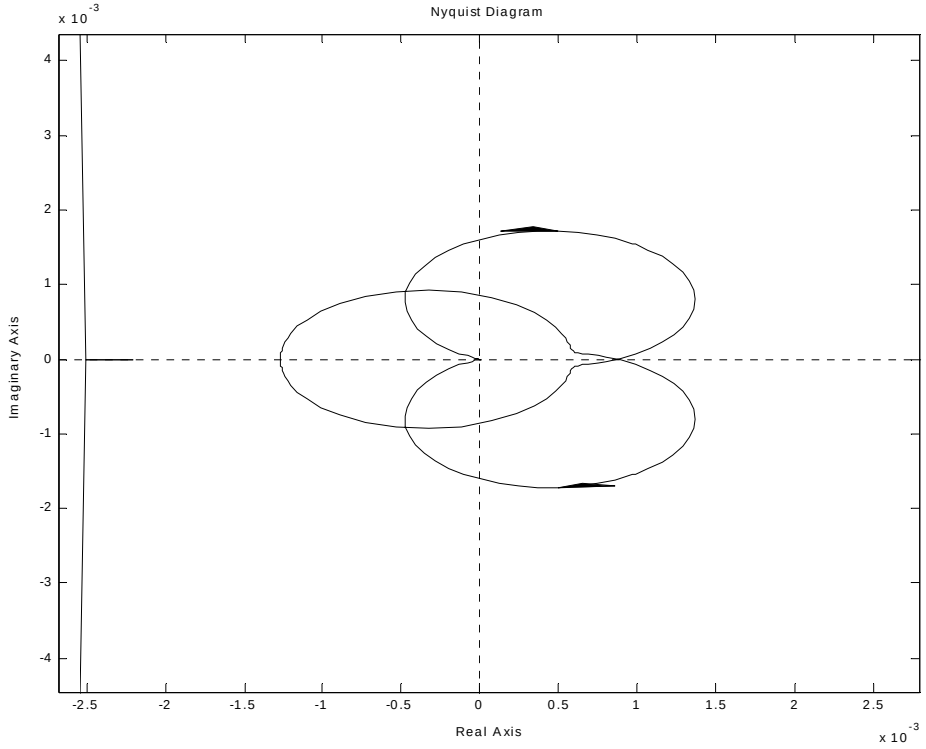


a

Fig. 5.52 Plot of Conditions for Scenario 4. a) Plot of Condition 1 for Scenario 4

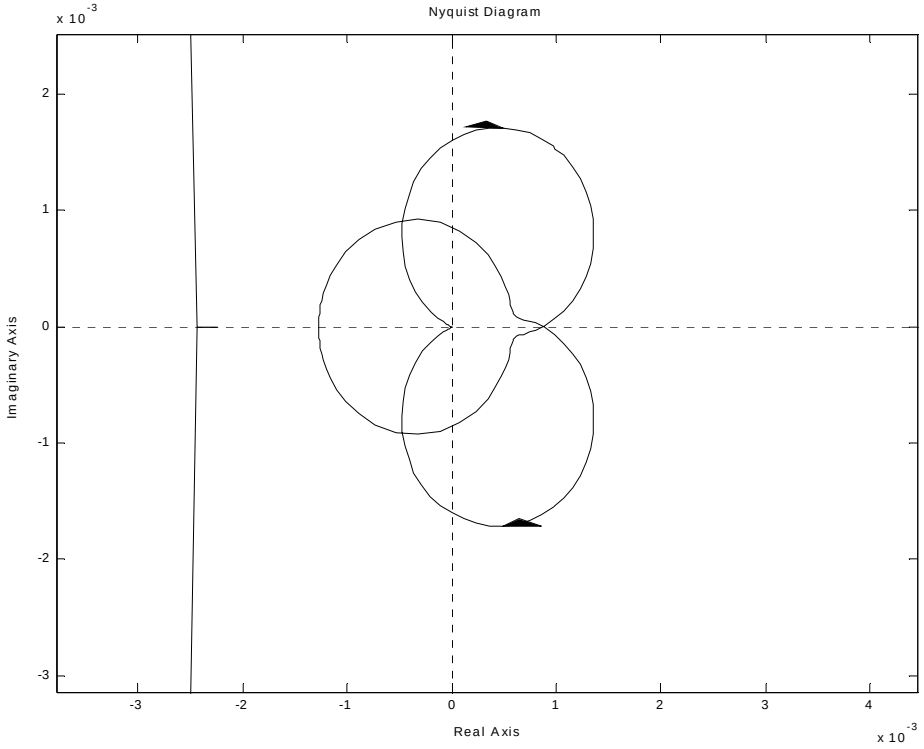


b

Fig. 5.52 Continued. b) Plot of Condition 2 for Scenario 4

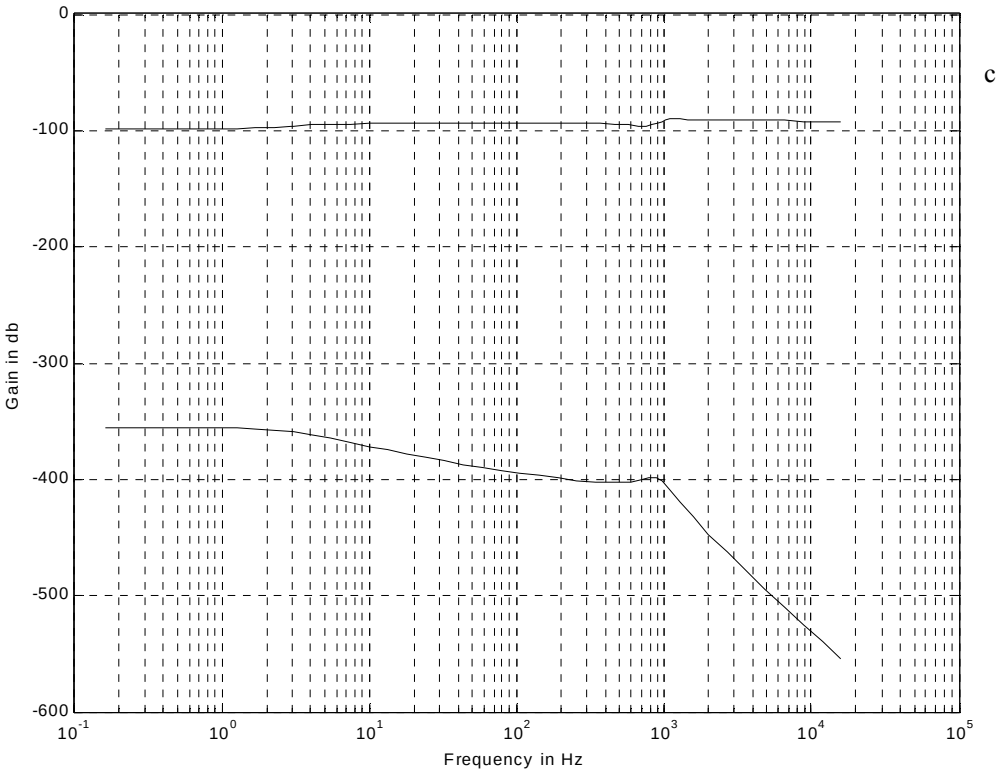


Fig. 5.52 Continued. c) Plot of Condition 3 for Scenario 4

5.4.5 Scenario 5

Evaluating the conditions in (5.4) for Scenario 5 also yielded the results that the scenario was stable, as was previously visually observed. There are no intersections between the areas within the disk of the forbidden region (of which only a portion is shown left of the full trajectory of the Nyquist contour) and the Nyquist contour of Conditions 1 and 2. Also, the region above the upper curve was not traversed by the lower curve in Condition 3. These results are presented in Fig. 5.53a-Fig. 5.53c. A major

factor in the similarity of the results for all the scenarios is the linear gain remained the same in all scenarios.

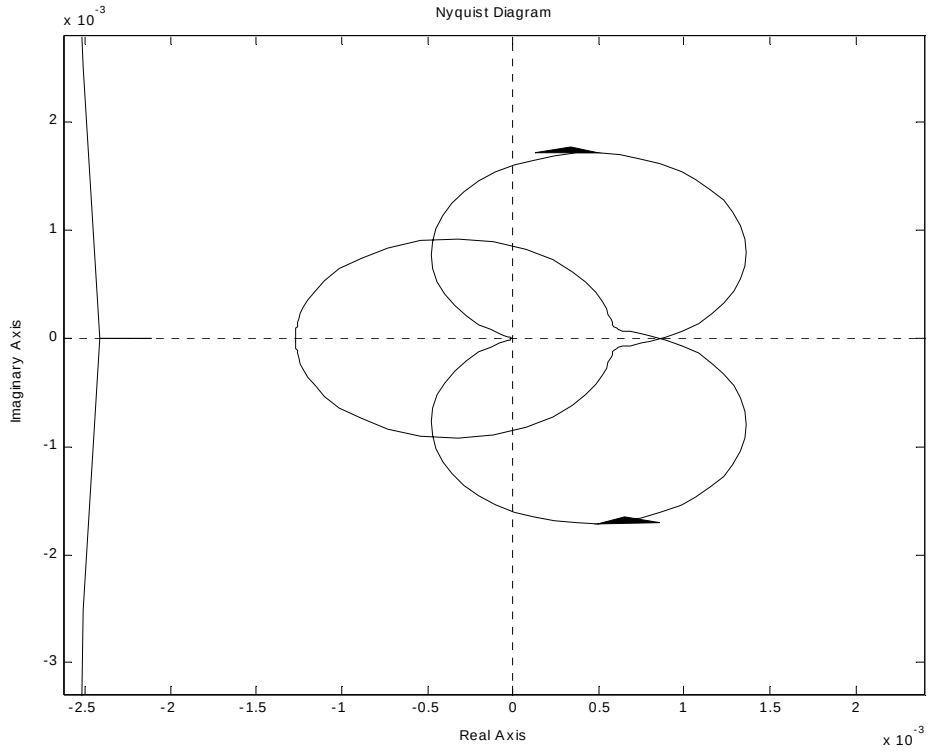


a

Fig. 5.53 Plot of Conditions for Scenario 5. a) Plot of Condition 1 for Scenario 5

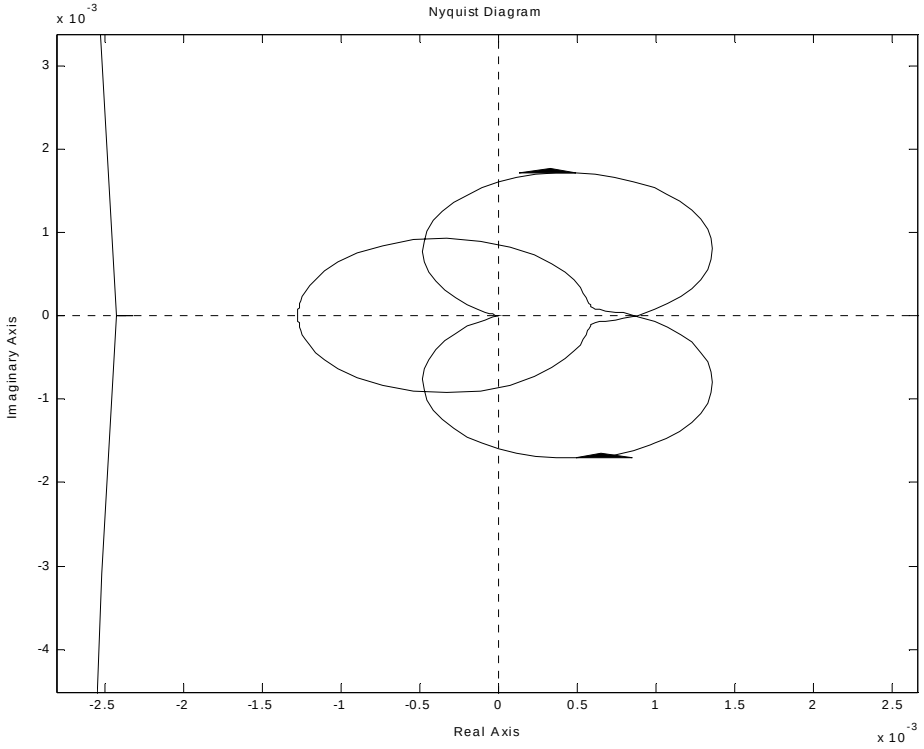


b

Fig. 5.53 Continued. b) Plot of Condition 2 for Scenario 5

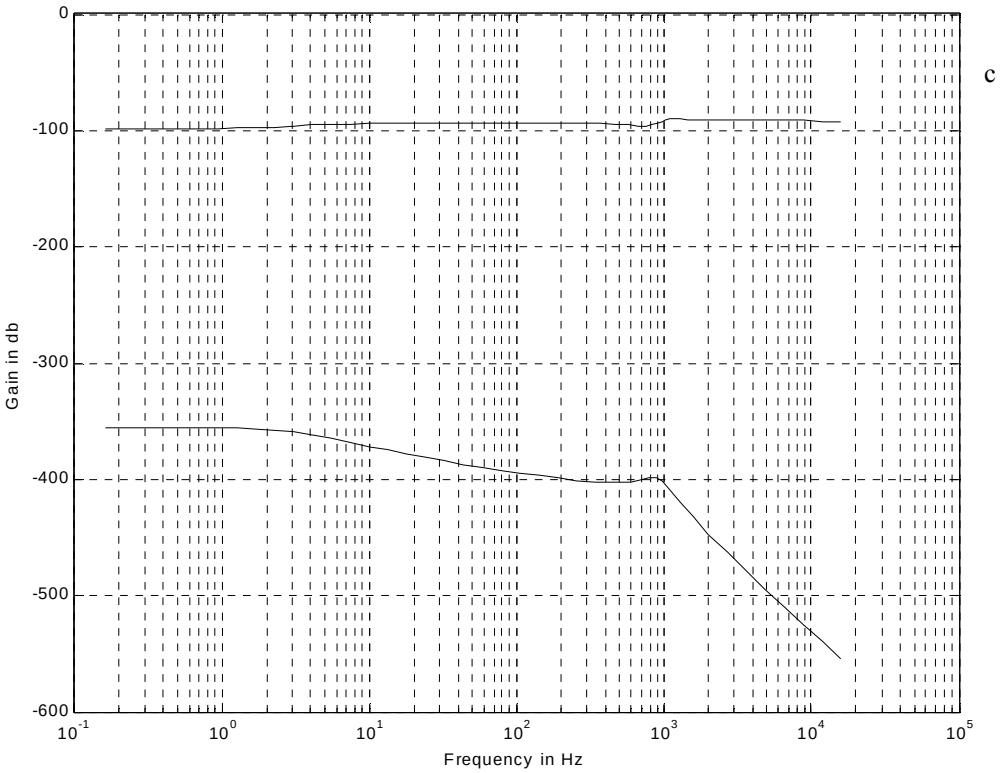


Fig. 5.53 Continued. c) Plot of Condition 3 for Scenario 5

### 5.4.6 Scenario 6

Evaluating the conditions in (5.4) for Scenario 6 also yielded the results that the scenario was stable as was observed. There are no intersections between the areas within the disk of the forbidden region (of which only a portion is shown left of the full trajectory of the Nyquist contour) and the Nyquist contour of Conditions 1 and 2. Also, the region above the upper curve was not traversed by the lower curve in Condition 3. These results are presented in Fig. 5.54a-Fig. 5.54c.

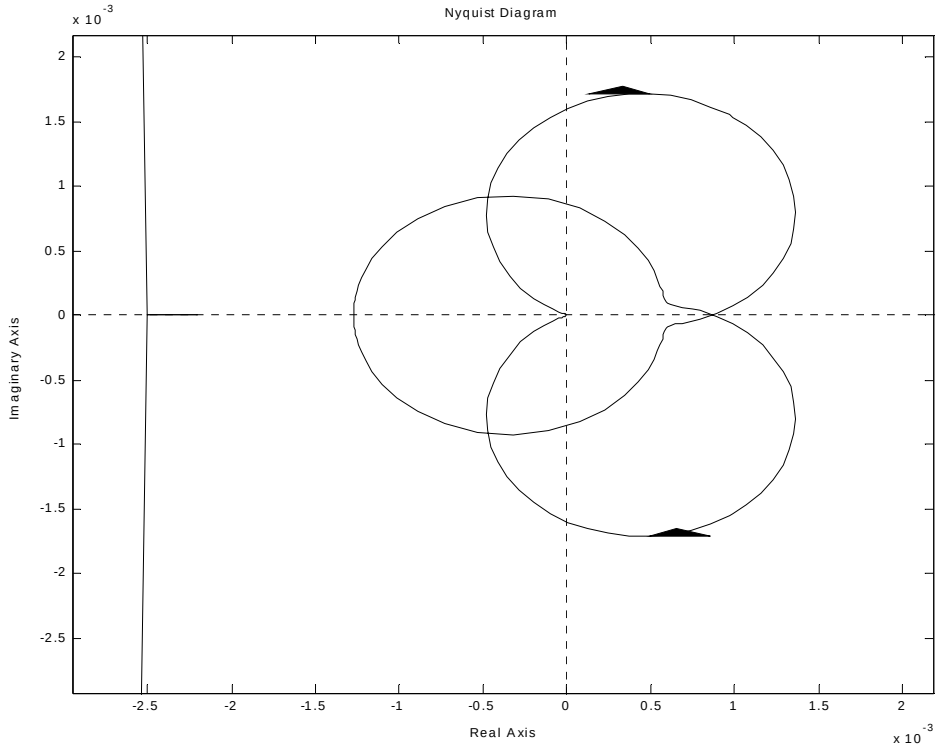


a

Fig. 5.54 Plot of Conditions for Scenario 6. a) Plot of Condition 1 for Scenario 6

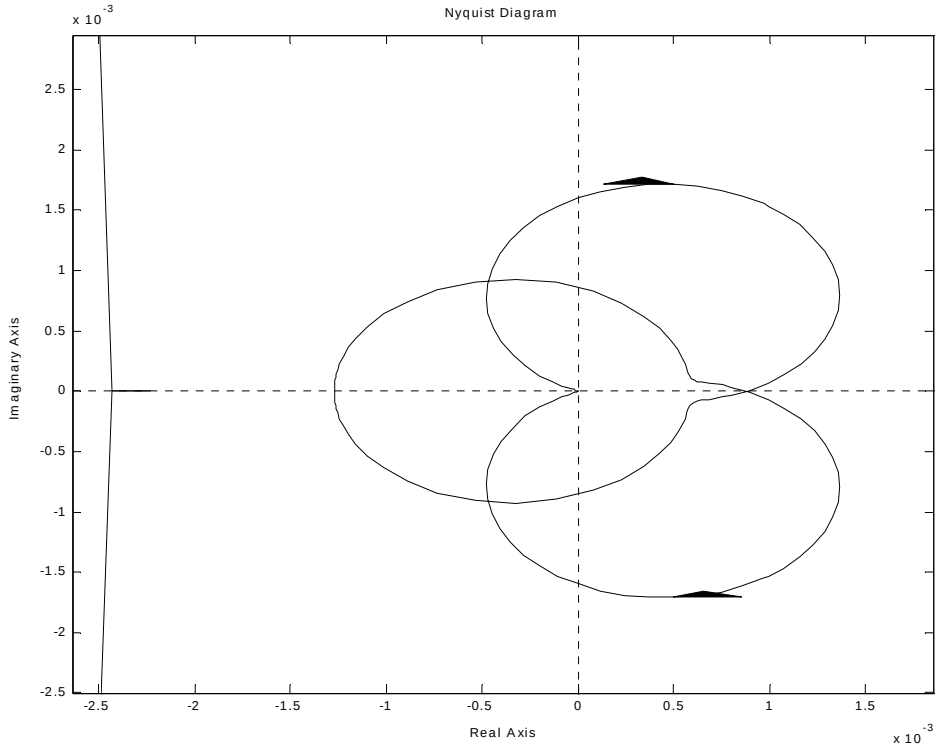


b

Fig. 5.54 Continued. b) Plot of Condition 2 for Scenario 6

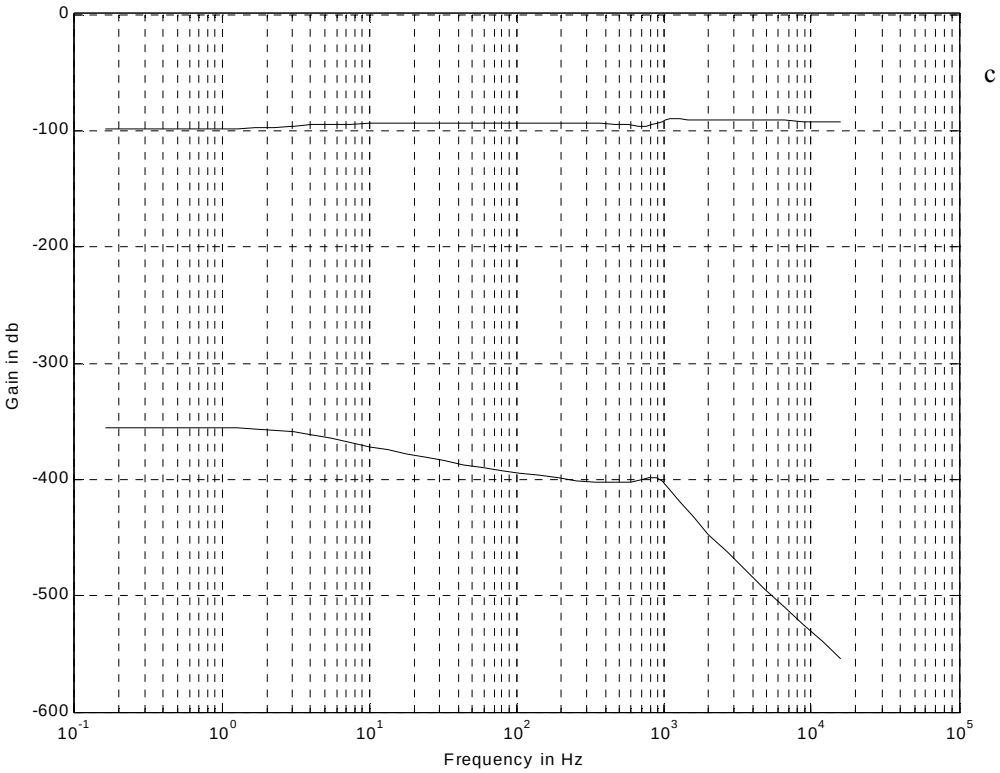


Fig. 5.54 Continued. c) Plot of Condition 3 for Scenario 6

### 5.4.7 Scenario 7

Evaluating the conditions in (5.4) for Scenario 7 also yielded the results that the scenario was stable as was observed. There are no intersections between the areas within the disk of the forbidden region (of which only a portion is shown left of the full trajectory of the Nyquist contour) and the Nyquist contour of Conditions 1 and 2. Also, the region above the upper curve was not traversed by the lower curve in Condition 3. These results are presented in Fig. 5.55a-Fig. 5.55c.

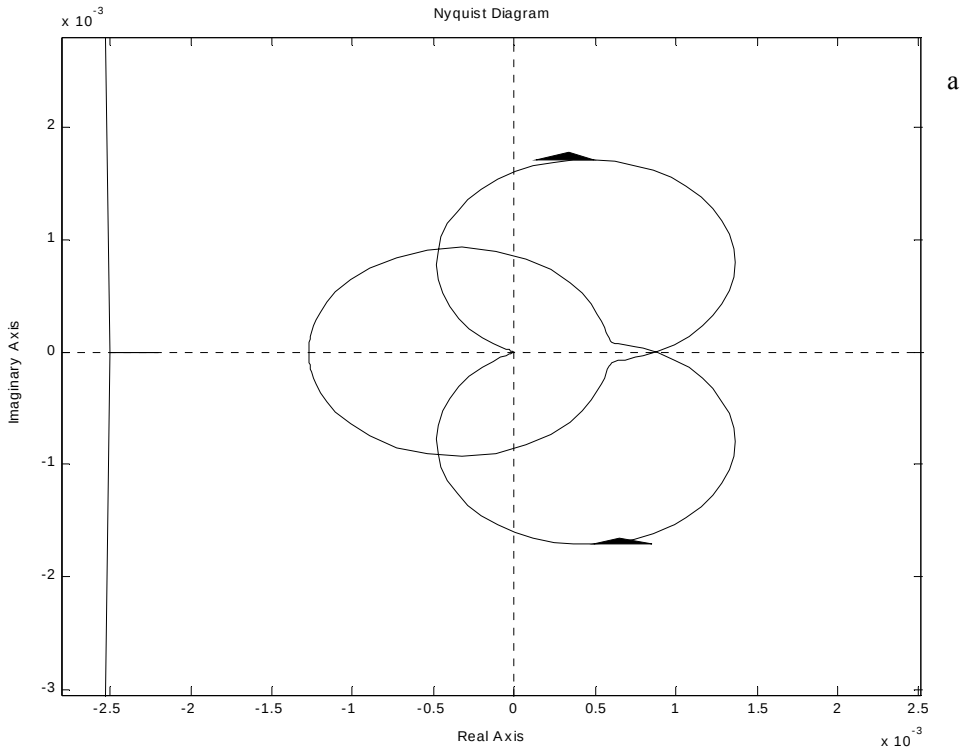


a

Fig. 5.55 Plot of Conditions for Scenario 7. a) Plot of Condition 1 for Scenario 7

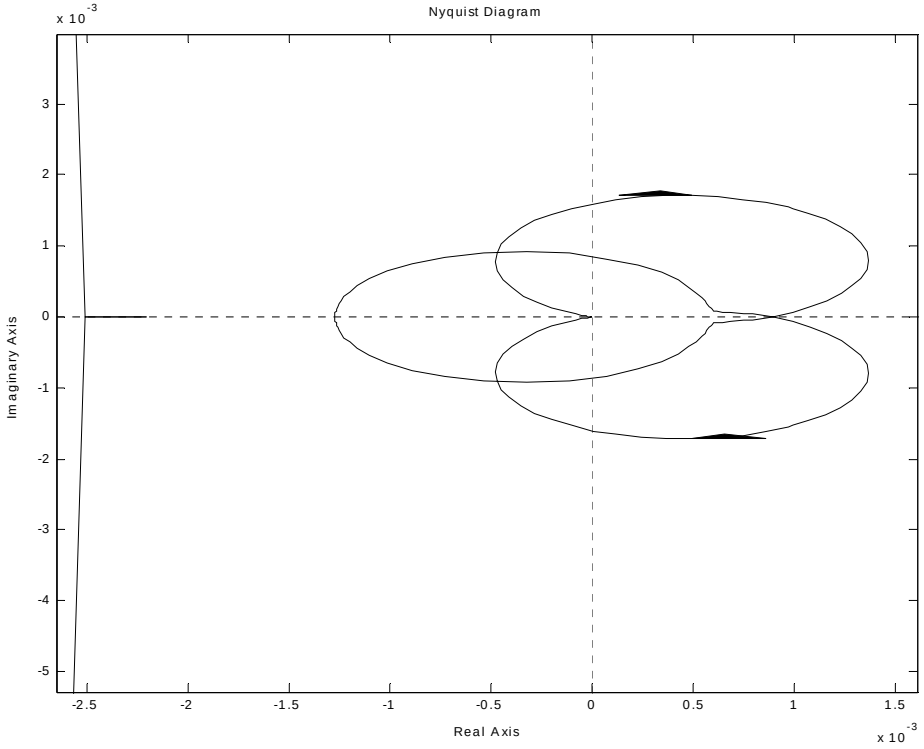


b

Fig. 5.55 Continued. b) Plot of Condition 2 for Scenario 7

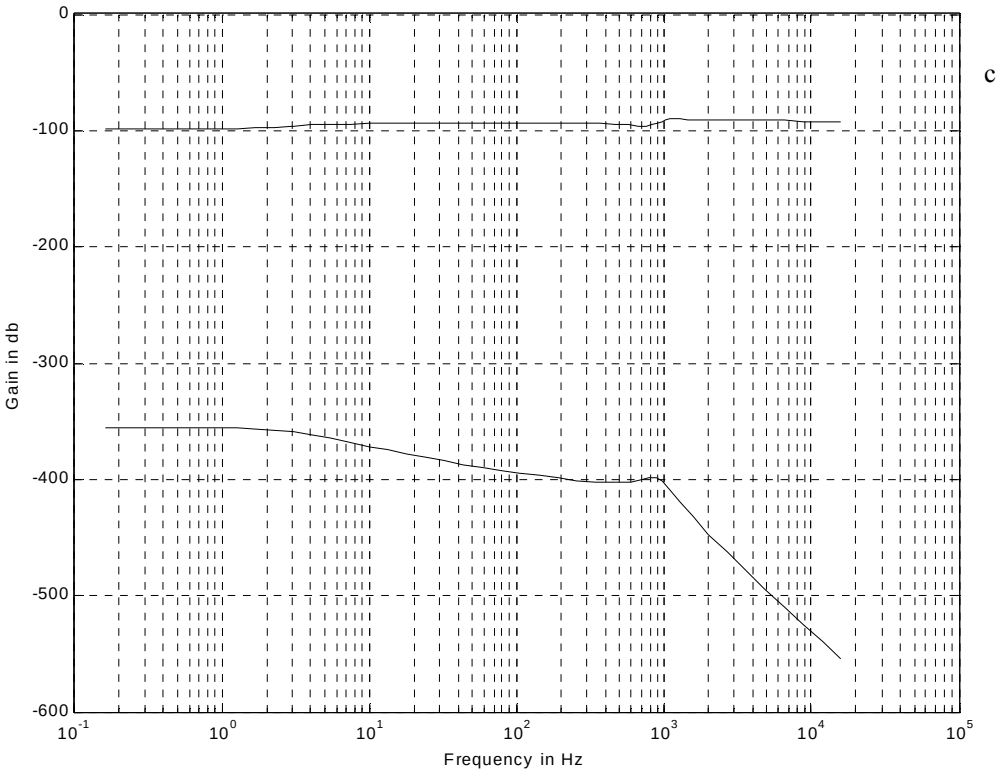


Fig. 5.55 Continued. c) Plot of Condition 3 for Scenario 7

### 5.4.8 Scenario 8a

Evaluating the conditions in (5.4) for Scenario 8a yielded the results that the scenario was stable at the bus of interest. It was, however, observed that the system showed some tendency to instability before protection operated. This was not significant, which is why it is supposed that stability assessment methodology declaring the system stable at the intrazonal bus is accurate. The significant signs of instability were on the interzonal bus and the generator busses, signals of which are not used in the stability assessment at this step, since they are not the interface of interest. There are no intersections between the

areas within the disk of the forbidden region (of which only a portion is shown left of the full trajectory of the Nyquist contour) and the Nyquist contour of Conditions 1 and 2. Also, the region above the upper curve was not traversed by the lower curve in Condition 3. These results are presented in Fig. 5.56a-Fig. 5.56c.

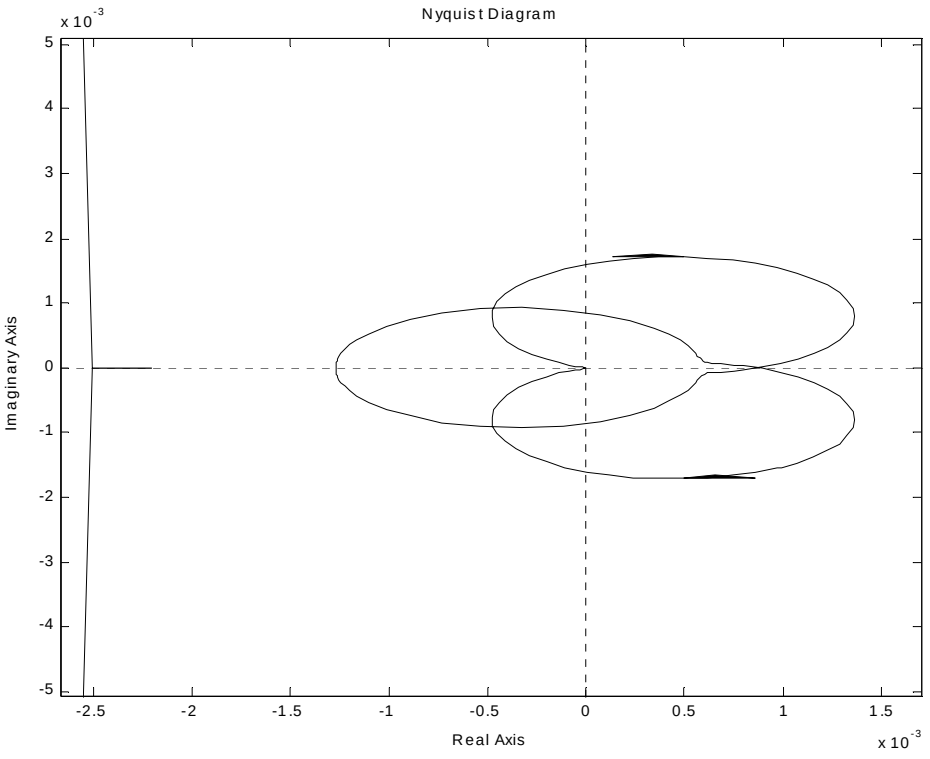


a

Fig. 5.56 Plot of Conditions for Scenario 8a. a) Plot of Condition 1 for Scenario 8a

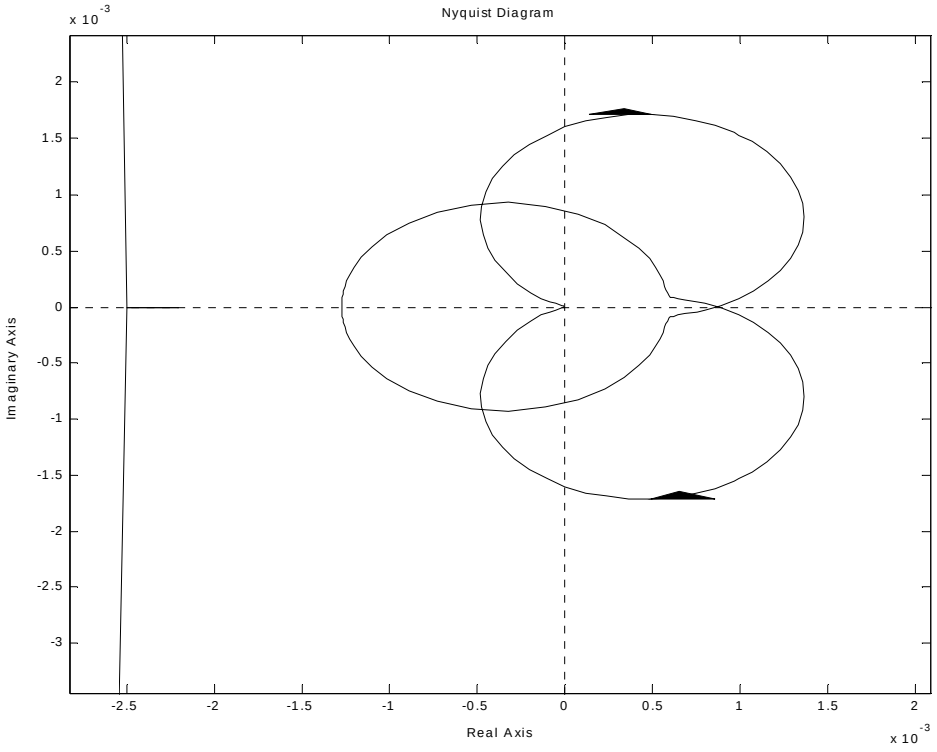


b

Fig. 5.56 Continued. b) Plot of Condition 2 for Scenario 8a

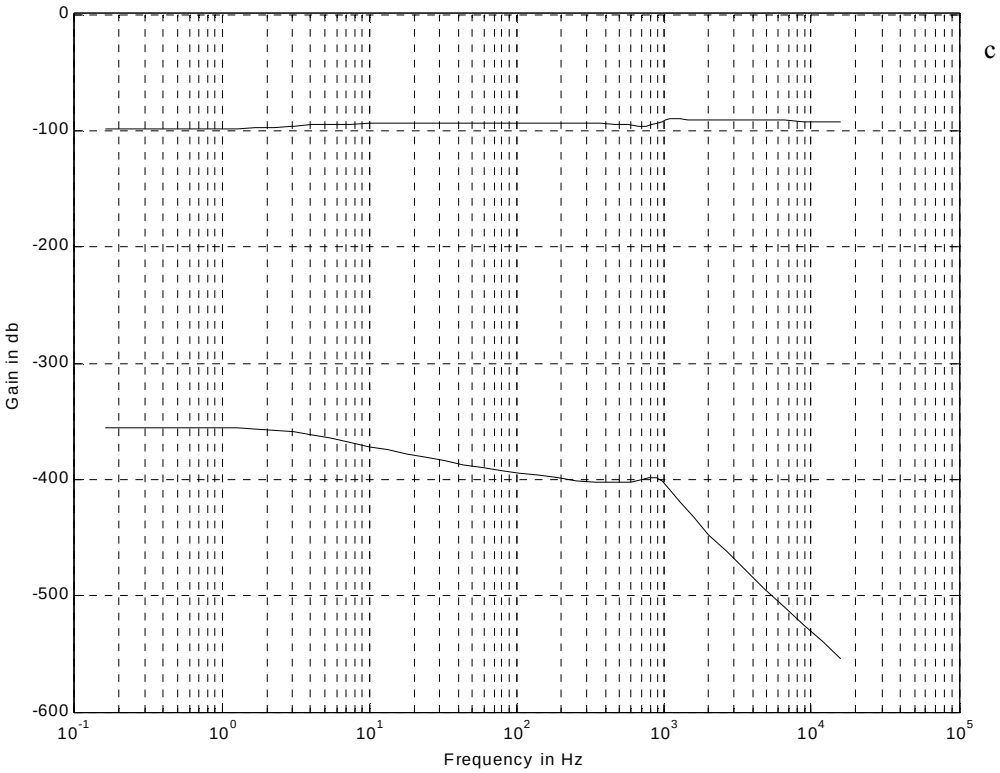


Fig. 5.56 Continued. c) Plot of Condition 3 for Scenario 8a

### 5.4.9 Scenario 9a

Evaluating the conditions in (5.4) for Scenario 9a yielded the results that the scenario was stable at the bus of interest. It was, however, observed that the system showed some tendency (more than Scenario 8a) to instability before protection operated. This was still not significant, which is why it is supposed that stability assessment declared the system stable. The significant signs of instability, however, were on the interzonal bus and the generator busses, signals of which were not used in the stability assessment for this case, since they were not the interface of interest. The methodology, therefore, accurately

assessed the intrazonal bus as stable for Scenario 9a. In the figures there are no intersections between the areas within the disk of the forbidden region (of which only a portion is shown left of the full trajectory of the Nyquist contour) and the Nyquist contour of Conditions 1 and 2. Also, the region above the upper curve was not traversed by the lower curve in Condition 3. These results are presented in Fig. 5.57a-Fig. 5.57c.

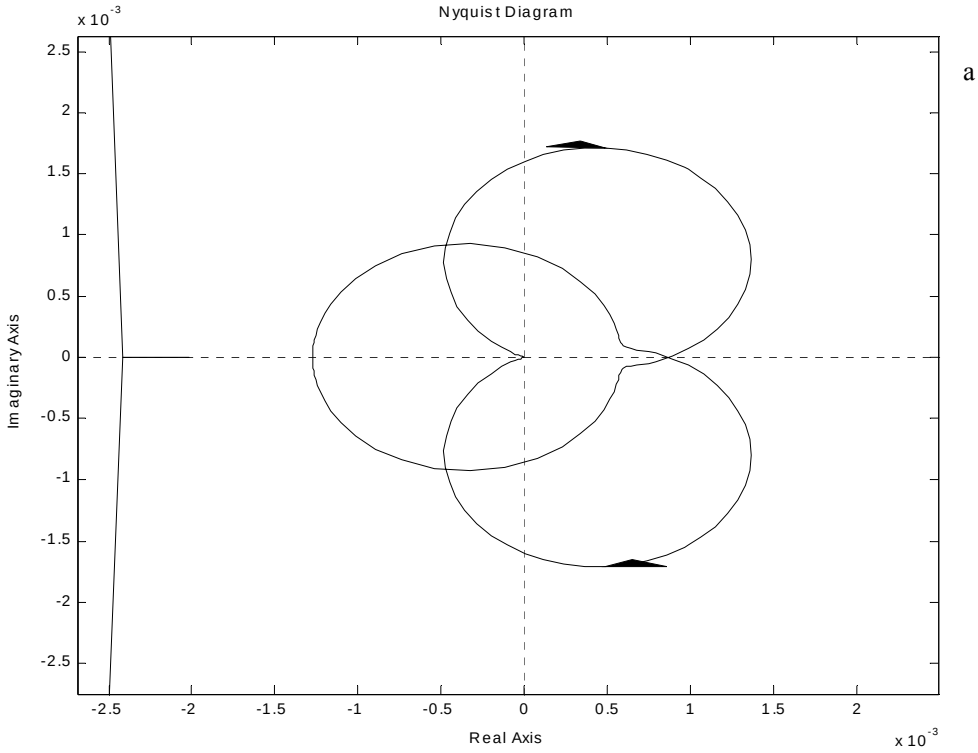


Fig. 5.57 Plot of Conditions for Scenario 9a. a) Plot of Condition 1 for Scenario 9a

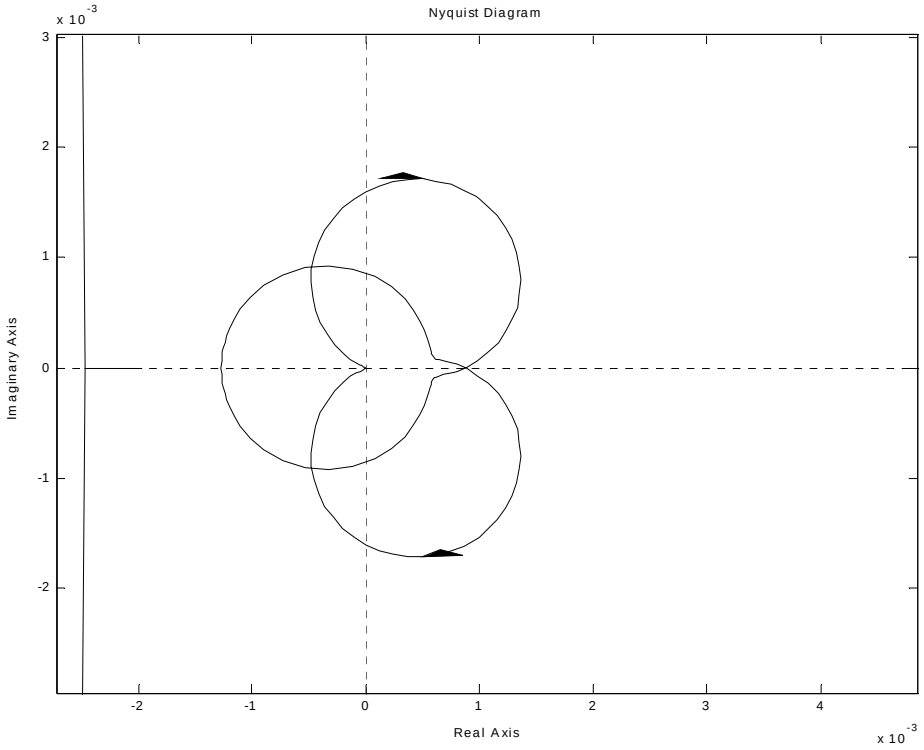


b

Fig. 5.57 Continued. b) Plot of Condition 2 for Scenario 9a

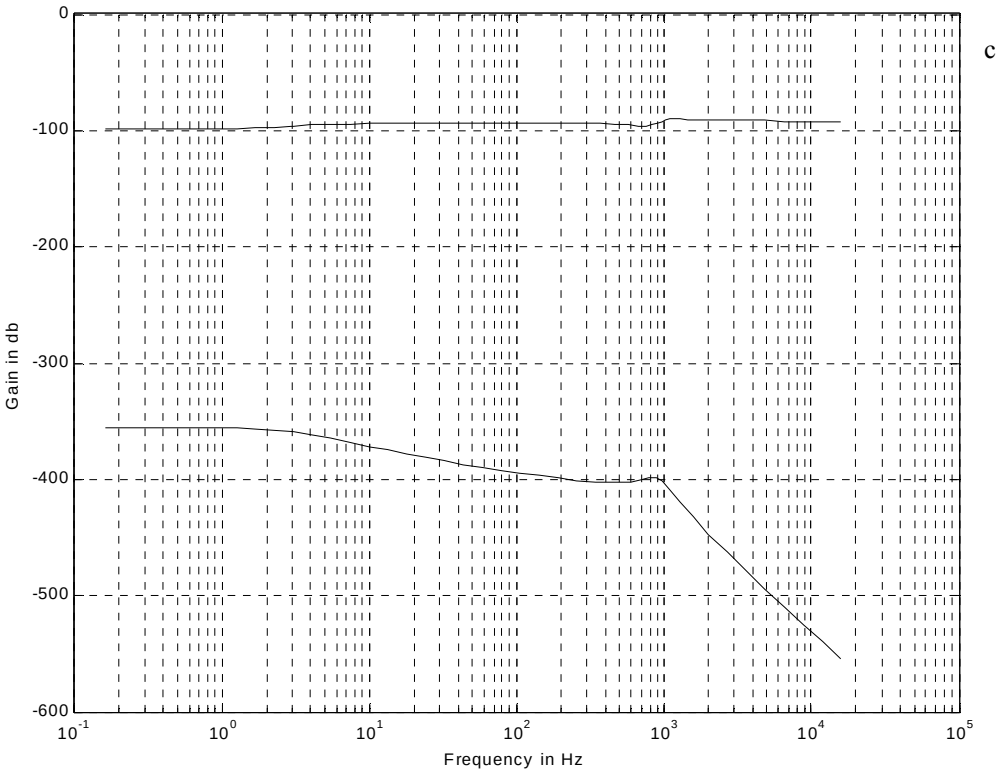


Fig. 5.57 Continued. c) Plot of Condition 3 for Scenario 9a

### 5.4.10 Scenario 8b

Using the methodology to assess whether the system was unstable as observed on the interzonal bus on the port side yielded some conflicting results. On the one hand, using coupled linear gains yielded the correct results of instability as shown in Fig. 5.58a through to Fig. 5.58c, using the decoupled linear gains as required by the methodology yielded contrary results as shown in Fig. 5.59a – Fig. 5.59c. To further substantiate the unlikelihood of this coincidental occurrence are the signals of both the actual and decoupled signals for the linear gain part of the subsystems in Fig. 5.60a- 5.60h. Figures a through d are the decoupled small signals results while, e through h are the actual small signal results. They show that the decoupling was properly done and the signals accurately replicated. Reasons for this discrepancy can be that the software was not solving identically in both cases. The results show that Scenario 8b could not be determined by the methodology.

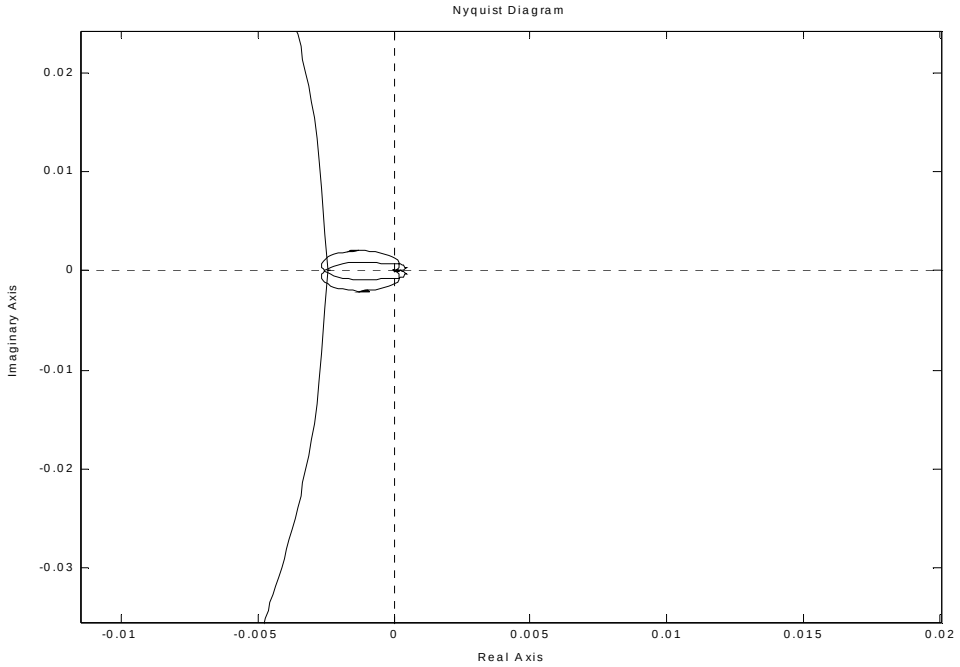


a

Fig. 5.58 Plot of Conditions for Scenario 8b. a) Plot of Condition 1 for Scenario 8b

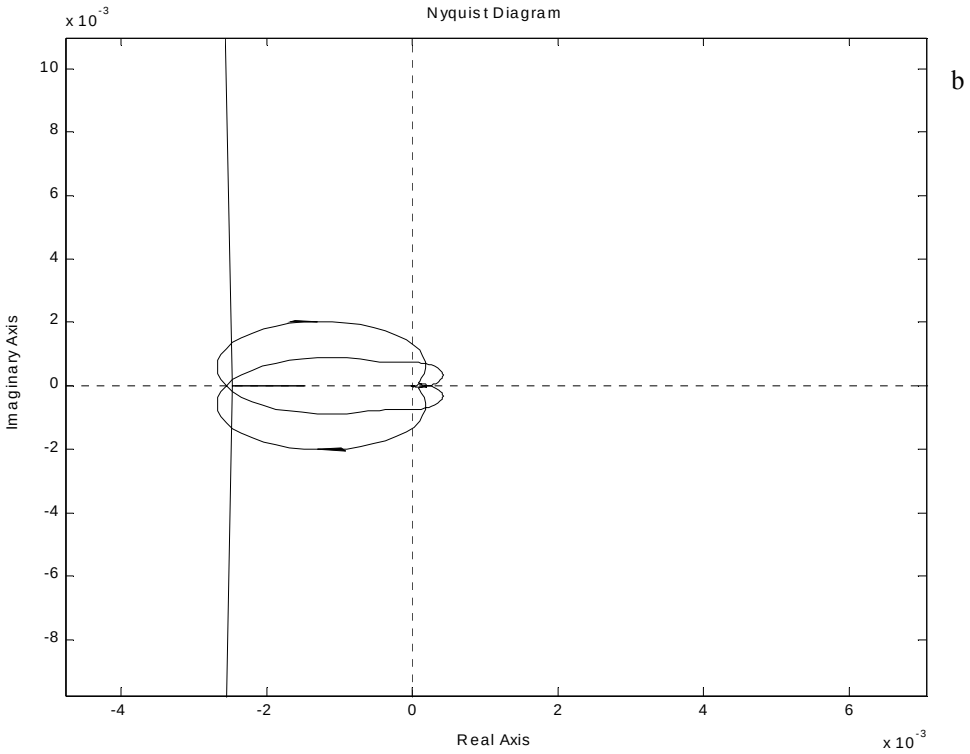


b

Fig. 5.58 Continued. b) Plot of Condition 2 for Scenario 8b

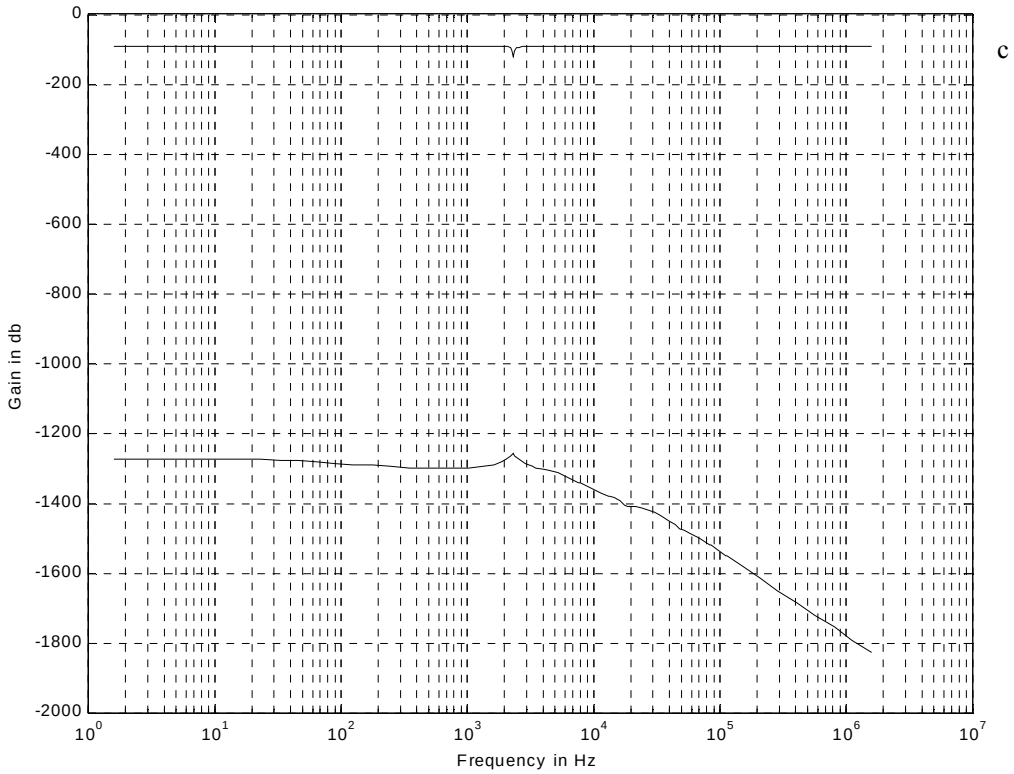


Fig. 5.58 Continued. c) Plot of Condition 3 for Scenario 8b

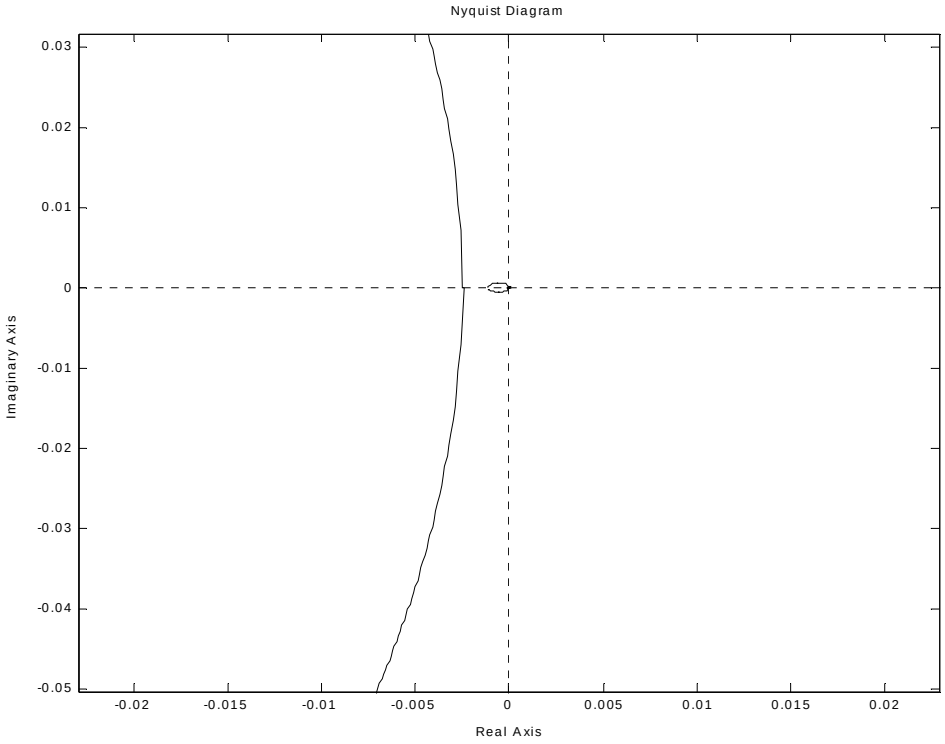


a

Fig. 5.59 Plot of conditions for Scenario 8b with decoupled systems. a) Plot of Condition 1 for Scenario 8b

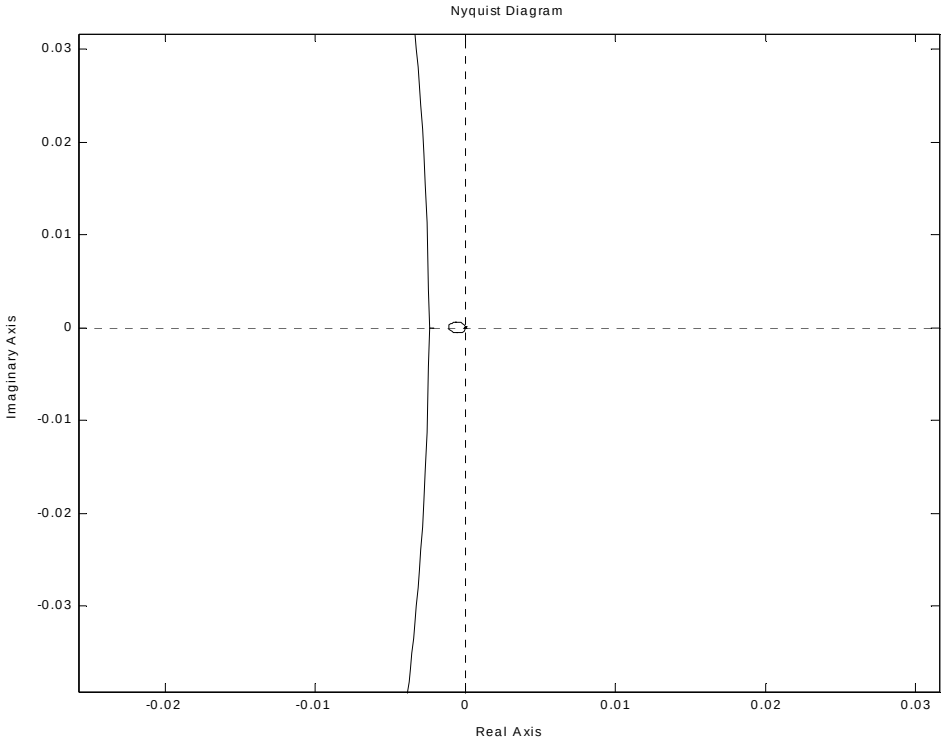


b

Fig. 5.59 Continued. b) Plot of Condition 2 for Scenario 8b

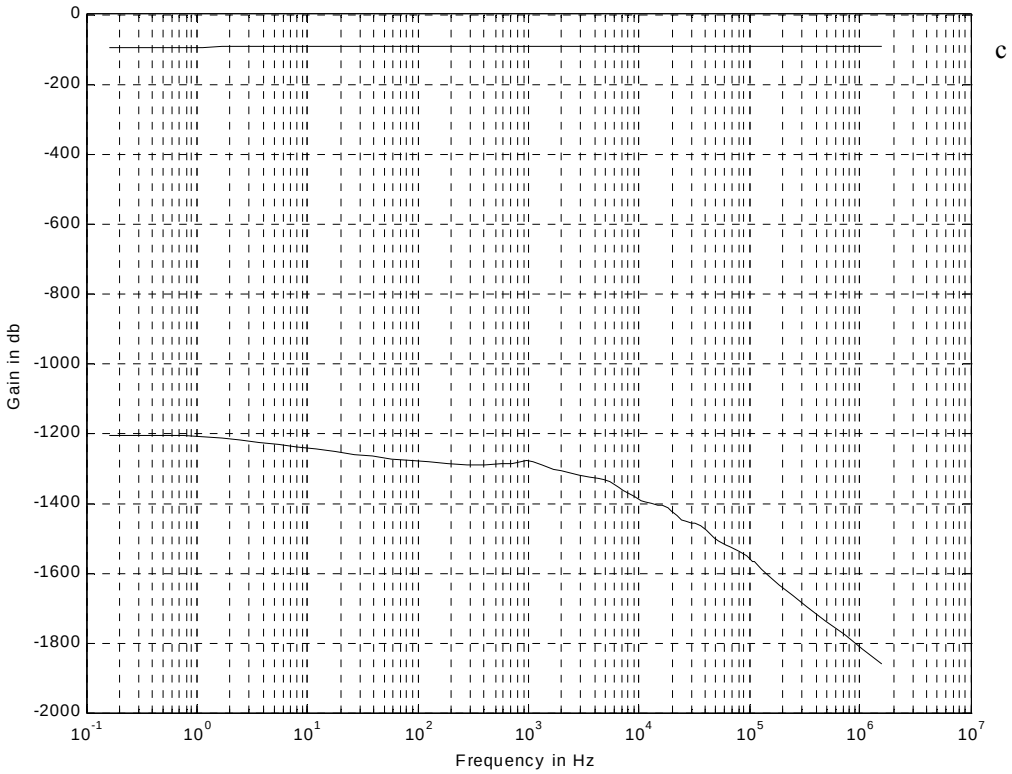


Fig. 5.59 Continued. c) Plot of Condition 3 for Scenario 8b

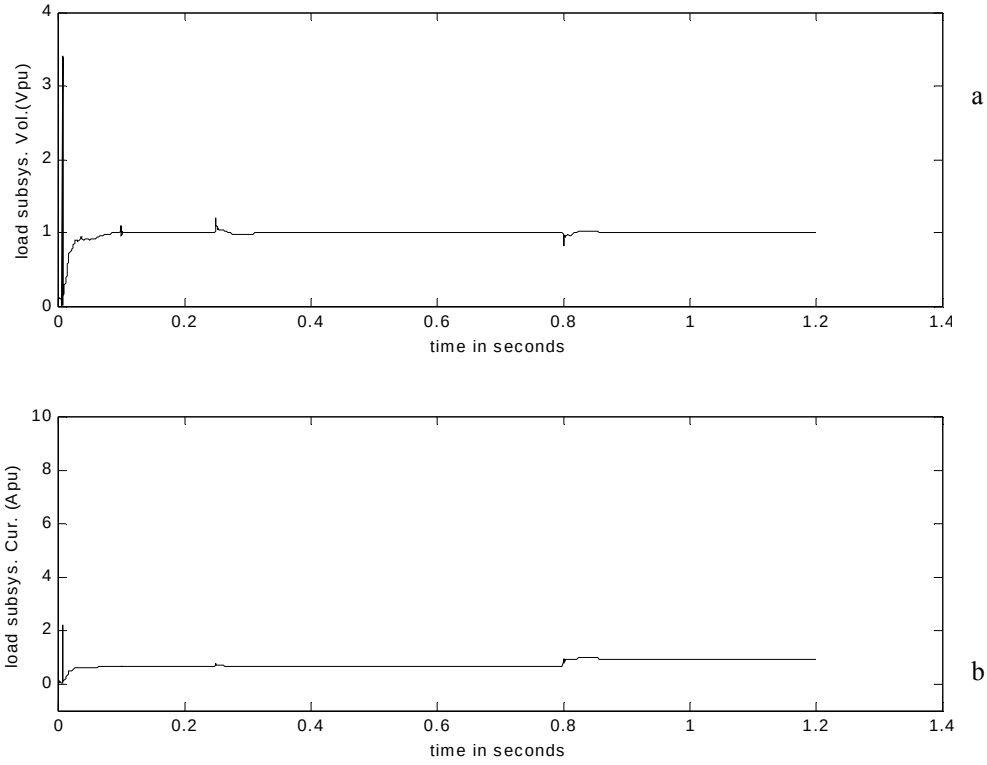


Fig. 5.60 Perturbation model and coupled simulation results for Scenario 8b. a) Load subsystem voltage for small signal with decoupled subsystems in pu b) Load subsystem current for small signal with decoupled subsystems in pu

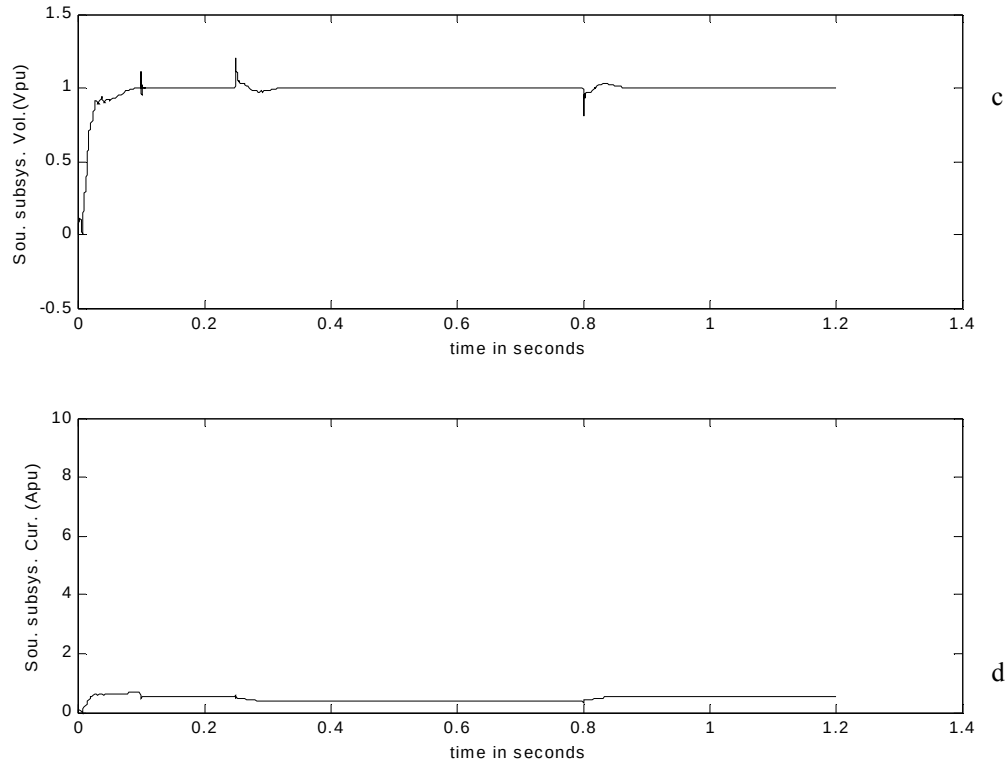


Fig. 5.60 Continued. c) Source subsystem voltage for small signal with decoupled subsystems in pu

d) Source subsystem current for small signal with decoupled subsystems in pu

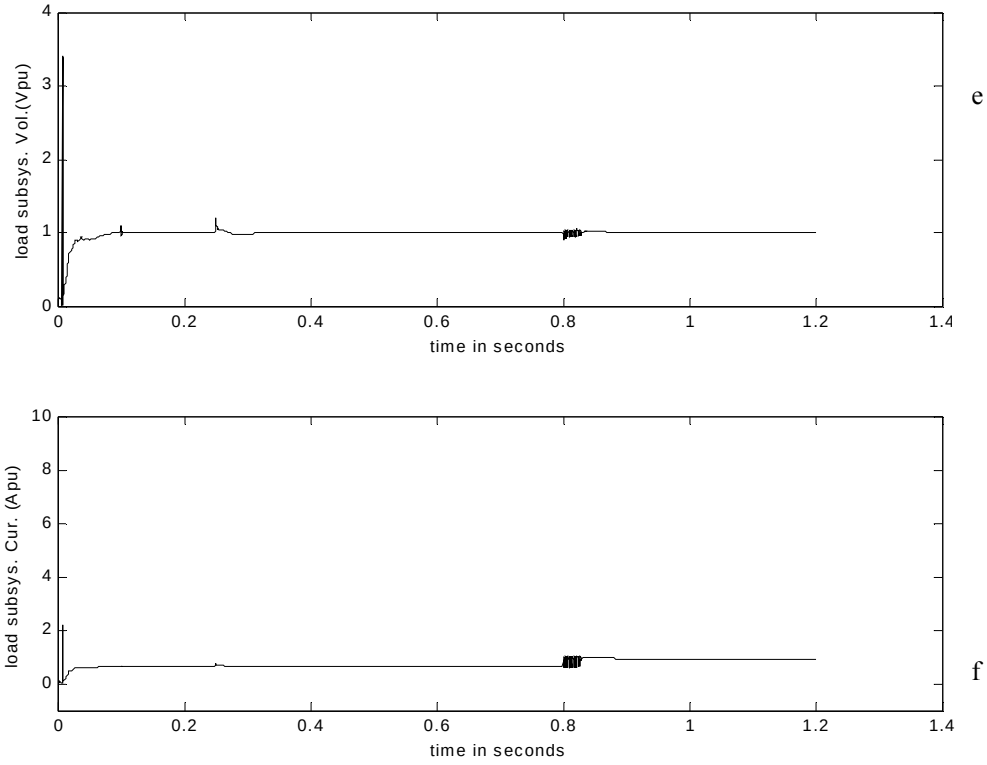


Fig. 5.60 Continued. e) Load subsystem voltage for small signal with coupled subsystems in pu

f) Load subsystem current for small signal with coupled subsystems in pu

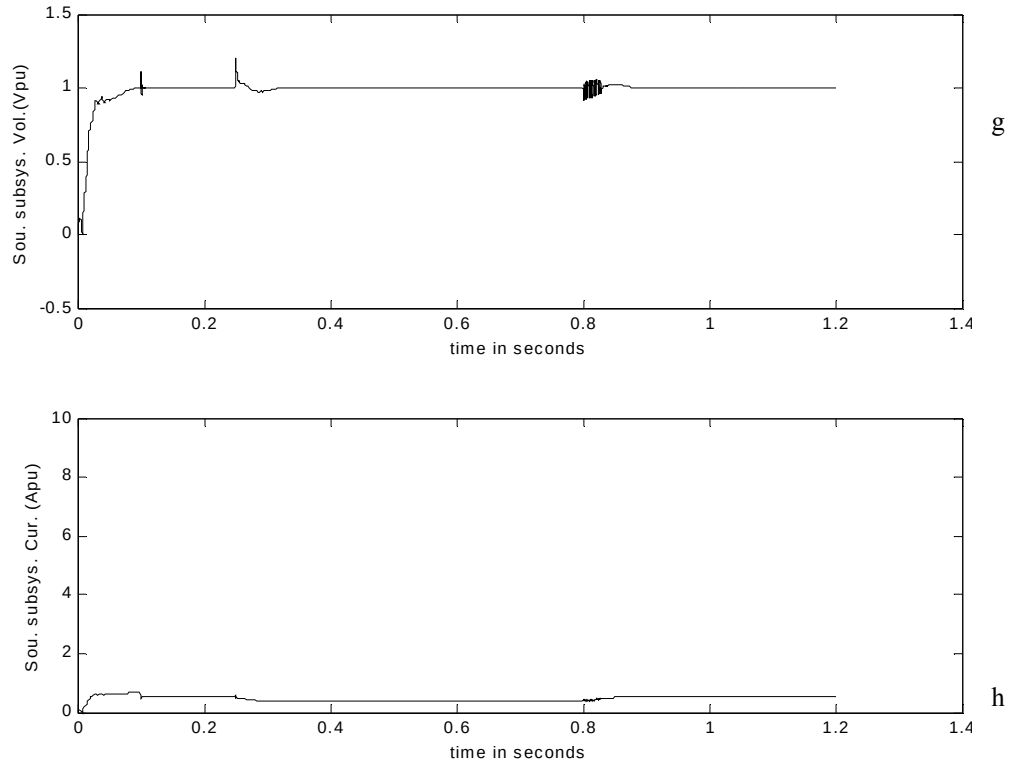


Fig. 5.60 Continued. g) Source subsystem voltage for small signal with coupled subsystems in pu

h) Source subsystem current for small signal with coupled subsystems in pu

### 5.4.11 Scenario 9b

Using the methodology to assess whether the system was unstable as observed on the interzonal bus on the port side also yielded some abnormal results. On the one hand, using coupled linear gains yielded extremely large gains as shown in Fig. 5.61a through to Fig. 5.61c (where the large contours are the nyquist while the some circle is the forbidden region), using the decoupled linear gains as stipulated in the methodology yielded small and large gain results as shown in Fig. 5.62a – Fig. 5.62c (Where the large

contours in Condition 1 are the nyquist contours and the large contours in Condition 2 is the forbidden region). To further substantiate the unlikelihood of this abnormality are the decoupled signals for the nonlinear gain part of the subsystems in Fig. 5.63a- 5.63d. Figures a through d are the interface signals which generated the abnormality. The reason for this abnormality could not be explained but it might be errors in computer simulation from solvers and stability code which could not be deciphered.

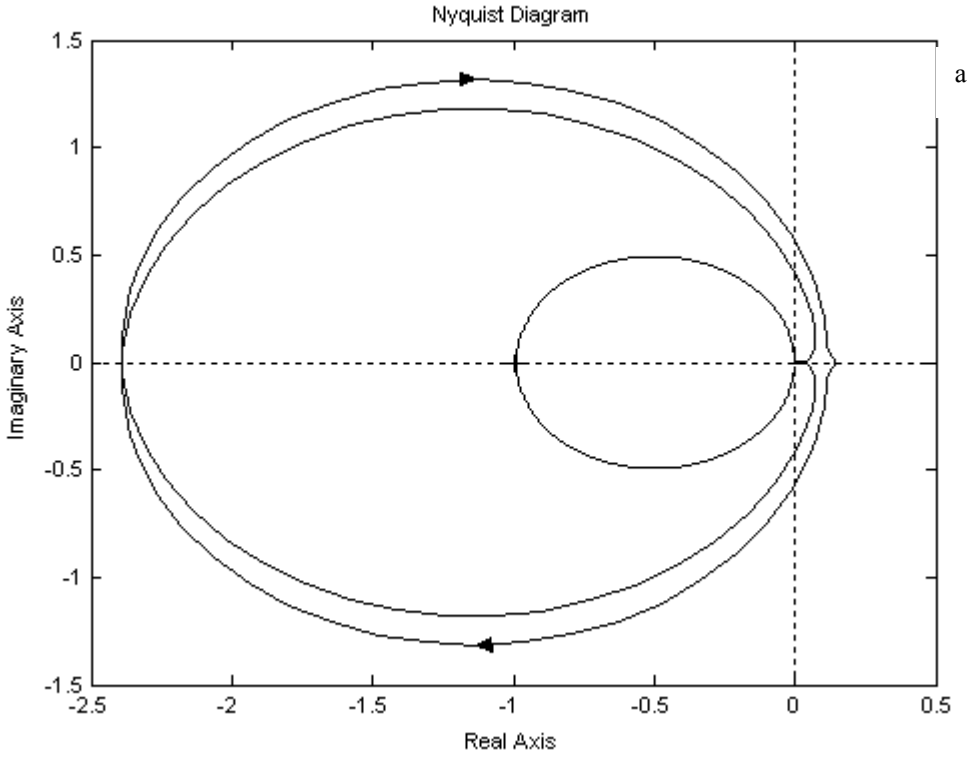


Fig. 5.61 Plot of conditions for Scenario 9b. a) Plot of Condition 1 for Scenario 9b

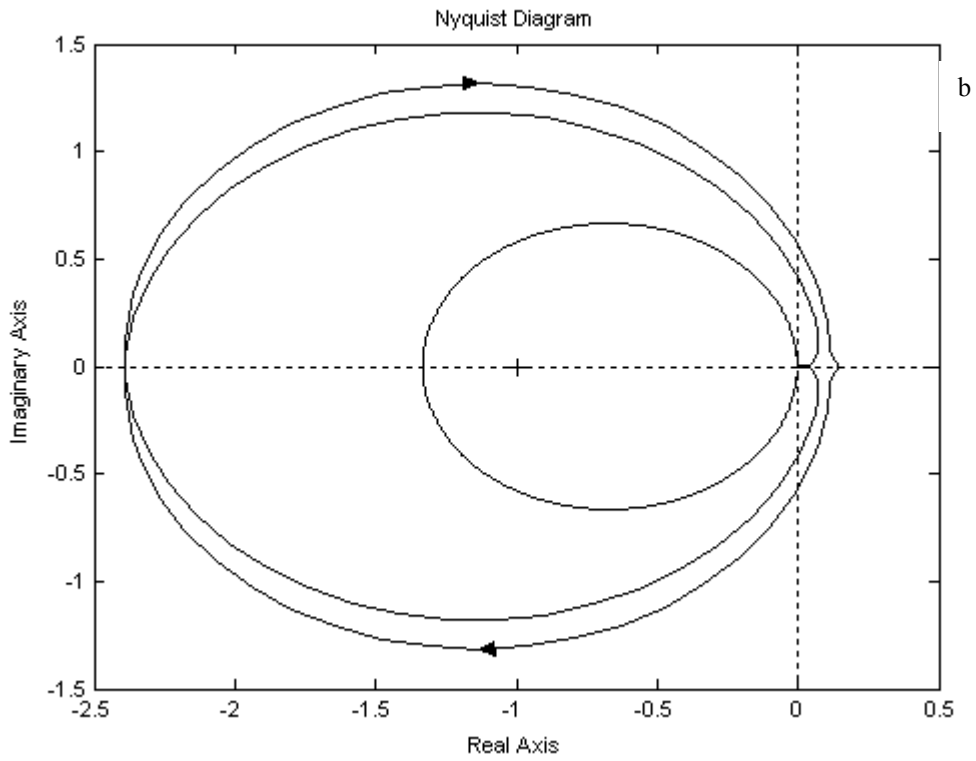


Fig. 5.61 Continued. b) Plot of Condition 2 for Scenario 9b

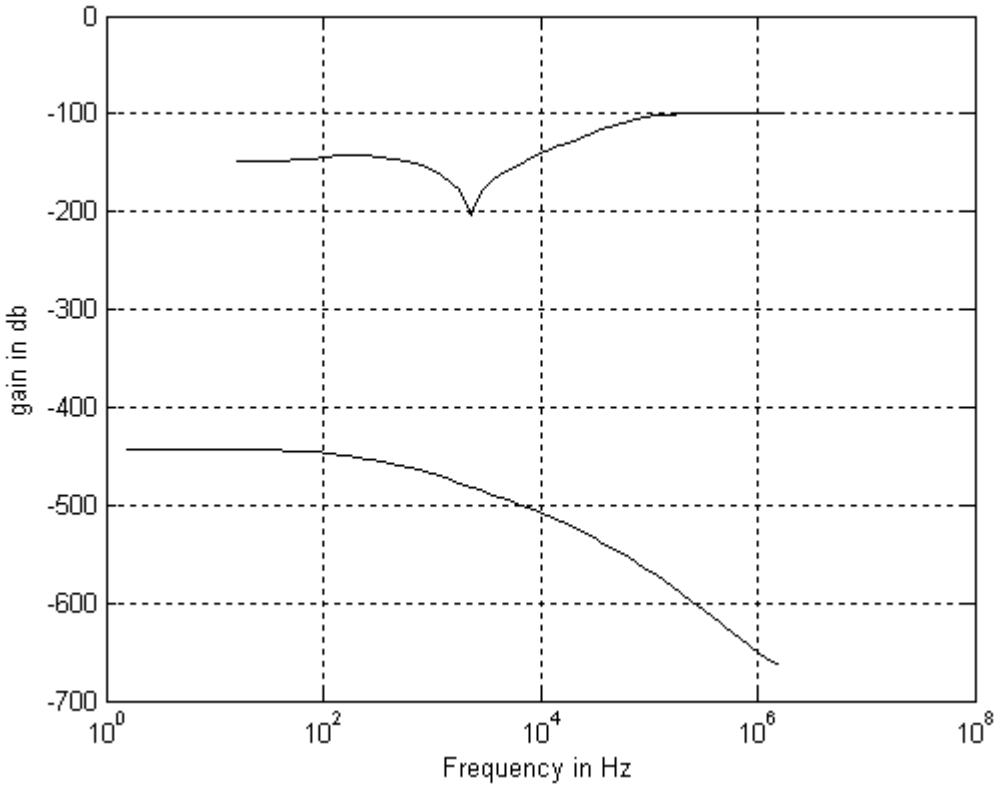


c

Fig. 5.61 Continued. c) Plot of Condition 3 for Scenario 9b

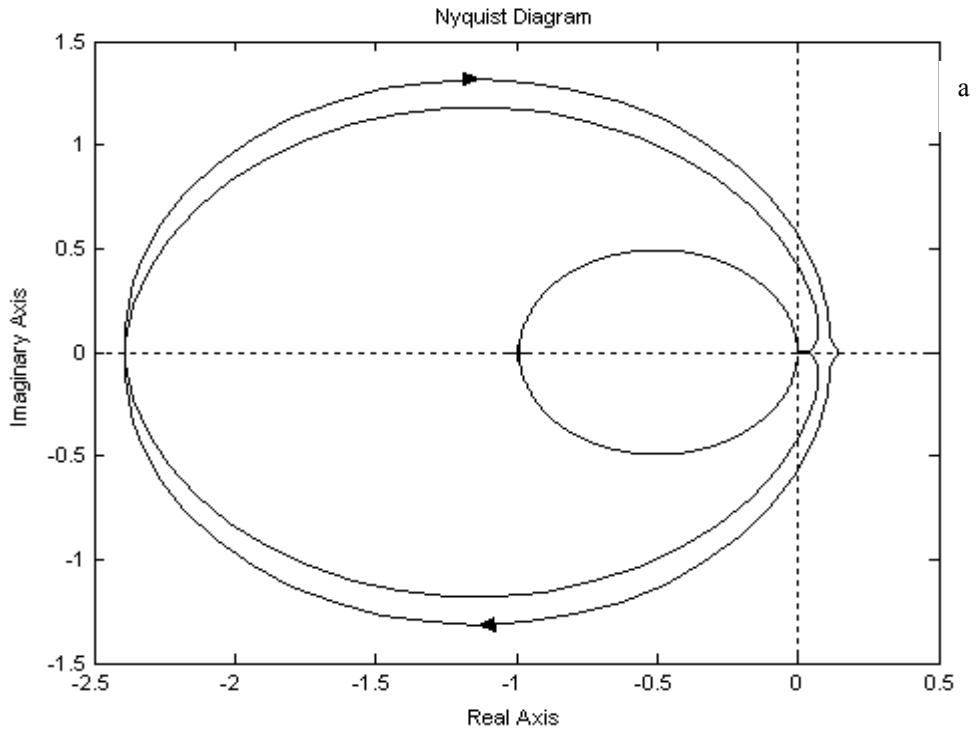


a

Fig. 5.62 Plot of conditions for Scenario 9b with decoupled systems. a) Plot of Condition 1 for Scenario 9b

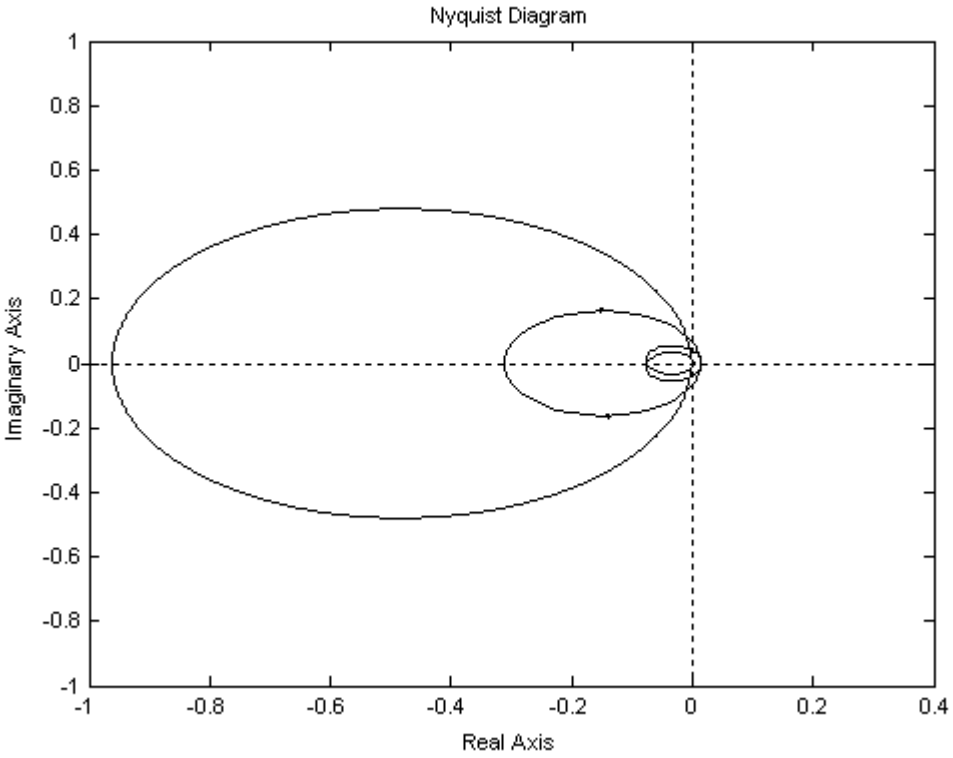


b

Fig. 5.62 Continued. b) Plot of Condition 2 for Scenario 9b

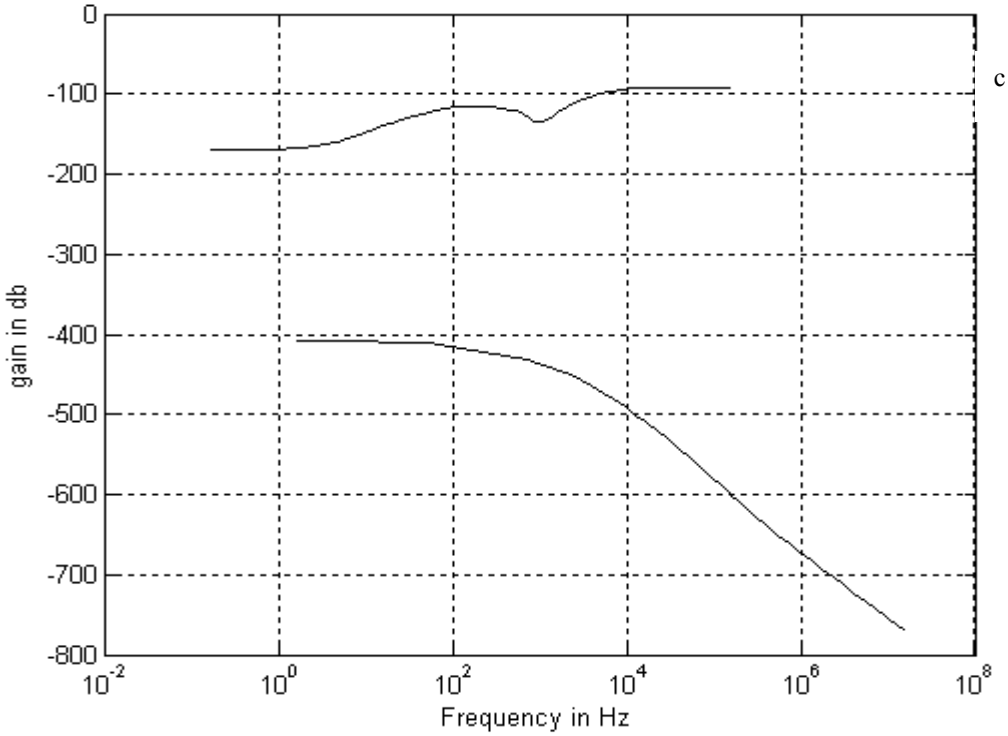


Fig. 5.62 Continued. c) Plot of Condition 3 for Scenario 9b

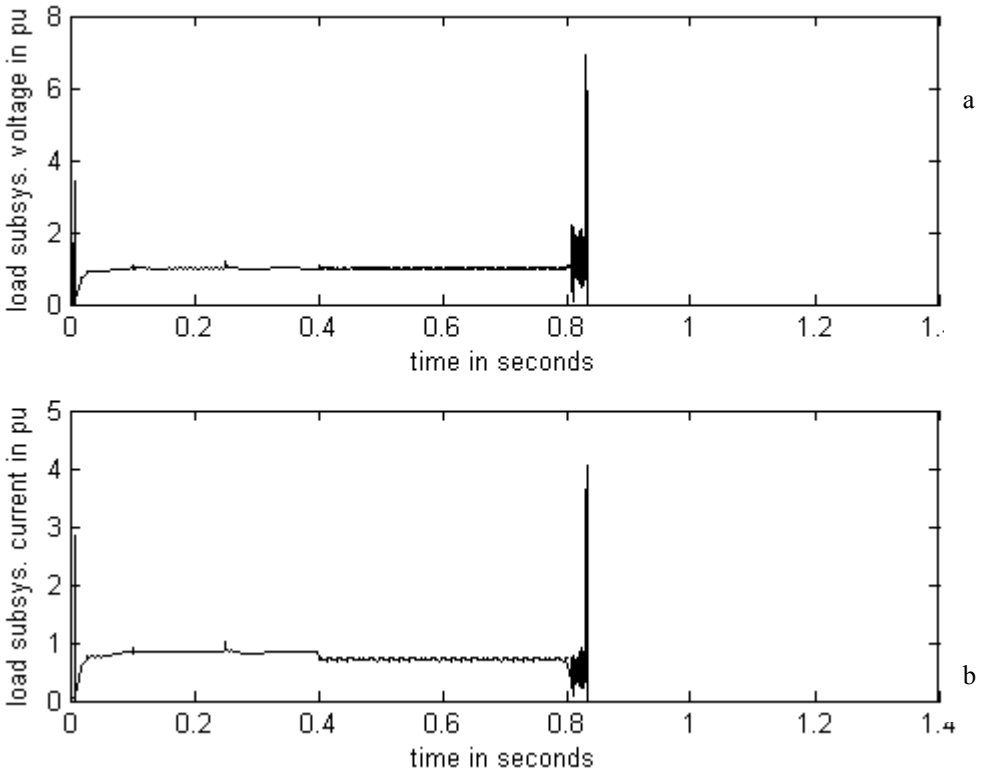


Fig. 5.63 Perturbation model large signal simulation results of Scenario 9b. a) Load subsystem voltage for large signal with decoupled subsystems in pu b) Load subsystem current for large signal with decoupled subsystems in pu

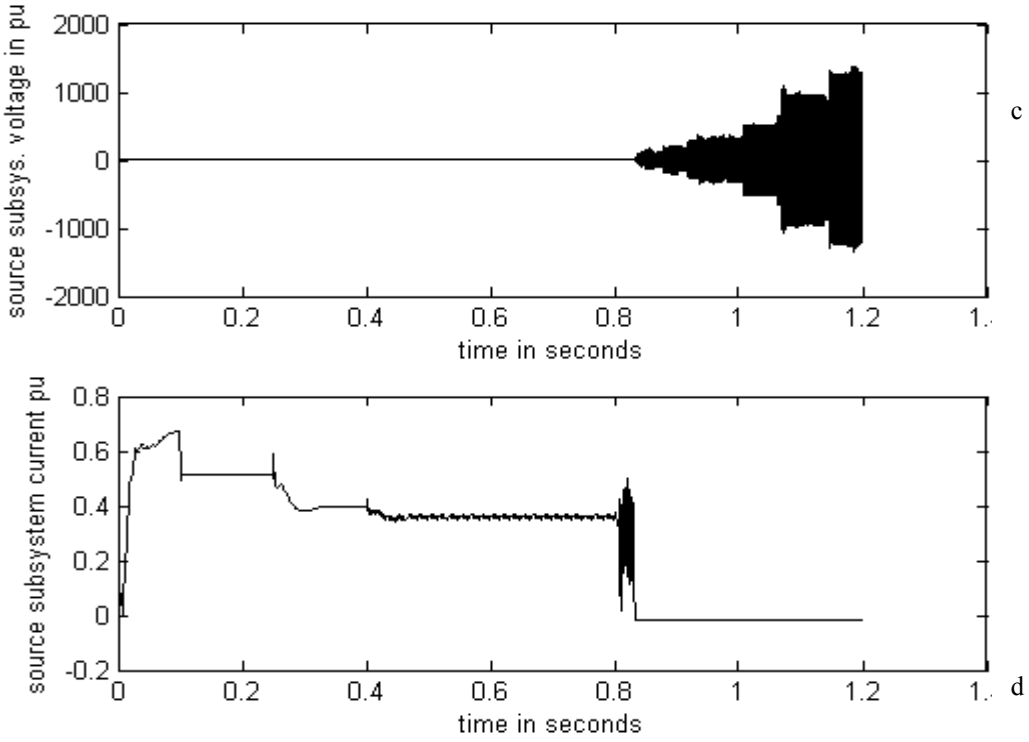


Fig. 5.63 Continued. c) Source subsystem voltage for large signal with decoupled subsystems in pu

d) Source subsystem current for large signal with decoupled subsystems in pu

## 5.5 Stability Margins

To determine the stability margins (the worst margin) of each scenario from the profiles of the stability conditions, the shortest distance (s) between the stability condition trajectory and the forbidden region profile was calculated. Since the shortest distance between two planes is a straight line and touches both planes at an angle perpendicular to the planes, the value of s is real. The value for s is also positive only since it is defined as the 'distance' between the planes or points. For Conditions 1 and 2 the s value is in magnitude, but it was converted to decibels (db) by multiplying the log of the magnitude by 20. The value for s in Condition 3 is already in db. It was also

important to identify the frequency at which the worst margins occurred. For Conditions 1 and 2, the frequency was obtained by discovering the frequency at which cTs was evaluated to give the gain magnitude of the point on the cTs (open loop gain of Condition 1 or 2), contour which forms a part of the shortest line. For Condition 3 the frequency of the worst margin was found by simply reading the x axis of the stability condition plot. The results of the stability margins are presented in Table 5.7. It was determined that the frequencies at which worst margins occur were from 0.25 to 0.82 hertz. This indicated that an AC/DC system of this nature was unstable only about the fundamental of the DC circuit from this feedback type of instability.

Table 5.7
Stability margins for reconfiguration scenarios

| | Condition 1 | | | Condition 2 | | | Condition 3 | |
|---|---|---|---|---|---|---|---|---|
| | Magnitude | db | Frequency Hz | Magnitude | db | Frequency Hz | db | Frequency Hz |
| Scenario 1 | 1.13E-03 | -5.8977E+01 | 2.54E-01 | 1.20E-03 | -5.8453E+01 | 4.05E-01 | 3.5000E+02 | 0.5 |
| Scenario 2 | 1.20E-03 | -5.8438E+01 | 5.12E-01 | 1.17E-03 | -5.8607E+01 | 2.54E-01 | 3.5000E+02 | 0.5 |
| Scenario 3 | 1.21E-03 | -5.8316E+01 | 4.05E-01 | 1.25E-03 | -5.8062E+01 | 5.12E-01 | 3.5000E+02 | 0.5 |
| Scenario 4 | 1.28E-03 | -5.7890E+01 | 8.16E-01 | 1.14E-03 | -5.8831E+01 | 2.54E-01 | 3.5000E+02 | 0.5 |
| Scenario 5 | 1.17E-03 | -5.8607E+01 | 6.46E-01 | 1.19E-03 | -5.8504E+01 | 3.21E-01 | 3.5000E+02 | 0.5 |
| Scenario 6 | 1.22E-03 | -5.8298E+01 | 4.05E-01 | 1.14E-03 | -5.8862E+01 | 2.54E-01 | 3.5000E+02 | 0.5 |
| Scenario 7 | 1.23E-03 | -5.8237E+01 | 2.54E-01 | 1.19E-03 | -5.8474E+01 | 2.54E-01 | 3.5000E+02 | 0.5 |
| Scenario 8a | 1.27E-03 | -5.7931E+01 | 8.16E-01 | 1.24E-03 | -5.8138E+01 | 3.21E-01 | 3.5000E+02 | 0.5 |
| Scenario 9a | 1.09E-03 | -5.9244E+01 | 2.54E-01 | 1.20E-03 | -5.8417E+01 | 2.54E-01 | 3.5000E+02 | 0.5 |
| Scenario 8b | 1.25E-03 | -5.8062E+01 | Not available | 1.2E-03 | -5.8416E+01 | Not available | 1.1E+03 | 0.2 |
| Scenario 9b | 10.0E-3 | 2.0000E+01 | Not available | unstable | unstable | Not available | 3.0E+02 | 10 |

## 5.6 Summary

In this chapter the definitions of the reconfiguration scenarios were made, the actual simulations of the reconfiguration scenarios in the coupled system were done, and results were presented. The decoupled system was perturbed to contain the reconfiguration information and the stability assessment methodology was applied to infer the stability conclusions of the intrazonal DC bus on the port side. The errors of the perturbation modeling have been calculated and presented. It was reported in this chapter that the test system was quite stable except for cases of severe load shedding and that during severe load shedding, the intrazonal bus was stable but the upstream busses were not. This was not however properly verified by the methodology since the attempt to do this failed in Scenarios 8b and 9b.

Chapter VI will contain further discussions of the study in collective terms sighting merits and demerits of the performance. Issues such as “which scenario had the best stability margin” will be discussed and reasons will be suggested for what the observations and inferences were. A discussion of why problems arose and why marginal at best success was recorded for verification of instability at other busses will be made.

# CHAPTER VI

# RECONFIGURATION CATALOGUE

## 6.1 Overview

In this chapter, a discussion of the results of Chapter V is presented in collective terms. The merits of the performance of the test IPS are shown using the results of the performance of all nine scenarios. Similarly, the limits of the test IPS are also shown which were obtained from observations of the results. Conclusions are then made about the limitations of reconfiguration of a PEBB-based integrated shipboard power system. Also, in this chapter some general analysis of results are presented which will be called the reconfiguration catalogue

## 6.2 Merits of Performance

All nine scenarios indicate that at the 775V intrazonal DC bus on the port side, the system is stable. There was noise on the intrazonal DC bus response for varying reasons: (1) there were ARCP converter setting limitations and subsequent noisy converter responses to loading as can be seen in Scenario 6 - Figs. 5.22-5.25 (2) filter impedance mismatching at low loading levels existed as can be seen in Scenarios 8 and 9 – Figs.5.33-5.37 and (3) the mode of controller, which, for current controlled during reconfiguration, triggered controller response that introduced noise – Figs. 5.18. The power system performance is not very noisy, even though the state space model generated instantaneous values of the various models. However, the models all ignored

the harmonics which was a reason for such good performance. The test IPS can be said to show good stability overall compared to older ship power system architecture. This can be seen from the fact that the reconfiguration activities, representing all the types of reconfiguration situations yielded stable results. It can be inferred that the decoupling of the generator frequency and load frequencies contributed to these stability results. This frequency decoupling which has been addressed in literature for DC distribution shipboard power system architectures [9] may be the reason why the stability issues of the IPS is better than older AC Radial and AC Zonal shipboard power system architectures.

The system responses to the various scenarios remained within a narrow range of stability margins but considering that range Fig. 6.1 through Fig. 6.3 show how the scenarios fared with one another. It can be seen from the figures that Scenario 9a gave the worst margin for Condition 1 of the stability conditions, Scenarios 4 and 6 gave the worst margin for Condition 2, and the gain for Condition 3 was the same for scenarios 1 through 9. As stated in stability margin discussion in Chapter V, the closest distance of gain trajectory and the forbidden region was the worst stability margins. The numbers on the x axis of Figs. 6.1-6.3 are the scenario labels.

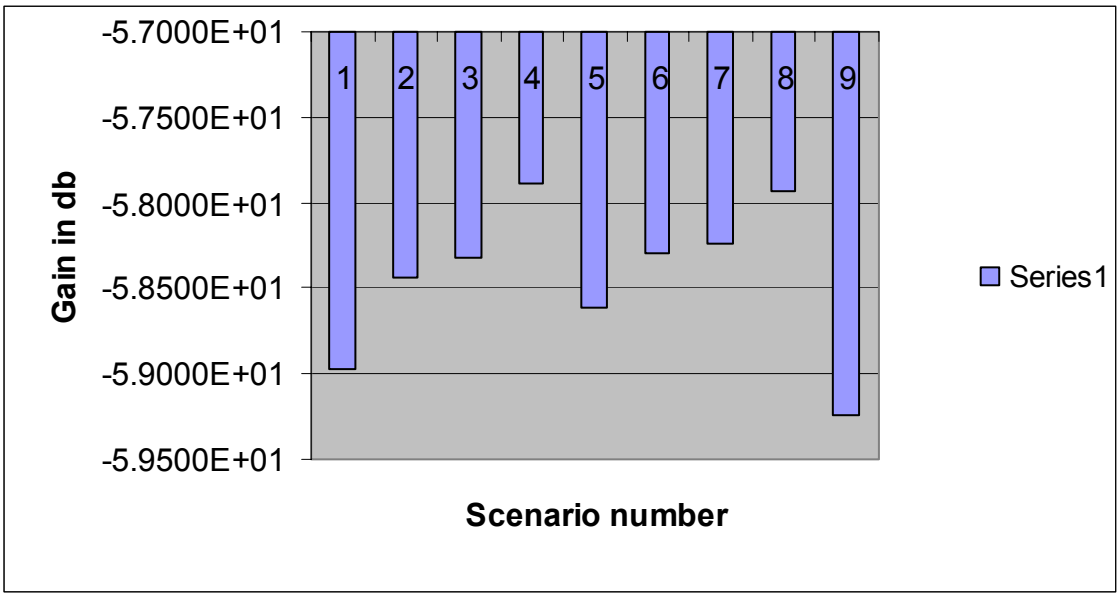


Fig 6.1 Plot of Condition 1 stability margins

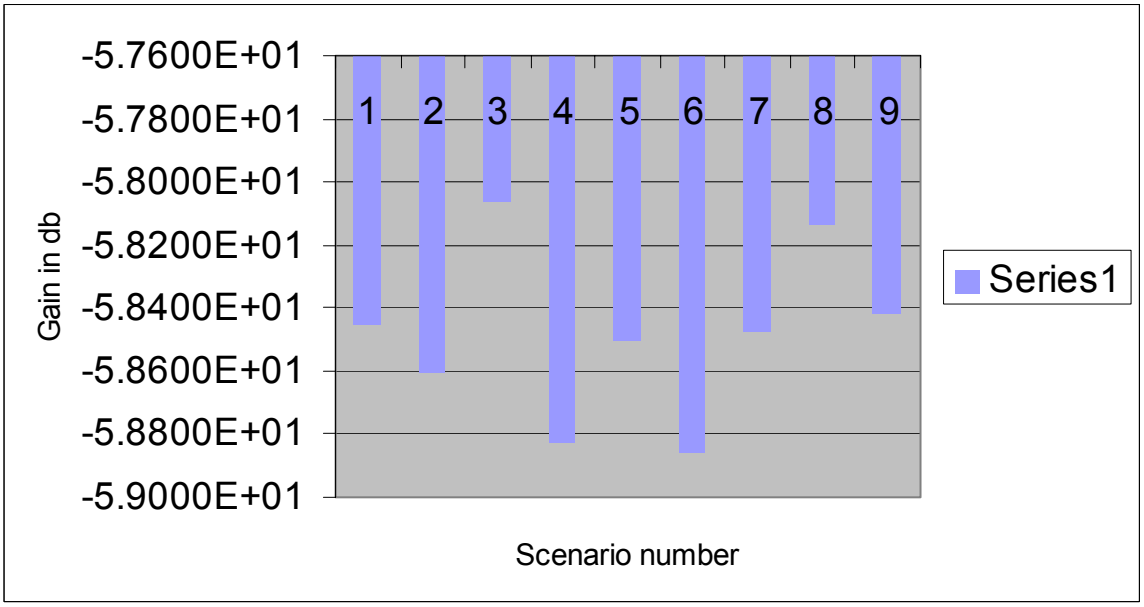


Fig 6.2 Plot of Condition 2 stability margins

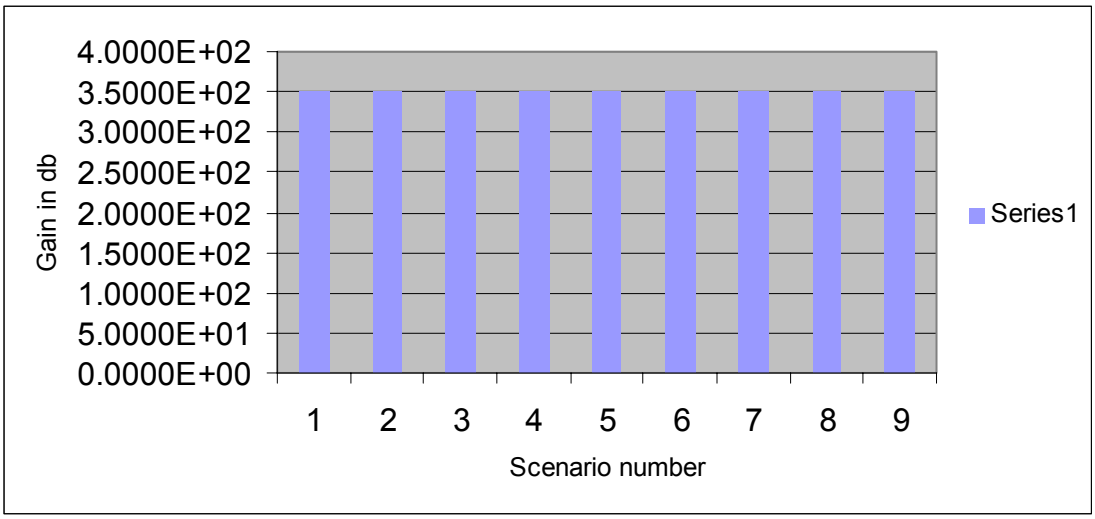


Fig 6.3 Plot of Condition 3 stability margins

Stability recorded from the stability assessment at the intrazonal DC bus on the port side was good. However, visual observations and some stability assessment show problems with Scenarios 8a and 9a for upstream busses. This was further investigated which required the decoupling of the system at the interzonal bus on the port side. It was observed that the methodology's corroboration of the visual observation of instability at that bus ran into some problems with abnormal results being recorded in Scenarios 8b and 9b. A comparison of degrees of instability could not be made between Scenario 8b and 9b because of these abnormalities. Also, frequencies could not be selected for the stability margins for Scenario 8b and 9b. But visual observations indicate that the instability is worse in Scenario 9b. Scenario 8b and 9b only exist in the decoupled form as stated in Chapter V since they represent Scenarios 8a and 9a, respectively, in the

actual reconfiguration scenarios. The system behaved as expected in all reconfiguration scenarios except for spikes observed in actual simulations in scenarios 1-3.

## 6.3 Limits of Performance

The responses reported in all the scenarios have limited interpretation due to the number of protective devices modeled for the system. Protection not modeled includes low voltage relays, reverse power relays, and under frequency relays. One more factor that contributed to the limitation of interpretation is that harmonics were ignored. Reasons for the simplification causing the limitations are that so little data are known about the system from the Navy and that the Navy data are often not inferable from those in commercial systems. The limitations were however not severe ones, because reconfiguration by load shedding, load addition and bus transfer operation could still be properly staged in the system through the proper use of switches, circuit breakers and bus transfers units. The UPS which is another form of protection for the system loads was also not modeled in this system, due to the load dynamics not being investigated in depth. The controllers served to preserve the magnitude of voltage or current signals seen by the converter's downstream components, such that the low voltage relays absence was not a real problem. However, solving the limitations, may lead to the problems seen on the interzonal busses of Scenarios 8a and 9a being alleviated.

## 6.4 Catalogue

The general information that could be extracted from the study is contained in Table 6.1 as follows.

Table 6.1

Reconfiguration scenarios catalogue

| Scenario | DC bus stability assessment | | Global stability assessment |
|---|---|---|---|
| | Visual | Methodology | Visual |
| Scenario 1 | Stable | Stable | Stable |
| Scenario 2 | Stable | Stable | Stable |
| Scenario 3 | Stable | Stable | Stable |
| Scenario 4 | Stable | Stable | Stable |
| Scenario 5 | Stable | Stable | Stable |
| Scenario 6 | Stable | Stable | Stable |
| Scenario 7 | Stable | Stable | Stable |
| Scenario 8a | Stable | Stable | Unstable (because of Scenario 8b) |
| Scenario 9a | Stable | Stable | Unstable (because of Scenario 9b) |
| Scenario 8a evaluated at interzonal bus | Unstable | Could not be determined | Unstable (because of Scenario 8b) |
| Scenario 9a evaluated at interzonal bus | Unstable | Unstable | Unstable (because of Scenario 9b) |

Conclusions that can be drawn from the analysis of the IPS system during reconfiguration are that the system can be easily reconfigured as long as shedding of large loads is avoided, and that the system is even more stable, when the operating frequencies of any subsystem within the system are well above 1Hz. This is because the worst margins were discovered at frequencies around 1Hz.

## 6.5 Summary

This chapter has discussed the results of the study in collective terms. It has presented the findings of a study on a PEBB-based integrated shipboard power system during reconfiguration and has shown the stability to be good within some limiting factors. These factors include magnitudes of loads that can be shed at any instance and avoidance of sub-harmonics within any subsystem. In Chapter VII, which is the conclusion, further comments will be made about the study, and future work will be laid out with emphasis placed on improving the contributions the study has presently. The application of the study will be discussed.

# CHAPTER VII

# CONCLUSIONS

## 7.1 Overview

The main goal of the study presented in this dissertation was to study system issues that occur during reconfiguration on a PEBB-based integrated shipboard power system such as the IPS. Six issues were found in this study to be important. One issue, DC bus stability of the intrazonal bus particularly, was investigated in depth. Supplementary goals of this dissertation research included contributing to a discussion of stability assessment methodology of an AC/DC power system, for which there was an application of an existing methodology. In uniquely applying the large scale AC/DC power system stability methodology [31] to a system during reconfiguration, innovative use of the perturbation to the decoupled version of the system was made. Contributions to the application of the large scale AC/DC power system stability methodology included accurately perturbing a baseline system with a perturbation containing the reconfiguration activity information. An important goal was analyzing the data generated from the stability assessment to infer conclusions on the limitations of the test IPS with regards to stability during reconfiguration.

## 7.2 Conclusion

The findings of this study on the PEBB-based integrated shipboard power system during reconfiguration are: (1) the intrazonal DC bus on the port side of the system is

stable for all reconfiguration operations investigated. (2) Load shedding to low system loading is problematic within the test IPS. (3) High frequency operation is good for the PEBB-based integrated shipboard power system since lower stability margins are found at lower frequencies. This last finding improves the system performance of the IPS because of the additional fact that audible acoustics are better at frequencies higher than 20kHz [9]. (4) Another source of noise in AC/DC power systems was discovered to be converter settings and controller response, especially in current controlled controllers. (5) Load loss due to overvoltage could be an important problem to look into, especially with a high amount of static loads in the system. The just mentioned finding was observed in the spikes that appeared in scenarios 1-3 results.

Contributions made in this study included insights gained about the phenomenon of reconfiguration in the test IPS with regards to its stability during reconfiguration, the science of perturbation modeling and a subsequent approximation analysis.

## 7.3 Future Work

The work of reducing the limitations of the performance of the test IPS, as contained in Chapter VI could not be done at this stage of the dissertation research. More protection as are currently being used in the military could be modeled in the test IPS. For the immediate future, more reconfiguration scenarios could be devised and more complicated scenarios can be investigated. More attempts could be made to properly verify the instabilities observed on the interzonal bus on the port side in Scenarios 8a and 9a which were attempted in Scenarios 8b and 9b in this research with a little success.

## 7.4 Project Applicability

The information gathered from the study is expected to be passed on to the military where it is hoped that it will help in efficient development of the IPS which is currently in the development stage. The Navy currently has a test bed at the Naval Warfare Center at Annapolis, Maryland, and the problems discovered and insights gained from the study could be of reasonable importance to the prototype testing presently being carried out. It is expected that systems level issues raised in this study could possibly help in fine tuning the development of converter designs being carried out by the military vendors and might reduce the cost of the eventual IPS shipboard power system.

## 7.5 Remarks

The work in this study was divided into three sections. They were modeling, simulation, and stability assessment. The complexities in modeling could not be understated. Simulation was extensively carried out and a lot of analysis went into stability assessment. This chapter has presented the concluding thoughts on the study, the work involved in the study has been shown, and the achievements of the study reiterated.

# REFERENCES

[1] N. Doerry, H. Robey, J. Amy, and C. Petry, "Powering the Future with the Integrated Power System," *Naval Engineers Journal*, pp. 267-282, May 1996.

[2] K. T. Chau, and C. C. Chan, "Nonlinear Identification of Power Electronic Systems," in *Proceedings of 1995 International Conference on Power Electronics and Drive Systems, 1995*, vol. 1, pp. 329-334.

[3] A. Emadi, and M. Ehsani, "Multi-Converter Power Electronic Systems: Definition and Applications," in *IEEE 32nd Power Electronics Specialists Conference,* Vancouver, Canada, 2001, pp. 1230-1236.

[4] G. S. Thandi, R. Zhang, K. Xing, F. C. Lee, and D. Boroyevich, "Modeling, Control and Stability Analysis of a PEBB Based DC DPS," *IEEE Transactions on Power Delivery,* vol. 14, pp. 497-505, April 1999.

[5] Z. Ye, K. Xing, S. Mazunder, D. Borojevic, and F.C. Lee, "Modeling and Control of Parallel Three-Phase PWM Boost Rectifiers in PEBB-Based DC Distributed Power Systems," in *IEEE Applied Power Electronics Conference and Exposition Proceedings part 2,* Kuala Lumpur, Malaysia, February 1998, pp. 1126-1132.

[6] D. Heping, K. Xing, and F. C. Lee, "Investigation of Soft-Switching Techniques for Power Electronics Building Blocks (PEBB)," in *IEEE Applied Power Electronics Conference and Exposition Proceedings part 2,* Kuala Lumpur, Malaysia, February 1998, pp. 633-639.

[7] K. J. Karimi, A. Booker, and A. Mong, "Modeling, Simulation, and Verification of Large DC Power Electronics System," in *Proceedings of the 27th Annual IEEE Power Electronics Specialists Conference,* 1996, vol. 2, pp. 1731-1737.

[8] Y. Dote, and R. G. Halt, "Review of Intelligent Control, Power Electronic Systems," *IEEE Power Engineering Review,* vol. 19, pp. 44-44, September 1999.

[9] J. G. Ciezki, and R. W. Ashton, "A Technology Overview for a Proposed Navy Surface Combatant DC Zonal Electric Distribution System," *Naval Engineers Journal,* vol. 111, pp. 59-69, May 1999.

[10] J. G. Ciezki, and R. W. Ashton., "The Resolution of Algebraic Loops in the Simulation of Finite Inertia Power System," in *Proceedings of the 1998 IEEE International Symposium on Circuits and Systems,* ISCAS'98, Monterey, California, June 1998, pp. 342-345 1998.

[11] U.S. Naval Academy Annapolis Maryland, "ONR Control Challenge Problem," U.S. Naval Academy Website, www.usna.edu/EPNES/ONR Control Challenge.pdf, January 2002, pp. 1-15.

[12] J.G. Ciezki, and R. W. Ashton, "Selection and Stability Issues Associated with a Navy Shipboard DC Zonal Electric Distribution System," *IEEE Transactions on Power Delivery,* vol. 15, no. 2, pp. 665-669, April 2000.

[13] T. Ericsen, "Power Electronic Building Blocks-a Systematic Approach to Power Electronics," in *IEEE Power Engineering Society Summer Meeting 2000*, vol. 2, pp. 1216-1218, July 2000.

[14] F. C. Lee, and D. Peng, "Power Electronics Building Block and System Integration," in *Proceedings of the Third International Power Electronics and Motion Control Conference PIEMC 2000,* vol. 1, pp. 1-8, August 2000.

[15] K. T. Kornegay, "Design Issues in Power Electronic Building Block (PEBB) System Integration," in *VLSI '98 System Level Design Proceedings IEEE Computer Society Workshop,* Orlando, Florida, April 1998, pp. 48-52.

[16] H. N. Robey, "Propulsion/Power Options-present to 2010 Timeframe, Point Paper for Aegis Advance Planning Cell," *Naval Surface Warfare Center Carderock Division,* NSWCCD Code 808, August 1995, pp. 1-27.

[17] J. Borraccini, W. Ruby, T Duong, D. Cochran, E. Roth et al "Demonstration of Power Electronic Building Block (PEBB1) Function and Plans for PEBB2 and PEBB3," in *GOMAC'97 Digest*, Las Vegas, Nevada, pp. 415-418.

[18] N. Doerry, and J. C Davis, "Integrated Power System for Marine Application," *Naval Engineers Journal*, vol. 106, pp. 77-90, May 1994.

[19] N. Doerry, H. Robey, J. Amy, and C. Petry, "Powering the Future with the Integrated Power System," *Naval Engineers Journal*, vol. 108, pp. 267-282, May 1996.

[20] C. Whitcomb, personal communication (email), Office of the Assistant Secretary of Defense (public affairs) Washington D.C., January 6, 2000.

[21] T. Ericsen, and A. Tucker, "Power Electronics Building Blocks and Potential Power Modulator Application," in *Power Modulator Symposium 1998*, Rancho Mirage, California, pp. 12-15, June 1998.

[22] W. Ruby, R. Cooley, J. Borraccini, M Cannell, J. Sullivan et al, "Power Electronic Building Block Design and Hardware Demonstrator-Results from December 1996 through May 1998," *Power Systems World ,*in *Proceedings of the Conference for Power Electronics, Power Quality and Intelligent Motion (PCIM),* Nunberg, Germany, November 1998, pp. 1-6.

[23] T. B. Dade, "Advanced Electric Propulsion Power Generation and Power Distribution," *Naval Engineers Journal,* vol. 106, pp. 83-92, March 1994.

[24] J. Mayer, "An Efficient Method of Simulating the Detailed Electromechanical Response of Industrial Power Systems," in *Proceedings of the IEEE Industrial Applications Society Annual Meeting1994*, vol. 3, pp. 2103-2109, October 1994.

[25] M. Belkhayat, R. Cooley, and E. H. Abed, "Stability and Dynamics of Power Systems with Regulated Converters," in *Proceedings of IEEE International Symposium on Circuits and Systems 1995, ISCAS '95*, vol. 1, pp. 143-145, May 1995.

[26] A. Emadi, and M. Ehsani, "Dynamics and Control of Multi-Converter DC Power Electronic Systems," in *Proceedings of the IEEE 32nd Annual Power Electronics Specialists Conference, PESC 2001*, vol. 1, pp. 248-253, October 2001.

[27] R. Zhang, F. C. Lee, D. Boroyevich, C. Liu and L. Chen, "AC Load Conditioner and DC Bus Conditioner for a DC Distribution Power System," in *Power Electronics Specialists Conference 2000,* vol. 1, pp. 107-112, September 2000.

[28] S. D. Sudhoff and S. F. Glover, "Three-Dimensional Stability Analysis of DC Power Electronics Based Systems," in *Power Electronics Specialists Conference 2000,* vol. 1, pp. 101-106, September 2000.

[29] S. D. Sudhoff, S. F. Glover, P. T. Lamm, D. H. Schmucker and D. E. Delisle, "Admittance Space Stability Analysis of Power Electronic Systems," *IEEE Transactions on Aerospace and Electronic Systems,* vol. 36, no. 3, pp. 965-973, July 2000.

[30] S. D. Sudhoff, D. H. Schmucker, R. A. Youngs and H. J. Hegner, "Stability Analysis of DC Distribution Systems Using Admittance Space Constraints," in *AES 98, Conference Proceedings of Institute of Marine Engineers* part 1, pp. 43-52, 1998.

[31] P. Huynh and B. H. Cho, "A New Methodology for the Stability Analysis of Large Scale Power Electronics Systems," *IEEE Transactions on Circuits and Systems-I Fundamental Theory and Applications,* vol. 45, no. 4, pp. 377-385, April 1998.

[32] P. Huynh, "Stability Analysis of Large Scale Power Electronics Systems," Ph.D. Dissertation, Virginia Tech, Blacksburg, Virginia, 1994.

[33] J. Lui, X. Feng, F. C. Lee, and D. Borojevich, "Stability Margin Monitoring for DC Distributed Power Systems Via Current / Voltage Perturbation," in *Proceedings of IEEE 16th Annual Applied Power Electronics Conference and Exposition,* vol. 1, pp. 745-751, October 2001.

[34] R. De Doncker, D. Divan, and M. H. Kheraluwala, "A Three-Phase Soft-Switched High-Power-Density DC/DC Converter for High-Power Applications," *IEEE*

*Transactions on Industry Applications*, vol. 27, no 1, pp. 63-73, January / February 1991.

[35] M. H. Kheraluwala, and D. Divan, "High Power Density DC-to-DC Converters for Aerospace Applications*," Final Report,* July 1989-December 1990, University of Wisconsin, Madison, 1991, pp. 37 –94.

[36] M. H. Kheraluwala, "High-Power High-Frequency DC/DC Converters," Ph.D. Dissertation, University of Wisconsin, Madison,1991.

[37] C. M. Wildrick, F. C. Lee, B. H. Cho and B. Choi, "A Method of Defining the Load Impedance Specification for a Stable Distributed Power System," *IEEE Transactions on Power Electronics,* vol. 10, no. 3, pp. 280-285, May 1995.

[38] R. W. De Doncker, D. M. Divan, and M. H. Kheraluwala, "A Three-Phase Soft-Switched High Power Density DC/DC Converter for High Power Applications," in *IEEE-IAS Conference Proceedings*, Pittsburgh, Pennsylvania, October 1988, pp. 796-805.

[39] M. H. Kheraluwala, R. W. Gascoigne, D. M. Divan, and E. Bauman, "Performance Characterization of a High Power Dual Active Bridge DC/DC Converter," in *IEEE Industry Applications Society Annual Meeting,* vol. 2, pp. 1267-1273, 1990.

[40] M. H. Kheraluwala, R. W. Gascoigne, D. M. Divan and E. D. Baumann, "Performance Characterization of a High-Power Dual Active Bridge DC-DC Converter," *IEEE Transactions on Industry Applications,* vol. 28, no. 6, pp. 1294-1301, November / December 1992.

[41] N. H. Kutkut, G. Luckjiff and D. Divan, "A Dual Bridge High Current DC-to-DC Converter with Soft Switching Capability," in *IEEE Industry Applications Society Annual Meeting,* New Orleans, Louisiana, October 1997, pp. 1398-1405.

[42] H. G. Rickover, and P. N. Ross, "Fault Protection on Shipboard AC Power Distribution Systems" *AIEE Transactions,* vol. 63, pp. 1109 – 1120, 1944.

[43] E. C. Mericas, and H. H. Hansen, "Generator Behavior in Response to Suddenly Applied Loads and Low Impedance Faults in the Shipboard Electrical System", *Naval Engineers Journal*, pp. 637 – 650*,* November 1962.

[44] D. E. Johnson, J. L. Hilburn, and J. R. Johnson, *Basic Electric Circuit Analysis*, Second Edition, Prentice Hall Inc, Englewood Cliffs, New Jersey, 1984.

[45] P. M. Anderson, and A. A. Fouad, *Power System Control and Stability*, IEEE Press, New York, 1993.

[46] B. T. Kuhn, S. D. Sudhoff., and C. A. Whitcomb, "Performance Characteristics and Average Value Modeling of Auxiliary Resonant Commutated Pole Converter Based Induction Motor Drives", *IEEE Transactions on Energy Conversion,* vol. 14, no. 3, pp. 493 –499, September 1999.

[47] R. D. Middlebrook, and S. Cuk, "A General Unified Approach to Modelling Switching Converter Power Stages", *Int. J. Electronics 1977,* vol. 42, no. 6, pp. 521 –550.

[48] A. Trzynadlowski, *The Field Orientation Principle in Control of Induction Motors*, Kluwer Academic Publishers*,* Boston, Massachusetts, 1994.

[49] J. O. Bird, *Electrical Circuit Theory and Technology*, Butterworth Heinemann, Boston, Massachusetts, 1997.

[50] ___ , "Switches, Bus Transfer, Electric Power Automatic and Manual (Metric)", *DOD-S-17773B*, Military Specifications, Amendment 3, September 7, 1993.

[51] MathWorks Inc. *MATLAB The Language of Technical Computing – Using MATLAB,* The Mathworks Inc., Natick, Massachusetts, 1984-2000.

[52] MathWorks Inc. *MATLAB The Language of Technical Computing – Using Simulink*, The Mathworks Inc., Natick, Massachusetts, 1990-2000.

[53] W. D. Stevenson Jr. and J. J. Grainger, *Power System Analysis* McGraw-Hill Inc.,New York, 1994.

[54] J. P. Norton, *An Introduction to Identification*, Academic, New York 1986.

[55] J. D. Ward, personal communication, Math Department, Texas A&M University College Station, Texas, December 2000.

[56] E. W. Cheney, *Introduction to Approximation Theory*, AMS Chelsea Publishing, Providence Rhode Island, 1982.

# APPENDIX A

**Problem Statement**

Prove that the Plant models (H) of the load subsystem and the source subsystem, which are determined for a certain configuration of the shipboard power system can, in the presence of changing topology, be approximated by a constant baseline part model and changing part gotten through applying correct perturbation signal.

Summary is $H_3(j\omega)$ + Perturbation model $\approx$ $H_2(j\omega)$.

$H_3(j\omega)$ is the nonlinear representation of the baseline plant. While $H_2(j\omega)$ is the nonlinear representation of the actual plant.

| List of Symbols | |
|---|---|
| $H(j\omega)$ | Plant model in frequency domain |
| $r_{uy}(\iota)$ | Cross correlation function of u and y |
| $r_{uu}(\iota)$ | Auto correlation function of u |
| $h(t)$ | Plant model in time domain |
| $R_{UY}(j\omega)$ | Transform of $r_{uy}(\iota)$ equivalent to the power spectral density (PSD) |
| $R_{UU}(j\omega)$ | Transform of $r_{uu}(\iota)$ equivalent to the power spectral density (PSD) |
| $H_1(j\omega)$ | Plant model after automatic Reconfiguration |
| $H_2(j\omega)$ | Plant model after restoration activities |
| $H_3(j\omega)$ | Arbitrary baseline plant model |
| $P$ | Any perturbation model |
| $P_1$ | Output Perturbation |
| $P_2$ | Input Perturbation |
| $P_3$ | Given scenario Perturbation |
| $C$ | Restoration reconfiguration model |
| $\delta$ | Approximation error for part I of proof |
| $P_P$ | First Trial perturbation model |
| $\varepsilon$ | Approximation error for part II of proof. Error between $P_P$ and $P_3$ |

**Proof**

The output power spectral density of any function y(w) is given by the fourier transform of the cross correlation function $r_{uy}(\tau)$. Similarly, the input power spectral density of any input signal u(w) is given by the fourier transform of the auto correlation function $r_{uu}(\tau)$. Eqn. (A-1) – Eqn. (A-9) are obtained from [54]. Eqn. (A-1) and Eqn. (A-2) are the standard representation of the cross and auto correlation functions

$$r_{uy}(\tau) = \lim_{T\to\infty} \frac{1}{2T} \int_{-T}^{T} u(t)y(t+\tau)dt \tag{A-1}$$

$$r_{uu}(\tau) = \lim_{T\to\infty} \frac{1}{2T} \int_{-T}^{T} u(t)u(t+\tau)dt \tag{A-2}$$

An alternative representation for the cross correlation function is Eqn. (A-3). Eqn. (A-3) is not used further in this proof

$$r_{uy}(\tau) = \int_{0}^{t_s} h(t)r_{uu}(\tau)dt \tag{A-3}$$

Where $t_s$ is the settling time. $r_{uy}(\tau)$ and $r_{uu}(\tau)$ can be redefined so that their transforms exist as Eqn. (A-4) and Eqn. (A-5).

$$r_{uy}(\tau) = \frac{1}{2T} \int_{-T}^{T} u(t)y(t+\tau)dt \tag{A-4}$$

$$r_{uu}(\tau) = \frac{1}{2T} \int_{-T}^{T} u(t)u(t+\tau)dt \tag{A-5}$$

The transform can then be written as Eqn. (A-6)

$$R_{UY}(j\omega) = \Im\left[r_{uy}(\tau)\right] = \int_{-\infty}^{\infty} r_{uy}(\tau)e^{-j\omega\tau}d\tau \tag{A-6}$$

Substituting Eqn. (A-4) into Eqn. (A-6) we get Eqn. (A-7) and by extension we can get Eqn. (A-8).

$$R_{UY}(j\omega) = \left(\frac{1}{2T}\right)U(-j\omega)Y(j\omega) \tag{A-7}$$

$$R_{UU}(j\omega) = \left(\frac{1}{2T}\right)U(-j\omega)U(j\omega) \tag{A-8}$$

$$H(j\omega) = \frac{R_{UY}(j\omega)}{R_{UU}(j\omega)} \tag{A-9}$$

The numerator of the RHS of Eqn. (A-9) can be nonlinear and so can the denominator, as a result of the transformation. There are therefore two ways that the plant model $H(j\omega)$ in Eqn. (A-9) can be changed.

[1] Change $H(j\omega)$ directly, and therefore obtain new $R_{UY}(j\omega)$ and $R_{UU}(j\omega)$.

[2] Change $R_{UY}(j\omega)$ and $R_{UU}(j\omega)$ such that new desired $H(j\omega)$ results.

**Engineering Application**

Electrical activity on ship results in different plant models. Let $H_1(j\omega)$ be platform response to assure power to vital loads. A series of supplementary reconfiguration actions follows to bring the system to exact desired configuration $H_2(j\omega)$. $H_2(j\omega)$ is known, but $H_1(j\omega)$ is unknown. Since $H_1(j\omega)$ is unknown, select a baseline plant model $H_3(j\omega)$ (known because predetermined) such that $H_3(j\omega)$ + perturbation model $\approx H_2(j\omega)$.

Approximation theory is needed in estimating the error resulting from substituting $H_1(j\omega)$ + counter activities $\approx H_2(j\omega)$ with $H_3(j\omega)$ + perturbation model $\approx H_2(j\omega)$ and in minimizing the maximum of the error from substituting $H_3(j\omega)$ + perturbation model for $H_2(j\omega)$. Perturbation model is composed of the first electrical activities and the counter activities. These are to be modeled using tripuls,rectpuls and randn functions. Only two parameters can be varied in the perturbation model. They are voltage and current and not physical connectivity.

**Part I**

Theorem on Existence of Best Approximation of $H_3(j\omega)$ + $P_3$ $\approx$ $H_2(j\omega)$ for $H_1(j\omega)$ + C $\approx$ $H_2(j\omega)$.

Refer to Eqn. (A-9) – definition of Plant model in the frequency domain. Repeat Eqn. (A-9) here for convenience.

$$H(j\omega) = \frac{R_{UY}(j\omega)}{R_{UU}(j\omega)} \tag{A-9}$$

It follows that

$$H_2(j\omega) = \frac{R_{(UY)_2}(j\omega)}{R_{(UU)_2}(j\omega)} \tag{A-10}$$

For the sake of focus lets replace the sign $\approx$, in the theorem, with = , this can be done away with at any point in the proof. So,

$$H_1(j\omega) + C = \frac{R_{(UY)_2}(j\omega)}{R_{(UU)_2}(j\omega)} = H_2(j\omega) \tag{A-11}$$

Let us take a baseline plant model $H_3(j\omega)$ such that (A-12) results.

$$H_3(j\omega) = \frac{R_{(UY)_3}(j\omega)}{R_{(UU)_3}(j\omega)} \tag{A-12}$$

We would like to perturb $Y \to Y_P$ and $U \to U_P$ so that

$$H_3(j\omega) + P_3 = \frac{R_{(UY)_3}(j\omega) + P_1}{R_{(UU)_3}(j\omega) + P_2} \tag{A-13}$$

Taking a long division of Eqn. (A-13) [55],

$$R_{(UU)_3}(j\omega) + P_2 \overline{\left) \begin{array}{c} H_1(j\omega) \\ \hline R_{(UY)_3} + P_1 \\ \hline \dfrac{H_1(j\omega)R_{(UU)_3}(j\omega) + H_1(j\omega)P_2}{R_{(UY)_3}(j\omega) + P_1 - H_1(j\omega)(R_{(UU)_3}(j\omega) + P_2)} \end{array}\right.} \tag{A-14}$$

Eqn. (A-14) is true if $H_3(j\omega) \geq H_1(j\omega)$

$$H_3(j\omega) + P_3 = H_1(j\omega) + \frac{R_{(UY)_3}(j\omega) + P_1 - H_1(j\omega)(R_{(UU)_3}(j\omega) + P_2)}{R_{(UU)_3}(j\omega) + P_2} \tag{A-15}$$

We need to estimate the maximum error and minimize it such that

$$\left| C - \frac{R_{(UY)_3} + P_1 - H_1(j\omega)(R_{(UU)_3}(j\omega) + P_{2)}}{R_{(UU)_3}(j\omega) + P_2} \right| = \delta \tag{A-16}$$

Where $\delta$ is a small positive number.

Eqn. (A-16) is a standard metric, obeying all the metric properties of reflexivity, positivity, symmetry and triangle inequality.

Let $$\frac{R_{(UY)_3} + P_1 - H_1(j\omega)(R_{(UU)_3}(j\omega) + P_2)}{R_{(UU)_3}(j\omega) + P_2} \equiv P \tag{A-17}$$

Therefore Eqn. (A-16) can be rewritten as

$$|C - P| = \delta \tag{A-18}$$

Standard proof of existence follows which is from [56]. It is rewritten here.

Let there be a set, C, such that $(a : a \in C)$. $P \subset C$ or vice versa where P is a set such that $(x : x \in P)$.

Let P denote a compact set in the metric space (C,d) proof is in [55]. d is the metric defined in Eqn. (A-18).

Prove that to each point $(a : a \in C)$ of the space there corresponds a point in P of minimum distance from a.

**Proof of part I [56]**

Let $\delta = \inf(d(a,x) : x \in P)$

By definition we may find a sequence of points $x_1, x_2, x_3, \ldots$ in P with the property that $d(a,x_n) \to \delta$ as $n \to \infty$. By the compactness of P we may assume that the sequence converges to a point $x^*$ of P (for basis check [55]). By the triangle inequality postulate we have that

$$d(a,x^*) \le d(a,x_n) + d(x_n,x^*) \tag{A-19}$$

The left-hand side of this inequality in Eqn. (A-19) is independent of n and the right-hand side approaches $\delta$ as $n \to \infty$. Therefore $d(a,x^*) \le \delta$. However, $x^* \in P$, $d(a,x^*) \ge \delta$. Therefore $d(a,x^*) = \delta \bullet$

**Part II**

By generalization we have Eqn. (A-11) is as (A-20).

$$H_3(j\omega) + P_p \approx \frac{R_{(UY)_2}(j\omega)}{R_{(UU)_2}(j\omega)} = H_2(j\omega) \tag{A-20}$$

$$H_3(j\omega) = \frac{R_{(UY)_3}(j\omega)}{R_{(UU)_3}(j\omega)} \tag{A-21}$$

Similar to earlier process

$$H_3(j\omega) + P_p = \frac{R_{(UY)_3} + P_1}{R_{(UU)_3} + P_2} \tag{A-22}$$

Taking a long division of Eqn. (A-22) [55]

$$R_{(UU)_3}(j\omega) + P_2 \overline{\left| \begin{array}{c} H_2(j\omega) \\ \hline R_{(UY)_3}(j\omega) + P_1 \\ \hline H_2(j\omega)R_{(UU)_3}(j\omega) + P_2 H_2(j\omega) \\ \hline R_{(UY)_3}(j\omega) + P_1 - H_2(j\omega)(R_{(UU)_3}(j\omega) + P_2) \end{array} \right.} \tag{A-23}$$

Eqn. (A-23) is true if $H_2(j\omega) \langle \left[ \left[ \frac{1}{H_3(j\omega)} \right]^{-1} + \left[ \frac{P_2}{R_{(UY)_3}(j\omega)} \right]^{-1} \right]$

$$H_3(j\omega) + P_p = H_2(j\omega) + \frac{R_{(UY)_3}(j\omega) + P_1 - H_2(j\omega)(R_{(UU)_3}(j\omega) + P_2)}{R_{(UU)_3}(j\omega) + P_2} \tag{A-24}$$

$$P_p - \left[ \frac{R_{(UY)_3}(j\omega) + P_1 - H_2(j\omega)(R_{(UU)_3}(j\omega) + P_2)}{R_{(UU)_3}(j\omega) + P_2} \right] \equiv P_3 \quad \text{(A-25)}$$

Therefore need to estimate the error in Eqn. (A-25).

$$\text{Let } \frac{R_{(UY)_3}(j\omega) + P_1 - H_2(j\omega)(R_{(UU)_3}(j\omega) + P_2)}{R_{(UU)_3}(j\omega) + P_2} = \varepsilon \quad \text{(A-26)}$$

Such that ε is the error of the approximation. (We assume that $P_3$ is the perturbation of equality.) It is needed that ε is minimized such that $\varepsilon \cong 0$. Then it is desirable to find P such that $\varepsilon \cong 0$. Standard way to do this is to take the derivative of ε with respect to P and set it to 0. However, doing this yielded no new information from Eqn. (A-26).

Easiest practical way to do this is to solve for the unknown in Eqn. (A-26) with ε experimentally determined to be the smallest value possible. $H_2(j\omega)$ is known and ε is determined experimentally. $P_1$ is set by $P_2$ (all Ps are initially unknown and are degrees of freedom) Therefore the unknown $P_2$ is computable and is needed to approximate the perturbation model $P_3$. If, however, ε is small it is to be neglected without losing confidence in method♦

# VITA

Adeoti T. Adediran earned her B.Sc. in electrical engineering from the University of Ibadan, Ibadan, Nigeria in 1987 and earned her M.S. in electrical engineering from the University of Tennessee, Knoxville, Tennessee in 1991. She is receiving her Ph.D. degree in electrical engineering at Texas A&M University in December 2003. From the fall of 1998 through the spring of 2002 she worked as graduate research assistant in the Power Systems Automation Laboratory at Texas A&M University. From fall 2002 through summer 2003, she worked with the National Emergency Response and Rescue Training Center, Texas A&M University as student technician. She is a student member of the IEEE, Phi Kappa Phi and IFUW. She can be contacted at adeoti@ee.tamu.edu or 2112 W. Clearwater Ave. Kennewick WA 99336